R. van der Meer

Glass Flood Defences

A theoretical and practical assessment of the impact resistance of Glass Flood Defences to floating debris

Source cover photo: http://fenexcorp.com/product/oversized-flood-barrier-and-window/

Glass Flood Defences

A theoretical and practical assessment of the impact resistance of Glass Flood Defences to floating debris

By

Roos van der Meer
Student number: 4089308

in partial fulfilment of the requirements for the degree of

Master of Science
in Structural Engineering

at the Delft University of Technology,
to be defended on Thursday 15 November, 2018 at 15:00.

Supervisor:	Prof.ir. R Nijsse,	TU Delft
Thesis committee:	Dr.ir. F.A. Veer	TU Delft
	Ir. W.F. Molenaar	TU Delft
	Ing. J. Staphorsius	Arcadis
	Ir. F. Lenting	Arcadis

An electronic version of this thesis is available at http://repository.tudelft.nl/.

“Intelligence is the ability to adapt to change”
-Stephen Hawking

Preface

This thesis is submitted in partial fulfilment of the requirements for the degree of MSc in Civil Engineering at Delft University of Technology. The research was carried out in cooperation with Arcadis Nederland and supervised by Delft University of Technology.

This thesis presents the exploratory research and testing of the impact resistance of a glass flood defence against floating debris. Some people say we are living in the “Glass Age”, and after this research I could not agree more; glass continues to amaze me as a structural material. With endless possibilities and improving material properties, I can safely say that this material is here to stay and will conquer markets other than just glazing. With good hopes that the glass flood defence will be implemented on a larger scale in the Netherlands the coming years, I am proud to say I was part of the experimental research of the glass flood defence.

I would like to thank my graduation committee for their enthusiastic and supporting approach. Ing. John Staphorsius and Ir. Fred Lenting for letting me conduct my thesis at Arcadis and helping me whenever I was in need. I want to thank Ir. Wilfred Molenaar for the discussions and advice on the report structure and the coarse-to-fine research approach. Rob Nijsse and Fred Veer for sharing their knowledge on the subject and for giving me the opportunity to do experimental research in the Stevin II laboratory, which really was the highlight of my MSc Structural Engineering.

I want to thank everyone at Arcadis who made my stay a pleasurable experience, and especially Dennis Kooijman for his help and guidance with the FEM analysis and for sharing his knowledge on glass structures.

I also want to thank everyone involved in sponsoring and performing of the impact-tests: Berthold Reiter from IBS Techniks for making the aluminum frame structure available for me to use in the tests; Kees Dorst for ordering the three glass panels on behalf of the Waterschap Limburg; and the laboratory employees Kees, Ruben, Jan, John and Louie for their flexibility and professional solutions to some of the challenges we encountered in the experiments.

Special thanks to my modern and large loving family, who support me unconditionally in life and keeping me sane throughout the process of graduating. The prospect of making them proud was a strong motivation for me to finish my study at the TU Delft. My sisters Sterre, Chaja, my brother Bas and my close friends Saskia, Tosca, Vera, Amber and Zoë for always believing in me and my competence to obtain my engineering degree. My bonus parents Pierre, Marion, and Mischa for raising and loving me as one of their own.
Especially involved in this thesis were my father Bert van der Meer, who helped me transport a heavier impact object twice as the glass proofed to be stronger than expected in the impact experiments. And my mother, Paula Steenwinkel, who reviewed and proofread my final thesis and for being the most caring mother imaginable.

Lastly, I want to thank Jelle for his love and endless patience to deal with my stubbornness and sometimes chaotic being, while giving me indispensable advice on the way to become an engineer.

R. van der Meer
Delft, November 2018

Abstract

Ever since the catastrophic storm surge that flooded a large part of the Netherlands in 1953, the Dutch have been updating and improving their flood defence system. The most recent update of the flood safety standards, the “Wettelijk BeoordelingsInstrumentarium 2017(WBI2017)”, calls for many alterations to the current flood defence system. The WBI2017 went into practice on the 1st of January 2017, and uses a risk based, fully probabilistic approach.

In the far south of the Netherlands, the river Meuse flows through the landscape. It flooded twice in the 1990s, causing a lot of economic damage. Emergency measures, such as demountable flood walls, were taken to prevent future flooding. And while this solution was to the liking of the inhabitants, the recent update in the flood safety standard calls for a more permanent structure. In the search for an alternative and permanent solution, a glass flood wall was suggested.

Nowadays there are not many examples of glass used in a flood defence in Dutch practice, and certainly not as part of a primary flood defence. It can be classified as an innovation, from which little is known from a flood and structural safety perspective. Glass is used globally to retain water in numerous applications such as aquaria, under water glazing, glass bottom boats, etcetera; therefore, water pressure is not seen as a high risk to the glass. What happens when floating debris hits the glass structure? Impact on glass can result in immediate failure, where the water retaining function could be lost. This thesis aims to answer this question, by theory and later on by impact experiments in a dry setting.

This thesis is built up in three main parts. In the first part; ‘Background’, the chapter “Location analysis“ describes the geographical context, in which the glass flood defence can be placed. A brief history of flooding, and an analysis of the environment and hydraulic boundary conditions is given alongside some earlier findings of the Flood Risk in the Netherlands (FloRis) on risk and potential damages. The next chapter presents existing literature related to the material glass, which plays a lead role in this thesis, as it makes the solution innovative and new. The chemical, mechanical and physical properties, geometrical limitations, pitfalls and weaknesses are given, after which the behavior and interlayer properties are presented for laminated glass. The background ends with a chapter about the Norms, Codes and standards that are applicable to the glass flood defence.

In the second part; ‘Calculations’, first the design of the structure and it’s properties and detailing is explained. The properties of the glass panel from the design is then used to determine the effective thickness and stress limits in the glass according to the NEN2608;2014 in chapter 7. It was found that when using the interlayer Sentryglass, and with a short duration load such as an impact, the effective thickness of the glass can be close to the thickness of the glass in reality. In chapter 8, a Finite Element Model is used to predict stresses caused by two main load situations: High water up to the top of the structure and impact loading. A simplified spring model is used to determine the maximum energy that can be absorbed by the structure. Using conservative assumptions, the critical impact energy was found to be $490\ Nm$. From analysis with different effective thicknesses, it was concluded that the structure still fulfils the Eurocode with one broken layer to withstand the high water loads in Ultimate Limit State (ULS).

To analyze the safety of this type of structure at the locations along the Meuse, a failure probability analysis is done in chapter 9. Based on the standards of the WBI2017, it was found that the structure can be safe enough to comply with the new flood safety standards, but more information should be gathered about the probability of an impact, and the possible impact objects.

In the last part of the thesis; ‘Experiment’, the findings of the experiments are presented. The experiment was conducted in the Stevin II laboratory at the TU Delft, and the impact capacity of

three separate panels with identical properties were examined. An aluminum supporting structure was used, a glass flood defence design from the German manufacturer IBS Technics. Two impact objects were used, and all three panels withstood the minimal kinetic energy of $490\ Nm$. The last panel could not be broken by the impact objects available, and was fractured using a steel hemisphere, mounted on one of the impact objects. This steel detail fractured the front two layers, indicating that the panel did not fail due to bending. The steel hemisphere tore apart in the impact. After the impact tests, the residual capacity was assessed by placing a concrete block of approximately 1200 kg onto an area of $0.5 \times 0.5m$ in the middle of the glass panel to imitate moments due to water pressure. The outer layer was still intact, and the panel carried this static load without any problem. After a few days, the last layer was fractured with a hammer and the static load test was repeated on the panel with three broken layers. Apart from a few centimeters deflection, the broken panel carried the load, proving that the residual capacity was sufficient to carry the maximum water pressure.

Nomenclature

Abbreviations

Abbreviation	Explanation
BRS	Borosilicate glass
DFPP	The Dutch Flood Protection Program
EET	Enhanced Effective Thickness
ER	Economic Risk
FloRis	Flood Risk in the Netherlands
GFD	Glass Flood Defence
HBN	Hydraulische Belasting Niveau
HWBP	HoogWaterBeschermingsProgramma
IR	Individual Risk
LEFM	Linear Elastic Fracture Model
LK	Leidraad Kunstwerken
SGP	SentryGlass Plus
SLS	Soda Lime Silica glass
SR	Societal risk
STOWA	Stichting Toegepast Onderzoek Waterbeheer
TAW	Technische Adviescommissie voor de Waterkeringen
WABO	Wet Algemene Bepalingen Omgevingsrecht
WBI	Wettelijk Beoordelings Instrumentarium
WTI	Wettelijk Toets Instrumentatium (OLD WBI)

Since a few different country glazing codes are investigated, it is practical to keep the different abbreviations in mind for glass types:

Abbreviation	UK	USA	Netherlands	Germany
AG	Float Glass	Annealed Glass (AG)	Vlakglas	Floatglas (Float) spiegelglas
HSG	Heat-strengthened glass (HSG)	Heat-strengthened glass (HSG)	Thermisch-Versterkt glas	Teilvorgespanntes Glas (TVG)
FTG	Toughened Glass	Fully Tempered Glass (FTG)	Thermisch gehard glas	Einscheiben-Sicherheitsglas (ESG)
FTG-H	Toughened Glass with heat-soak test	Fully Tempered Glass with heat-soak test	Thermisch gehard glas met heat-soak test	Einscheiben-Sicherheitsglas mit Heiβlagerungstest (ESG-H)
LSG	Laminated Safety Glass	Laminated Safety Glass	Gelaagd glas	Verbund-Sicherheitsglas (VSG)

Symbols

Symbol	Explanation	Unit
a	Length of the shortest side of the panel acceleration	[mm] [m/s]
A	Area Loading surface	[m] [m]
A_d	Equivalent static force inflicted by a collision	[kN]
B_1	Length of the loading area parallel to side B	[mm]
c	Corrosion constant	[-]
C	Constant	[-]
δ	Delta Dirac function (with the integral of δ equal to one)	[-]
E	Modulus of elasticity Occurring force Energy Economic risk	[N/mm²] [kN] [Nm] [€]
F	Force	[kN]
F_{dx}	Design value of the frontal collision force	[kN]
F_{dy}	Design value of the lateral collision force	[kN]
F_R	Collision force due to friction	[kN]
$f_{b;k}$	The characteristic bending strength of prestressed glass	[N/mm²]
$f_{g;k}$	characteristic bending strength of glass	[N/mm²]
$f_{mt;u;d}$	Design value of the bending strength	[N/mm²]
G	Shear modulus	[N/mm²]
γ	Safety factor	[-]
$\gamma_{m;A}$, γ_M	Material factor of annealed glass	[-]
$\gamma_{m;V}$	Material factor of prestressed glass	[-]
H	Length of the panel in mm	[mm]
H_1	Length of the loading area parallel to side H	[mm]
k	Spring stiffness Support factor	[N/m] [-]
k_a, k_{sf}	Surface effect factor	[-]
k_e, k_{ed}, k'_{ed}	Edge(and hole) quality factor	[-]
k_{mod}	Modification factor	[-]
k_σ	Tension factor according to table C.3 (NEN)	[-]
k_{sp}	The factor for surface structure	[-]
k_w	Factor for bending according to table C.3 (NEN)	[-]
k_v	Heat treatment factor	[-]
k_z	Loading zone factor	[-]
l	Length of the panel perpendicular to l_0	[mm]
l_0	Length of the unsupported side of the panel in	[mm]
L_A	Form factor dependent on the length and width of the panel	[-]
L_σ	Form factor for tension dependent on the form and support situation of the panel	[-]
L_w	Form factor for bending dependent on the form and support situation of the panel	[-]
m, M	Mass	[kg]
μ	Friction coefficient by a lateral collision (advised value =0.4)	[-]
n	Number of plates	[-]
ω	Frequency	[1/s]
ω_j	Contribution failure probability space	[-]
ω_0	Eigenfrequency	[1/s]

$\boldsymbol{\varphi}$	Angle of incidence	[°]
$\boldsymbol{\psi}$	Reduction factor	[-]
$\mathrm{Q_k}$	Characteristic load quantity	[kN]
$\boldsymbol{R_M}$	Reduction factors of partial factor	[-]
$\boldsymbol{\sigma}$	Stress	[]N/mm²]
$\boldsymbol{t}$	1. Thickness 2. Time duration	[mm] [s]
$\boldsymbol{u}$	Displacement	[m]
$\boldsymbol{\dot{u}, v}$	Velocity	[m/s]
$\boldsymbol{\ddot{u}, a}$	Acceleration	[m/s²]
$\boldsymbol{v}$	Poisson number	[-]
$\boldsymbol{x}$	Smallest distance from side l to the middle of the loading area according to C.1 in mm, where $\frac{x}{l} \leq 0.5$	[mm]
$\boldsymbol{y}$	Distance from side l_0 to the middle of the loading area according to C.1	[mm]

Table of contents

Part III

List of figures

List of tables

1. Introduction

1.1. Problem analysis

1.1.1. Intro

In the most southern province of the Netherlands, the higher grounds of the Limburg hills seem a safe alternative to the larger part of the country which is beneath sea water level. These are the areas people will flee to if disaster happens and the sea dikes cave. But as one of the biggest rivers in the Netherlands slices this landscape in half, it is also an area exposed to flood risk. This area is prone to flooding of the Meuse river, which originates from mountain waters in the French alps and debouches in the Dutch delta. As is historically the case with waterways, people are thriving and settling there because of the many opportunities such a large river can provide in trading, irrigating, traveling, bathing and fishing. Nowadays it still attracts people as they love to live by the water. Unfortunately a river can also be a large risk; high water levels can flood the area and cause large financial damage and casualties. In Limburg there are many settlements and villages next to the Meuse. According to the latest update in the Dutch Flood Protection Program many dikes along the Meuse are not up to the desired safety standard. These flood defences often lack in height. An innovative solution is needed as for many of the dikes, there is no room to heighten and widen the dikes without obstructing the direct inhabitants and their view on to the dikes. Increasing the dike height often meets a lot of resistance from the surrounding public, causing a lot of tension between the waterboards and the people they aim to protect. This report describes the first structural assessment of an innovative solution to these problems: a glass flood wall. The use of the material glass in a flood defence has not been widely accepted in the Netherlands but it offers a permanent solution: Its transparent nature maintains the view on the river, while its reputation as a structural material is growing and improving by the day.

1.1.2. Historic background of flood defences in the Netherlands

In the year of 1953 multiple dikes breached in the south of the Netherlands due to high water levels caused by a storm surge combined with spring tide. 1863 people lost their lives together with thousands of animals. This catastrophe sparked a change in flood management, and a delta committee was formed. They later presented a proposal for safety standards for the flood defences, while advising to shorten the coastline. The building of the famous Dutch Delta works were set in motion and have protected the delta successfully ever since.
In the 1990's the winters of 1993 and 1995 brought extremely high river discharges in the Meuse and Rhine river systems. 250.000 people had to be evacuated as flood safety could not be guaranteed. Large areas along the Meuse and Rhine were inundated and these events initiated many emergency measures and the "Room for the River" projects. [Jonkman et al.,(2017)]
The most recent update in the flood safety standards, the WBI2017 standard, called for major improvements on many of the Dutch flood defences. This included a lot of river dikes along the Meuse that need to be increased in height and strength. [Jonkman et al.,(2018)]

1.1.3. Problem indication

The case in Limburg is severe, where at some locations along the Meuse the height needs to be increased by more than two meters. Such heights have not been protected by glass flood walls in or outside of the Netherlands. Currently, the waterboard makes use of demountable flood defences, which have a large disadvantage over a permanent structure. A permanent structure is desirable to rule out failure related to closing/erecting the structure in an emergency situation and cut costs on the long term. With a glass structure, these requirements will be met. It is a desirable solution to build a transparent retaining wall, but little is known about the structural robustness of these structures; structural application of glass is relatively new which results in limitations in the guiding regulations. More information on the structural safety of this structure is needed before this solution can be implemented along the Meuse.

1.1.4. Problem definition

What is the main problem?

- The strength and robustness of a glass flood wall against the impact of floating debris is unknown.

What are the sub problems?

- A glass retaining wall is innovative, and never used at a large scale in terms of height and length. Therefore, little to no information on the structural safety against impact is present.
- There is no information on residual strength of glass in case of a calamity like a collision. More information on this subject is needed.
- Glass calculation methods are not harmonized on a European level.
- The material glass has a wide range in strength properties, and its limit strength depends on many factors including fabrication, finishing and loading.
- Impact models depend on many factors and modelling an impact on glass is very complex due to the brittle and unpredictable nature of the material.

1.2. Research principles

1.2.1. Goal

The main incentive of this research is to assess if a glass wall is safe enough to be used as flood defence in the Netherlands, meanwhile complying with the (local) safety standards. This will be accomplished by both theoretical and practical assessments on a given flood defence design of significant height. If such a design is considered to be safe enough it can be placed at more locations later on, provided that the loading conditions are similar to or lesser than the considered project.

1.2.2. Relevance

Research on the impact on glass by driftwood or floating debris has only be done by computer models and is never tested in practice or in laboratory tests. The response of a structure on such an impact is hard to model accurately. There are also no reliable methods available to research the ability of glass to withstand impact loads. Unfortunately, scaling of the glass tests is impossible due the large influence of small flaws and impurities in the material. Real life testing of the loads on glass is therefore a very common way to assess the structural safety of the glass such as the impact capacity. Since the response of the laminated glass to such an impact is unknown, this research is relevant to all stakeholders considering glass as part of a flood defence. It is also an addition to the many applications glass is nowadays used for, if deemed suitable as a flood defence.

1.2.3. Scope

If used correctly, glass is known to withstand water and wind pressures without any problems(aquaria, underwater windows, submarine windows, hurricane windows). But impact from hard or fast objects can cause permanent and fatal damage to the structure. The river flows with low velocities lateral to the structure, but the floating objects can be of large masses. Therefore the impact on glass by a “large mass/low velocity object” will be the main subject of research.
The model and the probabilistic analysis are based on one design: a 2x2 meter 3x19mm thick glass panel laminated with Sentryglass and supported by an IBS aluminum frame(this choice is explained in chapter 6). Other types of structure or designs are not considered in this research. Also, only the failure mechanism of “Structural failure” is considered, as “Overflow/Overtopping” and “Piping” are very location bound and miss relevance to the structure itself.

1.3. Research questions

1.3.1. Main research question

- Can a glass flood wall be structurally safe enough to withstand impact loads from floating debris?

1.3.2. Sub questions:

Location specific

- What are the risks to the glass structure at the location?
- What is the height that needs to be retained at the location?

Probabilistic analysis

- What is the allowed probability of failure for a structure at the project location?
- What are the failure modes of the glass flood defence?
- What is the probability of failure for the mechanism structural failure?

Material

- How do you determine the strength of a laminated glass panel (including foils)?
- What are possible sizes for the glass panel?
- What are the structural properties of glass?

Experiment

- What is the maximum energy that can be absorbed by the structure in case of a collision by an object of organic material?
- In case of breakage, is there any residual strength of the glass panels to withstand water and wave pressure that is present during or after collision?

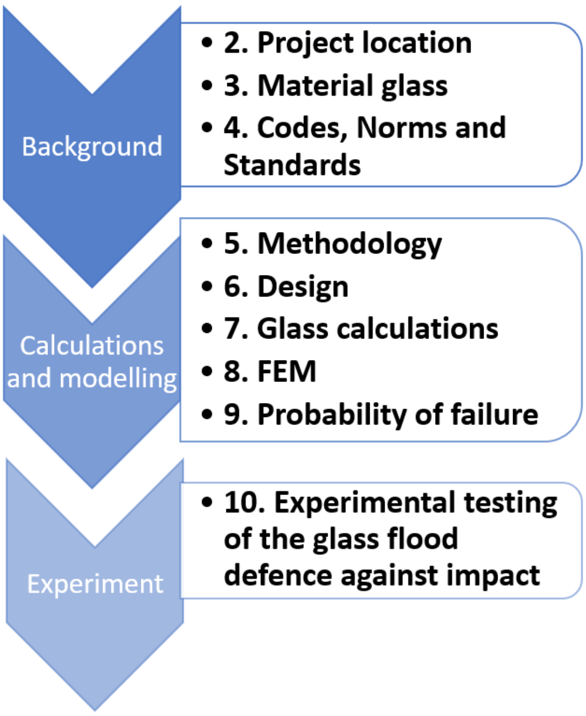

Figure 1-1: Thesis structure

1.4. Thesis Outline

In Figure 1-1, the chapters between the intro and conclusion are divided into three main parts: Background: in these chapters the background and existing literature are analyzed and relevant information about the project location, the governing legislation in building codes, and the material glass are presented to the reader. These chapters form the basis of this research, as is illustrated in the research pyramid: Figure 1-2 .
The next steps are theoretical. In the part "Calculation and modelling", the given design is used for strength calculations with glass calculation methods from three different country building codes (Dutch, German and Italian). This existing theory is then used to model the structure with the Finite Element Method (FEM) in SCIA Engineer. With this FEM model, an impact analysis is performed. To finalize the calculations, a failure probability analysis is done on the failure mechanism "Structural failure".

Due to the fact that existing models and methods are unreliable given the unpredictable nature of glass, a laboratory experiment is conducted at the TU Delft Laboratory Stevin II. The set-up, description of impact object, expectation and outcome of these laboratory experiments are presented in chapter 10. The results of the experiment are analysed and compared to the theoretical outcome, where after the conclusions, discussion and recommendations follow.

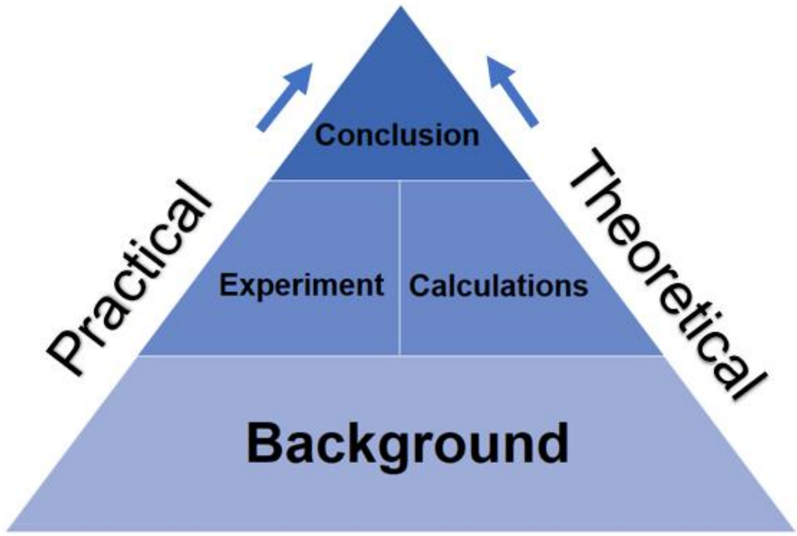

Figure 1-2: Research pyramid

Part I: Background

2. Project location

2.1. Introduction

This chapter describes the physical context of the problem. It’s goal is to gain insight in the hydraulic boundary conditions and risks that the glass flood defence will face if constructed in this area.

2.2. Area of interest

2.2.1. Waterboard Limburg

The task of a waterboard (waterschap), is managing all water related aspects in a certain area. Waterschap Limburg is the outcome of the recent merger between waterschap Peel and Maasvallei and waterschap Roer and Overmaas. It is responsible for managing the water system in the whole province of Limburg, the most southern province of the Netherlands. In 1993 and 1995 a large part of the area flooded, which gave impulse to the desire to upgrade the flood defence system in Waterschap Limburg. On the image below the possible locations for a glass flood wall are presented and on the right the river boundaries of the 1993 and 1995 flood can be seen.

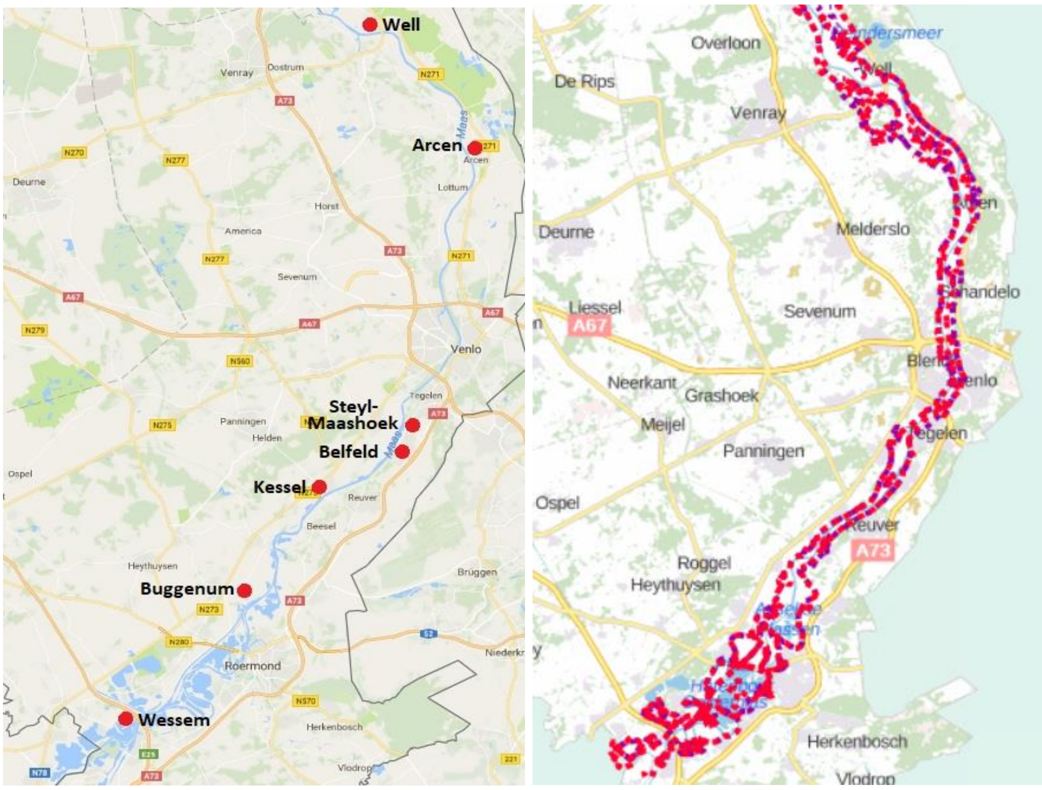

Figure 2-1:Left: Possible project locations [Google Maps (2017)]; Right: Flood boundaries of the Meuse in the 1995(red) and 1993(purple) floods [Pim platform(2018)]

2.3. Arcen

2.3.1. Design principles

The glass flood defence can be implemented on multiple locations along the Meuse, but for the case study one particular location, Arcen, is investigated more deeply. The design principles acquired from an intern Arcadis report are in summary:

- The governing water height that needs to be retained is NAP+18.40 m

- The possibility of drifting ships is small, there are no mooring places in the direct neighborhood
- Upstream a camping is present, from which canoe's/kayaks might float to the flood defence
- According to the Maas-model of Rijkswaterstaat(RWS) the water speed present at the location will be 1.90 m/s
- Kinetic energy is assumed to have an angle of incidence of 22.5°

For more information about the other locations the reader is referred to Appendix G.

2.3.2. History of flooding

On 20th of December, the town of Arcen was overwhelmed by a Meuse flood. Due to bad communication and the lack of help, people were still strolling the streets moments before the water flooded the town. Some parts of the village even faced water levels up to 2 meters. [Limburg1 (2013b)] In 1995, Arcen prepared for the flood with sand bags, which successfully protected most of Arcen, as can be seen by the red line in Figure 2-4: indication flood defence line [Arcadis(2017)]. Not all locations along the Meuse were successful in keeping their feet dry in 1995.


Figure 2-2: Rescue operation 1995 flood. [Source: https://beeldbank.rws.nl, Rijkswaterstaat / Henri Cormont]

Figure 2-3: Emergency measures proved to be successful in Arcen [Source: https://beeldbank.rws.nl, Rijkswaterstaat / Henri Cormont]

2.3.3. Geographical location flood defence line

As can be seen from the images below the 1993 flood affected a much larger part of Arcen than the 1995, although higher water levels occurred. Arcen was better prepared and therefore a new disaster was averted.

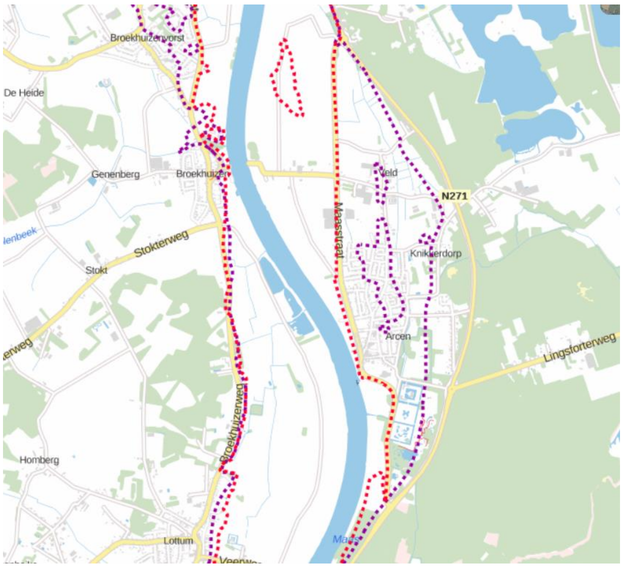

Figure 2-4: indication flood defence line [Arcadis(2017)]

Figure 2-5: Flood boundaries Arcen in the 1995(red) and 1993(purple) floods [Source: pimplatform.nl]

2.3.4. Height map Arcen

The 1993 flood inundated almost all of Arcen, and it is easy to see where the water stopped and why; in Figure 2-6: Bathtub Arcen (Source: AHN2 PDOK, Actuality: 2008-2012) one can see that Arcen is surrounded by much higher ground. This makes the area a river floodplain, protected by one dike. Due to this bathtub situation, the storage capacity of Arcen is limited. If a breach occurs, the water levels can rise fast. This is what happened in 1993.

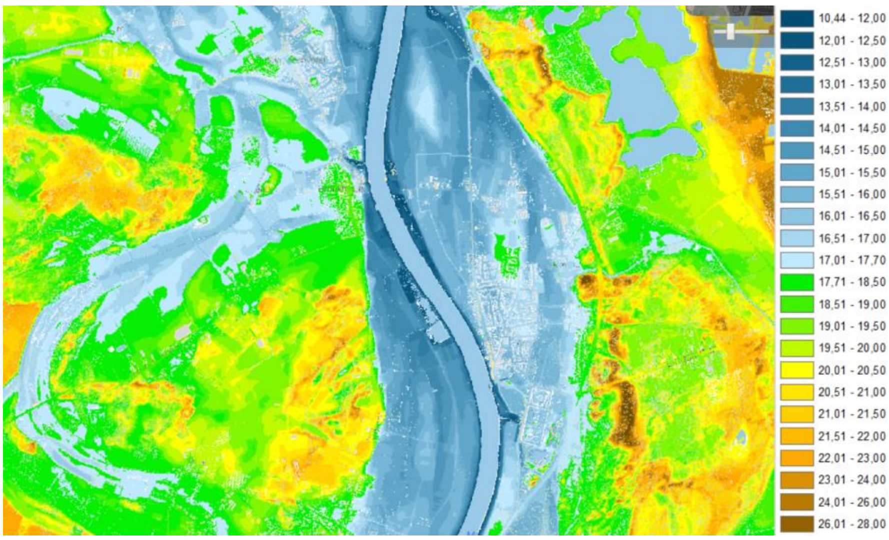

Figure 2-6: Bathtub Arcen (Source: AHN2 PDOK, Actuality: 2008-2012)

2.4. Current situation

2.4.1. Visualization

The 90’s floods called for additional emergency measures such as the demountable flood defences. As can be seen from the pictures below, this type of flood defence is almost invisible until high water levels are to come. Unfortunately, too many locations require this solution, which makes the amount of demountable flood defences unsafe. The locations of the demountable flood defences sometimes cross private gardens. At these locations a more aesthetic pleasing solution is required, and thus glass becomes a viable option for a permanent barrier.

Figure 2-7: The invisibility of the demountable flood defences [Source: https://www.bedandbreakfast.nl/bed-and-breakfast-nl/arcen/b-b-maaszicht/4832/]

Figure 2-8:Erecting the demountable flood defences [Source: Facebook page Waterschap Limburg]

2.4.2. Hydraulic boundary conditions

Water and wave levels

The water levels in the river Meuse can vary a few meters between high and low water. The measure location of Arcen has been dissolved since 1995. The information is retrieved by interpolation between the measurements of Well and Venlo and can differ slightly from reality.

Table 2-1: Indication water levels Well and Venlo

Water level	Height [NAP+m] Well	Height [NAP+m] Venlo
Low water level	<11.05	<11.05
Normal water level	11.05-12.60	11.05-14.60
Above normal water level	>12.60	>14.60
High water level	>14.30	>16.60
Extremely high water level	>1500	>17.90

In appendix O the Water levels, wave heights and wave periods and their yearly probability of occurrence are extracted [Hydra/pimplatform(2018)]:

Table 2-2: Yearly probability of occurrence of water levels, wave heights and wave periods

Yearly Pf	Water level without uncertainty addition [NAP+m]	Wave height [m]	Wave period [s]
1/10	15.869	0.546	2.278
1/30	16.368	0.604	2.354
1/100	16.845	0.661	2.433
1/300	17.208	0.712	2.499
1/1000	17.497	0.763	2.56
1/3000	17.695	0.809	2.613
1/10000	17.902	0.861	2.666
1/30000	18.092	0.909	2.712

2.4.3. Risk

In the VNK report, Arcen (dike-trajectory 65) is one of the dike-trajectories that were examined. The results of this report are published on the Rijkswaterstaat website. A brief explanation of the following risks is found in chapter 2. The following information is given in the Veiligheid Nederland in Kaart(VNK) report about the location Arcen:

Table 2-3: Summary VNK findings on Arcen

	Flood risks
Probability of flooding P_f per year	$1/100$
Economic risk per year	€1.9 million
Mean damage per flooding	€40 million
Risk of fatality per year	0.03
Mean amount fatalities per flooding	1

Societal risk

The FN-curve of the societal risk of Arcen shows the number of casualties given a water level with a certain exceedance probability.

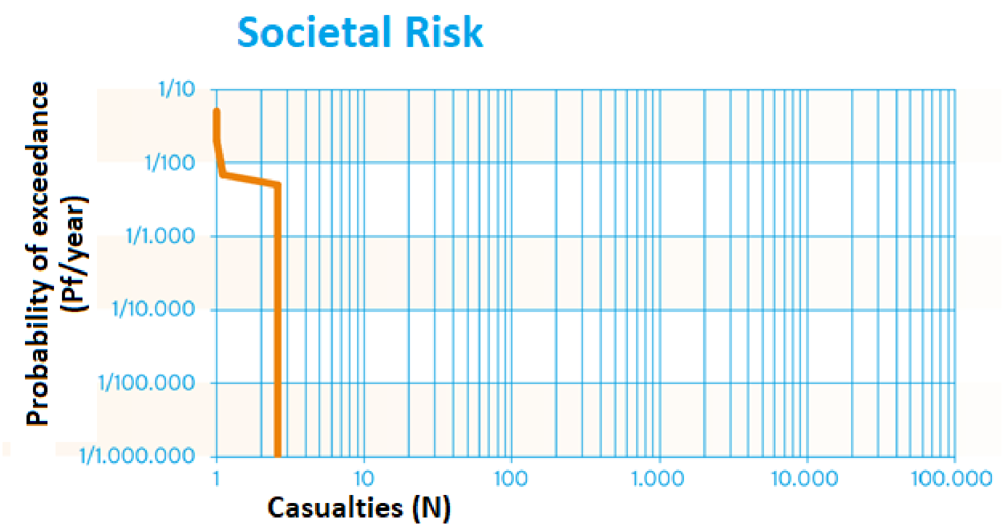

Figure 2-9: FN Curve Arcen [Rijkswaterstaat VNK Report(2015)]

Individual risk

The individual risk of flooding can be deduced from the figure below and is for location Arcen predominantly around the value of $1 \cdot 10^{-4}$. The probability of flooding in the i-viewer (a tool provided by Waterschap Limburg: www.pimplatform.nl) is $P_f = 1/420$ per dike section, which corresponds with the rounded value of $1/500$ according to the figure.

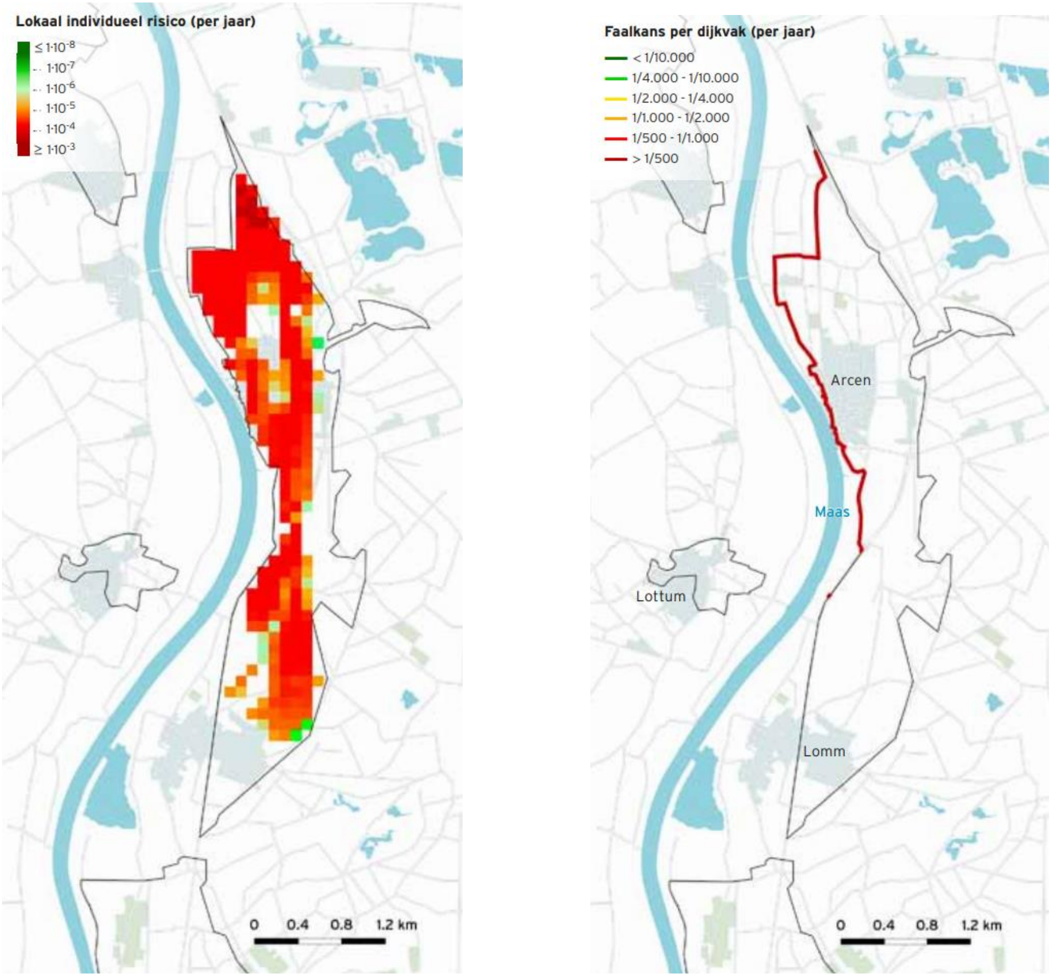

Figure 2-10: Individual risk and failure probability per dike section[Rijkswaterstaat VNK Report(2016)]

2.5. Reference projects

A few reference projects for glass flood walls, from the Netherlands and the UK, are presented in Appendix H. All the projects of glass flood walls in this report are still intact at the time of writing of this thesis. One case of severe overflow of the glass flood defence did happen at Keswick. In 2011, IBS Engineered Products Ltd installed a prestigious glass flood wall in the small town of Keswick. With an aluminum frame and EPDM seal. It is part of the Environment Agency's flood risk management scheme to protect the area from the river Greta. Supposedly the largest of its kind in terms of squared meters: 94 m². The length of this flood defence is about 120 meters. Source: [VolkerStevin (2012)]

Figure 2-11: The flood defence before and after overtopping. Photo credit: Stuart Holmes

During storm Desmond heavy rainfall flooded the river and the large amount of water overtopped the flood defence [itv News, 2015], leaving many people disappointed in the recently built, expensive glass wall. But this failure was only due to overtopping, and no structural failure occurred. While the water level was at its maximum, floating debris and trees crashed into the flood defence at high flow velocities, but leaving only superficial damage. The glass panels withstood the loads they were designed for and gave the town extra time to evacuate. The large impact the water had on the road behind the wall could be seen the day after the storm: a large part of the sidewalk washed away and left a deep scour hole. [BBC, 2016]

Figure 2-12: a tree washed over the flood wall. Photo credit: Dan Potts

Figure 2-13: a scour hole was left behind the structure after the flood. Photo credit: Rick Cooper

3. Material glass

3.1. Introduction

In this chapter the mechanical, physical, geometrical and chemical properties of glass are presented. A few structural applications and methods to create redundant glass structures are explained, after which the behavior and properties of laminated glass and interlayers is elaborated on in more detail.

3.2. Usage of glass

3.2.1. Brief history of glass

In the earliest ages of mankind, only natural formed glass was used, mostly as weapons. Obsidian; black volcanic glass was carved into sharp arrowheads and knife points for hunting and warfare. These objects are well known by anyone ever visiting a museum about prehistory.
The Roman writer Plinius the elder describes in his Magnum Opus “Historia Naturalis” a tale about the first men who made glass by accident. A Phoenician soda trader ship lands ashore to cook a meal on the beach. Having no stones to support their cooking pots, they placed soda blocks from their ship instead. While the temperature rose, the soda fused with the sand on the beach and became glass[Nijsse (2003)].

Glass used as windows started off as hand-made round plates, called crown glass. A ball of hot glass was blown, cut open, and while spinning it at high speed, a larger area formed due to the centrifugal force. Around the 1900’s a method for drawing glass was developed and made larger windows more available to the public. Larger structures with glass could be designed. The production of glass skyrocketed after the 1955’s invention of floating glass. This method slowly lets the molten glass continuously “flow” over a bath of molten tin. The gravity flattens the upper surface, while the lower surface is flattened by the tin. The end product is an infinitely long sheet of almost perfectly flat glass, which is cut in smaller sheets for better handling and transportation. With this method, the glass became much cheaper and used in facades and windows on a large scale. Nowadays 90% of the production of glass is floating glass.

3.2.2. State of the art

In recent years, improving technologies and knowledge about glass make that it is also used in load bearing structural applications. By laminating glass sheets or multiple components together a more redundant structural member can be obtained. Intensive research on the strength, lifetime, environmental impact of different types of interlayers and new methods to shape and use glass are still in development.

Figure 3-1:Chanel facade PC Hooftstraat, source [Yellowtrace(2017)]

3.2 Material properties

3.2.1 Chemical composition and structure

The majority of glass used in structures is soda lime silica glass (SLS), with some safety applications like fire protection glazing using borosilicate glass (BRS). The latter has a high resistance against temperature changes and acid but is also more expensive. In the scope of this research, we will only look at soda lime silica glass applications.

Table 3-1: Chemical composition of SLS glass according to [EN 572-1: 2004]

Material	Symbol	Mass [%]
Silica sand	SiO_2	69-74
Lime (Calcium Oxide)	CaO	5-14
Soda	Na_2O	10-16
Magnesia	MgO	0-6
Alumina	Al_2O_3	0-3
Others	-	0-5

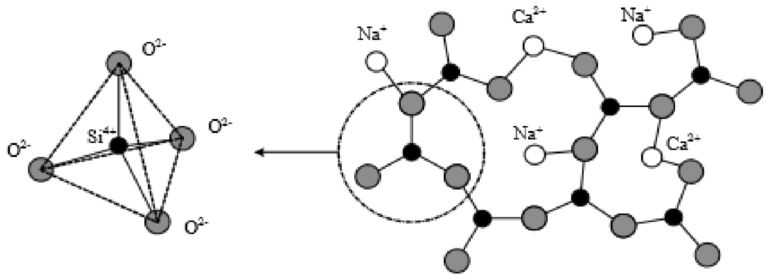

Figure 3-2: Chemical schematization of SLS glass from: Bos(2009)

Different compositions of the glass influence among others the melting temperature, viscosity and thermal expansion. Impurities are often added to lower the melting temperature and decrease the costs and energy usage of the manufacturing. [D. Vitalis(2017)]

3.2.2 Physical properties

Table 3-2: Physical properties SLS glass, source EN 1748-1-1:2004; EN 572-1:2004, with adaptations from Haldimann(2006)

Property	Dimension	SLS Glass
Density ρ	kg/m³	2500
Knoop hardness $HK_{0.1/20}$	Gpa	6
Young's modulus E	Mpa	70 000
Poission's ratio v	-	0.23 (for research applications)
Coef of thermal expansion α_T	$10^{-6}K^{-1}$	9
Specific thermal capacity c_p	$Jkg^{-1}K^{-1}$	720
Thermal conductivity λ	$Wm^{-1}K^{-1}$	1
Average refractive index within the visible spectrum n	-	1.52
Emissivity ε	-	0.837

3.2.3 Geometrical properties

It is advisable to use standard sizes of glass sheets for efficient design and lower costs. The standard maximum size is 3.21x6.0m, but this can be cut in any size if needed. Longer elements are possible, but not standard. The following nominal thicknesses are manufactured:

- 2, 3, 4, 5 and 6 mm with a tolerance of 0.2 mm
- 8, 10 and 12 mm with a tolerance of 0.3 mm
- 15 mm with a tolerance of 0.5 mm and
- 19 and 25 mm with a tolerance of 1.0 mm.

A thickness of 25 mm is possible, but costs go up. [European Commission(2014)]

3.3 Types of glass

Annealed glass (AG)

Almost all sheets of glass nowadays are produced with the floating method, which is explained earlier. If we are talking about these kind of glass sheets, there are three main types of flat glass that can be distinguished. If, after the floating process, the glass is not treated in any other way it is called annealed glass. After production, the bending strength smaller if one loads the tin-bath side in tension, but after usage this effect wears off.

Heat-strengthened glass (HSG)

The second type of glass can be retrieved by tempering the annealed glass. This process heats up the glass to 620-675 °C and then cools the glass with air. This causes the outside of the glass to harden, while the inside is still hot. Due to shrinking, tensile stresses form in the inside of the glass, while the outside is loaded in compression. This glass is called heat-strengthened or heat-toughened glass. [Haldimann, (2006)]

Fully tempered glass (FTG)

The third type is produced by the same process as for heat strengthened glass, but cooled down faster, producing fully tempered glass. This glass is also called safety glass as it is usually stronger, and shatters into small fragments when it breaks. In the Guidance of European Structural Design of Glass Components, it is referred to as Thermally Toughened Glass (TTG). [Sadlecek et al. (1995)] pointed out in his paper that the higher the internal prestressing, the higher the disintegrating force when such a panel is damaged, resulting in these small dice-like fragments. It is generally accepted that the abrupt disintegration of FTG is caused solely by the sudden loss of internal force equilibrium, although that is contradicted by F.P. Bos in his doctoral thesis. The small fragments are less sharp and serious human injury due to cutting is less likely. In comparison to the first two types of glass, it has little to no residual strength after failure. But its higher internal stresses make this the strongest type of glass. These internal stresses can, however, in combination with thermally expanding nickel-sulfide inclusions, suddenly cause the glass panel to break. This spontaneous failure can be prevented to a certain extend by testing the panels in heat-soak baths. [Haldimann, (2006)] Uneven tempering can also be the cause of this kind of failure. [Veer (2017)]

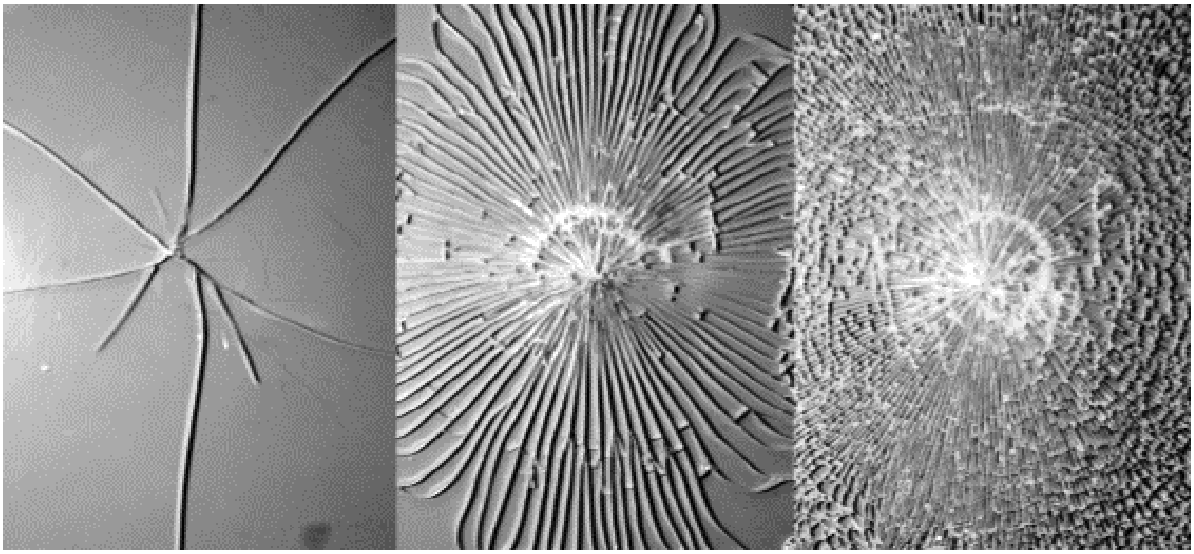

Figure 3-3: From left to right: Annealed glass; heat-strengthened glass; fully tempered glass (Haldimann, (2006))

Chemically tempered glass (CTG)

There is also the option to chemically strengthen the glass, in this case the prestressing only penetrates a few millimeters into the glass. It can be a very good solution when thin, durable glass is necessary; for example in telephone screens. The chemically strengthening process using ion-exchange can be used to make thinner, lighter, and even flexible glass, that has a high resistance against scratching.

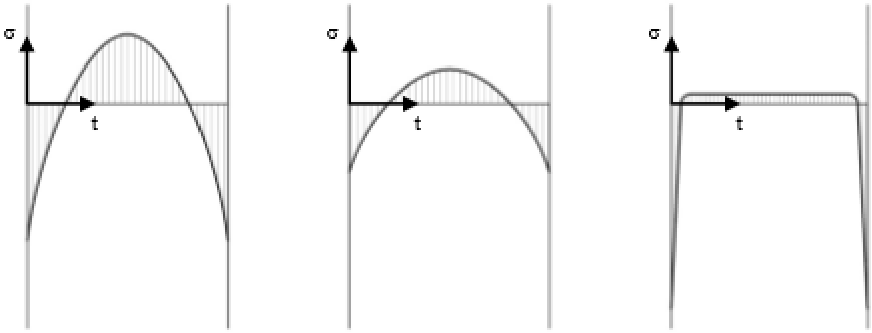

Figure 3-4: From left to right: stress distributions of respectively FTG, HSG and CTG [F.P. Bos(2009)]

3.4 Mechanical properties

3.4.1 Behavior

Brittleness

Unfortunately, glass is famous for of the most notorious failure behavior a material can have: brittle fracture. The material gives absolutely no failure warning, and when overloaded, cracks cause permanent damage. To avoid brittle failure, multiple methods are used to increase the safety of glass elements.

Viscosity

Glass flows and can be poured while it is hot. But when it cools down to room temperature it reaches a viscosity of 10^{20} Pa s, flow effects of a material with such a high viscosity would not be visible to the naked eye in millions of years. Due to these “low” flow effects, redistribution of forces does not happen and caused the brittle behavior. [Haldimann, (2006)]

Elastic modulus (Young’s modulus)

Being almost the opposite of ductile, it exhibits almost perfect linear elastic stress-strain behavior until failure, and no strain hardening takes place. The glass element fails when the stress at the tip of one flaw reaches its critical value. [Haldimann, (2006)]

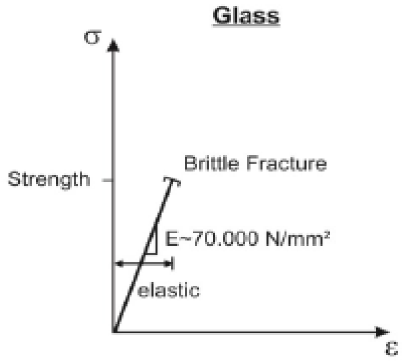

Figure 3-5: Stress-strain diagram glass [European commission (2014)]

3.4.2 Strength

Compression, tensile and bending strength

According to the European Commission (2014), the theoretical tensile strength of glass is extremely high; with values between $5000 - 8000\ MPa$ found in physical calculations. In practice, the bending strength of annealed glass lies between $30 - 80\ MPa$.
In the *Guidance for European Structural Design of Glass Components*(2014), the Dutch NEN, and the Italian CNR code it is advised to use the following nominal values for the surface stress:

Table 3-3: Bending strength of different types of glass

	Nominal bending strength f_k[N/mm²]
AG	45
HSG	70
FTG (or TTG)	120

Glass is strong in compression, but in practice the glass will experience tensile stresses near the introduction points of the load because of the Poisson effect, resulting in tensile failure long before the critical compressive stresses are reached. In the determination of glass strength, the time component of the loading has influence on the design strength. Unintentional eccentric loading can be fatal. Especially when slender glass elements are loaded axially, buckling failure is almost certain as the tensile stresses due to eccentricities or eccentric loading will become too large. [Haldimann (2006)]

3.4.3 Pitfalls

Besides the overall fragility of glass, a few more aspects need to be taken into consideration when using glass in structures.

Surface quality

The strength and in particular the tensile strength of glass depend heavily on the surface quality. Under compression surface flaws, or so-called Griffith flaws, are pushed together, but in tension these cracks will grow further as there is no mechanism in the glass to stop the crack growth. [Nijsse (2003)] Crack propagation usually happens at a certain speed called “the crack velocity”, which is very variable and hard to predict. In HSG, FTG and CTG small surface flaws will be pushed closed as the surface is prestressed by the tempering process. [Haldimann (2006)]

Stress corrosion

Although glass does not corrode like metals do, there is a deterioration phenomenon to glass that is called stress corrosion. A chemical reaction between water and glass causes a tensile crack to grow. By loading glass over a duration of time in combination with a humid environment, stress corrosion becomes an issue. [European commission (2014)] In combination with inability of glass to redistribute forces, these micro-cracks grow and the glass can fail because of this effect. Stress corrosion is mainly considered to happen when loading and moisture exposure happen at the same time.

Local connections

Due to the fact that there is minimal distribution of forces within the glass, peak stresses can cause the glass to fracture. Gradually introducing the forces and the use of ‘soft’ intermediate materials like neoprene, pure aluminum, nylon or EPDM between connections is important to avoid premature failure and maximizing the strength of the material [Presentation Christian Louter]. ‘Hard on hard’ material contact should be avoided at all times. Many glass panels have failed because the connections were not introduced properly.

Thermal expansion

The thermal expansion coefficients of steel are much larger than that of glass. To avoid unnecessary stresses, a soft interlayer like neoprene, pure aluminum, nylon or EPDM should be used to account for the thermal expansions. [D. Vitalis(2017)] Also, thermally expanding nickel-sulfide inclusions, can suddenly cause the glass panel to break. Heat-soak tests can significantly mitigate the risk of spontaneous failure due to the nickel-sulfide inclusions. [Haldimann, (2006)]

3.5 Structural safety

3.5.1 Four aspects in glass safety

In engineering safety is often expressed in terms of risk, which is usually defined as probability*consequence. If the failure probability of glass could be reduced, using it in structures would become cheaper and easier for contractors, while giving architects the freedom to use more glass in their designs. In *Safety Concepts in Structural Glass Engineering: Towards an Integrated Approach* F.P. Bos states there are four element safety properties: damage sensitivity(Σ), relative resistance®, redundancy(m), and fracture mode(A, B or C). A common way to increase the safety in structural glass is to create redundancy or alternative load paths.

3.5.2 Redundancy in glass

To compensate the unreliable characteristics of glass, structural glass needs to be redundant. This means that a single glass piece can never be used as structural element. To create redundancy in a glass element, it is usually glued or laminated with multiple components or with other materials. A few examples are given below.

Laminated glass

Sheets of glass can be laminated together. A laminated pane consists of a few glass sheets, laminated together by an interlayer, usually polyurethane foil (PVB foil) and sometimes a sacrificial outer layer. The latter can be on both sides of the laminated glass, depending on the impact risks on each side. This type of glass is also called safety glass, and is used in numerous applications like bulletproof glass, anti-burglary windows, car windshields, but also in structural applications like floors, walls and fins. [Delincé et al. (2008)] Laminated glass will be elaborated on more in the end of the chapter as it will be the main focus of this research.

Reinforced glass

Another method to increase the safety of glass is to reinforce it. There is many ongoing research on reinforced glass elements, with materials that can take up tensile forces. Reinforcing can be done with metals, but also more transparent materials like glass fiber and Kevlar. Reinforcing glass with glass fiber lets it keep its transparent feature, while working against the brittle failure behavior of glass. Bending tests on glass fiber reinforced glass beams showed promising post-breakage results. [Louter et al. (2010)]. Glass reinforcement makes use of the residual compression strength that is present after failure. Like reinforced concrete, the glass element has to crack first, before the reinforcements start to "work". After the cracking of the glass, people can see the element is overloaded and repair, replace or support the element in time.

Bundling

Other measures to give the structural member more redundancy is to increase the number of components. Laminating the glass is one example of bundling, but it does not have to stop with flat surfaces glued together; The bundled column is another example of an experimental redundant structural element; it consists of multiple glass rods, glued together in a bundle. If one of the rods fails, the forces are distributed over the other rods (if not overloaded), something that is not possible inside in one single glass element. Bundling can reduce the large safety factor that has to be used for structural glass elements. The bundled column concept is currently used in the 14 m spanning glass pedestrian bridge at the TU Delft Campus.

Usage of solid objects

The main reason larger solid glass objects are not very common is the same as why fully tempered glass sometimes spontaneously fails. When the inner part of the object is still hot, the outside is already cooling down and solidifying. The internal shrinkage pulls the outside skin in compression. Usually this is a positive feature, allowing the outside to take up more tensile stresses and more external force (as "Prince Rupert's drops" spectacularly show). But if the internal stresses become too large; the object shatters. To help settle the stresses and shrinkage in a better way, the cooling process has to be slowed down. For the glass bricks used in the glass facade of the Chanel store in the PC Hooftstraat (Figure 3-1:Chanel facade PC Hooftstraat, source [Yellowtrace(2017)]) the cooling process takes around 3 days. This makes the glass bricks a lot more expensive than their earthly counterparts. They are, however, a spectacular sight and structurally safe due to the many alternative load paths.

3.6 Laminated glass

3.6.1 Intro

Introduced already in the previous paragraph, laminated glass panels are combined sheets of AG, HSG, or FTG. They are basically sandwich structures and have different mechanical behavior than solid objects. The interlayers are used to "glue" the panels together, and are usually thermoplastics with visco-elastic behavior. Temperature, loading duration and intensity influences the mechanical properties of the interlayers. It is an effective way to obtain larger thicknesses, safety and redundancy in a glass panel. When shattered, but not completely punctured, the pieces of the glass layers will form a mesh and together with the laminating material can have significant residual strength. This can be an important feature for hydraulic structures if after an impact, the water retaining function can be preserved.

3.6.2 Manufacturing

Laminated glass for outside usage usually comes with a sacrificial outer layer. This outer layer protects the inner layers against impact, scratching and vandalism. The sacrificial layer is not to be taken into account when calculating the strength or effective thickness of the glass. Laminating with PVB or SG are both usually done by autoclaving; first, glass panes are washed and foils are positioned, then the panel is heated up to 70°C and rolled to press out air bubbles and blisters, then the assembly is put under pressure(0.8 MPa) and heated up to 140°C.

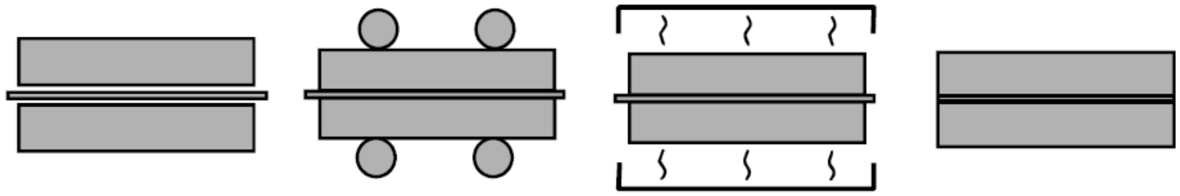

Figure 3-6: The process of autoclaving [European Commission Erasmus Mundus, Ungureanu, V., & Jordão, S. (2014)]

3.6.3 Structural interlayers

PVB

The most used interlayer nowadays is PVB, or polyvinyl butyral. Like all thermoplastics, its properties depend heavily on the temperature of the environment. The most commonly used sheets have a thickness of 0.38 mm, while 2-4 sheets are used between glass layers. [European commission(2014)]. For larger projects, the sheets of 0.38 mm can be manufactured up to a width of 3.22 and a length of 1500 m(on a roll).

SGP

Alternatives for PVB are on the rise, and since its introduction in 1998, the stiffer SentryGlass© interlayers by DuPont de Nemours showed promising results for structural glass applications [Louter et al. (2010)]. Sentryglass is an Ionoplast interlayer. Its main advantages over common PVB is the remaining stiffness after failure. According to the manufacturer Dupont and licensee Kuraray SentryGlass is up to five times stronger and up to 100 times stiffer than other types of interlayers and was initially designed for hurricane proof glazing. It can be used to create hurricane-, impact-, and blast resistant glass. It keeps its clarity for many years and is less susceptible to yellowing and less vulnerable to moisture exposure than other interlayers. [Kuraray(n.d.); (Dupont(n.d.)]
SGP can be manufactured in flat sheets of thicknesses 0.89, 1.52, 2.29 and 3.05, with a width of 1.52 and on a roll of 0.89 mm with widths of 1.21, 1.52, and 1.83 meter, up to a length of 200 meter. [European Commission Erasmus Mundus, Ungureanu, V., & Jordão, S. (2014)]

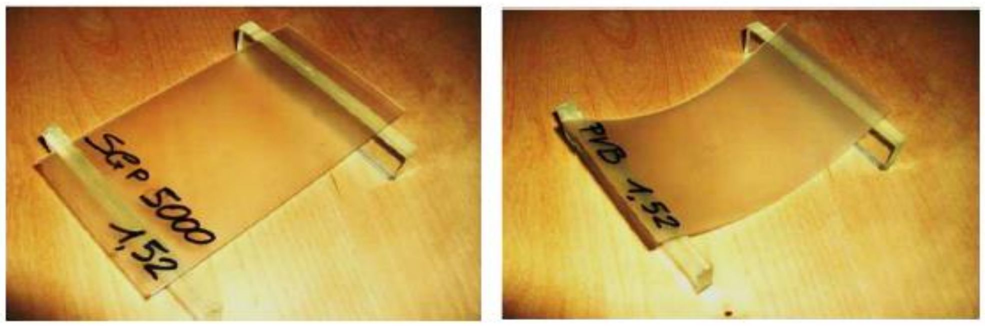

Figure 3-7: left: Sentryglass foil; right: PVB foil.[European Commission Erasmus Mundus, Ungureanu, V., & Jordão, S. (2014)]

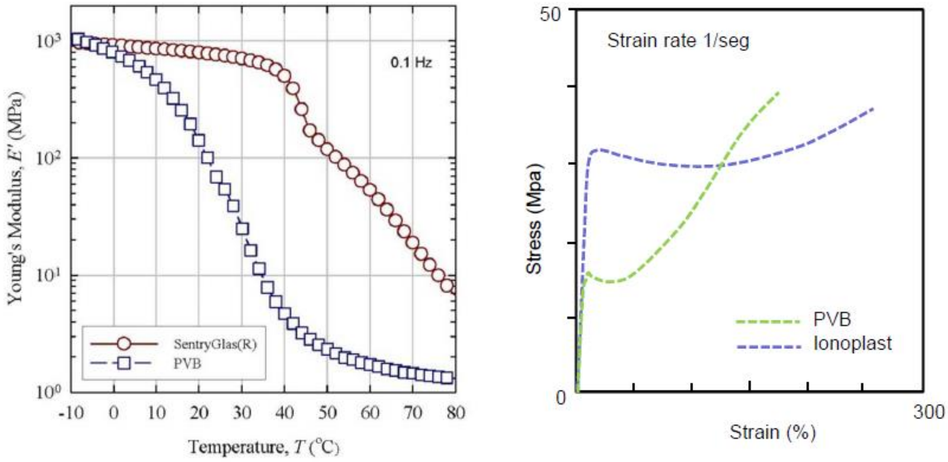

Figure 3-8: Youngs modulus of PVB and SG under different temperatures, [European Commission Erasmus Mundus, Ungureanu, V., & Jordão, S. (2014)]

SGP VS. PVB

SGP and PVB are both thermoplastics. This means they can be reshaped and get rid of permanent plastic deformation when heated above a certain temperature. Unfortunately, this usually also means strength loss at higher temperatures. Because the glass transition temperature differences between the two materials the stress-strain behavior between SGP and PVB deviates significantly. With a higher elastic modulus, tensile strength and shear modulus (not at all temperatures), SGP exhibits superior behavior over PVB as a reinforcing material, but also after breakage. The high stiffness and tensile force of the SGP foils transfer compressive forces that the broken glass can still withstand. This means there is a much higher remaining bending capacity than for conventional PVB. [Bos(2009)]

Other laminates

Other possible interlayers are EVA (EthylVinylAcetate), TPU (Thermoplastic PolyUrethane) and cast resins. Because their properties are not as strong and durable as PVB and SGP (or unknown), they are often not allowed in safety glass. [Bos (2009)] These interlayers are therefore not considered in the scope of this project.

Table 3-4: Mechanical properties (indicative) of PVB and SGP, source: European Commission Erasmus Mundus, Ungureanu, V., & Jordão, S. (2014)

Property	**Dimension**	**PVB**	**SGP**
Density ρ	[Kg/m³]	1070	950
Shear Modulus G	[Gpa]	0-4	-
Poisson's ratio v	[-]	≈0.50	≈0.50
Thermal expansion coef. $\boldsymbol{\alpha_T}$	$[K^{-1}]$	$80 \cdot 10^{-6}$	-
Tensile strength $\boldsymbol{f_t}$	[Mpa]	>20	34.5
Elongation at failure $\boldsymbol{\varepsilon_t}$	[%]	>250-300	400
Elastic Modulus E	[N/mm²]	18	300
Glass transition temp.$\boldsymbol{T_g}$	[°C]	~10-15	~55-60

The interlayer properties presented in Table 3-4: Mechanical properties (indicative) of PVB and SGP, source: European Commission Erasmus Mundus, Ungureanu, V., & Jordão, S. (2014) depend heavily on temperature and duration of loading. Manufacturers like Kuraray and DuPont de Nemours offer different interlayers for different purposes, some relevant applications for laminated safety glass are proposed at the end of the chapter.

Interlayer thickness

According to X. Zhang et al. the thickness of the interlayer contributes significantly to the penetration resistance. Besides improved penetration resistance, also the overall thickness will increase. It will however be decreasing the shear resistance between panels, resulting in a lower coupling factor. Because penetration resistance due to an impact is important in keeping the water retaining function and the thickness of the interlayer also contributes positively to the post-breakage strength and stiffness, it is preferred to use a significant thickness of the interlayer.

3.6.4 Structural behavior of laminated glass

The behavior of laminated glass depends on the stage of cracking, because it consists of two, or multiple glass panes. At first, it behaves as a sandwich structure, with the layers interacting with each other while being intact. But after cracking, this interacting changes and different mechanisms occur.

Pre-cracking phase

The pre-breakage behavior of laminated glass in bending can be described as the lower and upper limit of respectively; two separate panels sliding over each other; or one monolithic glass panel of the same thickness. Properties of the interlayers and therefore the pre- and post-breakage behavior of a glass panel depend heavily on the temperature, but a glass panel used outside will normally not be subjected to such extreme temperatures.
The cooperative strength between interlayer SGP and glass layer can be almost 90% compared to a solid glass panel in short term loads. [Arcadis (2017)]

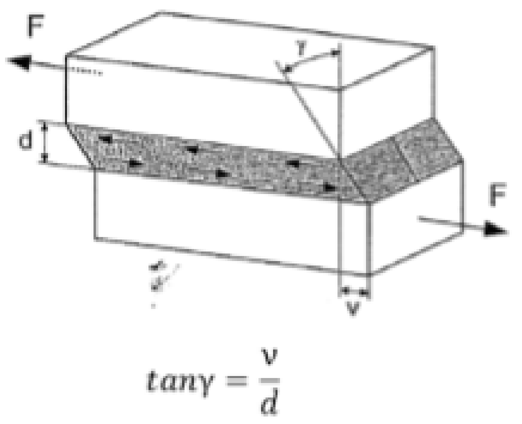

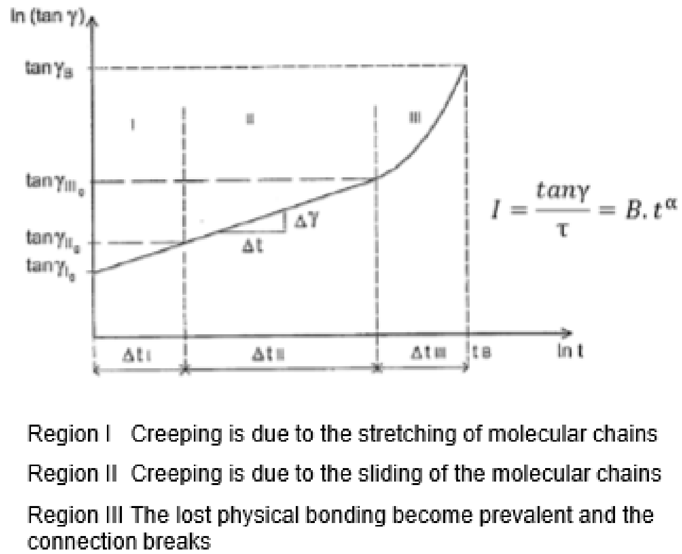

Figure 3-9: Interaction between layers under short term loading [European Commission Erasmus Mundus, Ungureanu, V., & Jordão, S. (2014)]

Figure 3-10:Behavior of the interlayer under long term loading [European Commission Erasmus Mundus, Ungureanu, V., & Jordão, S. (2014)]

Post-cracking phase

Laminated glass has residual strength after breakage. This is due to the interlayer keeping the pieces together, uses the compression capacity of the broken pieces, and transferring tensile stresses through the interlayer. A. Kott and T. Vogel found a remaining capacity of 25% of the ultimate failure load in a PVB-laminated double layer of annealed glass. [Bos (2009)]

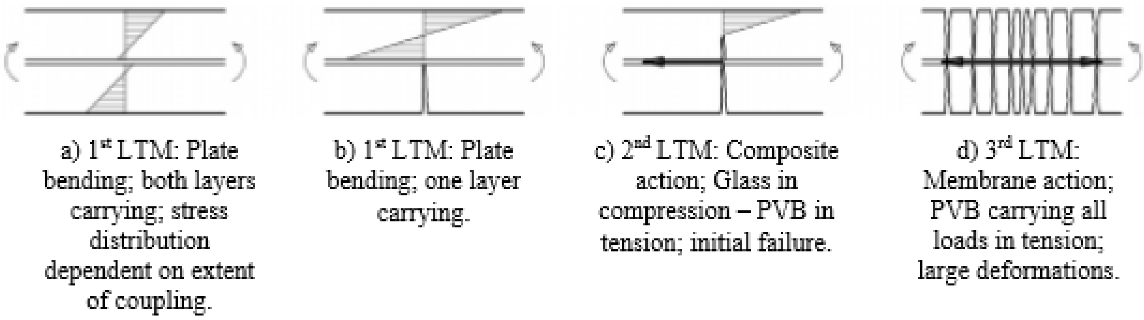

Figure 3-11:Different stages of Load Transfer Mechanisms (LTM) [Bos (2009)]

Residual strength

As is described in the post-cracking phase, not all structural capacity is lost in laminated panels when cracking occurs. The parameters having the most influence on the residual capacity of a laminated panel are: [Delincé et al. (2008)][European Commission(2014)]:

- Composition and strength of the glass section
- The mechanical properties of the interlayer
- The adhesion strength between glass and interlayer
- The size of the glass shards(which depend on glass type and failure scenario)
- Supports and bearing type

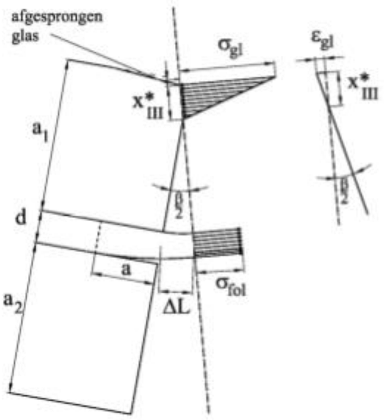

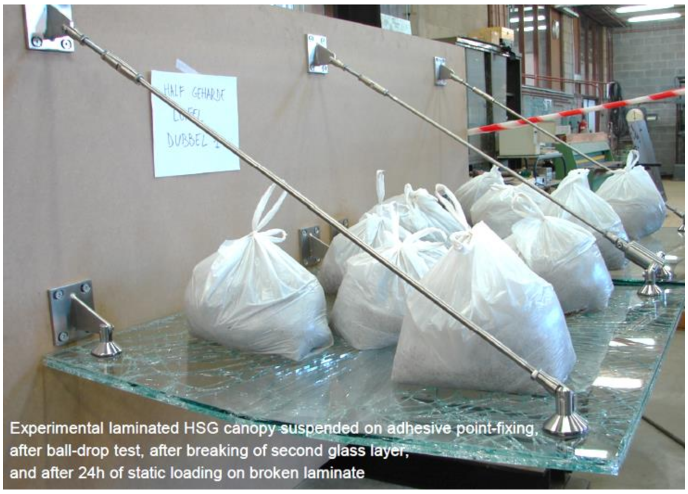

Figure 3-12: Force equilibrium of broken panel, source: [Delincé et al. (2008)]

Figure 3-13:residual strength test with static load [TU Delft presentation Structural Glass]

3.6.5 Structural safety of laminated glass

The safety of a glass element however stays a subject of debate, and in most cases glass elements still have to be experimentally tested before they can be used for structural applications. On the Eurocodes website (checked 28-09-2017) it is stated that a glass Eurocode is still under construction. There is, however, a report available called "*Guidance for European Structural Design of Glass Components*", which was released in 2014. It is a draft for the first version of the Eurocodes for glass, and gives advice on the manufacturing, calculations and handling of glass products. More on the Eurocodes and Dutch NEN norms in the next chapter "Norms, Codes, and standards".

4. Norms, codes and standards

4.1 Introduction

In the following paragraphs the relevant norms, codes and standards that apply on the glass flood defence are presented and briefly summarized. As the glass flood defence is a multidisciplinary structure, a few of these standards overlap and the most conservative code or method must be followed.

4.2 Flood safety

4.2.1 Intro

In the Netherlands a hydraulic structure or flood defence has to comply with multiple codes; the codes for building structures, and codes for flood safety. For the structure, the Eurocodes and the NEN norms need to be followed in the design and execution process. These are based on a semi probabilistic approach with safety factors and design checks. But in flood safety a different set of rules apply, which has been updated as of 2017. From then on, flood safety will be done on a more risk based approach, using probabilistic modelling to determine the safety of a flood defence.

4.2.2 Water act

The Dutch water act came into effect from 22 December 2009, and is the result of a merge out of eight laws. The water act manages surface- and groundwater, and improves cohesion of water management and spatial planning in the Netherlands. It strives to decrease administrative burdens and minimize the amount of laws. It is expected to be remain enforced until the environmental act replaces it in 2021. [Helpdesk water (n.d.)]

4.2.3 Flood risk (WBI2017)

Per 1 January 2017 the new flood safety standards of the WBI2017(former WTI2017) went in practice, replacing the former “Maximum water level methodology” from 1958 and the “Maximum hydraulic load methodology” from 1996. The Dutch Flood Protection Program(DFPP), which is translated from the Dutch name: Hoogwater Beschermings Programma(HWBP), pursues a fully probabilistic approach. The vision, approach and instruments on the “how to” are stated in the WBI2017(abbreviation of the Dutch “het Wettelijk Beoordelings Instrumentarium”). In 9, the probabilistic approach of the WBI2017 is explained.

4.2.4 LKR (Stowa)

STOWA is the abbreviation for Stichting Toegepast Onderzoek Waterbeheer (Foundation of Applied Research for Water Management). It gathers, stores, spreads and assesses new and old knowledge and provides information and guidance for waterboards and other relevant organizations such as the LKR (Leidraad Waterkerende Kunstwerken).

4.3 Structural Safety

4.3.1 Bouwbesluit (Housing act)

Het bouwbesluit (Dutch building regulations/Building Act) are a set of construction rules with minimum standards for buildings as housing, offices, shopping stores, hospitals etc to guarantee (fire) safety and living comfort. It references to the NEN- and Eurocodes for calculation methods. From 2012 it also includes demolition- and usage regulations.

4.3.2 Eurocode

The Eurocodes are the product of the wish for a standardization in European building codes, the Building Act. This now consists of 10 reports on the material properties, design, and construction of different building aspects, with the 11th in the making for structural glass. Sometimes National

Annexes are included to provide methods and loads that are applicable to different countries, for example higher snow loads for Austria than for the Netherlands.

Table 4-1: Summary of Eurocodes

	Code	Subject
1	1990-x-x	Basis of structural design
2	1991-x-x	Actions on structures
3	1992-x-x	Concrete
4	1993-x-x	Steel
5	1994-x-x	Steel-Concrete
6	1995-x-x	Wood
7	1996-x-x	Masonry
8	1997-x-x	Geotechnical structures
9	1998-x-x	Earthquake resistance
10	1999-x-x	Aluminum
11	2020-x-x	Glass

In the writing of this report, there is no Eurocode on **structural** glass(only glazing) available yet. But in the meantime the *Guidance for European Structural Design on Glass Components*(2014) can be used for advised methodology and calculation methods. Eurocodes on the determination of the loads and the surrounding structure still hold. In the case of a glass flood defence in the Netherlands, the loads on the structure also need to be determined following the probabilistic WBI2017. There are however, codes on glazing structures and laminated safety glass. For the heavy-duty glazing, the panels are usually tested by means of a so called “ball drop test”, where the glass has to resist the impact of a ball with certain mass, dropped from a certain height, see 10.1.2. A summary of related codes is given in paragraph 4.3.4 .

4.3.3 NEN

The Eurocodes are valid throughout Europe, but on a national level, the National Standards hold. The Netherlands have the NEN Norms, which overlap with Eurocodes for the most part. NEN 2608 is the code used for the determination of glass dimensions and types of normal glazing. While the NEN2608 is meant for normal glazing, it can be used for structural designs in glass íf the engineer is careful; the regulations are young, and as a result still in continuous development.
NEN norms on laminated glass are: NEN-EN-ISO 12543-1, NEN-EN-ISO 12543-2 and NEN-EN-ISO 12543-3.

4.3.4 European glazing codes

The typical contribution of glass in a building is as glazing. To keep out the cold and let in the light, glass has been the main material to be used for windows, with improving characteristics every year.

Table 4-2: Summary of European Norms on glass, from presentation "Structural Glass"

Subject	Norm/code
Laminated safety glass	EN ISO 12543
Safety – Impact resistance	EN 12600
Safety in case of fire	Resistance to fire: EN 13501-2 Reaction to fire: EN 13505-1 External fire behavior: prEN 13505-1 (CR 187)
Security	Burglar Resistant: EN 356 Bullet Resistant: EN 1063 (1999) Explosion: EN 13541

Mechanical strength	General basis of design- Design for uniformly distributed loads and triangular loads: prEN 13474-1:2005 Design for line and concentrated loads: prEN 13474-3: June 2008 Determination of interlayer shear transfer coefficient: prEN vwxyz_N255E: June 2008 Effective thickness concept: prEN N249a:2008
Sound attenuation	N 12758-1 (2008-Rev7) “MIM” test method: ISO DIS 16940
Light and Energy Transmission, Thermal Insulation	EN 410: : Determination of luminous and solar characteristics EN 673: Determination of the U-value
Assembly rules	EN 12488
Evaluation of conformity	EN 14449

4.4 Other

4.4.1 Vaarrichtlijn 2017 (Waterway Guidelines)

The Dutch waterway guidelines are relevant in this case as this give an indication of extend in which shipping on the river is prohibited during high and low water levels. For longer time-span high water levels such as on the river Meuse, the governing high water is set to the water level that is exceeded once for 24 hours in the last ten years. For recreational shipping, the governing water level is one that is exceeded 2% of the time in the summertime(1 April – 1 October).

4.4.2 Innovations

In the WBI2017 tools and models are presented to assess the reliability of dikes and dunes, but unfortunately no formal software tools exist for the strength assessment of hydraulic structures [Implementing risk based flood defence standards (2016)] Glass structures are therefore not a part of the WBI2017 set of normative rules for Dutch flood safety. They can be marked as an innovative flood defence. For new techniques An instruction manual on how to deal with these kind of innovations can be found on the WBI website and is called: “Handreiking Innovaties Waterkeringen (Groene versie)”. Innovating is encouraged as ‘there is no progress without innovation’.

4.4.3 WABO (Wet Algemene Bepalingen Omgevingsrecht)

The WABO (roughly translated: Law general regulation of environmental rights) provides the environmental permit. This environmental permit is one integrated permit for building, housing, monuments, space, nature and environment. [www.infomil.nl]

Part II: Calculations

5. Methodology

5.1 Introduction

In this chapter the methods used for the glass calculations, the FEM model and the probability of failure are briefly explained. A more extensive explanation of the calculations and input for the FEM model and failure probability analysis can be found in respectively Appendix E, H and I.

5.2 Glass calculations

The theory used for glass strength calculations is not given on a European level yet; therefore there is no universal method on how to deal with glass structures and certainly not with glass flood defences in the Netherlands. J.P. Bos made a clear overview in his doctoral thesis of the methods that are used in different countries or continents for calculating the strength or maximum allowed load of the glass. This was mostly based on the methods Haldimann compared in his own doctoral thesis. Most of these methods overlap or come down to the same; the allowable stress method, this method involves the intensity and duration of the load. This method of the allowable stress is also used in the NEN, and a few other countries in Europe.

The choice is made to compare the methods from the Dutch, German and the Italian codes for glass. The Dutch code NEN 2608 is important to give prove of theoretical strength in the country where the flood defences will be placed. The German code is reviewed because a few suppliers of glass flood walls(IBS, Thyssen Krupp) are based in Germany and use the German standard for glass, TRLV-2006-08. And last but not least, the Italian code is investigated as it uses the most recent research[European commission(2014)].

Calculations on the glass are done with a few variations of the allowable stress method to determine the most suitable approach. This will also give insight in to the differences between countries. First, hand calculations are done to determine the effective thickness of the glass panel in two different load situations.

Calculations are done for a $2x2\ m$ panel with $3 \times 19\ mm$ FTG and $2.19\ mm$ Sentryglass foils(see Chapter 8: “Design”). There are two main load cases:

“Fundamental loading” combination 1

The typical load situation for the glass panels will be that of high water levels in the river Maas. The normative load combination is that of static water pressure and wave loading. The load is a distributed load over the whole area of the glass and its duration is one month.

“Incidental” combination 2

A large object floats on the river during the flood, this can be a loose boat, a tree or floating debris. It collides into the structure with a certain speed and angle. The load is a concentrated load over an area of $100\ mm$ by $100\ mm$ in the middle of the plate, with an impact duration of one second.

These are done while complying with the Eurocode for basic structural design in terms of loading conditions for Ultimate Limit State(with safety factors) and Serviceability Limit state (no safety factors). All three codes provide a method to determine the allowable stress and a method to determine the effective thickness of a laminated panel.

The allowable stress and effective thickness methods from the NEN are used for the FEM model, as these are governing at the project location.

5.3 FEM

A finite element model is made with SCIA Engineer, using the results from the glass calculations based on the NEN2608 and the design of the IBS structure. As the FEM model uses displacements to calculate the stress distribution, the stresses from the model based on the displacement- effective thickness are conservative.
The kinetic energy of the impact must be translated into deformation and spring energy in both the structure and impact object. This is done by modelling the structure in SCIA, and assume the impact object is infinitely stiff to be on the conservative side($k_b = \infty$).

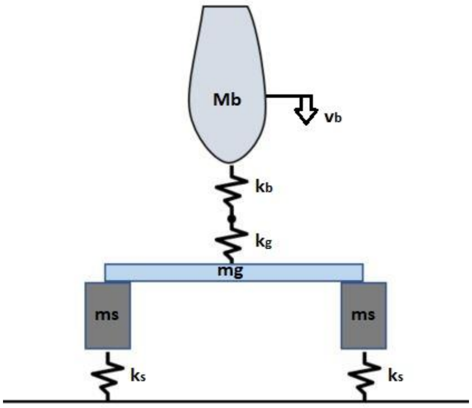

Figure 5-1: Simple spring model

To use the FEM model to approach the maximum impact capacity a few assumptions are made:

- The impact energy is absorbed only by the structure
- The effective thickness in the model is based on displacement-effective thickness
- The impact load is determined based on a static equilibrium
- The impact area is $100\ mm$ by $100\ mm$
- Kirchoff's theory for slender plates is used
- The effective glass thickness at the time of impact is $53\ mm$ according to the NEN 2608
- The allowable stress for an impact is $92.1\ N/mm^2$
- The side posts are assumed to be fully clamped into the foundation

All input for the FEM model can be found in Appendix I.

5.4 Probability of failure

A failure probability analysis is done based on the methods provided in the WBI2017 report "Toetsspoorrapport Sterkte en stabiliteit puntconstructie" which translates to: "Assessment report Strength and Stability". The failure tree in Figure 5-2 is translated and adapted to the situation of a permanent retaining wall without the possibility of opening and closing the structure.

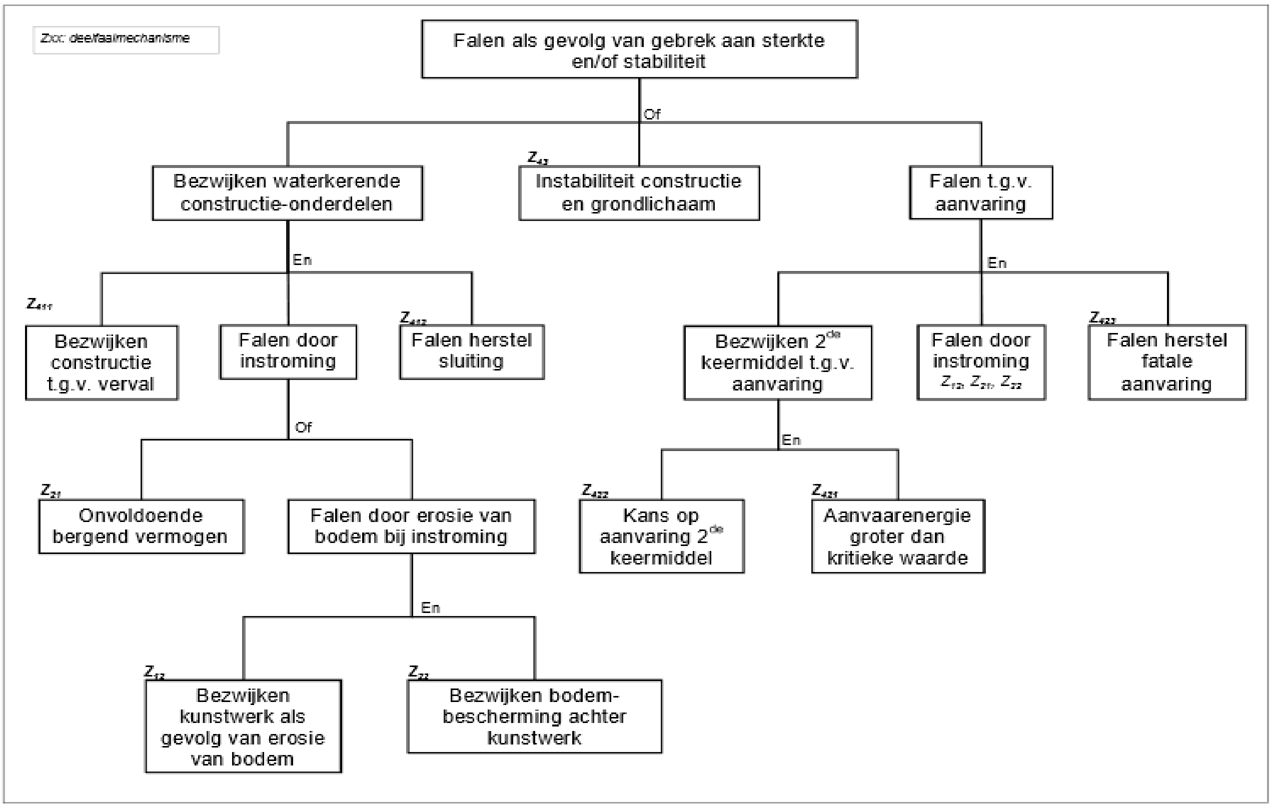

Figure 5-2: Failure probability tree "Structural failure" [WBI 2017. (2015)]

Every sub-mechanism, has its own Z-function. Some of the Z-functions depend on structural details and must be defined by the user, and some are defined in the report and can be used directly if the parameters are inserted. All is done with probabilistic distributions of the parameters, where some of the distributions are already known or obtained from data, and others are estimated using the assessment report. An explanation on the Z-functions, the parameters and results are presented in the Appendixes I and J.

5.5 Experiment

To assess the strength of an impact on glass in a certain situation, it is advised to do tests with the true size of the glass structure as the accuracy of existing models is not sufficient. Scaling of the tests is not possible due to the large effect flaws and cracks, scratches, the surface- and edge quality have on the strength of the glass.
The experiments are done in the Stevin II laboratory, with the design explained in chapter 6. The set-up of the experiment is simple: A tree is used as a pendulum, which is dropped on to the glass from increasing heights until glass breakage. From the height and impact speeds, an approximation of the kinetic energy can be derived.
After the impact tests, a static load will be put on the glass, with resembling moments caused by high water levels on the panel.

6. Design

6.1 Introduction

The design that is being assessed will consist of three main parts: The glass panel, the Aluminum frame and the side supports. The frame and side posts are provided by IBS Technics GMBH, and is made of extruded Aluminum; AW6005 for the posts and AW6082 for the framework. This chapter describes the design in detail. The glass calculations, FEM model and probability of failure are based on this design.

Figure 6-1: The installed IBS glass flood defence system [IBS]

6.2 Glass panel

With the design restrictions of the frame and the requirements the design leads to the following dimensions:

6.2.1 Dimensions

The dimensions of the glass panel are given, and the choices are explained in table 6.1.

Table 6-1: Dimensions of the glass panel

Dimension	Amount	Explanation
Height	1909 mm	The height of the structure is determined for every location and the usual heights for the glass flood wall are between 0.8 and 1.2 meter height. In this case the height of the flood wall is chosen to be 2000 mm high. The glass panel needs to have a height of 1909 mm to gain a total flood height of 2000 mm.
Width	1850 mm	The width of a conventual glass flood defence by IBS ranges from 1.75 to 2.5 meters. To decrease glass thickness and post dimensions the center to center distance is chosen to be around 2000 mm, this results in a panel width of 1850 mm.
Thickness glass	3 x 19 mm	The IBS structure accepts a range of total panel thickness between 30-70 mm. Therefore logical configurations of glass panes are: 3x19 mm, 4x15 mm, 5x12 mm. 3x19 mm is the cheapest option (less layers to laminate) and a larger thickness of individual glass panes has a positive effect on the stiffness and strength of the panel.
Thickness interlayer	2 x 2.28 mm	Recommended by manufacturer.
Total thickness	61.56 mm	The total thickness adds up to 61.56 mm, therefore meets the thickness requirements of the IBS frame.

6.2.2 Glass types

The glass type that will be used is Fully Tempered Glass (FTG) for a few reasons:

- The thickness restriction called for a slightly stronger glass to be able to withstand significant impact if the total thicknesses of around 60 mm were the outcome from the possible glass configurations.
- The manufacturer does not produce HSG in the thickness of 19 mm.
- It is a more conventional type of glass and is more likely to be used in the flood defences

6.2.3 Interlayer

The interlayer is chosen to be Sentryglass foil due to its superior properties over PVB foil, and it is likely that this will be used in the glass flood defences. The foils in the test sample has a thickness of 2.28 mm, as recommended by the glass supplier.

6.3 Frame structure

6.3.1 Material

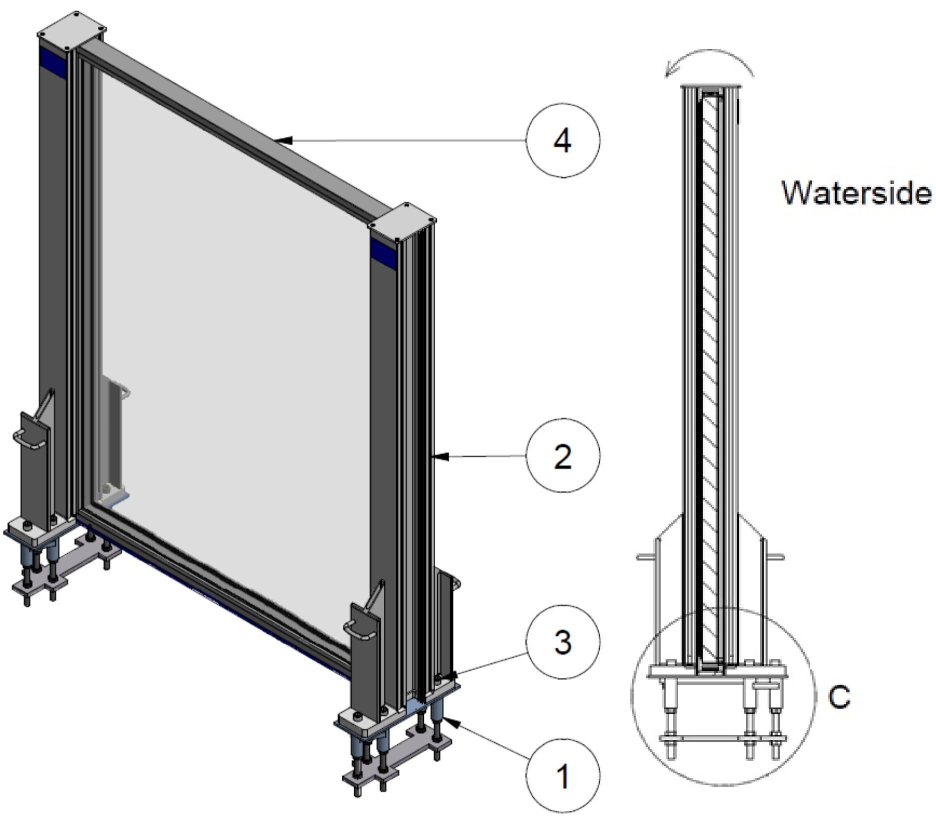

Figure 6-2: The glass flood defence [IBS]

Figure 6-3: Side view glass flood defence [IBS]

In Table 6-2 the members of the IBS structure are presented. It consists of three main parts; the frame, the anchor plates and the side posts, where the side posts are secured into the foundation by connecting the anchor plate with the side posts using the round head screws. The frame, containing the glass panel, is placed between the space of the I-profiles of the posts, creating a hinged bearing.

Table 6-2: Specification detailing frame structure

Number	Name	Specifics	Material
1	Anchor plate	AP100K-T05	Stainless steel: 1.4301 (grade 304)
2	Aluminum post	MS100K-G	AW6005
3	Round head screws	DIN 912 M24 x 110	Stainless steel: 8.8 (800 N/mm²)
4	Frame	H1926xV2500	AW6082

6.3.2 Detailing

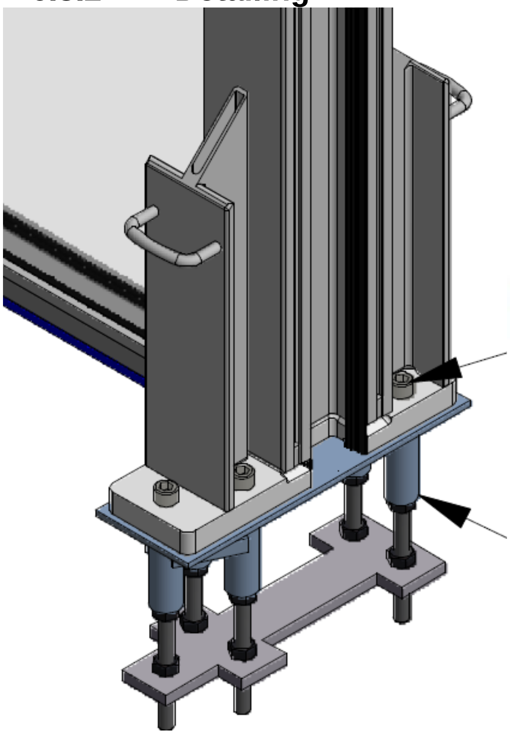

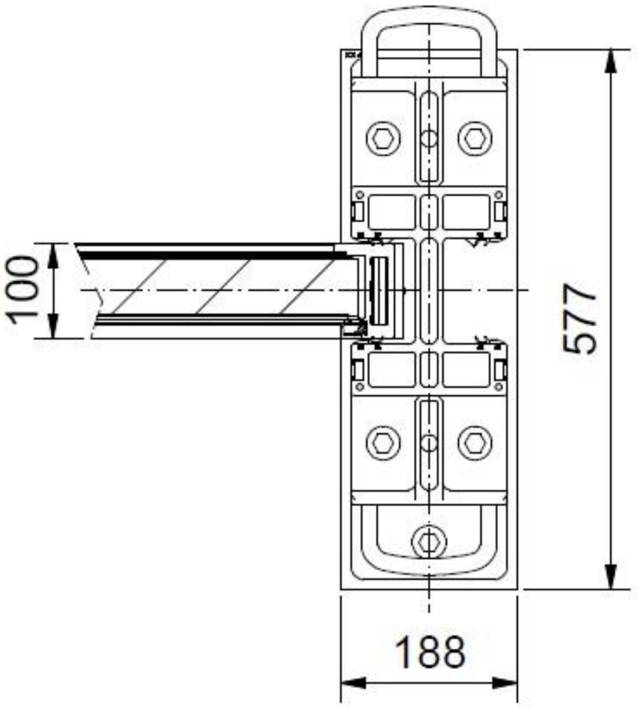

Figure 6-4: Anchoring of side support in 3D

Figure 6-5: Anchoring of side support top view

For more details on the supporting structure the reader is referred to the supplier IBS Technics GMBH or the author.

6.3.3 Proven strength

In the flood that hit the small town of Keswick, large pieces of floating debris like trees were found near and even on top of the glass floodwall, see Figure 6-6. This suggests that the system is robust enough to withstand these kinds of loads.

Figure 6-6: a tree washed over the glass flood defence during a flood [http://www.flood-defenses.com/flood-protection/catastrophe-protection/glas-walls]

7. Glass calculations

7.1. Intro

In this chapter the behavior and calculation methods for a laminated glass panel are explained, after which the effective thickness and limit stress are determined with the methods from the NEN 2608:2014 for two main load cases. For more information on the other methods the reader is referred to Appendix E.

7.2. Laminated glass with three plies

7.2.1. Two load cases

Calculations are done for a $2 \times 2\ m$ panel with $3 \times 19\ mm$ FTG and $2.19\ mm$ Sentryglass foils (see Chapter 6, Design”). There are two main load cases:

“Fundamental loading” combination 1

The typical load situation for the glass panels will be that of high water levels in the river Maas. The normative load combination is that of static water pressure and wave loading. The load is a distributed load over the whole area of the glass and its duration is one month.

“Incidental” combination 2

A large object floats on the river during the flood, this can be a loose boat, a tree or floating debris. It collides into the structure with a certain speed and angle. The load is a concentrated load over an area of $100\ mm$ by $100\ mm$ in the middle of the plate, with an impact duration of one second.

7.2.2. Layered and monolithic behavior

Laminated glass is a composite material, meaning that it consists of multiple materials that work together. In this case, it is fully tempered glass and the interlayer material Sentryglass. Because it is a panel made from different layers of varying material it can be called a sandwich panel. To approach the stiffness and behavior of a sandwich panel, or a laminated glass panel, it is common to transform the panel into a fictitious panel of only one material, using coupling factors between the governing material and effective thicknesses of that material. There is an upper- and lower boundary in the coupling factor:

0 : No coupling, glass plates slide over each other (low stiffness)

1 : Fully coupled, the panel behaves as if it was monolithic (high stiffness)

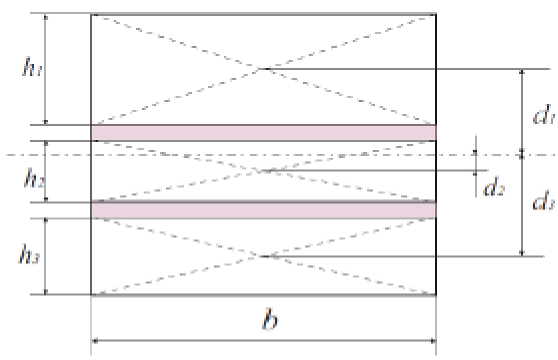

Figure 7-1:The layered panel [CNR-DT 210/2013(2013)]

7.2.3. Equivalent/effective thickness method according to the NEN 2608

For calculations with layered glass, the glass panel can be assigned an equivalent thickness. This equivalent thickness $t_{gg;u}$ can be used for displacement and stress checks, and can be determined by the following formulas:

$$t_{gg;u} = MIN(t_{gg;i;u})$$

$$t_{gg;i;u} = \sqrt{\frac{(1-\omega_\sigma)\cdot\sum_{j=1}^{n} t_{pl;j}^3 + \omega_\sigma \cdot \left(\sum_{j=1}^{n} t_{pl;j}\right)^3}{t_{pl;i} + 2\cdot\omega_\sigma\cdot t_{m;i}}}$$

In ULS, and:

$$t_{gg;ser} = \sqrt[3]{(1-\omega_W)\cdot\sum_{i=1}^{n} t_{pl;i}^3 + \omega_W \cdot \left(\sum_{i=1}^{n} t_{pl;i}\right)^3}$$

In SLS, where:

$t_{gg;u}$ = the equivalent thickness of layered glass in ultimate limit state(ULS) , in mm
$t_{gg;i;u}$ = the design thickness of a glass plate in a layered glass panel in ULS, in mm
$t_{gg;ser}$ = the equivalent thickness of layered glass in serviceability limit state(SLS) , in mm
ω_σ = coupling factor of the interlayer in stress $0 \le \omega_\sigma \le 1$
ω_W = coupling factor of the interlayer in bending $0 \le \omega_w \le 1$
$t_{pl;j,i}$ = the glass plate thickness of glass panel i or j in mm
n = the number of glass plates in the panel
$t_{m;i}$ = the distance from the middle of the glass plate i, and the middle of the glass panel, without taking the thickness of the interlayer into account.

7.2.4. The design value of plate thickness of glass pane i

The design thickness of the glass panel needs to be determined by the following formula:

$$t_{pl;i} = t_{pl} = t_{nom} - \Delta_t$$

Where:

$t_{pl;i}$ = the glass plate thickness of glass panel i, in mm
t_{pl} = the glass thickness of a single glass sheet, in mm
t_{nom} = the nominal thickness of a single glass sheet, in mm
Δ_t = the maximum allowable deviation, in mm

For a glass plate with thickness of 19 mm, Δ_t is 1.0 mm.

$$t_{pl;i} = t_{pl} = 19 - 1 = 18$$

7.2.5. Coupling factors

The effective thickness method uses coupling factors determine the cooperation between the plates. The coupling factors are determined by the following formulas:

$$\omega_\sigma = \frac{1}{1+\frac{\beta}{L_\sigma}}; \qquad \omega_W = \frac{1}{1+\frac{\beta}{L_W}}; \qquad \beta = \frac{1}{2}\cdot\frac{\pi^2}{L_A^2}\cdot\frac{E_g}{1-v_g^2}\cdot\frac{X}{G_{tl}}$$

Where:

L_W = form factor of bending dependent on the shape and supporting conditions of the plate
L_σ = form factor of stress dependent on the shape and supporting conditions of the plate
L_A = form factor dependent on the length and width of the plate
E_g = elasticity modulus of glass (=70 000 N/mm²)
v_g = Poisson number of glass (= 0.23)
X = maximum value of equations below
G_{tl} = shear modulus of the interlayer (also determined at the EET method)

X is the maximum value of: $X_1 = \sum_{i=1}^{n-1}(t_{pl;i} + t_{V;i})$ or $X_2 = \sum_{i=2}^{n}(t_{pl;i} + t_{V;i-1})$

In which
$t_{V;i-i}$ = The thickness of the interlayer, in mm

Since we use glass plies and interlayers of identical thickness, X_1 and X_2 are the same value.

7.2.6. Support situation

The configuration of the glass used in the IBS structure is $3x19\ mm$ FTG with Sentryglass foils, and the FEM model of the IBS structure showed that the glass is mainly supported by the side supports and is therefore 2-sided supported. For a 2-sided supported panel the following equations can be used:

$L_A^2 = l_0^2$; $L_w = 1.002 \cdot \left(\frac{2 \cdot l_0}{z}\right)^{-0.04354}$; $L_\sigma = 1.832 \cdot \left(\frac{2 \cdot l_0}{z}\right)^{-0.60906}$; $z = \frac{B_1 + H_1}{2}$

Where
L_A = the form factor dependent on the length and width of the panel
l_0 = the length of the unsupported side of the panel in mm
L_w = the form factor for bending dependent on the form and support situation of the panel
L_σ = the form factor for tension dependent on the form and support situation of the panel
B_1 = the length of the loading area parallel to side B in mm
H_1 = the length of the loading area parallel to side H in mm

For both load situations:
$\frac{B}{H} = \frac{2}{2} = 1$; $k_w = 1.002$; $k_\sigma = 1.832$;

For load situation 1:
B_1=2m; H_1=2m

For load situation 2:
B_1=0.1m; H_1=0.1m

7.2.7. Shear modulus

The shear modulus of the interlayer is assumed to be 114 MPa(see Appendix E for explanation).

7.2.8. Results effective thickness

Load situation 1:

$$t_{gg;i;u} = \sqrt{\frac{(1-\omega_\sigma) \cdot \sum_{j=1}^{n} t_{pl;j}^3 + \omega_\sigma \cdot \left(\sum_{j=1}^{n} t_{pl;j}\right)^3}{t_{pl;i} + 2 \cdot \omega_\sigma \cdot t_{m;i}}} = 53.69\ mm$$

$$t_{gg;ser} = \sqrt[3]{(1-\omega_W) \cdot \sum_{i=1}^{n} t_{pl;i}^3 + \omega_W \cdot \left(\sum_{i=1}^{n} t_{pl;i}\right)^3} = 50.01\ mm$$

Load situation 2:

$$t_{gg;i;u} = \sqrt{\frac{(1-\omega_\sigma) \cdot \sum_{j=1}^{n} t_{pl;j}^3 + \omega_\sigma \cdot \left(\sum_{j=1}^{n} t_{pl;j}\right)^3}{t_{pl;i} + 2 \cdot \omega_\sigma \cdot t_{m;i}}} = 52.56\ mm$$

$$t_{gg;ser} = \sqrt[3]{(1-\omega_W) \cdot \sum_{i=1}^{n} t_{pl;i}^3 + \omega_W \cdot \left(\sum_{i=1}^{n} t_{pl;i}\right)^3} = 53.10\ mm$$

See Appendix P, Maple files for the input and calculation. As can be seen from the results, the effective thicknesses of the two load cases are of the same order of magnitude and are similar.

7.2.9. Allowable stress method according to the NEN 2608

The design value for the bending strength is calculated with the following formula:

$$f_{mt;u;d} = \frac{k_a \cdot k_e \cdot k_{mod} \cdot k_{sp} \cdot f_{g;k}}{\gamma_{m;A}} + \frac{k_e \cdot k_z \cdot (f_{b;k} - k_{sp} \cdot f_{g;k})}{\gamma_{m;V}}$$

Table 7-1: Explanation of symbols "Design value of strength" according to the NEN

Symbol	Meaning	Formula or explanation	Value
$f_{mt;u;d}$	Design value of the bending strength	See above	TBD
k_e	The factor for the edge quality	Heat strengthened Loaded out of plane	1.0
k_a	The factor for the surface effect	$1.664 \cdot A^{-(\frac{1}{25})}$ for concentrated load or non-linear calculation of bending stress 1.0 for distributed loading	TBD
A	The loading surface	$H1 \times B1$ of the load in mm^2	TBD
k_{mod}	The modification factor	$(\frac{5}{t})^{\frac{1}{c}}$	TBD
c	Corrosion constant	For middle zone For edge zone	18 16
t	Time duration of loading	Dependent on situation	TBD
k_{sp}	The factor for surface structure	Float glass	1.0
$f_{g;k}$	The characteristic bending strength of glass	Float glass	45 [N/mm²]
$f_{b;k}$	The characteristic bending strength of prestressed glass	Fully Tempered Glass	120 [N/mm²]
$\gamma_{m;A}$	The material factor of glass	Other load than isochoric pressure or wind pressure	1.8
$\gamma_{m;V}$	The material factor of prestressed glass	Fixed	1.2
k_z	Factor for the loading zone	It is assumed the load will not occur in the corners of the glass, and these will partly be protected	1.0

7.2.10. Results allowable stress

The following value for the design bending strength for a short duration load is calculated:

$$t = 3;\; A = 100 \cdot 100 = 100000;\; k_a = 1.664 \cdot 100000^{-\left(\frac{1}{25}\right)} = 1.151\,;\; k_{mod} = (\frac{5}{t})^{\frac{1}{c}} = 1.0288$$

$$f_{mt;u;d} = \frac{1.151 \cdot 1.0 \cdot 1.0288 \cdot 1.0 \cdot 45}{1.8} + \frac{1.0 \cdot 1.0 \cdot (120 - 1.0 \cdot 45)}{1.2} = 92.1\ MPa$$

The following value for the design bending strength for a long duration load is calculated:

$$t = 60 \cdot 60 \cdot 24 \cdot 30 = 2592000$$
$$A = 0.1 \cdot 0.1 = 0.01$$
$$k_a = 1.0$$

$$k_{mod} = (\frac{5}{t})^{\frac{1}{c}} = 0.481$$

$$f_{mt;u;d} = \frac{1.0 \cdot 1.0 \cdot 0.481 \cdot 1.0 \cdot 45}{1.8} + \frac{1.0 \cdot 1.0 \cdot (120 - 1.0 \cdot 45)}{1.2} = 74.53\ MPa$$

Table 7-2: Allowable stress per load situation

Load situation	Duration and load area	
1	Duration: 3-5 sec Load surface area: 0.1x0.1m	92.10 [MPa]
2	Duration: 1 week Load surface area: 2x2m	74.53 [MPa]

7.2.11. Summary of methods

The Italian code has similar methods for the effective thickness and limit stress. The German code assumes no coupling between the separate glass panes and also has a predefined limit stress. A summary of the values of the three different codes is given in Table 7-3: Summary of results different methods below

Table 7-3: Summary of results different methods

Code		Stress effective thickness $[mm]$	Displacement effective thickness $[mm]$	Stress limit $[N \backslash mm^2]$
NEN	Concentrated short load:	53.00	53.96	92.10
	Distributed long load	53.03	52.45	74.53
CNR	Concentrated load:	57.1	57.1	71.40
	Distributed load	57.4	57.4	62.58
TRLV		25.96	25.96	50

It can easily be seen that the German glass code is the most conservative in all methods, which results in more expensive glazing, as more material is needed to withstand the same loads. The Dutch NEN code is used in continuing calculations and the FEM model, as it is the governing code in the Netherlands.

7.3. Effective thickness of two plies

The effective thickness in the case that one of the plies breaks is also calculated. If two plies break the effective thickness is assumed to be the design thickness(see 7.2.4) of one ply: 18 mm. In reality the residual strength depends on which side the glass is broken, as broken layers exhibit residual capacity in compression. This influence is neglected.

Load situation 1:

$$t_{gg;i;u} = \sqrt{\frac{(1-\omega_\sigma) \cdot \sum_{j=1}^{n} t_{pl;j}^3 + \omega_\sigma \cdot (\sum_{j=1}^{n} t_{pl;j})^3}{t_{pl;i} + 2 \cdot \omega_\sigma \cdot t_{m;i}}} = 35.88\ mm$$

$$t_{gg;ser} = \sqrt[3]{(1-\omega_W)\cdot\sum_{i=1}^{n} t_{pl;i}^3 + \omega_W\cdot(\sum_{i=1}^{n} t_{pl;i})^3} = 35.72\ mm$$

Load situation 2:

$$t_{gg;i;u} = \sqrt{\frac{(1-\omega_\sigma)\cdot\sum_{j=1}^{n} t_{pl;j}^3 + \omega_\sigma\cdot(\sum_{j=1}^{n} t_{pl;j})^3}{t_{pl;i} + 2\cdot\omega_\sigma\cdot t_{m;i}}} = 35.45\ mm$$

$$t_{gg;ser} = \sqrt[3]{(1-\omega_W)\cdot\sum_{i=1}^{n} t_{pl;i}^3 + \omega_W\cdot(\sum_{i=1}^{n} t_{pl;i})^3} = 35.74\ mm$$

See Appendix Maple filesK: Maple files for the input and calculation.

8. Finite Element Analysis

8.1. Intro

A FEM model is made with SCIA Engineer, input for the model is retrieved from the glass calculations and properties of the structure are extracted from the IBS design presented in chapter 6. An extensive explanation of all input is given in Appendix I.

For the limit stress, effective thickness and other material properties, the following NEN codes are used in the FEM model:

Table 8-1: Used standards

Material	
Glass	NEN-2608
Aluminum	NEN-EN 1999-1-1+A1:2011

8.2. Load case 1: Water pressure

In Appendix F the maximum allowed stress in the ULS of the glass is determined for a long duration distributed load according to the Dutch NEN:

$$74.53\ MPa$$

The stress-effective thickness for this load case according to 7.2.8:

$$t_{gg;ser} = \sqrt[3]{(1-\omega_W)\cdot\sum_{i=1}^{n} t_{pl;i}^3 + \omega_W\cdot\left(\sum_{i=1}^{n} t_{pl;i}\right)^3} = 50.01$$

Using the stress-effective thickness to calculate the stresses in the FEM model is conservative. In reality, the stresses will be lower by a factor of $\left(\frac{t_{gg;ser}}{t_{gg;i;u}}\right)^2$. Since in this case the stress- and displacement effective thicknesses are close to each other due to the strong interlayer, the true stresses are slightly smaller.

With a water pressure up to the structure of 2 meters and a safety factor of 1.5, the pressure at the bottom is $30\ kN/m^2$. since the maximum stresses are significantly less than the allowable stress in the glass, it is concluded that the glass is sufficiently strong to withstand water pressure.

8.2.1. 3D principal stress σ_1 with $t_{eff} = 50.01$

SLS

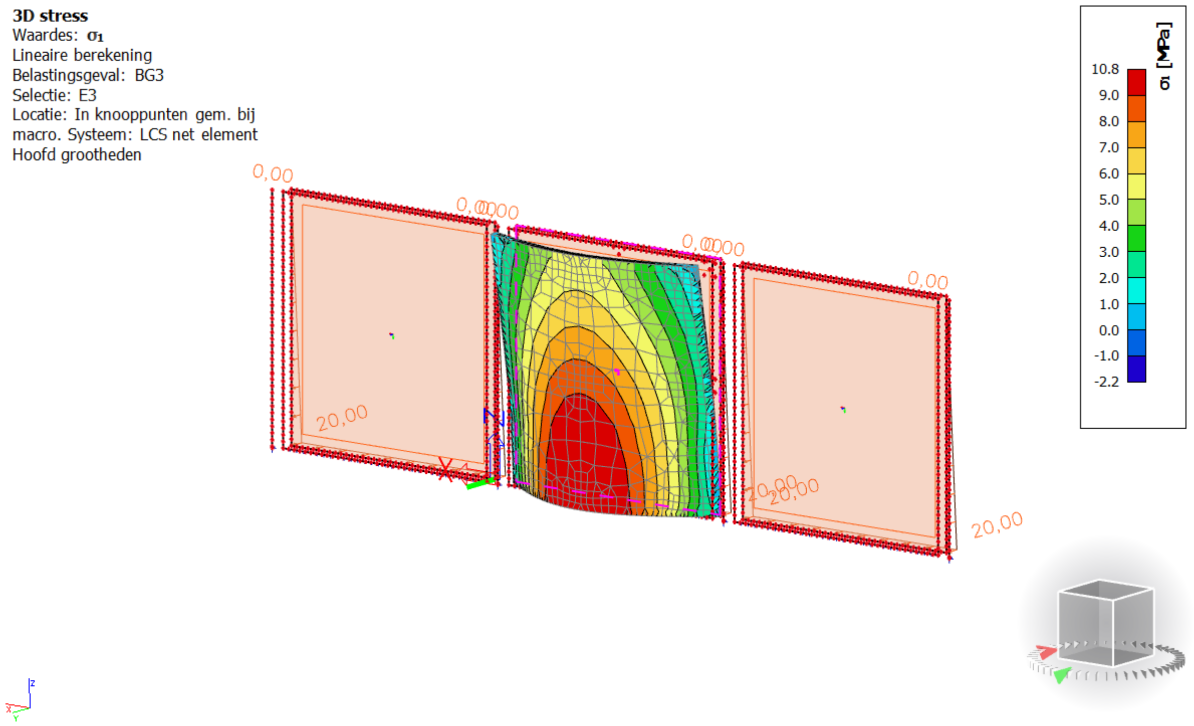

Figure 8-1: 3D principal stress σ_1 with t_eff=50.01 for the water pressure in SLS

Maximum tensile stress is $10.8\ N/mm^2 < 74.53\ N/mm^2$

ULS

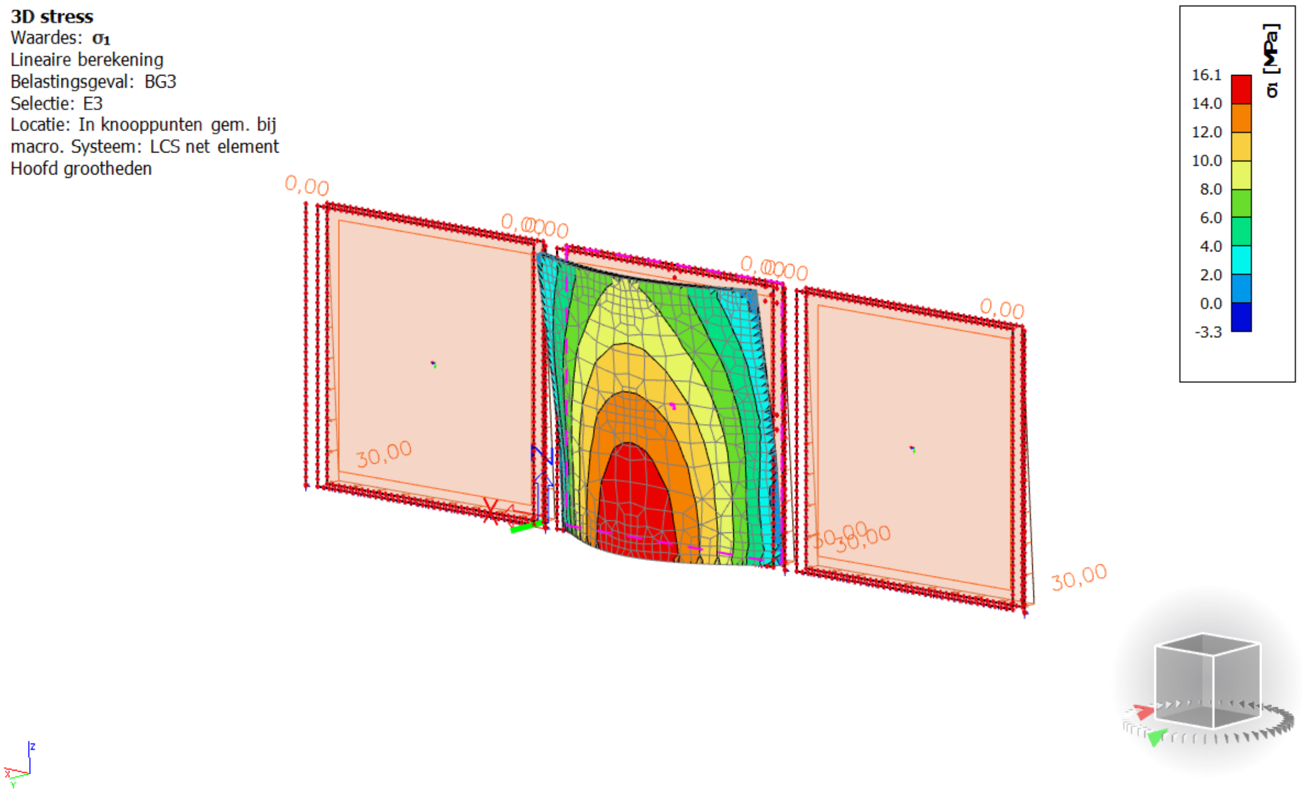

Figure 8-2: 3D principal stress σ_1 with t_eff=50.01 for the water pressure in ULS

Maximum tensile stress is $16.1\ N/mm^2 < 74.53\ N/mm^2$

8.2.2. 3D principal stress σ_2 with $t_{eff} = 50.01$

SLS

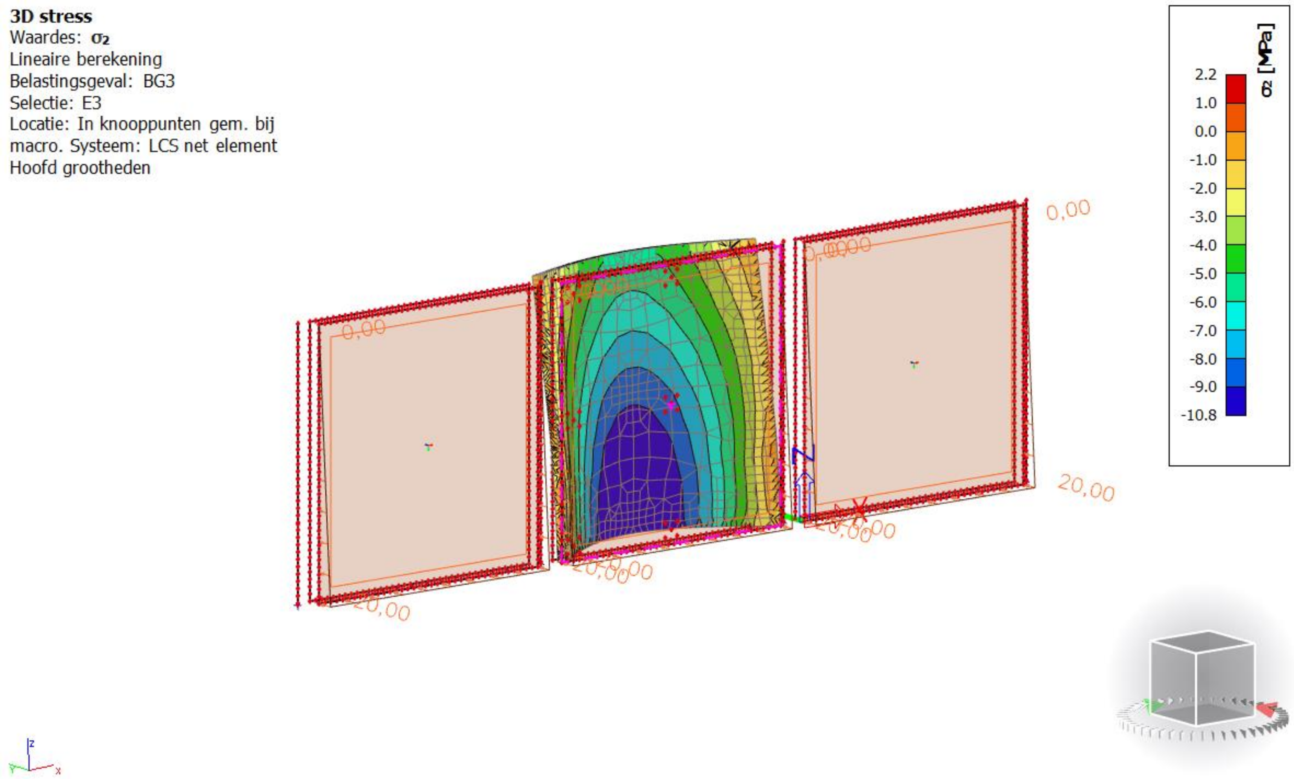

Figure 8-3: 3D principal stress σ_2 with t_eff=50.01 for the water pressure in SLS

Maximum tensile stress is $2.2\ N/mm^2 < 74.53\ N/mm^2$

ULS

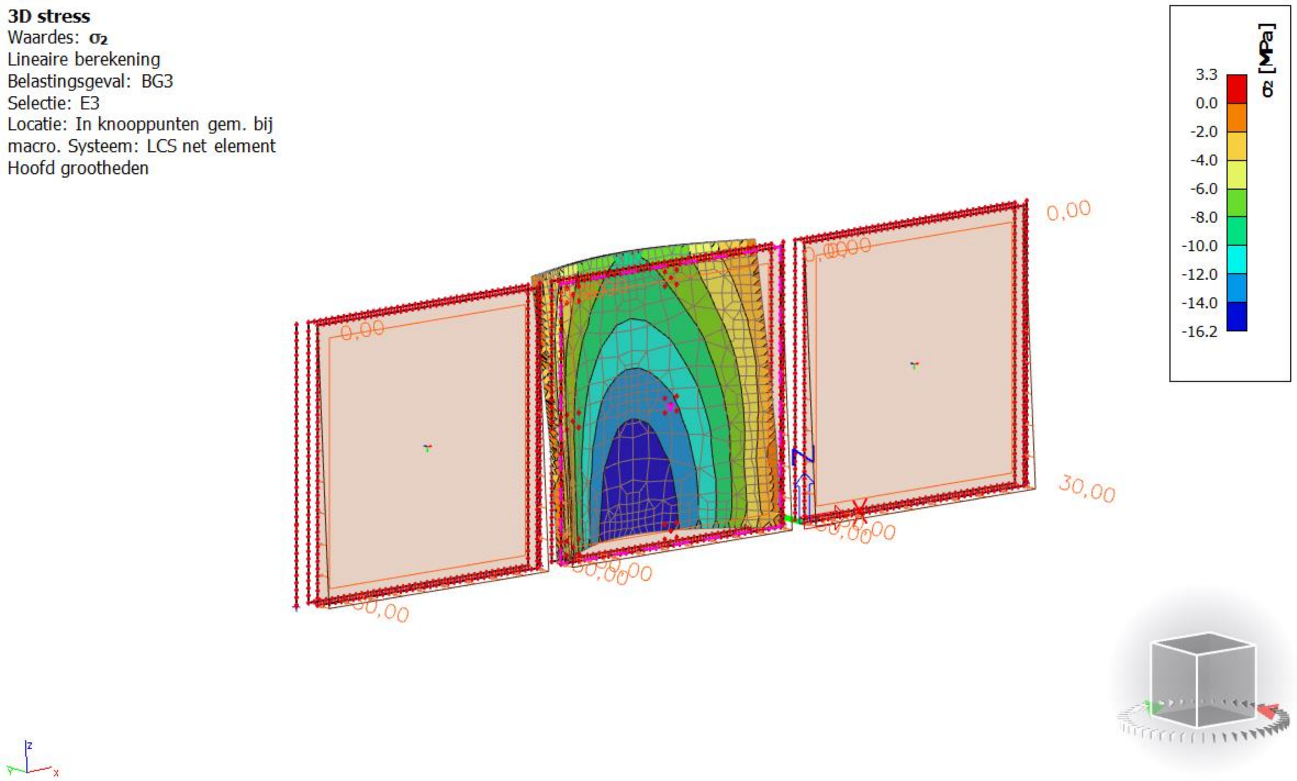

Figure 8-4: 3D principal stress σ_2 with t_eff=50.01 for the water pressure in ULS

Maximum tensile stress is $3.3\ N/mm^2 < 74.53\ N/mm^2$

8.2.3. 3D displacement u_{max}

SLS

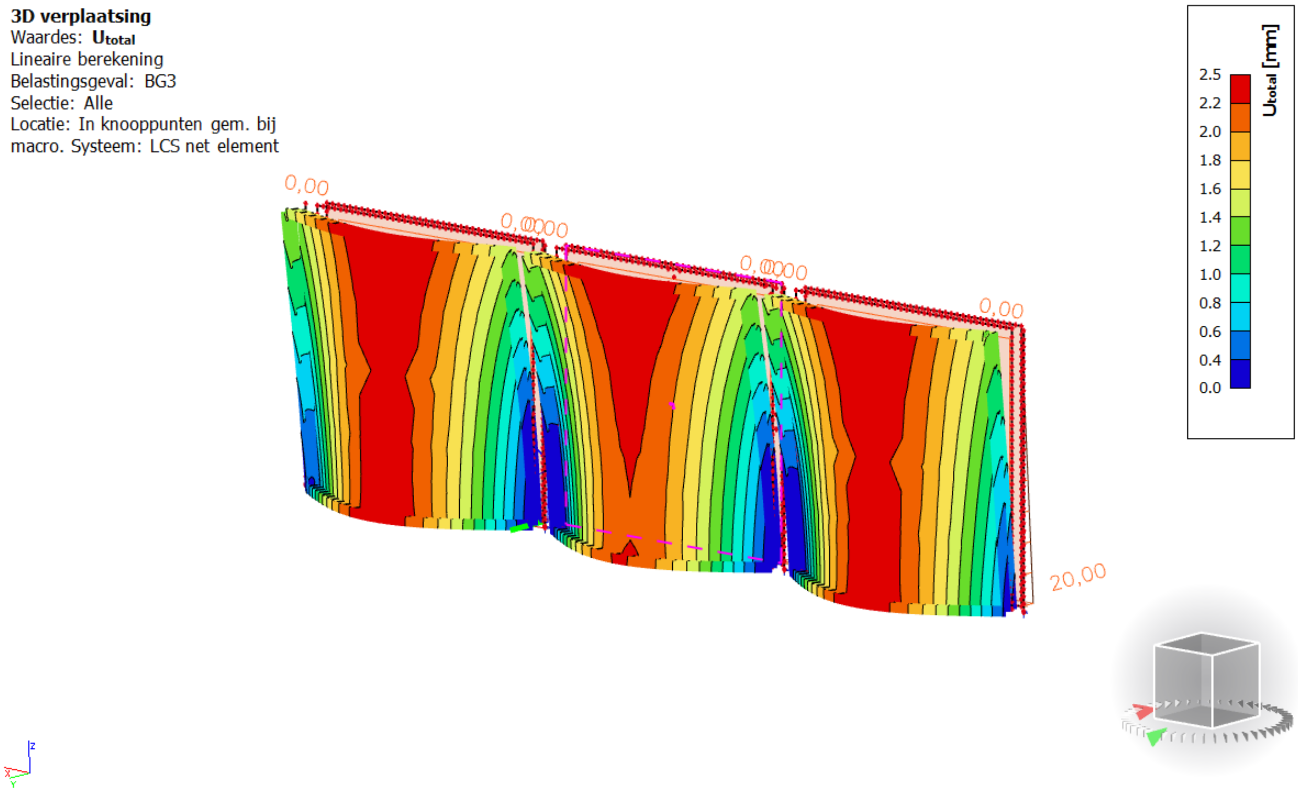

Figure 8-5: 3D maximum displacement u_max in SLS

Maximum displacement of the glass and aluminum structure is $2.5\ mm$.

ULS

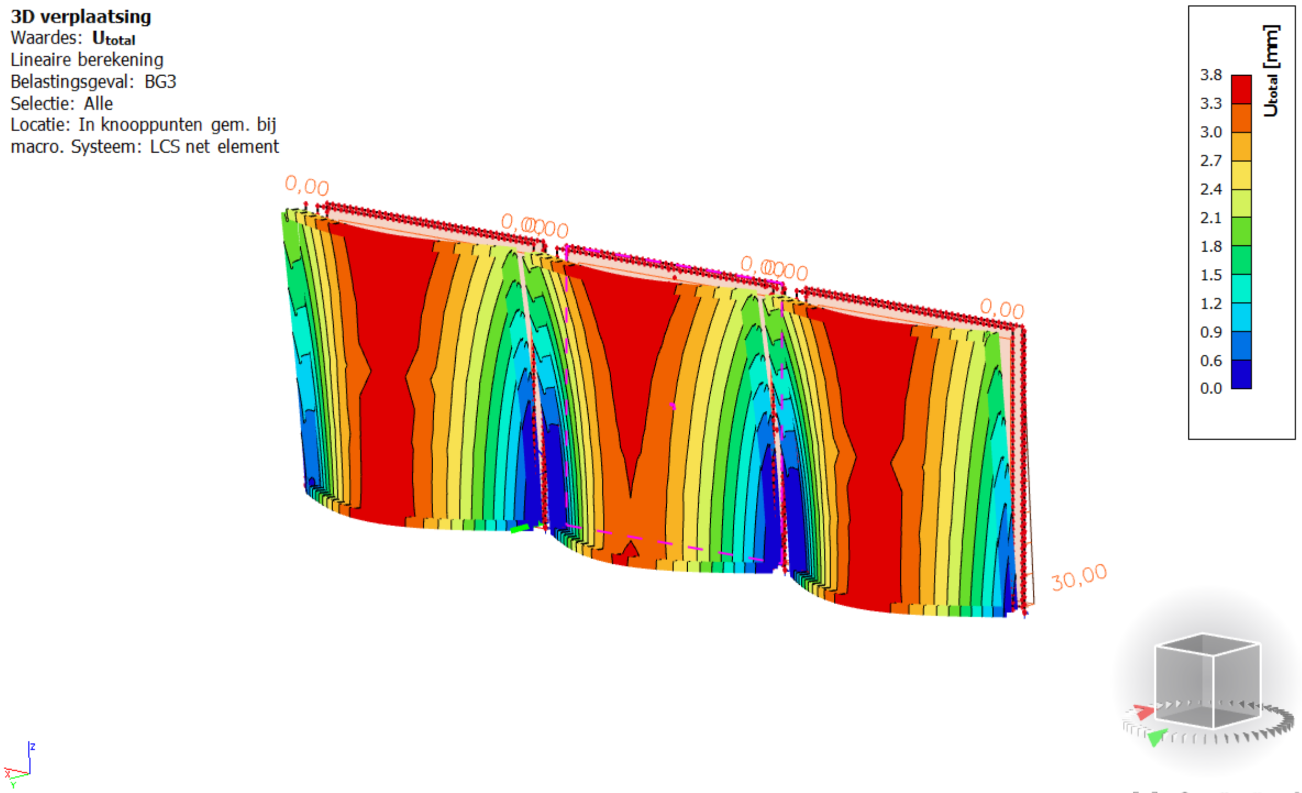

Figure 8-6: 3D maximum displacement u_max in ULS

Maximum displacement of the glass and aluminum structure is $3.8\ mm$.

8.3. Load case 2: Collision force

In the previous chapter and in Appendix F the maximum allowed stress in the ULS of the glass is determined for a short duration concentration load according to the Dutch NEN:

$$92.10\ MPa$$

With a concentrated force of $10200\ kN/m^2$ on a surface of $0.1x0.1m$, the iteratively found total load is $102\ kN$. The maximum principal stresses are $91.7\ N/mm^2$. As this is an incidental load situation, no safety factors are required for the load.

8.3.1. 3D principal stress σ_1 with $t_{eff} = 53\ mm$

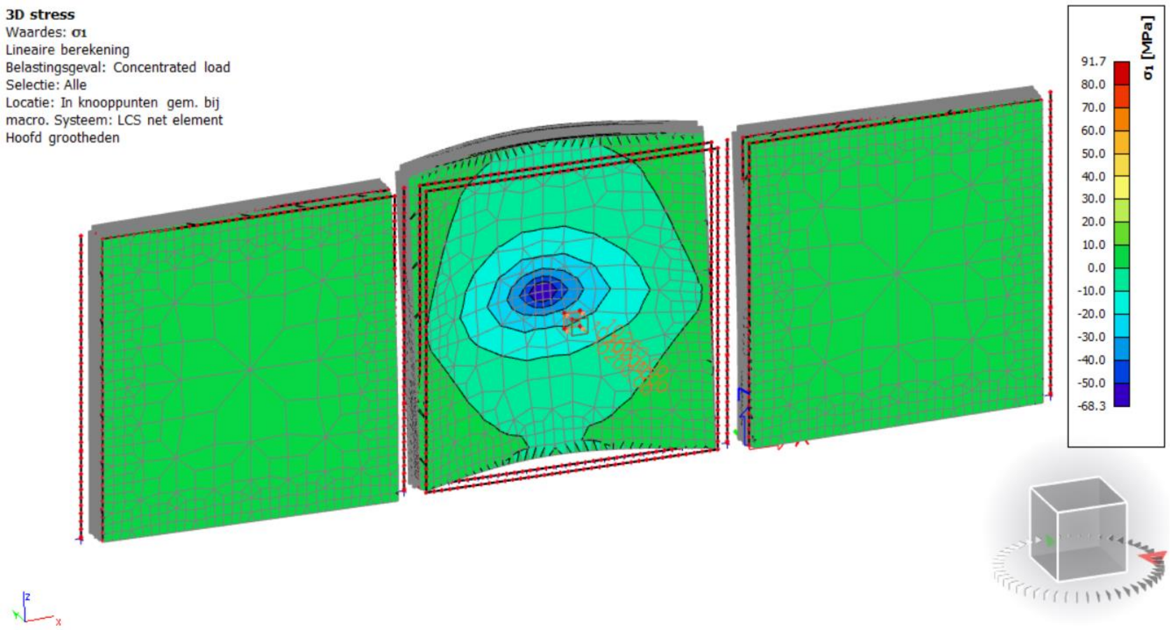

Figure 8-7: 3D principal stress σ_1 with t_eff=53 mm in SLS

8.3.2. 3D principal stress σ_2 with $t_{eff} = 53\ mm$

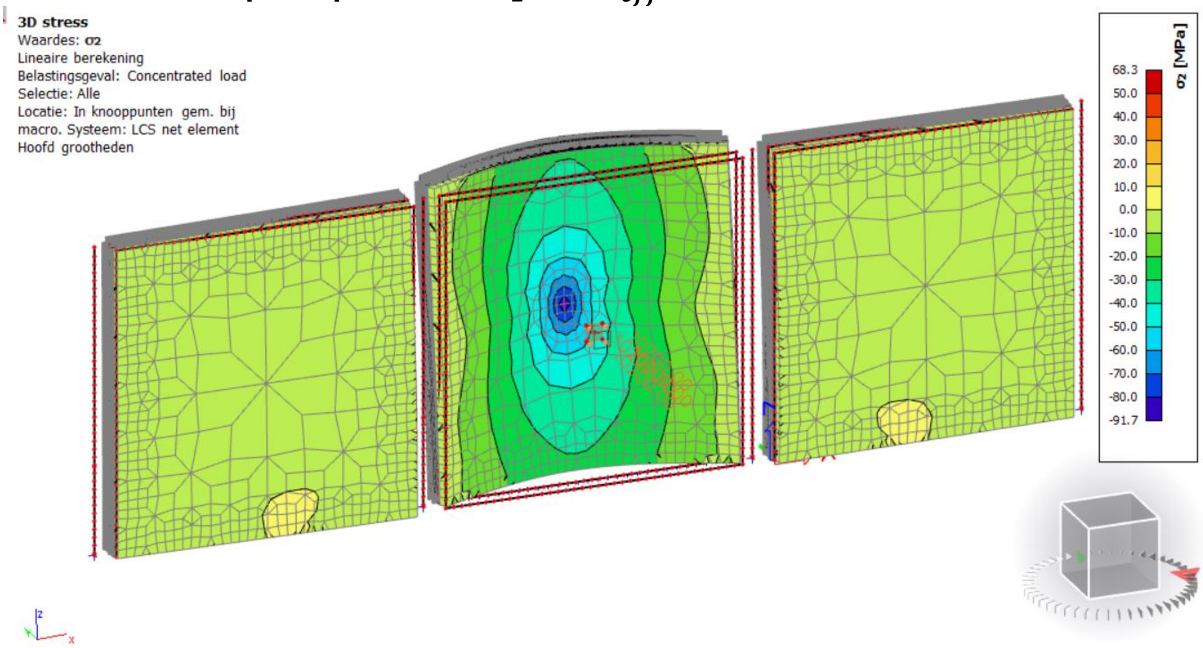

Figure 8-8: 3D principal stress σ_2 with t_eff=53 mm

And the maximum displacement is 9.6 mm.

8.3.3. 3D displacement u_{max}

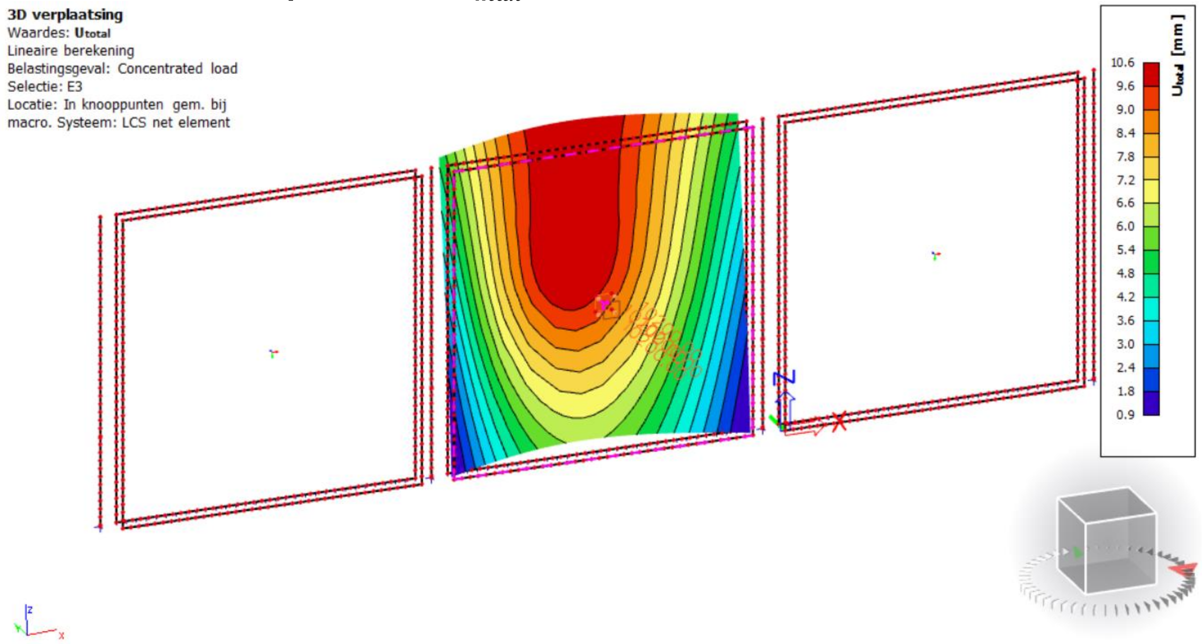

Figure 8-9: 3D displacement u_max for an impact load

At this point the critical stress according to the NEN is reached. The concentrated load is $102\ kN$ and the displacement $u_{max} = \Delta x = 0.096\ m$. According to the formula derived in Appendix B; the (linear) relation $F \cdot \Delta x = 2 \cdot E_{kin,max}$, the energy absorbed by the structure becomes:

$$E_{absorbed} = \frac{F \cdot \Delta x}{2} = \frac{102 \cdot 0.096}{2} = 0.490\ kNm = 490\ Nm$$

This value corresponds with the energy of a tree trunk of $200\ kg$, with a speed of $2.213\ m/s$

$$E_{kin} = 0.5 \cdot 200 \cdot 2.213^2 = 490\ kg \cdot m^2/s^2 = 490\ Nm$$

This energy is absorbed by the structure without inclination of the impact object, which is a conservative assumption.

8.4. Water level resistance after impact

In case of an impact, one, two or all plies can be broken. If the water level is still high at the time of impact, this can cause the panel to fail completely resulting in a flood. In the FEM model, the residual strength with the effective thicknesses of one and two plies is checked.
The maximum allowed stress for a long duration distributed load is:

$$74.53\ MPa$$

Similar to the analysis performed in 8.2; using the maximum allowed stress using the Dutch NEN, and the FEM model made in SCIA. Only the thickness is varied and the stresses are calculated in SLS and ULS. The found maximum stresses of 3 coupled plies, 2 coupled plies, two uncoupled plies and a single ply are summarized in the table below. The output of the FEM model for these situations can be found in Appendix H.

Table 8-2: Summary of the capacity of different thicknesses to withstand maximum water pressure in SLS and ULS

t_{eff}	σ_{max} in SLS	σ_{max} in ULS
$\mathbf{50.01\ mm}$	$\mathbf{10.8\ N/mm^2}$	$\mathbf{16.1\ N/mm^2}$
$\mathbf{35.72\ mm}$	$\mathbf{16.0\ N/mm^2}$	$\mathbf{24.1\ N/mm^2}$
$\mathbf{22.68\ mm}$	$\mathbf{27.3\ N/mm^2}$	$\mathbf{40.9\ N/mm^2}$
$\mathbf{18\ mm}$	$\mathbf{46.5\ N/mm^2}$	$\mathbf{69.8\ N/mm^2}$

It must be noted again that the stresses in coupled layers are based on the displacement-effective thickness, this is done to simplify the calculations and staying on the conservative side. The stresses of coupled layers are slightly smaller than presented in Table 8-2: Summary of the capacity of different thicknesses to withstand maximum water pressure in SLS and ULS with this interlayer and loading.

8.5. Conclusion

The minimum amount of kinetic energy that can be absorbed by the structure according to NEN2608;2014 glass calculations and the Finite Element Model is $490\ Nm$, if only deformation by the structure is considered in combination with pure bending.
With one glass layer fractured, with the panel still coupled or uncoupled by the laminate, there is still significant water pressure to retain.
From the impact analysis can be concluded that the more elastic(or plastic) deformation capacity is present at the impact location, the lower the equivalent static load. Adding more deformation capacity in the structure can be done without losing any structural safety can be done by adding a rotational spring at the bottom of the side posts or using a damper of some sort at the back of the structure to increase the deceleration distance. It is also possible to see if some material can be saved in the aluminum structure, decreasing costs and increasing deformation in case of an impact, but overloading and fatigue need to be kept in mind. A more ductile anchoring can be an option too.

Discussion:

There are no other methods for failure mechanisms other than bending, but it is likely that these can occur also. Shear, punching shear, longitudinal shear also occurs within the glass and may cause failure.
The NEN 2608 is a Dutch code used for the calculation of glazing, and not particularly for glass in structural applications. Nevertheless, the mechanisms and methods in this code can carefully be used to determine the stress limits and effective thicknesses.

9. Probability of failure

9.1. Introduction

This chapter provides an explanation of the WBI2017 methods, where after the results from a probabilistic analysis is presented. For a more extensive explanation of the used models and z-functions used to obtain the failure probability, the reader is referred to Appendix I.

9.2. Probabilistic approach

In the following paragraphs the essence of probabilistic risk assessment is explained. The definition of flood risk as adopted by the European Commission (2007) is as follows:

“”Flood risk” means the combination of the probability of a flood event and of the potential adverse consequences for human health, the environment, cultural heritage and economic activity associated with a flood event.”

Or in short:

$$Flood\ Risk = Probability \times Consequences$$

9.2.1 Z-functions

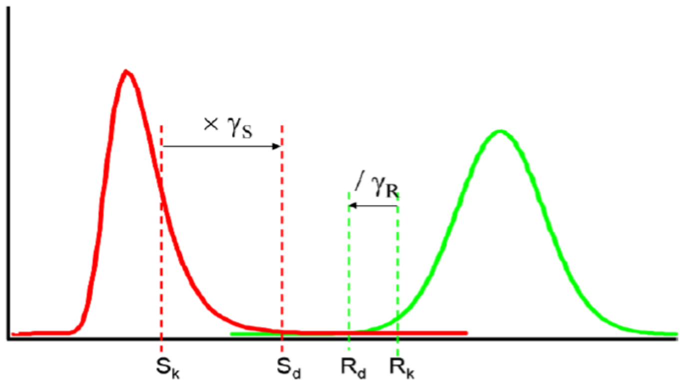

Figure 9-1:The limit state function of Load(red) and Strength(green)

In Figure 9-1:The limit state function of Load(red) and Strength(green) the well-known probability density functions of load and resistance are schematized. The surface area of the overlapping part is the failure probability represented in the limit state function or so-called Z-function: $Z < R - S$. R stands for Resistance, related to the strength of materials or elements. S stands for Sollicitation, relating to the Load. The overlapping surface area of these functions is the indication of the probability that the load is larger than the resistance of the element of material, or the probability of failure P_f.

Strength and load over a longer period of time

In time, the structure usually degrades in strength or resistance. A dike, for example, lowers in height due to subsidence. Simultaneously, its grass cover can degrade in quality, leading to a larger probability of failure. At the same time the loads(e.g. water levels, wind) fluctuate and sometimes increase, and the probability of exceedance of a certain critical value increases if the time period increases. In the figure below, the blue arrows represent investments like reinforcements, replacements and renovations of the structure.

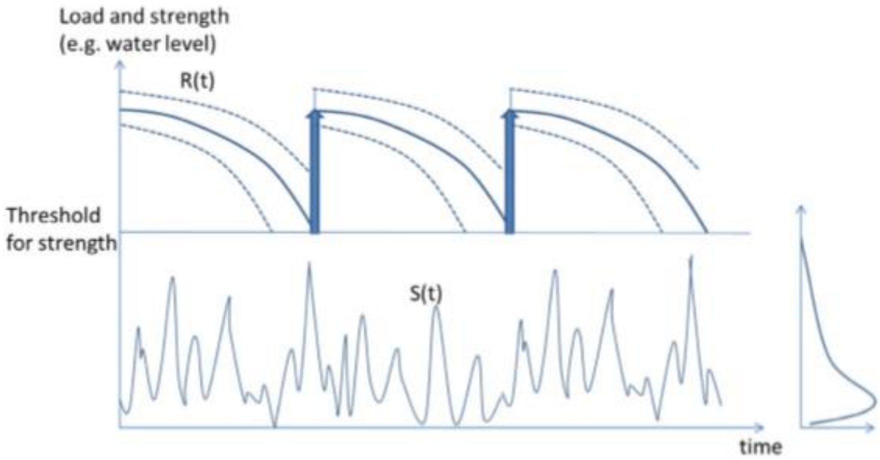

Figure 9-2:Schematic development of strenght and load over time. [S.N Jonkmal et al(2017)]

9.2.2. Probability of failure

The total system failure is build up from different sub-systems, where a failure in a subsystem causes total system failure. The probabilities of the sub systems add up to the total failure probability of the system. Because the different subsystems are sometimes correlated with each other, this will have to be taken into account when calculating the probability of failure of the total system. The probability P_f of failure of a dike-section consists of the probabilities of flooding of different failure mechanisms.

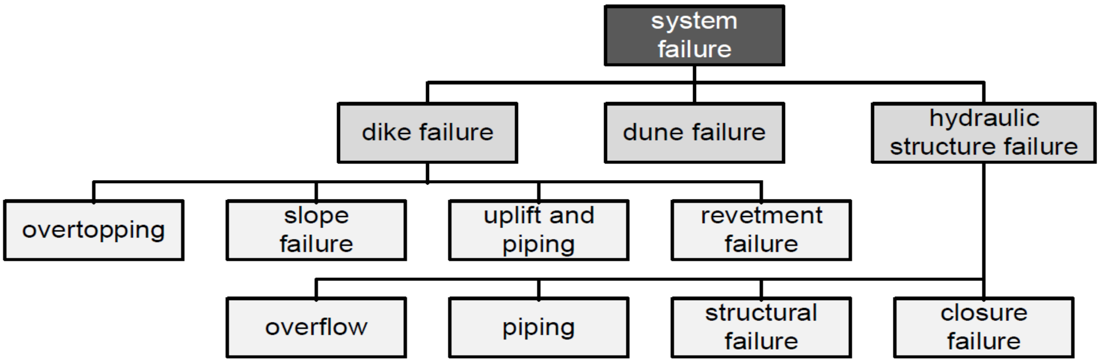

Figure 9-3:Failure tree of system failure [Jonkman, Jorissen, Schweckendieck, & Van den Bos, 2017]

In this report, only hydraulic structure failure is considered. Because this report only considers the glass flood wall as a permanent structure, the sub mechanism of “closure failure” is be neglected. More on the failure probability analysis of the glass flood defence can be found in Appendix I.

Type	Failure mechanism	Contribution ω_j
Dike	Overflow and wave overtopping	0.24
	Piping, heave and rupture of the cover layer	0.24
	Slope stability (inner slope)	0.04
	Outer revetment failure	0.10
Hydraulic Structure	Failure due to non-closure of hydraulic structure	0.04
	Piping at hydraulic structure	0.02
	Structural failure of hydraulic structure	0.02
Other		0.3
Total		1

Standard distribution of failure mechanisms, source Implementing risk based flood defence standards

For a hydraulic structure, usually a total contribution (ω_j) of 0.08 is suggested, while the structural failure usually has a maximum contribution of $\omega_j = 0.02$.

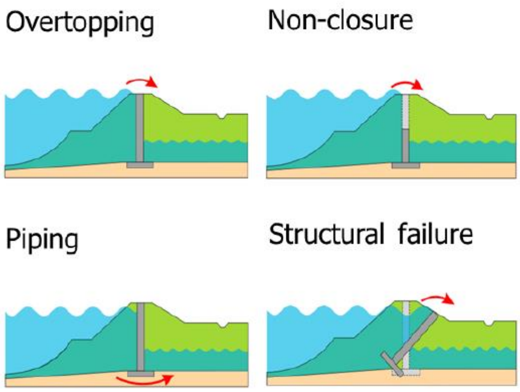

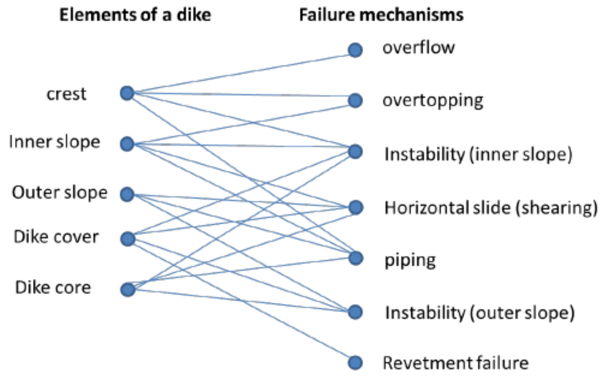

Figure 9-4:the different failure mechanisms related to a hydraulic structure with movable gates [Jonkman, Jorissen, Schweckendieck, & Van den Bos(2017)]

Figure 9-5:The failure mechanisms and dike elements are always interconnected [Jonkman, Jorissen, Schweckendieck, & Van den Bos (2017)]

Length effect

After the probability of failure of one of the mechanisms is determined, it needs to be multiplied with a length effect factor. The longer the dike trajectory, the larger the chance there is a weak link. The formula for the length effect factor is:

$$N_j = 1 + \frac{a_j \cdot L}{b_j}$$

In which:
N_j = the length effect factor [-]
a_j = fraction of the trajectory length that is sensitive to failure mechanism [-]
L = trajectory length [m]
b_j = length of a typical independent section for failure mechanism [m]

Probability of flooding

To determine the probability of flooding of an area, the total probability of flooding is the sum of the probability of failure of all dike sections together.

9.2.3. Risks

In the WBI standard, flood risk is not just the probability of failure of a dike trajectory, but also takes the consequence into account. WBI2017 considers three types of risk, namely; Economic Risk(ER), Individual Risk(IR), and Societal Risk(SR) and these are elaborated on below.

Individual risk

It is determined that for an individual in the Netherlands, the risk of a fatality caused by flooding must be $1 \cdot 10^{-5}$. In combination with the mortality rate per flooding(FN curves), the necessary failure probability of a dike trajectory can be determined.

$$IR(x,y) = \sum_i^n P_i F_{D,i}(x,y)(1 - F_{E,i})$$

Where:
$IR(x,y)$=individual risk at location (in the Netherlands $1 \cdot 10^{-5}$)
p_i=probability of scenario i [1/year]
$F_{D,i}(x,y)$= mortality at location (x,y) for a scenario i

$F_{E,i}$ = evacuation fraction for scenario i

[Jonkman et al., (2017)]

Financial risk

Flood risk can be quantified by means of the expected damage. According to Kaplan and Garrick (1981): Risk is a set of scenarios (*si*),each of which has a probability (*pi*) and a consequence (*di*). It can be expressed as the sum of all probabilities times their consequences.

$$E(d) = \sum_{S_t=1}^{n} p_i \cdot d_i$$

Societal risk

As seen above, consequences can be expressed in the terms of damage. But it can also be expressed in loss of life. For a flood prone area FN-curves or FD-curves can give good insight on the risks of that area. Where N stands for the number of fatalities and the D for the amount of damage.

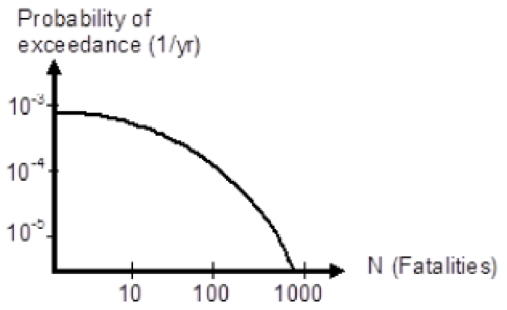

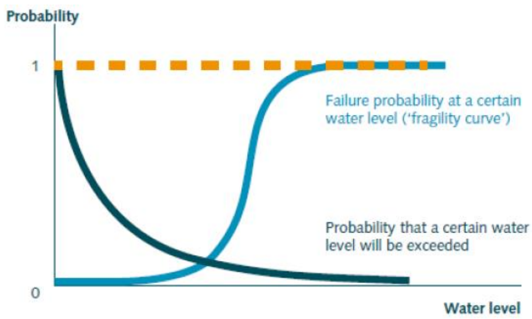

Figure 9-6:an FN-curve, the amount of fatalities caused by a flood and its probability [Jonkman, Jorissen, Schweckendieck, & Van den Bos(2017)]

Figure 9-7:fragility curve vs the probability of occurrence of a certain water level [Jonkman, Jorissen, Schweckendieck, & Van den Bos(2017)]

9.2.4. Failure probability percentage

For an hydraulic structure, the total failure probability space is 8%, in which the failure probability percentage for structural failure is 2%. In chapter one is found that the probability of failure of one section in Arcen is $1/470$. This means the failure probability of an hydraulic structure in that dike section must be less than:

$$P_{f;space} = 1/470 \cdot 0.02 = 4.255 \cdot 10^{-5}$$

A full probabilistic calculation for structural failure of the glass flood defence in location Arcen is done based on the WBI2017 standards. A hydraulic structure has 3 main failure modes:

1. Structural Failure
2. Overtopping/overflow
3. Piping

For one failure mode, 'Structural Failure', the Z-functions are obtained or determined and the probability of failure of each sub-mechanisms are calculated with Monte Carlo simulations in Prob2B. The Z-functions are explained and elaborated on in Appendix I. Input parameters are determined in Appendix I and Appendix J.

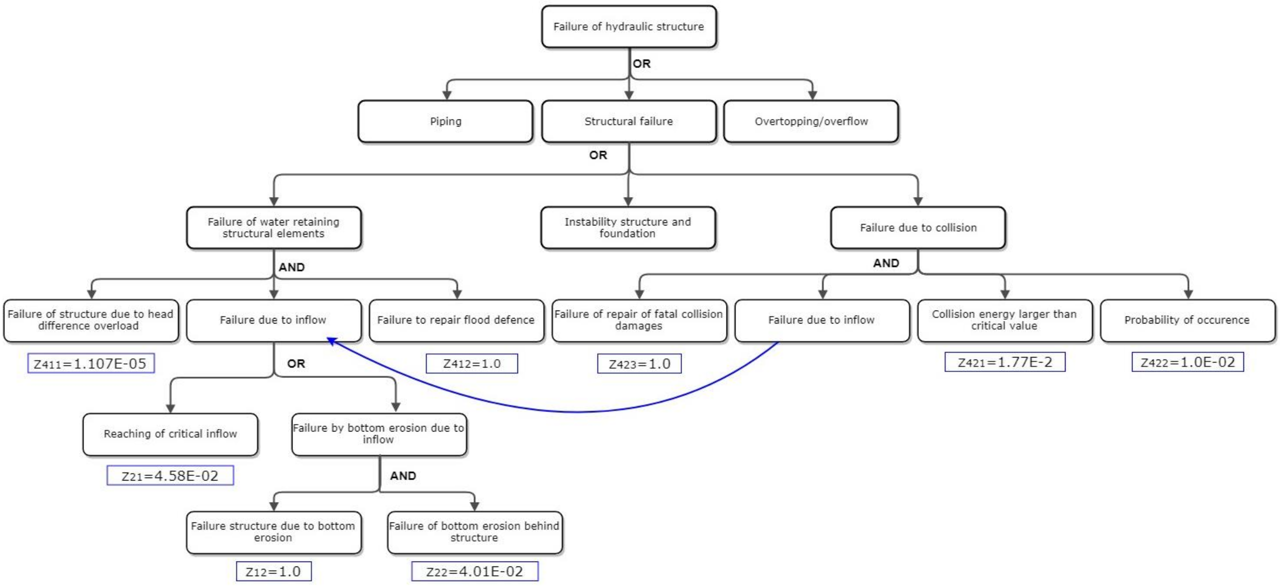

Figure 9-8: Failure mechanism tree

The sub- mechanisms of the failure mechanism “Structural Failure” are:

1. Failure of structure due to bottom erosion → Z_{12}
2. Failure due to the reaching of critical inflow → Z_{21}
3. Failure of bottom erosion behind structure → Z_{22}
4. Failure of structural parts due to head difference overload → Z_{411}
5. Failure to repair flood defence → Z_{412}
6. Collision energy larger than critical value → Z_{421}
7. Probability of occurrence of a collision → Z_{422}
8. Failure to repair the fatal collision damages → Z_{423}
9. Failure of structure due to instability of structure or its foundation → Z_{43}

9.3. Failure probability of the failure mechanism “Structural Failure’

The safety standard in dike trajectory 65 (Arcen) is $1/100$ [VNK/Pimplatform].The failure probability of a section of an hydraulic structure is extracted from the i-viewer and is $1/470$ per year. The failure probability space of an hydraulic structure is 0.08, with 0.02 reserved for structural failure [S.N. Jonkman et al.]. The total yearly failure probability space for this mechanism then becomes:

$$P_{f;space} = 1/470 \cdot 0.02 = 4.255 \cdot 10^{-5}$$

In comparison: the yearly failure probability of a structure in the Eurocode Consequence Class 2 is $1.30 \cdot 10^{-6}$(see Appendix Load specificationA). Which is more conservative.

OR-function

Due to sometimes unknown correlations between failure mechanisms and sub-mechanisms the failure probabilities per failure mechanism are not simply added when the OR function is used. Correlations are taken into account by giving an upper and a lower limit of the total failure probability. This means that the lower limit assumes full correlation between failure mechanisms, while the upper limit corresponds to the situation that the failure mechanisms are independent and there is no correlation between the failure probabilities. [S.N. Jonkman et al.]

Lower limit OR: $P_{combi} = Max(P_i)$

Upper limit OR: $P_{combi} = \sum(P_i)$

To be on the safe side, the upper limit must be assumed, and the probabilities are added up to each other. The reality will be in between.

AND-function

When the function AND is used, it means that all sub-mechanisms need to happen independently to cause system failure. Sometimes these sub-mechanisms are highly correlated and can therefore not be multiplied with each other. For example, when water retaining elements fail due to head difference overload, it is highly possible that the hydraulic load is high, and the probability of reaching the critical inflow is close to one. The lower limit in this case is that the failure mechanisms are completely independent and can be multiplied with one another. The upper limit assumes full correlation and the largest probability is governing.

Lower limit AND: $P_{combi} = P_1 \cdot P_2 \ldots \cdot P_i$
Upper limit AND: $P_{combi} = Max(P_i)$

When the failure probabilities of all sub-mechanisms are determined, the total failure probability $P_{f;total}$ can be derived by adding the independent failure mechanisms to each other:

$$P_{f;total} = P_{f;waterretainingelements} + P_{f;collision} + P_{f;instability}$$

9.4. Analysis failure tree

9.4.1. Brief analysis

Some correlations can be easily identified, as the probability of “Failure of the structure due to head difference overload” and “Failure due to inflow” are highly correlated. When “Failure of the structure due to head difference overload” occurs, “Failure due to inflow” almost certainly also occurs, this is the domino effect. The other way around is almost impossible: there is no inflow if the water retaining elements do not fail. This is not always the case, but for this particular structure, inflow becomes critical very fast as there is no inner water level.
Other failure mechanisms such as the “Probability of occurrence” of a collision and the “Collision energy larger than critical value” are independent.

In the sub mechanism “Failure of water retaining structural elements” it can be concluded that the upper limit is equal to the probability of failure of “Failure due to head difference overload” $Z_{411} = 1.107 \cdot 10^{-5}$.

In the sub-mechanism failure due to collision all events need to happen to cause a flood. The events are independent of each other, so the failure probability becomes:
Failure due to inflow =$4.01 \cdot 10^{-2} \cdot 1.0 + 4.58 \cdot 10^{-2} = 8.59 \cdot 10^{-2}$
Failure due do collision $= 1.0 \cdot 10^{-2} \cdot 1.77 \cdot 10^{-2} \cdot 8.59 \cdot 10^{-2} = 1.52 \cdot 10^{-5}$

9.4.2. Total failure probability:

$$P_{f;total} = 1.52 \cdot 10^{-5} + 1.107 \cdot 10^{-5}\left(+P_{f;instability} = assumed\ sufficient\right) = 2.627 \cdot 10^{-05}$$

This probability is smaller than the failure probability for a section at the location. More information about the probability of a collision and the distributions of floating debris in the Meuse is needed as to obtain a more accurate failure probability.

For more information on the used Z-functions and distributions of parameters the reader is referred to Appendix I and Appendix J.

9.5 Conclusion

From this failure probability analysis, it may be concluded that a glass flood defence can be safe enough to comply with the WBI2017 standards. But while many conservative assumptions were made, the failure probability should be investigated in more detail, and for more locations to obtain more accurate failure probabilities. The assumptions made in this analysis are based on one location, but every situation is different.

The aluminum structure and the glass itself are sufficiently strong to retain a water level up to the top of the structure. The failure probability can decrease:

- If there is potential remaining bearing capacity after glass breakage that may be taken into account
- If the experiments on the structure suggest a higher critical value of the collision energy
- A more detailed analysis of possible impact objects in the river is done
- The emergency measures that can prevent flooding after a fatal impact are taken into account
- There would be a bottom protection behind the structure

The failure probability can also increase if the probability of occurrence of an impact by significant floating debris is larger dan assumed. This is an interesting subject for further research as sizes, velocities, the material of floating objects, the damping of the water have large influence on the collision energy.

Discussion

The failure probability analysis done in this thesis holds a lot of uncertainties. Many of the Z-functions are based on standard values or conservative assumptions. It is wise to look closer into the critical failure mechanisms such as the probability of failure due to impact; where the probability of occurrence of such an event is very uncertain but has large influence on the total failure probability.

Part III: Experiment

10. Experiments

10.1. Introduction to glass experiments

10.1.1. Incentive

Since impact on glass is still under a lot of investigation and the modelling of impact on brittle materials is nowadays still inaccurate. Therefore, new glass applications are usually assessed by experimental testing. To be sure the glass can withstand the loads, they are applied on the glass without scaling of the tests.

10.1.2. Existing impact tests

“Pendulum test” or the “Soft body impact test”

In Europe, the pendulum test is the test described by the international standard EN 12600 (Table 4-2). This is usually an impact body like Figure 1-2, but in the Netherlands a bag of glass pearls is used to imitate the body of a person. This used to be a $50\ kg$ bag of sand.

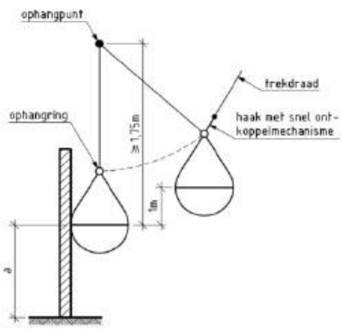

Figure 10-1: Pendulum test EN 12600 [GIB GMBH. (n.d.).]

Figure 10-2: Glass pearl pendulum test NEN 6702 [Schijf WVB. (n.d.).]

In accordance with the NEN 6702, structures with a possibility of ‘falling through’, need to be tested with the “glass pearl pendulum test”. These tests mimic a falling person, and it makes use of a bag of glass pearls of $50\ kg$, falling from a height of $1\ m$. After impact of the bag of glass pearls, the following checklist needs to be fulfilled to assure the safety of the glass. [Schijf WVB. (n.d.).]:

- The impact body cannot go through the separation
- The cohesion of the structure is intact
- No loosening of parts larger than $100\ mm^2$
- At fracturing, no openings occur where a ball of $100\ mm$ in diameter can go through
- No dangerous situations can occur that may cause injury
- The anchoring needs to stay intact

It is possible to apply this checklist to our own tests.

“Ball drop test” or “hard body impact test”

To assess the impact resistance against hard body impact, the ball drop test or hard body drop test described in EN356 (see Table 4-2), drops a $4.1\ kg$ steel ball on the glass from a height of $1.5 - 9\ m$. [FloodControlTV. (2012, July 2).]

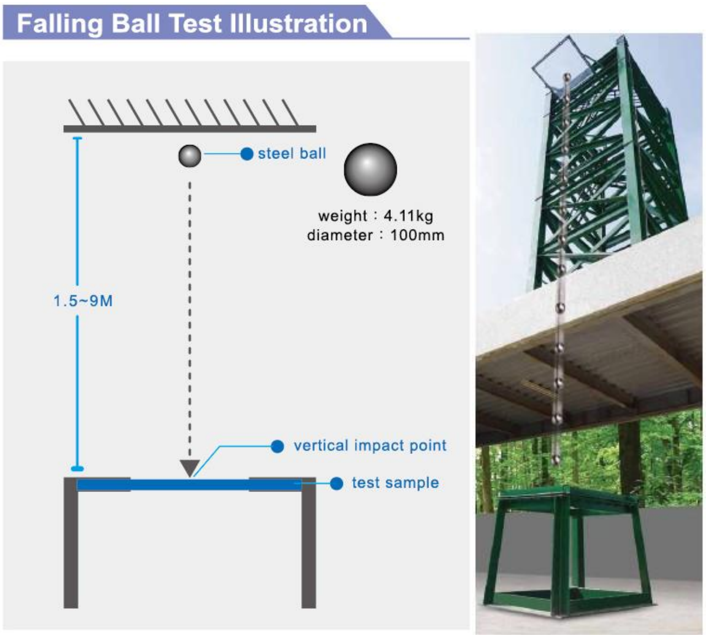

Figure 10-3: The ball drop test from EN 356 [Derstrong Enterprise. (n.d.).]

Hurricane glazing test

In the hurricane prone Northern America, impact tests are done to assess hurricane-resistant windows. Wooden objects of various size are shot at the glass window at high speeds, until it breaks. The window is then subjected to cyclic loading to simulate wind loading.

Figure 10-4: Hurricane glass test [Elite Window Film. (n.d.)]

Eurocodes and NEN codes do not specify the load combination of a severe impact followed by water and wave pressure on a safety glass panel. A comparable sequence of events occurs for hurricane conditions. The load combination for the impact-flood case is quite similar to the hurricane proof window testing procedure. The hurricane test protocol consists of two main parts; Impact loading by flying debris and thereafter cyclic loading by wind gusts. This can be translated to our loading case; impact by floating debris(smaller velocities but can be of larger masses), and water and wave pressure (static pressure with cyclic loading).

10.2. Experiments Stevin II Laboratory

10.2.1. Expectations

Model and calculations

By using conservative assumptions, the minimum amount of energy that needs to be retained by the glass flood defence is calculated for the middle of the panel in 8.3. The minimum amount of energy that the panel must be able to withstand due to pure bending according to the NEN2608 and FEM analysis from the previous chapters is:

$$490\ Nm$$

In B.4 is analyzed that the most unfavorable situation that can occur with a floating tree in the Meuse is approximately $1083\ Nm$.
In an internal Arcadis report, a value of $1000\ Nm$ is mentioned for impact loads from a tree, based on expert opinion.

Impact bending strength

The bending strength of glass is larger for an impact load, 120 for HSG and 170 for FTG [Heyder & Paulu]. These values are not used in the NEN and therefore the lower adjusted values of resp. 70 and 120 are used for stress limits. Alongside other conservative assumptions it is therefore expected that the outcome of the calculations are an underestimation of the strength.

Set up

Similar to the pendulum test prescribed by the EN 12600, the experiment will be done by raising the impact object to a certain height and fall against the glass. The height of the object is increased every time until the glass is damaged. In the following paragraphs, the tests are summarized. A more extensive report on the test results can be found in Appendix D.

10.2.2. Impact objects

We used two different trees for the impact tests, as after the first test impact object 1 turned out to be too light to cause damage to the panel.

Impact object 1

Table 10-1: Properties impact object 1

Property	Value
Length	$2.55\ m$
Diameter	$0.27\ m$
Weight	$140\ kg$
Species	Larch (Larix)
Origin	Gelderland (Holland)

Figure 10-5: Impact object 1

Impact object 2

Table 10-2: Properties impact object 2

Property	Value
Length	$2.20\ m$
Diameter	$0.40 - 0.45\ m$
Weight	$380\ kg$
Species	Red Oak (Quercus rubra)
Origin	Gelderland (Holland)

Figure 10-6: Impact object 2

10.2.3. Test 1

After a test run with the pendulum test on some left-over glass, we were ready to test the first panel. Since the glass panel weighs more than $500\ kg$, it had to be safely transported using a vacuum suction lifter to place it in the Aluminum frame.

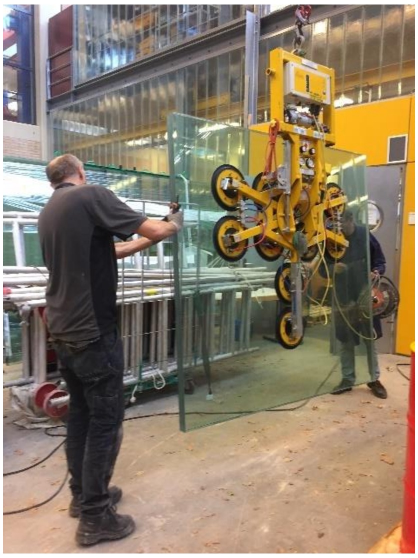

Figure 10-7: Vacuum suction lifter

Figure 10-8: placing the glass panel in the frame

After carefully placing the glass panel into the Aluminum frame, and securing it with click-profiles and EPDM seals, the panel had to be rotated. During rotating one of the corners unfortunately slammed on the Meccano set-up, causing the middle glass layer to fracture. Since there is still information to be gathered from this panel, it was decided to test it anyway and the panel was placed between the side posts.

Figure 10-9: Visible breakage pattern from lower corner

Figure 10-10: The complete structure test 1 with already fractured middle layer

The results from the video analysis are summarized in Table 10-3: Summary test 1 The minimal energy of $490\ Nm$ is reached and no further fracturing of glass occurred. Only impact object 1 was used for this test, after the test it was decided to get a heavier object for the next tests.

Table 10-3: Summary test 1

Test	Impact object	Speed	E_{kin}	Remarks
1.1	Object 1	$2.658\ m/s$	$494\ Nm$	Delamination, no glass damage
1.2	Object 1	$1.893\ m/s$	$250\ Nm$	Delamination spreads further, no glass damage
1.3	Object 1	$1.902\ m/s$	$253\ Nm$	Delamination spreads further, no glass damage

Because the middle layer was already fractured, something interesting happened after the first impact; the front glass layer seemed to delaminate partially. Where the layer was still laminated in the shape of a square, the outside of this laminated square was clearly loose from the rest of the panel. This delamination effect after impact can be a subject for further research.

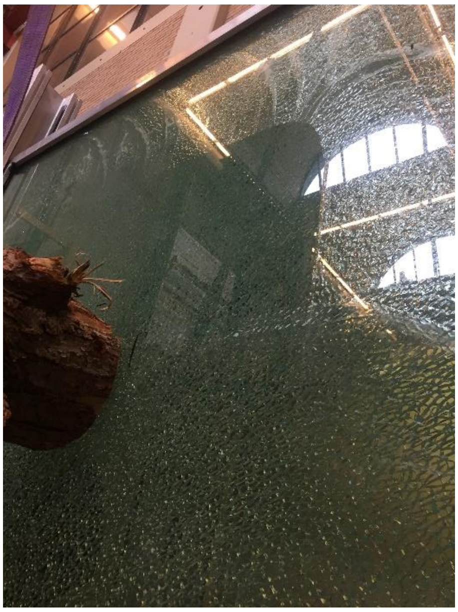

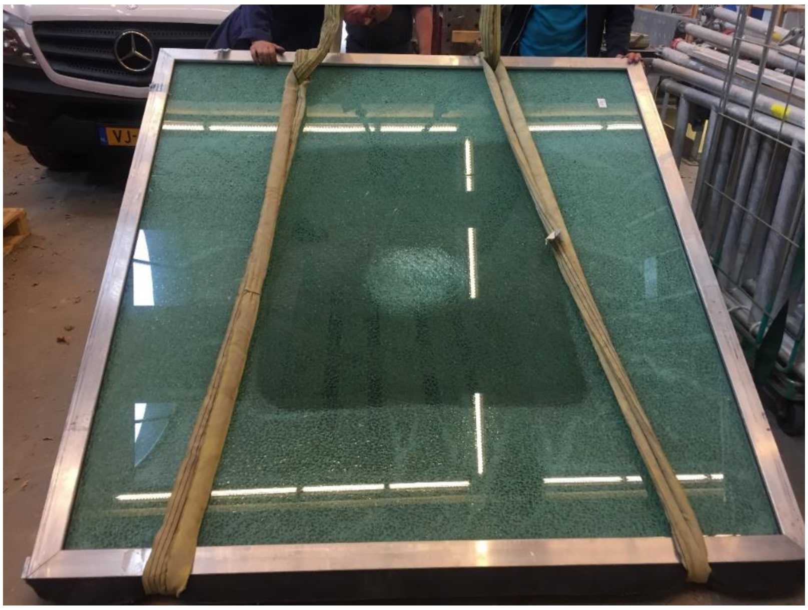

Figure 10-11: Visible delamination

Figure 10-12: The delaminated panel

10.2.4. Test panel 2

A total of eight tests were done. The panel eventually broke the two back layers by object 2 at a speed of 3.2 m/s. No delamination occurred and the three broken glass layers and two Sentryglass layers exhibited minimal deformation during transportation on the forklift.

Table 10-4: Summary test 2

Test	Impact object	Speed	E_{kin}	Remarks
2.1	Object 1	$< 2.83\ m/s$	$< 560\ Nm$	No damage.
2.2	Object 1	$< 2.83\ m/s$	$< 560\ Nm$	No damage.
2.3	Object 1	$2.83\ m/s$	$560\ Nm$	No damage.
2.4	Object 2	$< 3.0\ m/s$	$< 1710\ Nm$	No damage.
2.5	Object 2	$3.0\ m/s$	$1710\ Nm$	No damage.
2.6	Object 2	$3.2\ m/s$	$1946\ Nm$	Two layers fractured at the back of the glass.
2.7	Object 2	$3.1\ m/s$	$1826\ Nm$	Last layer fractured
2.8	Object 2	$3.29\ m/s$	$2056\ Nm$	No further damage except more glass falling from the three already broken layers.

After impact, two layers at the back side of the glass were shattered, indicating that the failure was due to a moment. Because there were two damaged layers, it was not possible to derive the origin of the failure from the crack pattern. But at the backside, the corner started to crumble as can be seen in Figure 10-14. This can be an indication that this location is vulnerable.

Figure 10-13: The panel after test 2.6

Figure 10-14: Crumbling of the lower corner

In test 2.7 the last and front layer also fractured. With three glass layers broken, the displacement of the glass at the location of impact increased enormously in test 2.8, therefore increasing the deceleration distance. This decreases the equivalent static load. With the panel acting more elastic, the impact object bounced back to a significantly larger height than the previous tests(Figure 10-15). This indicates that the kinetic energy was not fully absorbed by the structure, but stored in spring energy and returned in potential (height) energy.

Figure 10-15: Return height test 2.8

Figure 10-16: The three broken layers still laminated

Figure 10-17: The panel on the forklift

10.2.5. Test panel 3

Before test 3, the weight of impact object 2 to break the glass was assumed to be sufficient. But after the first 11 tests with impact object 1 and impact object 2 this assumption turned out to be false. As there was limited space in this part of the laboratory, the tree could not be pulled any higher. Therefore it was decided to rotate the tree at impact location so the face edge would hit the glass, see Figure 10-18. Since there was still no damage after these impacts, the top of the glass was tested in test 3.14 and 3.15. When this also did not cause any harm to the glass, the steel hemisphere from Figure 10-19: Impact with steel hemisphere test 3.17 was mounted on to the tree and this caused the two front layers to fracture in test 3.17. Between test 3.17 and test 3.22, an attempt was made to fracture the back of the glass, but this did not happen. After test 22, it was decided to stop the impact tests and proceed with test 4 with one layer intact.

Table 10-5: Summary test 3

Test	Impact object	Speed	E_{kin}	Remarks
3.1	Object 1	$< 2.364\ m/s$	$< 391\ Nm$	No damage.
3.2	Object 1	$< 2.364\ m/s$	$< 391\ Nm$	No damage.
3.3	Object 1	$2.364\ m/s$	$391\ Nm$	No damage.
3.4	Object 2	$< 3.150\ m/s$	$< 1885\ Nm$	No damage.
3.5	Object 2	$< 3.150\ m/s$	$< 1885\ Nm$	No damage.
3.6	Object 2	$< 3.150\ m/s$	$< 1885\ Nm$	No damage.
3.7	Object 2	$< 3.150\ m/s$	$< 1885\ Nm$	No damage.
3.8	Object 2	$< 3.150\ m/s$	$< 1885\ Nm$	No damage.
3.9	Object 2	$< 3.150\ m/s$	$< 1885\ Nm$	No damage.
3.10	Object 2	$< 3.150\ m/s$	$< 1885\ Nm$	No damage.
3.11	Object 2	$3.150\ m/s$	$1885\ Nm$	No damage.
3.12	Object 2 with edge of tree	$< 3.924\ m/s$	$< 2925\ Nm$	We put the lowest point of the pendulum behind the glass so the edge of the tree would hit the glass. Still no damage.
3.13	Object 2 with edge of tree	$3.924\ m/s$	$2925\ Nm$	No damage.
3.14	Object 2 – impact at top	$< 3.366 m/s$	$2153\ Nm$	We changed the location of impact to the top of the structure. No damage.
3.15	Object 2 – impact at top	$3.366 m/s$	$2153\ Nm$	No damage.
3.16	Object 2	$3.75\ m/s$	$2672\ Nm$	No damage.

3.17	Object 2 with steel sphere	$2.226\ m/s$	$941.46\ Nm$	Damaged by the steel sphere: the two front layers were shattered.
3.18	Object 2	$< 3.588\ m/s$	$< 2446\ Nm$	No further damage except more glass falling from the already broken layers.
3.19	Object 2	$< 3.588\ m/s$	$< 2446\ Nm$	No further damage except more glass falling from the already broken layers.
3.20	Object 2	$< 3.588\ m/s$	$< 2446\ Nm$	No further damage except more glass falling from the already broken layers.
3.21	Object 2	$< 3.588\ m/s$	$< 2446\ Nm$	No further damage except more glass falling from the already broken layers.
3.22	Object 2	$3.588\ m/s$	$2446\ Nm$	No further damage except more glass falling from the already broken layers.

Figure 10-18: Impact with face edge test 3.12 and 3.14

Figure 10-19: Impact with steel hemisphere test 3.17

After the impact with the steel hemisphere, delamination started to occur around the impact location, which is the opposite of what happened in Test 1, where the middle of the glass stayed laminated. The delamination pattern can be seen clearly in Figure 10-25 and Figure 10-26.

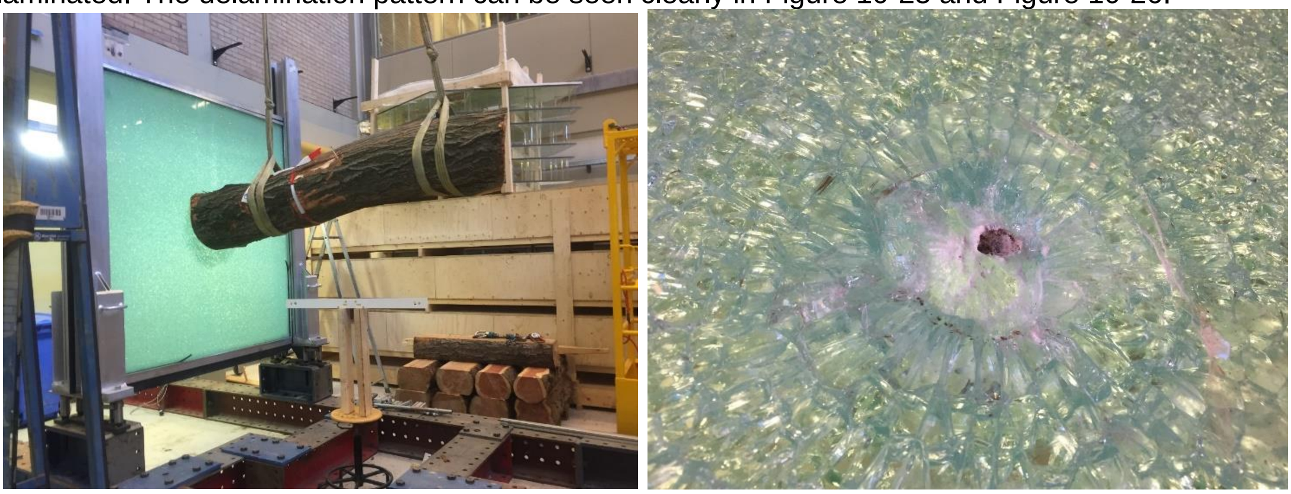

Figure 10-20: The broken panel with impact object 2

Figure 10-21: Location of impact

Figure 10-22: Discoloration around impact location

Figure 10-23: Broken panel 3

The steel hemisphere did not survive the hard-on-hard impact either, and exhibited brittle fracture, see Figure 10-24.

Figure 10-24: The broken steel hemisphere

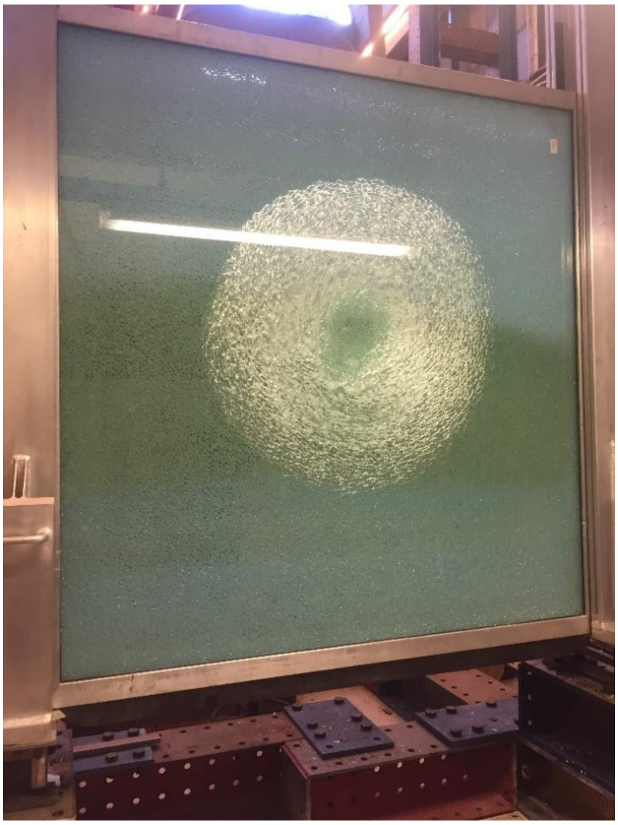

Figure 10-25: Delamination circle side view

Figure 10-26: Visible delamination in the panel

10.2.6. Test 4, remaining bearing capacity

Test 4.1

After D.5 Test 3, the panel had 2 broken layers, we put a concrete block of $1174\ kg$ on a surface of $0.5 \times 0.5\ m$, see Figure 10-27: The placing of the concrete block on a surface of 0.5x0.5 m. This approaches the moments in the panel that are caused by water pressure up to the top of the structure.

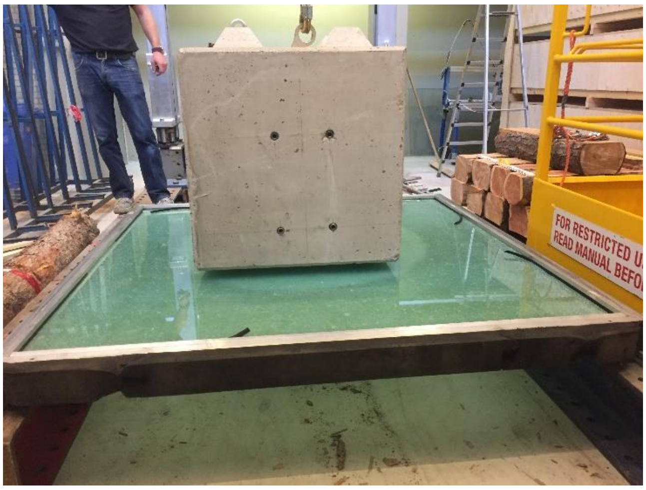

Figure 10-27: The placing of the concrete block on a surface of 0.5x0.5 m

Figure 10-28: Static load test

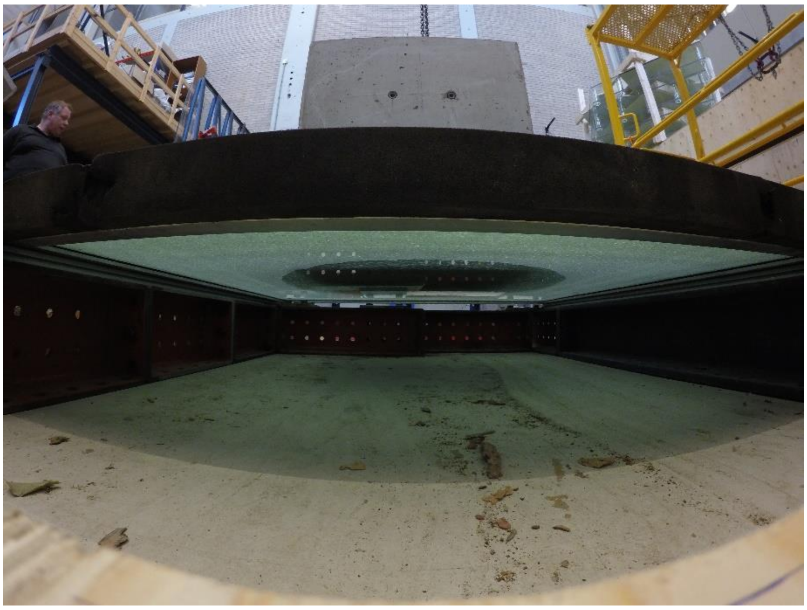
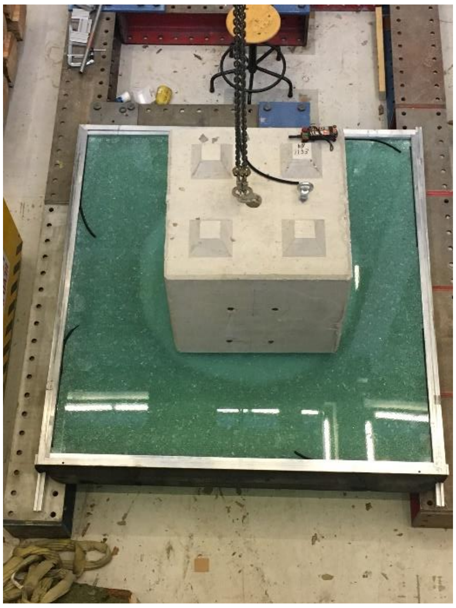

Figure 10-29: Static load test view from below

Figure 10-30: Static load test view from top

We left the load on the glass for three days, and nothing happened.

Test 4.2

After three days, we lifted the concrete of the glass, broke the third and last layer and put the weight back on. The glass cracked and squeaked for a few minutes, and deflected a few cm. Then it stopped and an equilibrium was reached. In Figure D-86, the impact point of the hammer is visible as a discoloration in the glass.

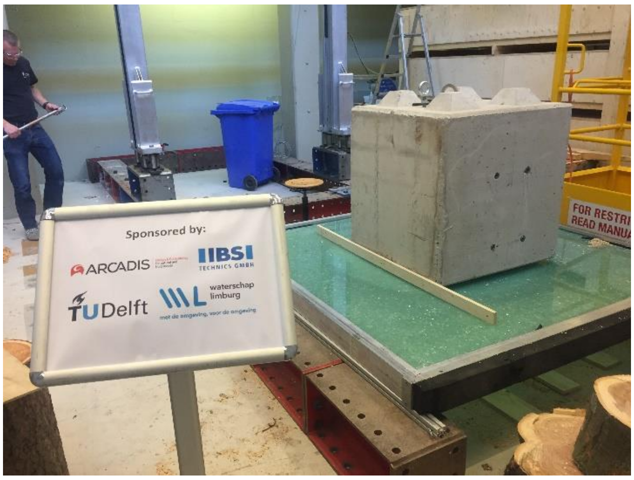

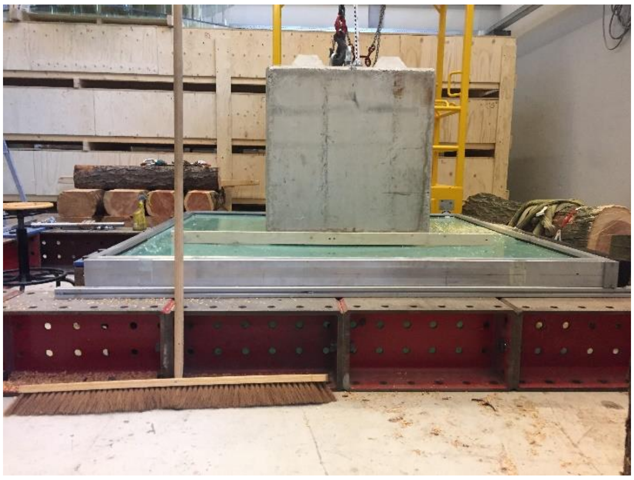

Figure 10-31: Free standing concrete block on three broken layers

Figure 10-32: Side view test 4.2

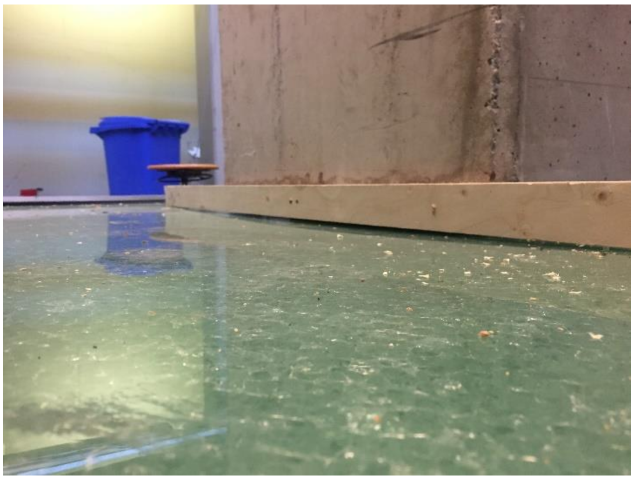
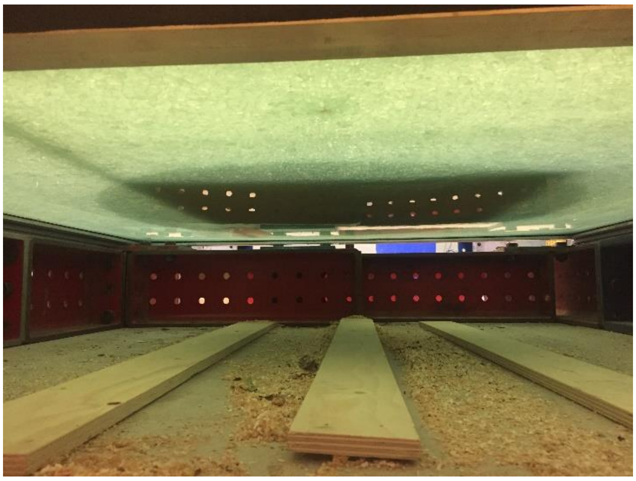

Figure 10-33: Visible sag of the panel

Figure 10-34: View under the panel, with location of hammer impact visible

10.3. Conclusion experiments

Conclusion results

All panels passed the limit of $490\ Nm$. Even with 1, 2 or 3 broken layers, the panels withstood the impact of the objects and the integrity of the structure was preserved according to the checklist from the pendulum test in 10.1.2. It can be concluded that, in the case of an impact, the thick glass is robust and has a high impact capacity concerning objects from organic material. Even with glass breakage there is sufficient residual strength to withstand more impacts and even significant static loads. The more layers were broken, the more elastic behavior the glass panel conducted, which results in the impact object bouncing back higher and higher.
The IBS structure withstood the loads without any problems, there was minimal visible damage except for some deformations in the frame profiles. The amount of material may be optimized to create a more elastic and economic structure.

Discussion

It was unfortunately not possible to obtain the displacements of the glass panel as the view was obstructed by the aluminum frame. The pure displacement was also compromised because along with the side posts, the test set up also deformed due to the large moments caused by impact of the heavy impact object. This caused a rotation, resulting in a larger deceleration distance. This larger deflection and rotation is more than assumed in the FEM analysis (no rotation). This must be kept in mind if the glass flood walls are constructed in reality; that the foundation might be stiffer, resulting in lower failure loads from impact.

In the static tests, the cyclic loading from waves is not taken into account. It is possible that if there is significant wave loading, the interlayer eventually collapses due to fatigue.
It is possible that due to fracturing, the glass is not watertight at the edges and progressive failure may be possible if the glass shards flush out (like the piping mechanism in dikes). This may be an interesting subject for further research.

Recommendations from the experiments

It is advised that in reality deformation/rotation space is incorporated in the design or foundation, so that in the case of an impact, there is a larger deceleration distance.
If there will be any other tests with these type of structures in the future, it may be interesting to test with HSG rather than FTG, as small mistakes can cause the complete layer to fracture immediately.

Delaminating of the panel after fracturing and impact can be investigated in further research on impact.

11. Conclusion, discussion and recommendations

11.1. Conclusions

The conclusions following the theory and experiment are given below.

11.1.1. Theory

The conclusions based on theory are divided into four main subjects:
Literature research on glass theory, the *glass calculations* and analysis of the different methods, the findings from the *FEM model* and the *probabilistic analysis* of the failure probability of the mechanism “structural failure”.

Literature research

- Glass exhibits brittle behavior and therefore impact loadings are far more of an issue than gradually introduced loads or distributed loads like wind or water pressure
- There is safety in numbers; adding more components to a glass member can increase the safety of a glass structure to almost the same level as other materials.
- After failure of all glass plies, laminated glass can still have significant residual capacity.
- Structural glass is still very much in development and there are no harmonized methods on how to calculate with structural glass within Europe.
- Due to the large spread in strength values found in research or structural codes, and the complexity of impact modelling, testing new glass applications on certain loads is necessary as there are no accurate methods to determine the minimal dimensions.
- Scaling of the tests is not possible due to the large effect flaws and cracks, scratches, the surface- and edge quality have on the strength of the glass.
- The disintegration of Fully Tempered Glass (FTG) is instant if failure somewhere in the glass occurs. This gives little to no residual capacity, or at least far less than an HSG or AG panel. Heat-Strengthened Glass (HSG) and Annealed Glass (AG) have a lower initial strength but better residual capacity after breakage.

Glass calculations

- The German structural glass code (TRLV) is very conservative compared to the Dutch and Italian codes, which results in more expensive and conservative design.
- For short duration loads such as an impact at low to normal temperatures, laminated glass acts almost as a monolithic pane of glass if a Sentryglass interlayer is used.
- The choice of interlayer is important and contributes significantly to the strength characteristics of laminated glass according to the Dutch and Italian methods and recent research. The German TRLV does not take the influence of the interlayer into account at all, which results in designing with the most economic option of interlayer, but not necessarily the most optimal.

FEM model

- The Aluminum side posts are very stiff and may be optimized to increase deformity to unburden the load on the glass in case of an impact (more deformation results in a longer deceleration distance, thus decreasing the concentrated load).
- It is therefore a good choice to use Aluminum over steel, as the modulus of elasticity of Aluminum ($70000\ N/mm^2$) is about 1/3 than that of steel ($210000\ N/mm^2$).

- A rotational spring can be built in at the foot of the structure, to increase deformity without decreasing the strength of the structure. This increases the impact capacity.
- The thickness and strength of the glass and the IBS Structure is more than sufficient to withstand the hydraulic loads.

Probabilistic analysis

Probabilistic analysis is an interesting way to find out hidden weaknesses and strengths of location bound specifics

11.1.2. Experiment

- After breakage, the panel still has significant residual capacity to withstand a static load of $1174\ kg$ on an area in the middle of the glass of $0.5 \times 0.5\ m$. This load causes similar internal moments in the panel as a water level up to the top of the structure in serviceability limit state, as analyzed with FEM analysis.
- The failure of FTG is sudden and can be caused by one small mistake or wrong inclination. The visibility is severely decreased if one glass layer fractures. With two fractured layers it is nearly impossible to see anything other than light and shadows through the glass. It can therefore be economical to use HSG, which exhibits even better residual capacity than FTG if laminated.
- Delamination between layers can occur if an already fractured layer is subjected to an impact loading.
- The more layers are fractured, the more elastic the glass panel behaves, resulting in lower impact loads due to a larger deceleration distance.

11.2. Discussion

11.2.1. Limitations and uncertainties

Glass calculations

- As there is no universal method to do calculations on glass, it is uncertain if the best/most accurate/safest method is used.
- The material glass is uncertain in itself, it has a wide range in strength and many factors contribute to eventual failure.
- Calculated with the NEN and CNR glass codes, there is a high coupling factor present if Sentryglass is used as interlayer, especially for short duration loads. This results in all cases in a coupling factor very close to 1. Which causes the effective plate thickness is to be close to the thickness for a monolithic glass plate of the same thickness including the foils. This may not be realistic on the long term and be an over-estimation of the strength.

FEM

- The modelling of an impact on brittle materials is very complex and time consuming, therefore a basic spring model is used to determine the critical impact load in this thesis.
- Only bending is considered as a failure mechanism in the glass, and this remains true if the impact object is of sufficiently soft material to prevent failure such as the fractured front layers of test 2.17. These were shattered by hard-on-hard impact, which can be the case for a boat's bow.
- The impact object is not modelled but represented as a static distributed load on a surface of $0.1 \times 0.1\ m$.

Failure probability analysis

This analysis is based on many uncertainties and assumptions and these are therefore not mentioned.

Experiment

- In the model the anchor posts are assumed to be fully clamped, while in the experiments this turned out not to be the case. This causes a longer deceleration distance and therefore a lower impact force. In reality this may be different.
- Only the impact of tree trunks was investigated in the tests, other impact objects and materials were not considered.

11.2.2. Experiments VS Theory

As it should be, the experiments showed far better results than the conservative calculations based on the NEN 2608 and FEM. The experiments gave more insight of the remaining bearing capacity of a broken panel, than could be found in literature. This remaining capacity can never be taken into account in practice, but it is an extra reassurance and is also used as safety check in other tests such as “Pendulum test” or the “Soft body impact test” and Hurricane glazing test.

11.2.3. Other aspects

Ecological

An obstruction for water usually is also an obstruction for (aquatic) life. A flood wall has a larger impact on the environment than a common levee with a mild slope and glass layer. The latter is easily implemented into a natural environment, whereas a glass wall is an obstruction to life in and out of water. Glass walls are responsible for countless amounts of bird-deaths each year. The ecological impact of glass flood walls was out of the scope of this research, but needs mentioning nevertheless.

Vandalism

It must be said, hard-on-hard impact on glass is still a large risk to the glass. It may nearly impossible to reach the inner layer by using a hammer or axe, certainly if sacrificial layers are applied, but the valued visibility and transparency is lost quickly. An option is to use a different type of glass like AG or HSG instead of FTG on the outer layers (or completely), as the fracture pattern has larger glass shards for more transparency and this is less “fun” to break. A combination will also increase the residual capacity, although this was already sufficient in the broken FTG panel to withstand the static tests.

11.3. Recommendations

The recommendations following this study are presented below:

- The aluminum structure (side posts) is very robust and safe; but to absorb an impact, it may be wise to use less material to create a more flexible structure. It can be optimized to create more deformation space and use less material, which also makes the structure a more economical option. Otherwise a rotational spring could be added to gain the same deformation space and decrease impact loads.
- It is uncertain if the glass is still water tight at the high water pressure up to the top of the structure with all layers broken. Progressive failure, like piping in a dike, may wash out glass particles causing the panel to fail eventually. This is interesting for further research.
- In the assessment of the static residual capacity of the panel, the impact of dynamic wave loading on the interlayer is not taken into account. In the American tests explained in the Hurricane glazing test paragraph, cyclic loading after breakage is part of the assessment. This may be interesting for future research.
- Look into the use of HSG glass rather than FTG glass. It has a lower initial strength, but also a lower breakage rate and higher residual capacity. Maybe add more layers with a smaller thickness as HSG is not available in $19\ mm$ glass thickness.
- The results of the experiment are not been used to re-validate the model due to time limitations. This can be interesting for further research, as the deformation of the set-up

during impact is not taken into account in the FEM model. Further validation can be used to improve the estimation of the critical impact energy.

- It is wise to improve the accuracy of the failure probability, this can be a MSc of its own.

Further research is required for:

- The probability of occurrence of an impact.
- The range of masses, velocities, materials, shapes of floating objects in the rivers.
- The impact of different types of impact objects (boats, cars, motorcycles).
- The rate of fatigue caused by cyclic wave loading in the Sentryglass interlayer after glass breakage.
- The water tightness and possible progressive failure (piping effect) due to washing out of glass particles (can be in combination with fatigue of the interlayer due to wave loading).
- The delamination after fracturing and impact.

Bibliography

Arcadis. (2016). *Toepasbaarheid van glas in waterkeringen* (Projectnummer: C03011.000435). Retrieved from intern network

Arcadis. (2017, 15 September) Memo ontwerpuitgangspunten glazen waterkeringen [memo]. Retrieved from intern network

BBC. (2016, 7 mei). Keswick's glass flood protection panels repaired. Retrieved from http://www.bbc.com/news/uk-england-cumbria-36236083

Blaauwendraad, J. (2006). *Plate analysis, theory and application*. Retrieved from Blackboard TU Delft

Bos, F. P. (2009). *Safety Concepts in Structural Glass Engineering: Towards an Integrated Approach*. Retrieved from https://repository.tudelft.nl/islandora/object/uuid:85191798-a57d-4be0-a0c0-7096dc2976fe?collection=research

Bower, B. (2016, 22 november). Glassmaking may have begun in Egypt, not Mesopotamia. Retrieved from https://www.sciencenews.org/article/glassmaking-may-have-begun-egypt-not-mesopotamia

CEN. (2007). *NEN-EN 1993-1-8:2006/NB:2007*. Retrieved from https://www.nen.nl/NEN-Shop/Norm/NENEN-1993182006NB2007-nl.htm
EN 1993-1-1 art. 6.2.3

CEN. (2011). *NEN-EN 1090-2:2008+A1:2011 nl*. Retrieved from https://www.nen.nl/NEN-Shop/Norm/NENEN-109022008A12011-nl.htm

CEN. (2011). *NEN-EN 1999-1-1+A1*. Geraadpleegd van https://www.nen.nl/NEN-Shop/Norm/NENEN-199911A12011NB2011-nl.htm

CEN. (2016). *NEN-EN 1993-1-1+C2+A1:2016*. Retrieved from https://www.nen.nl/NEN-Shop/Norm/NENEN-199311C2A12016-nl.htm

Corning. (2015, September). Corning® Gorilla® Glass for Large Format Applications [Dataset]. Retrieved from http://www.corning.com/microsites/csm/gorillaglass/PI_Sheets/CGG_PI_Sheet_Large_Cover.pdf

Delincé, D., Callewaert, D., Belis, J., & Van Impe, R. (2008, April). Post breakage behavior of laminated glass in structural applications. Retrieved from https://www.researchgate.net/publication/265988738_Post-breakage_behavior_of_laminated_glass_in_structural_applications

Derstrong Enterprise. (n.d.). EN 356 Falling Ball Test. Retrieved November 6, 2018, from http://www.derstrong.com.tw/EN356-Certificate.htm

DuPont. (n.d.). Laminated Glass Interlayers for Stronger, Safer Glass. Retrieved September 28, 2017, from http://www.dupont.com/products-and-services/construction-materials/safety-glass-interlayers/brands/sentryglas-ionoplast-interlayer.html

Elite Window Film. (n.d.). Missile impact and cyclic test loading. Retrieved 7 November 2018, from http://ftl-incinfo.com/index.php/testing/impact-cyclyc-load-testing

European Commission. (2014). *Guidance for European Structural Design of Glass Components* (Support to the implementation, harmonization and further development of the Eurocodes). Retrieved from https://bib.irb.hr/datoteka/703795.lbna26439enn.pdf

European Commission Erasmus Mundus, Ungureanu, V., & Jordão, S. (2014). Advanced design of glass structures [College-slides]. Retrieved from http://www.ct.upt.ro/suscos/files/2013-2015/1E05/2E5_Glass_structures_L3_2014_VU.pdf

FloodControlTV. (2012, July 2). Glass Flood Barrier in Wells by Flood Control International [Youtube]. Retrieved November 5, 2018, from https://www.youtube.com/watch?v=ujJHfabjD24&feature=youtu.be

Flood Control International. (2017). *Glass Barriers*. Retrieved from http://www.floodcontrolinternational.com/PRODUCTS/FLOOD-BARRIERS/Glass-dl4.php

GIB GMBH. (n.d.). Fall protections. Retrieved November 6, 2018, from https://www.gib-gmbh.com/en/safety-technology/fall-protections/

Hagen, C. W. (2017). *Developments in reinforced glass beams* (Using post-tensioned GFRP strips, fibreglass fabric and sequential linear analysis). Retrieved from https://repository.tudelft.nl/islandora/object/uuid%3A22cf6e1e-7317-4140-84d1-d6b63caa2e36?collection=education

Haldimann, M. (2006). *fracture strength of structural glass elements – analytical and numerical modelling, testing and design* (Doctoral Thesis). Retrieved from https://infoscience.epfl.ch/record/89658/files/EPFL_TH3671.pdf

Heyder, F., & Paulu, F. (2012). A laminated glass wall will protect Warnemünde from high water. In F. Veer, R. Nijsse, & F. Bos (Eds.), *Challenging Glass 3, Conference on Architectural and Structural Applications of Glass* (pp. 75-82). Retrieved from http://www.sturmflutschutz-warnemuende.de/literature/505_Heyder_Paulu_flood_protecting_glass_wall_index_i1.pdf

Jonkman, S. N., Jorissen, R. E., Schweckendieck, T., & Van den Bos, J. P. (2017). *Flood Defences Lecture notes CIE5314* (2nd ed.). Retrieved from TU Delft Blackboard

Hartsuijker, C. (2001). *Toegepaste Mechanica, deel 2: Spanningen vervormingen , verplaatsingen*. Amsterdam, Nederland: Academic Service.

Helpdesk water. (n.d.-b). Waterwet. Retrieved October 5, 2018, from https://www.helpdeskwater.nl/onderwerpen/wetgeving-beleid/waterwet/

IBS engineered products. (z.j.). Glass Flood defence System. Retrieved from http://www.ibsengineeredproducts.co.uk/disaster-prevention/glass-walls/

Itv News. (2015, 5 december). Storm Desmond floods breach defences in Keswick. Retrieved from http://www.itv.com/news/update/2015-12-05/storm-desmond-floods-breach-defences-in-keswick/

Kentrop, J. (2016). *Design and reliability evaluation of a glass flood defence* (MSc. Thesis). Geraadpleegd van https://repository.tudelft.nl/islandora/object/uuid:7f4a8b7d-e00e-4818-8340-be1d3284b857/datastream/OBJ/download

Kuraray. (n.d.). SentryGlas®. Retrieved September 28, 2017, Retrieved from https://www.trosifol.com/https://www.trosifol.com/products/architecture/trosifolr-structural-security/sentryglasr/

Limburg 1. (2013, 15 december). Arcen 1993: Het water kwam door de stopcontacten. Geraadpleegd op 21 september 2018, van https://l1.nl/arcen-1993-het-water-kwam-door-de-stopcontacten-30025

Louter, C., Leung, C., Kolstein, H., & Vamberský, J. (2010). Structural Glass Beams with Embedded Glass Fibre Reinforcement. *Challenging Glass 2*, *1*, 439-448. Retrieved from uuid:a49771ad-26e1-453f-b69f-b590883dfc51

Rijkswaterstaat. (2014). *Eindrapportage Veiligheid Nederland in Kaart* (VNK). Retrieved from https://staticresources.rijkswaterstaat.nl/binaries/Eindrapport%20Veiligheid%20Nederland%20in%20Kaart_tcm21-63921.pdf

Mystery of Prince Rupert's Drop at 130,000 fps - Smarter Every Day [Video file]. (2013, March 22). Retrieved from https://www.youtube.com/watch?v=xe-f4gokRBs

Nijsse, R. (2003). *Glass in Structures*. Basel, Switzerland: Birkhäuser.

Oikonomopoulou, F., Bristogianni, T., Veer, F. A., & Nijsse, R. (2017, March 9). *The construction of the Crystal Houses façade: challenges and innovations*. Retrieved from https://repository.tudelft.nl/islandora/object/uuid%3Ad3f68471-ee0b-422e-93b9-b8438de5b8eb?collection=research

Oikonomopoulou, F., Van den Broek, E. A. M., Veer, F. A., Nijsse, R., & Bristogianni, T. (2017, April 10). Design and experimental testing of the bundled glass column. Retrieved from https://repository.tudelft.nl/islandora/object/uuid%3Ad020d5a3-ceee-4d70-b52e-ce85fd80cc67?collection=research

Schijf WVB. (n.d.). Glasparel slingerproef. Retrieved November 6, 2018, from https://www.schijf-wvb.nl/glasparel-slingerproef/

SCIA Engineer. (2016). *Handboek Doorsneden*. Retrieved from https://help.scia.net/download/17.0/nl/Cross-sections_nld.pdf

Sebastiaan N. Jonkman, Hessel G. Voortman, Wouter Jan Klerk & Saskia van Vuren (2018): Developments in the management of flood defences and hydraulic infrastructure in the Netherlands, Structure and Infrastructure Engineering, DOI: 10.1080/15732479.2018.1441317

Sectional characteristics calculated by FEM [Help]. (n.d.). Retrieved June 15, 2018, from https://help.scia.net/15.1/en/rb/crosssections/sectional_characteristics_calculated_by_fem.htm

Sedlacek, G., Blank, K. and Gusgen, J., (1995). *Glass in structural engineering.* The Structural Engineer, 73(2), 17-22.

STOWA. (2015). *Leidraad Toetsen op Veiligheid Regionale Waterkeringen* (STOWA 2015-15). Retrieved from http://stowa.nl/upload/publicatie2014/LTV%20regionale%20waterkeringen%202015/STOWA%20MODULE%20INTRODUCTIE%20MET%20BIJLAGEN%20EN%20REFERENTIE.pdf

Timoshenko, S., & Woinowsky-Krieger, S. (1959). *Theory of plates and shells* (2nd ed.). New York, USA: McGraw-Hill Book Company.

Veer, F., Louter, P., & Bos, F. (2009). *The strength of annealed, heat-strenghtened and fully tempered float glass*. Fatigue & Fracture of Engineering Materials & Structures, 32, 18-25

Vitalis, D. (2017). *Glass Sandwich Panel*. Retrieved from https://repository.tudelft.nl/islandora/object/uuid:8414bc7f-6dcc-49ad-b16b-2bc92a29fee6?collection=education

VolkerStevin. (2012, 16 februari). Unique glass wall preserves views of Keswick. Retrieved from http://www.volkerstevin.co.uk/en/news/detail/unique-glass-wall-preserves-views-of-keswick

Wagemaker. (2017). *Berekening* (Twee bruggen Prinses Irenestraat). Retrieved from https://www.odnzkg.nl/mozard/document/docnr/8401336,,7864674,/W17078%20RAP01_v10_pdf%20.pdf

Waterschap Limburg. (2017). *Crisisplan Waterschap Limburg* (Corsanummer: 1602416). Retrieved from https://www.waterschaplimburg.nl/publish/pages/3466/crisisplan_waterschap_limburg.pdf

Waterschap Peel en Maasvallei Venlo. (2016). *Evaluatie Regionale Wateroverlast 30 mei t/m 1 juli 2016*. Retrieved from https://www.waterschaplimburg.nl/publish/library/6/evaluatie_wateroverlast_juni_2016_wpm.pdf

WBI 2017. (2015). *Toetsspoorrapport Sterkte en Stabiliteit puntconstructies*. Retrieved from: https://www.helpdeskwater.nl/onderwerpen/waterveiligheid/primaire/beoordelen-wbi/producten-wbi/

WBI 2017. (2017). *Schematiseringshandleiding sterkte en stabiliteit kunstwerk*. Retrieved from https://www.helpdeskwater.nl/algemene-onderdelen/structuur-pagina/zoeken-site/@178897/laag-2-1/

Wierzbicki, T., & MIT. (2006). *Plates and shells*. Retrieved from http://hdl.handle.net/1721.1/45585

A. Load specification

A.1. NEN-EN 1990+A1+A1/C2:2011

A.1.1. Basis of structural design

Consequence class

In accordance of the European Standard EN 1990, the structure will be classified according to their consequences in case of failure. Glass is not known for its robustness, and structures containing glass need to be of a low consequence class or have a high redundancy. The Italian code CNR-DT 210/2013 for glass also includes a class zero.

Table A-1: Explanation Eurocode consequence classes [CNR-DT 210/2013]

Class	Code	Description	P_f (per 50 years)	P_f (per year)
Class 0	CC0	specifically non-structural construction products. Their failure has extremely limited consequences in economic, social and environmental terms and in terms of loss of human life.	Not Specified	Not specified
Class 1	CC1	structural elements. Their failure has limited consequences in terms of loss of human life and small or negligible consequences in economic, social or environmental terms. This category includes structures in buildings where people are present only occasionally and, by extension, those glass elements whose structural failure has limited consequences.	$4.83 \cdot 10^{-4}$	$1.335 \cdot 10^{-5}$
Class 2	CC2	structural elements. Their failure has medium consequences in terms of loss of human life and considerable consequences in economic, social or environmental terms. Examples of structures that belong to this class are residential or office buildings. By extension, the class includes all structural elements whose failure leads to consequences of a medium level of severity.	$7.235 \cdot 10^{-5}$	$1.30 \cdot 10^{-6}$
Class 3	CC3	structural elements. Their failure has high consequences in terms of loss of human life and very great consequences in economic, social and economic terms. Structures which belong to this class are public buildings, stages and covered grandstands, where the consequences of failure are high (for example concert halls, shopping malls susceptible to overcrowding, etc.). By extension, the class includes all structural glass elements whose failure has severe consequences.	$8.54 \cdot 10^{-6}$	$9.96 \cdot 10^{-8}$

For primary flood defences, consequence class CC3 is mandatory. This results in a yearly probability of failure of $9.96 \cdot 10^{-8}$ for a structural element. However, the consequences of flooding in this area are not so severe, and according to the NEN 2608:2014, the consequence class may be scaled down if in the risk analysis the consequences are concluded to be of an lower order OR all following requirements are met:

- The surface of the element is less than 20 m² (yes)
- The fundamental loading combination with extreme variable load is not the governing fundamental load combination (depends)

A.2. Load specifications

A.2.1. Partial safety factors

Table A-2: Partial safety factors

	Symbol	Factor
Self-weight glass	$\gamma_{G1,g}$	1.35
Self-weight other	γ_{G1}	1.35
Dead load	γ_{G2}	1.5
Variable load	γ_{Q}	1.5
Water and wave pressure	γ_{w}	1.5*
Incidental load (collision)	γ_{A}	1.0

A.3. Loading scenarios

There are three loading scenarios that need to be considered. For the reassurance of the public, it needs to be proven that the laminated glass panel can withstand a certain impact load and maintain its water retaining function. The following load scenarios are investigated and put in order. There are no permanent loads on the structure and self-weight is considered to be negligible.

A.3.1. Fundamental loading combination 1

The typical situation for the glass panels will be that of high water levels in the river Maas. The normative load combination is that of static water pressure and wave loading.
The general formula for the characteristic loading combination is:

$$E_d = E\{G_{k,j}; P; Q_{k,1}; \psi_{0,i} Q_{k,i}\} \; j \geq 1; i > 1$$

Which can be formulated as (the most unfavorable combination):

$$\sum_{j\geq 1} \cancel{\xi_j \gamma_{G,j} G_{k,j}} \text{"} + \text{"} \cancel{\gamma_P P} \text{"} + \text{"} \gamma_{Q,1} \mathrm{Q}_{\mathrm{k},1} \text{"} + \text{"} \sum_{i>1} \gamma_{Q,i} \psi_{0,i} Q_{k,i}$$

Of which both P(prestressing force) and G(self-weight) can be neglected. Water pressure and wave pressure are both variable loads, with water pressure being the governing variable load

$\gamma_{Q,1}$ = 1.25 $\mathrm{Q}_{\mathrm{k},1}$ = linear static water pressure up to the top
$\gamma_{Q,2}$ = 1.25 $\mathrm{Q}_{\mathrm{k},2}$ = Sainflou wave pressure
$\psi_{0,2}$ = 1.0

A.3.2. Incidental combination pre-failure 2

A large object floats on the river during the flood, this can be a loose yacht, a tree or floating debris. It collides into the structure with a TBD speed and angle. It is calculated in two combinations: water load up to the top of the structure with a point load also on top, and water pressure up to the middle of the structure, wave load(see wave load assumptions) from the still water level and a point load in the middle of the plate.

The general formula for the incidental loading combination is:

$$E_d = E\{G_{k,j}; P; A_d; (\psi_{1.1} \; or \; \psi_{2,1}) Q_{k,1}; \psi_{2,i} Q_{k,i}\} \; j \geq 1; i > 1$$

And can be formulated as:

$$\sum_{j\geq 1} \cancel{G_{k,j}} \text{"} + \text{"} \cancel{P} \text{"} + \text{"} A_d \text{"} + \text{"} (\psi_{1.1} \text{ or } \psi_{2.1}) \mathrm{Q}_{\mathrm{k},1} \text{"} + \text{"} \sum_{i>1} \psi_{2,i} Q_{k,i}$$

Of which both P(prestressing force) and G(self-weight) can be neglected.
A_d = the equivalent static force inflicted by a collision, see "loads"
$Q_{k,1}$ = linear static water pressure up to the middle of the structure
$\psi_{1.1}$ = instead of 0.5, a factor of 1.0 is chosen and the height of the water is reduced
$Q_{k,2}$ = Sainflou wave pressure $\psi_{2.2}$ = 0.3

Note: Speed, mass, stiffness, impact area and impact angle of the floating object have probabilistic distributions; which can be determined or estimated based on the available information and common sense.

A.3.3. Incidental combination post-failure 3

The glass panels are broken by a large mass impact, but are not punctured and still have residual strength. It is almost certain that in case of a floating object impact, there are also high water levels. The load combination after "failure" will be that of the water pressure, and cyclic wave loading. Glass itself is not susceptible to fatigue, but the interlayer is; therefore the number of wave-cycles is also a factor to take into account.
Note: Another large mass impact can lead to complete failure of the panel, but will not be taken into account as this is reasonably not possible to design the structure on. It will be included in the probability of failure when conducting the full probabilistic calculation.

A.4. Loads

There are many possible loads that could act on the structure, but the three governing loads are presented below. Wind loading, human-induced loads and collisions by cars are not taken into account as they are negligible compared to water- and wave pressure or an collision with floating debris.

A.4.1. Water pressure

The water in the river is fresh, 1000 [kg/m³], this results in a load of 10 [kN/m³]. The water level has a large spreading in the river Meuse and can vary a few meters.

A.4.2. Wave loading

Wave loading according to Sainflou is used for preliminary design. Since the waves occurring at the structure are wind waves, their wave length is estimated to be 2x the wave height. Wave height 1.5 m from the Arcadis report (used for overtopping?) is very large for the Maas river and may be unrealistic. Sainflou also leeds to an overestimation of the load for short waves. Therefore the design wave height is chosen to be 0.75m, with a wave length of 1.5 m.

A.4.3. Collision force or impact load

This dynamic force is incidental, with a very low probability of occurrence. It depends on many factors, of both the structure and incoming object. The equivalent static force can be calculated, however, methods on this subject vary enormously and a specific method for impact on laminated glass is not yet defined. The discussion on whether or not it is reasonable to design for this force is ongoing but an attempt is made to calculated this resultant force with the model described in Appendix B.

B. Collision Energy

B.1. NEN-EN 1991-1-7+C1+A1

B.1.1. Eurocode 1: Actions on structures - Part 1-7: General actions - Accidental actions

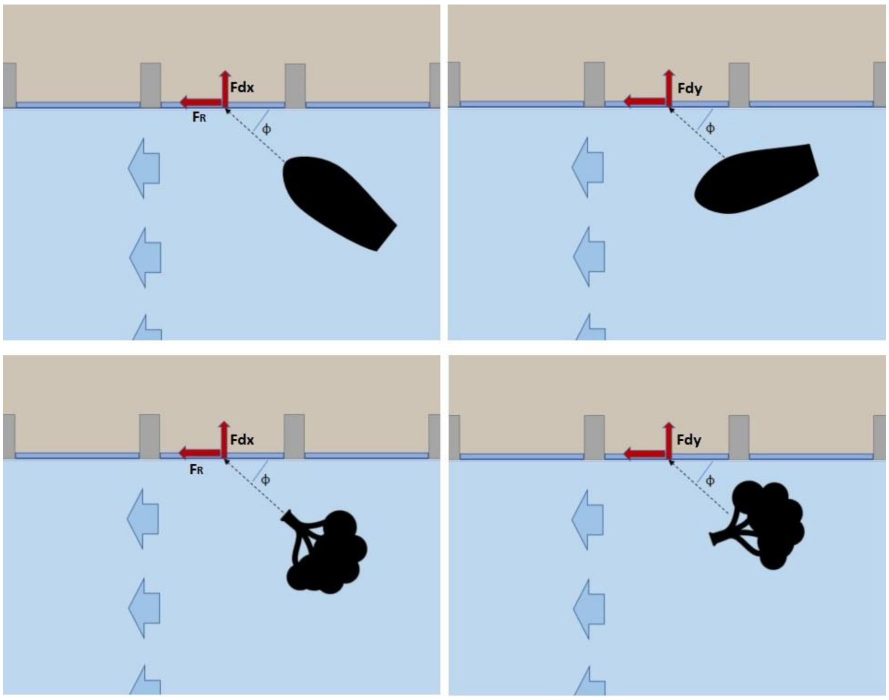

Figure B-1: Impact angle of floating objects

The following formula holds for F_R:

$$F_R = \mu \cdot F_{dy}$$
$$F_{dx} = F \cdot \sin(\varphi)$$

F = the total collision force
F_{dx} = the design value of the frontal collision force
F_{dy} = the design value of the lateral collision force
F_R = collision force due to friction
φ = angle of incidence
μ = the friction coefficient by a lateral collision (advised value =0.4)

According to the NEN-EN 1991-1-7+C1:2011/NB (National Annex to NEN-EN 1991-1-7+C1: Eurocode 1: Actions on structures - Part 1-7: General actions - Accidental actions) shipping area's where only touristic shipping takes place, it is advised to take the following forces into account:
F_{dx} = 500 kN
F_{dy} = 250 kN

When there is high water, no large ships are allowed on the river. High water usually occurs in wintertime, the amount of pleasure boats like small yachts and sailing boats are small but their presence is not forbidden(yet). It is also possible that smaller boats are drifting on the river by accident. The glass walls are at most locations placed parallel to the river stream, therefore it is assumed that there will be no frontal collision with a boat, but the design value for a lateral collision force is assumed to be sufficient for the preliminary calculations, 250 kN.

Unless specified otherwise: the speed of a colliding ship is assumed to be 3 m/s plus the speed of the water. In ports the speed of ships can be assumed to be 1.5 m/s. Since in our case, with high water, boats and ships are not allowed on the river, mainly drifting ships and debris will collide with the structure. The speed of the water is determined in the reference situation to be between 1.4-2.4 m/s at several locations along the Maas river and . The angle of incidence is the highest for Steyl-Maashoek, around 40°. Most of the other locations have smaller angles of incidence and a minimum is set at 22.5°.

B.2. Impact energy (Kinetic energy)

The well-known formula to calculate kinetic energy:

$$E_{kin} = \frac{1}{2}mv^2$$

Where:
m = Mass [kg]
v = Speed [m/s]

The formula for potential spring energy:

$$E_{pot} = \frac{1}{2}ku^2$$

k = Spring stiffness [kN/m]
u = Displacement [m]
Kinetic energy is usually measured in units of Joules (J); where one Joule is equal to 1 $kg \cdot m^2/s^2$.
Potential Energy is usually measured in $N \cdot m$, which are equal to Joules by the relation:

$$1\ N = 1\ kg \cdot \frac{m}{s^2}$$

The equivalent force (in N) that comes from the energy that excites the spring(the structure)
From Hooke's law (the force is proportional to the extension) follows:

$$F = k \cdot u$$

$$E_{pot} = \frac{1}{2}ku^2 = \frac{1}{2} \cdot F \cdot u \rightarrow F = \frac{2 \cdot E_{pot}}{u}$$

The relation between force, energy an spring stiffness becomes:

$$E_{pot} = \frac{1}{2}ku^2 \rightarrow u = \sqrt{\frac{2 \cdot E_{pot}}{k}} \rightarrow F = k \cdot \sqrt{\frac{2 \cdot E_{pot}}{k}} = \sqrt{2 \cdot k \cdot E_{pot}}$$

Because the kinetic energy of the incoming object needs to be absorbed by the structure, the structure's potential energy needs to absorb this energy. The law of conservation of energy states that no energy is lost, only transferred. Besides spring energy, which can be seen as the elastic deformation of the structural components, more energy can be transferred if the maximum potential spring energy is breached and permanent deformation starts to take place in the structure: plastic deformation or fracture. Glass does not exhibit plastic deformation and the energy is dissipated by fracturing. The law of conservation of energy assumes equilibrium:

$$E_{total} = E_{kin} + E_{pot} + E_{other} = 0$$

Where:

$$E_{pot} = E_{elastic} + E_{fracture} + E_{plastic}$$

$$E_{kin} = E_{object} + E_{water}$$

By neglecting the contribution of E_{other}(for example energy dissipating by the damping of the water) and $E_{plastic}$(the plastic deformation of the Aluminum frame structure) the simple case that the strength of the glass is governing, the frame is assumed to be infinitely stiff in comparison to the glass plate.

B.3. Kinetic energy of a berthing ship

An approximation of the kinetic energy of colliding ships can be found in the manual Hydraulic structures. The method for the calculation of berthing forces of ships is similar to an impact force. In this method the collision is modelled as a mass-spring system, with 3 masses and 3 springs which represent the ship, the water and the structure. For a preliminary design damping is neglected which results in a conservative approach. It must be added that this method is used for large berthing ships, therefore some of the parameters are estimated (instead of calculated) based on the situation of a “weak” structure and smaller boats.

The force on the structure can be calculated by:

$$F = k \cdot \Delta x = \sqrt{2 \cdot k \cdot E_{kin,max}}$$
$$\rightarrow k^2 \cdot \Delta x^2 = 2 \cdot k \cdot E_{kin,max}$$
$$\rightarrow k \cdot \Delta x^2 = 2 \cdot E_{kin,max}$$

We then arrive at the relation:

$$\rightarrow F \cdot \Delta x = 2 \cdot E_{kin,max}$$

Where:

F = the berthing or collision force
k = the spring stiffness of the structure
Δx = the displacement
$E_{kin,max}$ = the kinetic energy

The kinetic energy of the ship consists of the mass and velocity of the ship itself, but also the displaced water around the ship; added mass. The equation for the kinetic energy then becomes:

$$E_{kin} = \frac{1}{2}(m_s + m_w) \cdot v_s^2$$

If the stiffness of the structure is unknown; the amount of energy that needs to be absorbed by the structure is given by:

$E_{kin} = \frac{1}{2} \cdot m_s \cdot v_s^2 \cdot C_H \cdot C_E \cdot C_S \cdot C_C$ or $E_{kin} = \frac{1}{2}(m_s + m_w) \cdot v_s^2 \cdot C_E \cdot C_S \cdot C_C$

Table B-1: kinetic energy of a berthing ship explanation

Symbol	Meaning	Formula or explanation	Value
$\boldsymbol{m_s}$	the mass of the ship	$\rho \cdot L \cdot B \cdot D \cdot C_b$ or an estimation	3000 [kg] $(1000 \cdot 4 \cdot 1.5 \cdot 0.5)$

$\boldsymbol{m_w}$	the added mass of water	$\rho \cdot L \cdot \frac{1}{4} \cdot \pi \cdot D^2$	785 [kg] $(1000 \cdot 4 \cdot \frac{1}{4} \cdot 3.14 \cdot 0.5^2)$
$\boldsymbol{\rho}$	Specific weight of water	Fresh water	1000 [kg/m³]
$\boldsymbol{L}$	Length of the ship	-	~4 [m]
$\boldsymbol{B}$	Width of the ship	-	~1.5 [m]
$\boldsymbol{D}$	Draught of the ship	-	~0.5 [m]
$\boldsymbol{v_s}$	the velocity of the ship	$v \cdot \sin(\varphi)$ (with v=2.5 and φ=30)	~1.25 [m/s]
$\boldsymbol{C_H}$	the hydrodynamic coefficient	$\frac{m_s + m_w}{m_s} = 1 + \frac{D}{B}$	1.26
$\boldsymbol{C_E}$	the eccentricity coefficient	$\frac{k^2 + r^2 \cdot cos^2(\gamma)}{k^2 + r^2}$	0.816
$\boldsymbol{k}$	Radius of gyration	$(0.19 * C_b + 0.11) \cdot L$ With $C_b = 1.0$	1.2
$\boldsymbol{r}$	Distance between center of m_s and contact point	estimation	~2 [m]
$\boldsymbol{\gamma}$	Impact radius	Estimation	~30 [°]
$\boldsymbol{C_S}$	the softness coefficient	Weak structure	1.0
$\boldsymbol{C_C}$	the configuration coefficient	Damping of water between ship and structure	1.0

$$E_{kin} = \frac{1}{2} \cdot 3000 \cdot 1.25^2 \cdot 1.26 \cdot 0.816 \cdot 1.0 \cdot 1.0 = 2409.75\ Nm$$

This is an approximation of the kinetic energy of large ships, and may not be applicable in this case. It is a positive feature that this method takes the added mass of water into account, but this may also be a lot less due to the smaller dimensions and low velocities in this case.

B.4. Kinetic energy of a tree

Similar to the previous approximation of the kinetic energy of a ship, a simplified calculation can be done for other objects. The well-known formula of $E_{kin} = \frac{1}{2} m v^2$ can be used. Because the tree or tree-branch is carried by the water, there is no added mass.

With a mass of a tree ranging between 80-750 kg, with diameters ranging from 0.15-0.40 meters [Arcadis], and a flow velocity and angle of incidence for the different locations are given below:

Table B-2: Impact information different locations

Loacation	Flow velocity v	Angle of incidence α
Well	-	-
Arcen	1.9 [m/s]	22.5°
Steyl-Maashoek	1.33 [m/s]	40°
Belfeld	2.0 [m/s]	22.5°
Kessel	1.72 [m/s]	22.5°
Buggenum	1.40 [m/s]	22.5°
Wessem	2.4 [m/s]	Large (45° is assumed)

[Arcadis]

The impact speed perpendicular to the structure can be calculated with:

$$v_{\perp} = v \cdot \sin(\alpha)$$

And the speed parallel to the structure:

$$v_{=} = v \cdot \cos(\alpha)$$

The kinetic energy becomes:

$$E_{kin} = \frac{1}{2} m (v \cdot \sin(\alpha))^2$$

The most unfavorable situation occurs at Wessem, where $v_{\perp}$ can become

$$v \cdot \sin(\alpha) = 2.4 \cdot \sin(45) = 1.7 m/s$$

And

$$E_{kin} = \frac{1}{2} \cdot 750 \cdot (1.7)^2 = 1083.75\ Nm$$

In comparison to the laboratory tests: this is the same amount of kinetic energy as a tree of 140 kg, going at a speed of 3.93 m/s.

B.5. The impact load

The structure and its different parts all have their own stiffness which can be modelled as a multiple mass-stiffness system as long as elastic deformation takes place and no fracturing occurs.

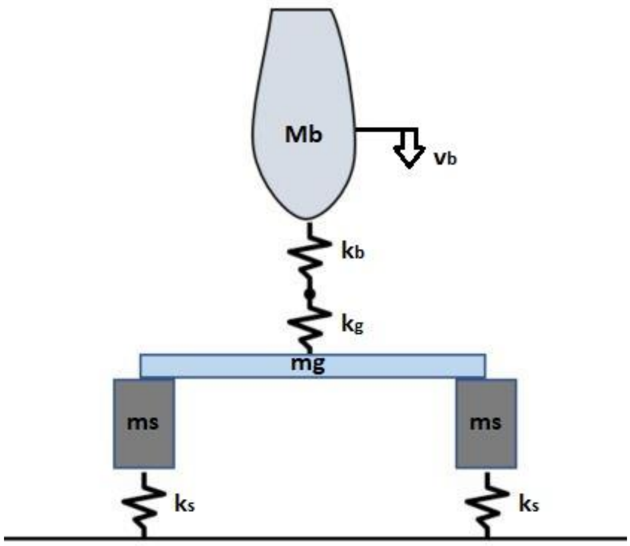

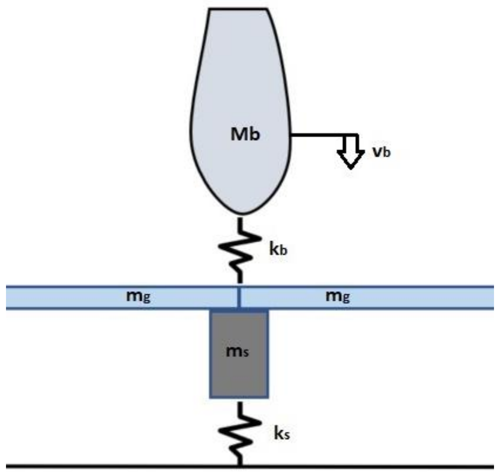

Figure B-2: Simple spring model impact on glass

Figure B-3: Simple spring model impact on side post

Where:

M_b = the mass of the boat
m_g = the mass of the glass panel
m_s = the mass of one support
k_g = the stiffness of the glass panel
k_s = the stiffness of one support
v_b = velocity of the boat perpendicular to the structure

B.6. Force distribution in the plate

There are 3 situations that can occur for the distribution of forces in the plate if the collision happens in the middle of the plate:

1. The panel as a wide beam
2. The panel as a simply supported plate
3. The panel as a high plate

The panel as a wide beam

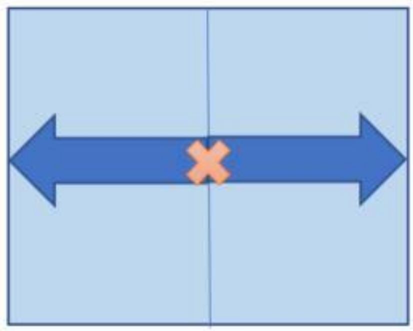

Figure B-4: the panel as a wide beam

The stress distributions in the plate are of the first order, in one direction and beam theory of the Euler Bernoulli beam (or Navier beam) is applied because of the low thickness-length ratio. See the equations for the beam stiffness below.

The panel as a simply supported square plate

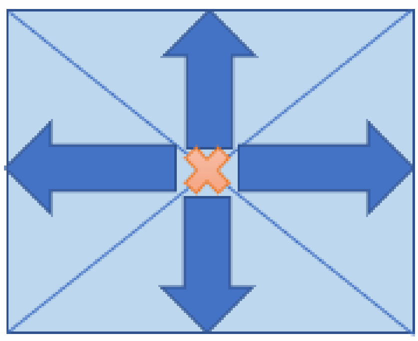

Figure B-5: The panel as a simply supported square plate

The stresses in the plate are of higher order and in two directions, they can be approximated with Kirchhoff-Love theory because the theory of thin plates applies.

The panel as a high plate(strip)

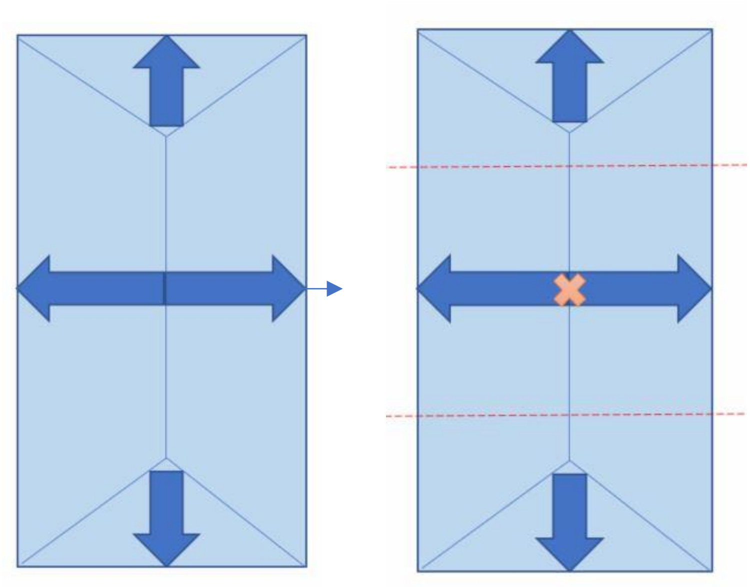

Figure B-6: The panel as a strip

The forces will be distributed for the large part like a beam, with a width assumed to be equal to the span of the plate.

It is assumed that the behavior of a square plate will be in between situation 1 and 2, situation 3 is mentioned as an alternative. We first assume the plate as a wide beam

B.7. Structure stiffness beam

The stiffness of the glass panel as a beam can be derived easily by forget-me-nots, simply supported on both sides. The beam stiffness becomes $EI = E \cdot \frac{1}{12} \cdot b \cdot h^3$, and spring stiffness k can be derived by using the forget-me-nots and convert the formula for the deflection into a formula for the spring stiffness k.

$$F = k \cdot u \rightarrow k = \frac{F}{u}$$

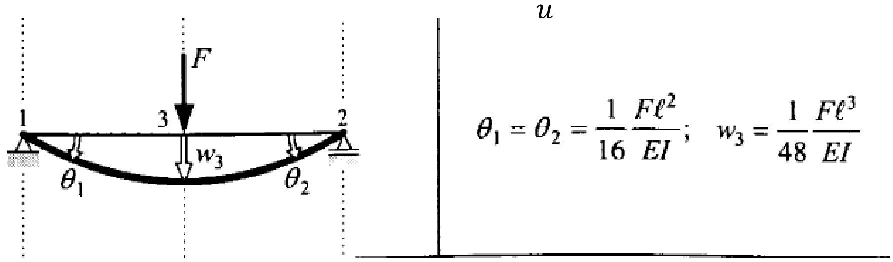

Figure B-7: Displacement simply supported beam with concentrated load

$$k = \frac{F}{u} = \frac{48EI}{l^3}$$

For a simply supported beam.

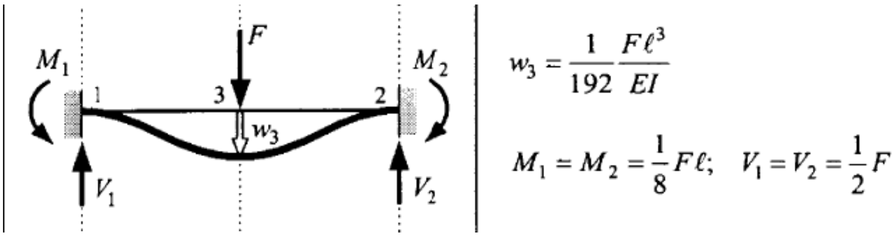

Figure B-8: Displacement clamped beam concentrated load

$$k_g = \frac{F}{u} = \frac{192EI}{l^3}$$

For a clamped beam. Since the glass panel is partly clamped in reality, the spring stiffness will be between these two values, but the most unfavorable situation is that of a simply supported beam.

Spring stiffness of the support beams

The spring stiffness of the support beams however, are a bit more complicated as the spring stiffness also depends on the height if the impact. The lower the impact, the stiffer the spring. In the forget-me-not the height of the impact is represented by l, and F is the impact force.

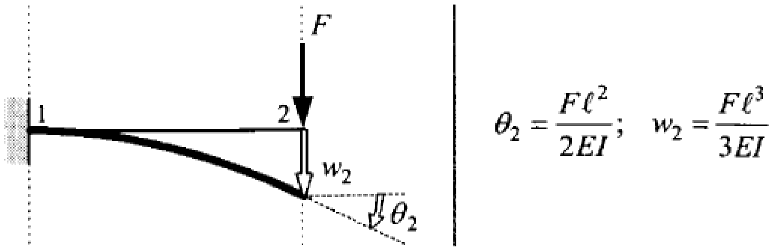

Figure B-9: Displacement cantilever concentrated load

$$k = \frac{F}{u} = \frac{3EI}{l(x)^3}$$

If the impact is on the glass, it is likely that the force F will be distributed over the two supports, and half of the load F is assumed to be uniformly distributed over the full support height. The deflection in the middle of the support is composed of the deflection of the distributed load up to the half of the height and an additional moment.

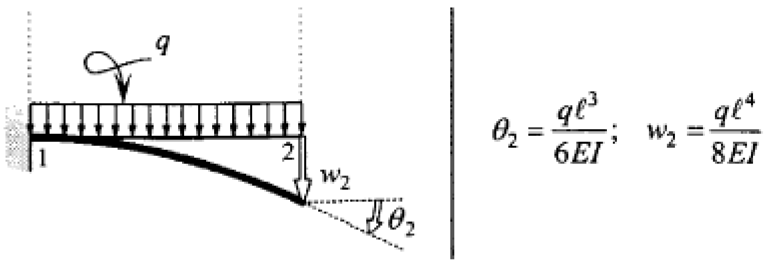

Figure B-10:Displacement cantilever distibuted load

$q = \frac{F}{2 \cdot l}$ and $q = u \cdot \frac{8EI}{l^4}$

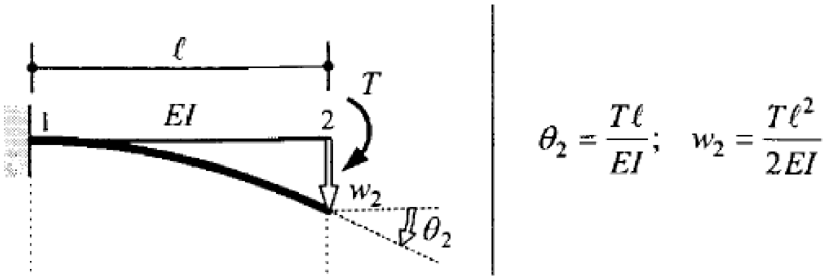

Figure B-11: Displacement cantilever with moment

$$T = \frac{1}{2} l \cdot q \cdot \frac{1}{4} l = \frac{1}{8} l^2 \cdot q (= \frac{F}{2 \cdot l}) = \frac{Fl}{16}$$

$$u = u_1 + u_2 = \frac{Fl^3}{16EI} + \frac{Fl^3}{32EI} = \frac{3}{32} \frac{Fl^3}{EI}$$

$$k = \frac{F}{u} = \frac{32EI}{3l^3}$$

The spring of the incoming object depends on the properties of the object, this can be a boat, large or small, which can have various bow-stiffness, and an assumption has to be made. Below the mean spring-stiffness of a few objects are presented.

Table B-3: Spring stiffness different objects

Type of object	Spring stiffness [kN/m]	Source
Car	300	NEN-EN 1991-1-7+C1+A1:2015 , table C.1
Wooden pole/tree	1508 kN/m	NEN-EN 338

B.8. Wooden pole

The spring stiffness of a wooden tree/beam or pole in axial direction is computed below. We take the mean bending elasticity E_{mean} of wood, and multiply this by the mean value of the section surface A.

$$N = EA \cdot \frac{du}{dx} = EA \cdot \varepsilon$$

Where the axial force N is the force F, $\varepsilon = u/l$ the extension $\left[\frac{m}{m}\right]$ and $k = EA/l$.

Table B-4: Dimensions/properties impact object tree

Properties/ dimensions	Symbol	Mean	Range	Source
E-modulus	E	$11.5 \cdot 10^3\ [kN/m^2]$	$[7-16] \cdot 10^3\ [kN/m^2]$	NEN-EN 338
Density	ρ	$435\ [kg/m^3]$	$350-520\ [kg/m^3]$	NEN-EN 338
Radius	r	$0.1875\ [m]$	$0.075-0.3\ [m]$	Arcadis/estimate
Surface area	A	$0.0594\ [m^2]$	$0.018-0.125\ [m^2]$	πr^2
Length	l	$3\ [m]$	$1-5\ [m]$	Estimate
Mass	m	77 [kg]	6.3-325	$A \cdot l \cdot \rho$

It is assumed the wood is softwood, and the bending and tension E-moduli of soft woods parallel to the grain range from $7000 - 16000\ N/mm^2$. The radius r (in Appendix D, Plate loading, this radius is called c) of a wooden pole or tree that can occur in the river can range from $75 - 300\ mm$. The surface area A then becomes πr^2.

$$k_b = EA/l\ = \frac{E\pi r^2}{l}[N/mm]$$

$$[N/mm] = [kN/m]$$

Lower limit: $k_b = 7 \cdot 10^3 \cdot \pi \cdot 0.075^2/3 = 42\ [kN/m]$
Upper limit: $k_b = 16 \cdot 10^3 \cdot \pi \cdot 0.3^2/3 =\ 1508[kN/m]$
Mean $k_b = 11.5 \cdot 10^3 \cdot \pi \cdot 0.1875^2/3 =\ 424[kN/m]$

Note that if the length of the pole increases, the stiffness becomes less, but the mass(and therefore kinetic energy) also increases. The upper- and lower limit are therefore divided by the mean length.

If the masses of the structure are neglected and the structure behaves like a spring; the limit of the elastic model is assumed to be when the outer glass ply reaches its critical bending stress. The methods of the NEN and CNR give equivalent thicknesses for displacement- and stress calculations. There must be equilibrium between the kinetic energy, and the potential spring energy stored in the structure on impact. With this model, the maximum energy that can be stored elastically can be determined. If the kinetic energy is larger than the calculated maximum, it is likely that the glass will break and energy will also be dissipated into the cracking of the glass.

Neglecting the mass of the structure, the springs are now combined into an equivalent spring:

$$\frac{1}{k_{eq}} = \frac{1}{2 \cdot k_s} + \frac{1}{k_g} + \frac{1}{k_b} \rightarrow k_{eq} = \frac{1}{\frac{1}{2 \cdot k_s} + \frac{1}{k_g} + \frac{1}{k_b}}$$

Because the springs are in series, the force in each spring is equal. The spring stiffness of the foundation is neglected.

The energy equation is simplified to:

$$E_{kin} = E_{pot} \rightarrow \frac{1}{2}mv^2 = \frac{1}{2}ku^2$$

$$\frac{1}{2}m_b v_b^2 = \frac{1}{2}k_{eq}u_{eq}^2 \rightarrow u_{eq} = \sqrt{\frac{m_b v_b^2}{k_{eq}}}$$

$$F_{eq} = k_{eq} \cdot u_{eq} = k_{eq}\sqrt{\frac{m_b v_b^2}{k_{eq}}} = \sqrt{m_b v_b^2 k_{eq}} = v_b\sqrt{m_b k_{eq}}$$

$$F_{eq} = v_b\sqrt{\frac{m_b}{\frac{1}{2 \cdot k_s} + \frac{1}{k_g} + \frac{1}{k_b}}}$$

$$UC = \frac{F_{eq}}{F_{max}}$$

F_{max} is the maximum static force that the structure can take and unity checks need to be done for the rest of the structure on shear force and moments. It is likely that the maximum moments in the glass panel are governing.

B.9. Literature

Arcadis. (2017, 15 September) Memo ontwerpuitgangspunten glazen waterkeringen [memo]. Retrieved from intern network

C. Plate loading

Classic beam theory can be extended by plate theory. Because the glass panels have small thickness compared to span ($t < \frac{1}{5}l$), shear deformation can be neglected and Kirchoff's plate theory is applied in the FEM model. If the glass plate behaves more like a plate than a wide beam the following relations are valid for the glass panel.

C.1. Plate theory

Like beam theory, deformations and rotations can be coupled to the applied loads and boundary conditions of a plate structure by kinematic, constitutive and equilibrium relations.

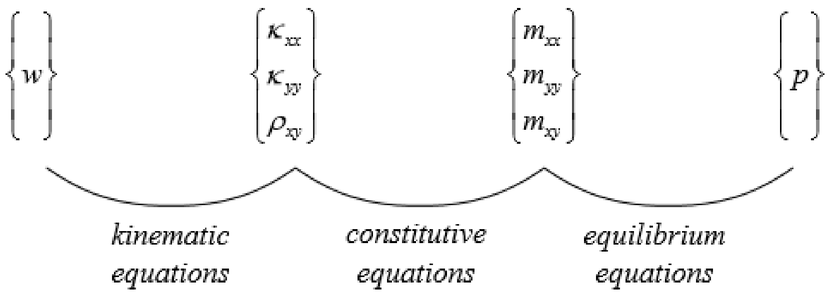

Figure C-1: Relations for a slender slab

C.1.1. Kinematic relation

the following kinematic relations hold:

$$\varphi_x = -\frac{\partial w}{\partial x}; \qquad \varphi_y = -\frac{\partial w}{\partial y};$$
$$\kappa_{xx} = -\frac{\partial^2 w}{\partial x^2}; \quad \kappa_{yy} = -\frac{\partial^2 w}{\partial y^2};$$
$$\kappa_{xy} = -\frac{\partial^2 w}{\partial x \partial y}; \text{ (or } \rho_{xy} = -2\frac{\partial^2 w}{\partial x \partial y};\text{)}$$

Where
v = is the deformation
φ = the local rotation
κ = the local curvature

C.1.2. Constitutive relation

The constitutive equations are(without shear deformation):

$$m_{xx} = D(\kappa_{xx} + v\kappa_{yy})$$
$$m_{yy} = D\left(v\kappa_{xx} + \kappa_{yy}\right)$$
$$m_{xy} = (1 - v)D\kappa_{xy}$$

Where
m = the local moment
D = the plate stiffness

$$D = \frac{Et^3}{12(1 - v^2)}$$

In matrix notation the constitutive relations from above read:

$$\begin{Bmatrix} m_{xx} \\ m_y \\ m_{xy} \end{Bmatrix} = D \begin{bmatrix} 1 & v & 0 \\ v & 1 & 0 \\ 0 & 0 & 1-v \end{bmatrix} \begin{Bmatrix} \kappa_{xx} \\ \kappa_{yy} \\ \kappa_{xy} \end{Bmatrix}$$

C.1.3. Equilibrium relation

The equilibrium equations are:

$$v_x = \frac{\partial m_{xx}}{\partial x} + \frac{\partial m_{yx}}{\partial y}$$
$$v_y = \frac{\partial m_{yy}}{\partial y} + \frac{\partial m_{yx}}{\partial x}$$
$$\frac{\partial v_x}{\partial x} + \frac{\partial v_y}{\partial y} + p = 0$$

Which result in the total equilibrium equation of:

$$-\left(\frac{\partial^2 m_{xx}}{\partial x^2} + 2\frac{\partial^2 m_{yx}}{\partial y \partial} + \frac{\partial^2 m_{yy}}{\partial y^2}\right) = p$$

C.1.4. Biharmonic plate equation

By substitution of the kinematic equations into the constitutive relations one obtains:

$$m_{xx} = -D(\frac{\partial^2 w}{\partial x^2} + v\frac{\partial^2 w}{\partial y^2})$$
$$m_{yy} = -D(v\frac{\partial^2 w}{\partial x^2} + \frac{\partial^2 w}{\partial y^2})$$
$$m_{xy} = -(1-v)D\frac{\partial^2 w}{\partial x \partial y}$$

The biharmonic plate equation is obtained:

$$D\left(\frac{\partial^4}{\partial x^4} + \frac{\partial^4}{\partial x^2 \partial y^2} + \frac{\partial^4}{\partial y^4}\right)w = p$$

And with the La Place operator written as:

$$\nabla^2 = \frac{\partial^2}{\partial x^2} + \frac{\partial^2}{\partial y^2}$$

The biharmonic plate equation can be written as:

$$D\nabla^2\nabla^2 w = p \rightarrow \nabla^4 w = \frac{p}{D}$$

C.2. Literature

Blaauwendraad, J. (2006). *Plate analysis, theory and application*. Retrieved from Blackboard TU Delft

Timoshenko, S., & Woinowsky-Krieger, S. (1959). *Theory of plates and shells* (2nd ed.). New York, USA: McGraw-Hill Book Company.

Wierzbicki, T., & MIT. (2006). *Plates and shells*. Retrieved from http://hdl.handle.net/1721.1/45585

D. Experiment

The results of the experiment are given in the next paragraphs. Only the tests just before, with and after failure are presented.

D.1. Impact object 1

Table D-1: Properties impact object 1

Property	Value
Length	$2.55\ m$
Diameter	$0.27\ m$
Weight	$140\ kg$
Species	Larch (Larix)
Origin	Gelderland (Holland)

Figure D-1: Impact object 1

D.2. Impact object 2

Table D-2: Properties impact object 2

Property	Value
Length	$2.20\ m$
Diameter	$0.40 - 0.45\ m$
Weight	$380\ kg$
Species	Red Oak (Quercus rubra)
Origin	Gelderland (Holland)

Figure D-2: Impact object 2

D.3. Test 1

Table D-3: Summary test 1

Test	Impact object	Speed	E_{kin}	Remarks
1	Object 1	$2.658\ m/s$	$494\ Nm$	No damage.
2	Object 1	$1.893\ m/s$	$250\ Nm$	No damage.
3	Object 1	$1.902\ m/s$	$253\ Nm$	No damage.

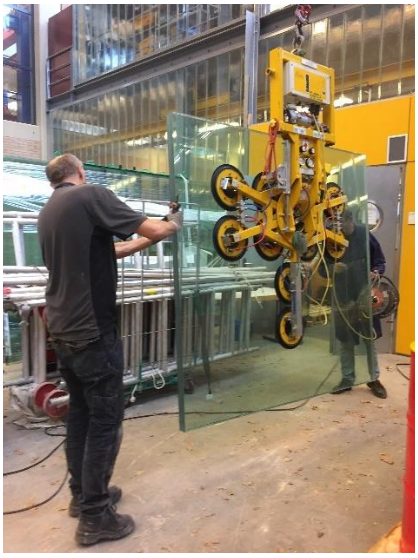

Figure D-3: Vacuum suction lifter

Figure D-4: placing the glass panel in the frame

After carefully placing the glass panel into the Aluminum frame, securing it with click-profiles and EPDM seals, The panel had to be rotated. During rotating one of the corners unfortunately slammed on the Meccano set-up, causing the middle glass layer to fracture. Since there is still information to be gathered from this panel, we decided to test it anyway and placed the panel between the side posts.

We then tested the panel with impact object 1:

D.3.1. Test 1.1

Panel 1; Impact object 1; test 1; delamination

The high speed camera is said to take 60 frames per second. The 4 frames 1.1.1, 1.1.2, 1.1.3 and 1.1.4 are taken apart right before impact without failure.

Approximately 8.86 cm displacement between frames. Frame 1.1.1-1.1.2 and 1.1.3-1.1.4 turned out to be the same, so there are 2/60 second between the frames instead of 1/60.

$$u/t = m/s = 0.0886/\frac{2}{60} = 2.658\, m/s$$

Figure D-5: Frame 1.1.1

Figure D-6: Frame 1.1.2

Figure D-7: Frame 1.1.3

Figure D-8: Frame 1.1.4

Reflection on test 1.1

Because the middle layer was already fractured, something interesting happened after the first impact; The front glass layer seemed to delaminate partially. Where the layer was still laminated in the shape of a square, the outside of this laminated square was clearly loose from the rest of the panel.

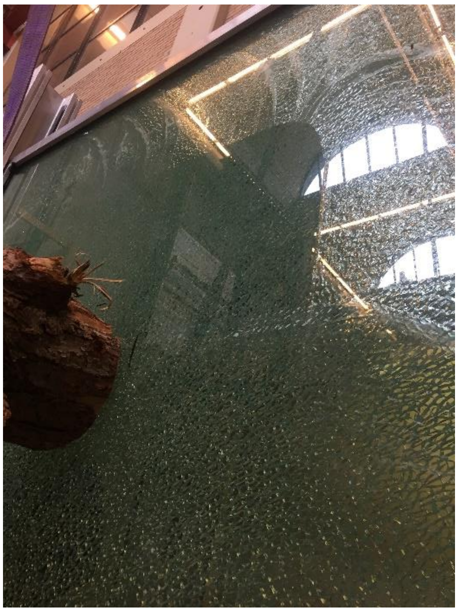

D.3.2. Test 1.2

Panel 1; Impact object 1; test 2; delamination spreads further
The high speed camera is said to take 60 frames per second. The 4 frames 1.2.1, 1.2.2, 1.2.3 and 1.2.4 are taken apart right before impact without failure.
Approximately 10 cm displacement between frames. Frame 1 and 2 turned out to be the same, so there are 2/60 second between the frames instead of 1/60.

$$u/t = m/s = 0.0631/\frac{2}{60} = 1.893\ m/s$$

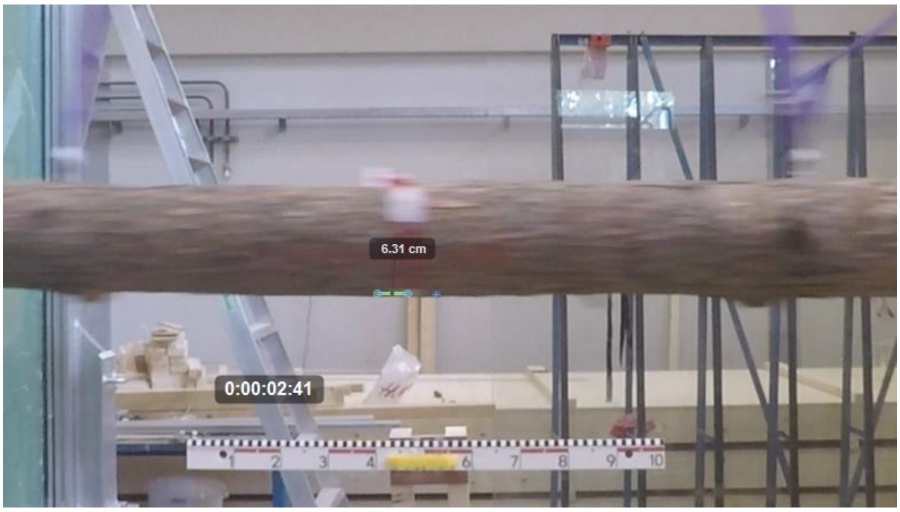

Figure D-9: Frame 1.2.1

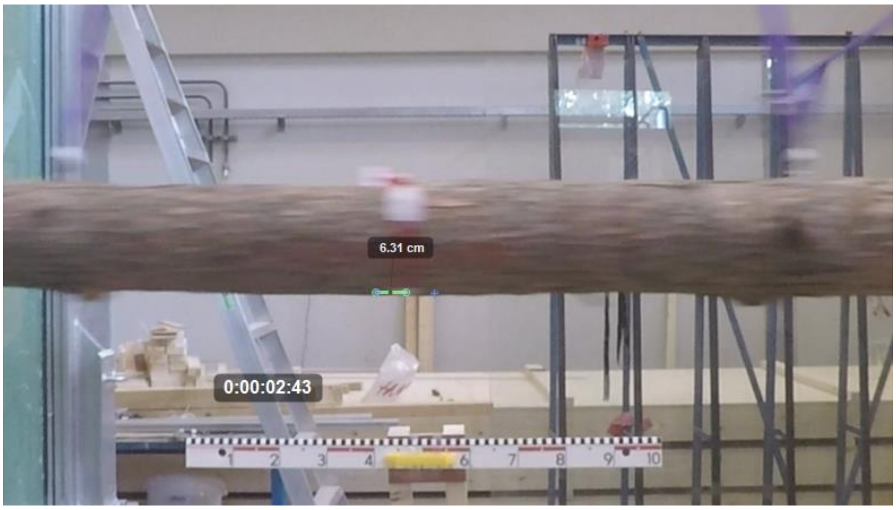

Figure D-10: Frame 1.2.2

Figure D-11: Frame 1.2.3

Figure D-12: Frame 1.2.4

D.3.3. Test 1.3

Panel 1; Impact object 1; test 3; delamination spreads further
The high speed camera is said to take 60 frames per second. The 4 frames 1.3.1, 1.3.2, 1.3.3 and 1.3.4 are taken apart right before impact without failure.

Approximately 10 cm displacement between frames. Frame 1 and 2 turned out to be the same, so there are 2/60 second between the frames instead of 1/60.

$$u/t = m/s = 0.0634/\frac{2}{60} = 1.902\ m/s$$

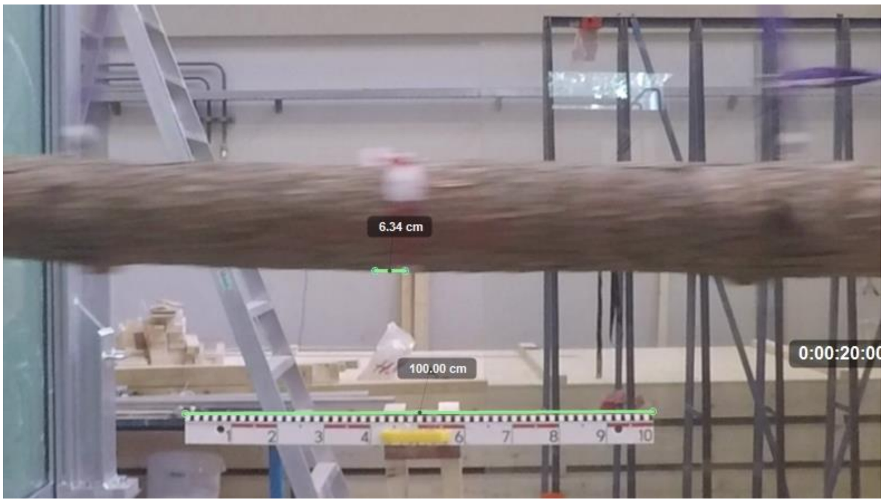

Figure D-13: Frame 1.3.1

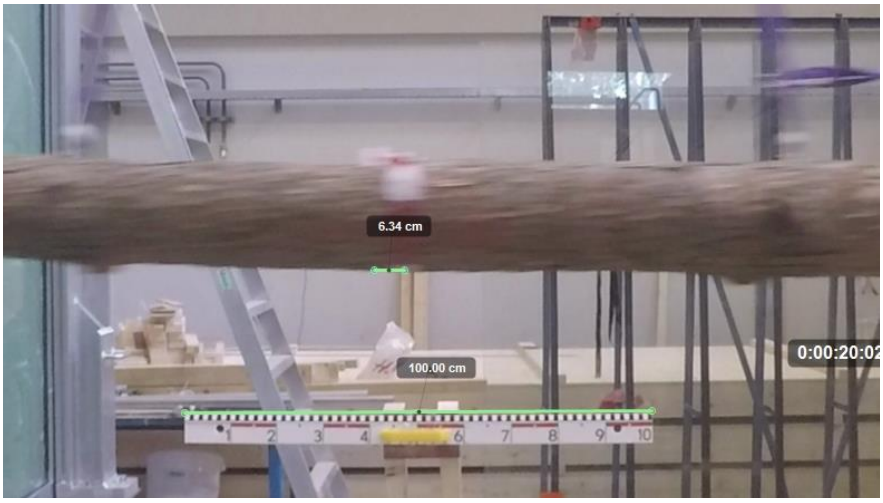

Figure D-14: Frame 1.3.2

Figure D-15: Frame 1.3.3

Figure D-16: Frame 1.3.4

Elaboration on test 1.3

Other than further delaminating, the impact object did not cause any more damage to the panel. Therefore it was decided to obtain a heavier object for the next tests. In Figure D-17, the laminated square is clearly visible, as is the location of impact.

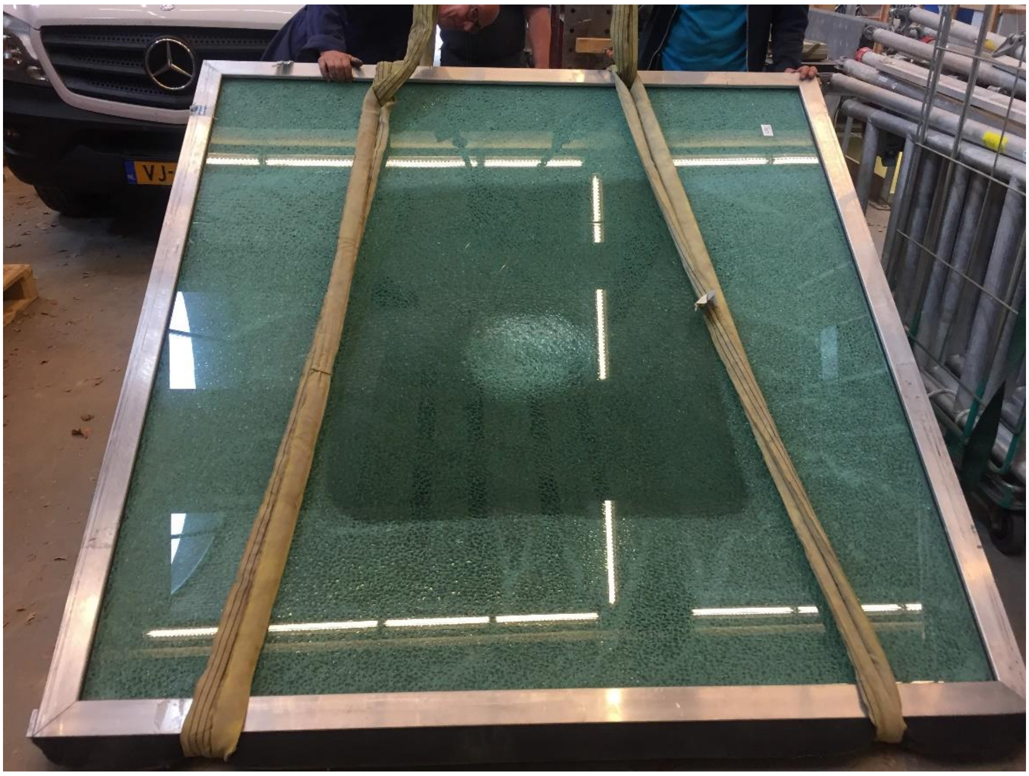
Figure D-17: The delaminated panel

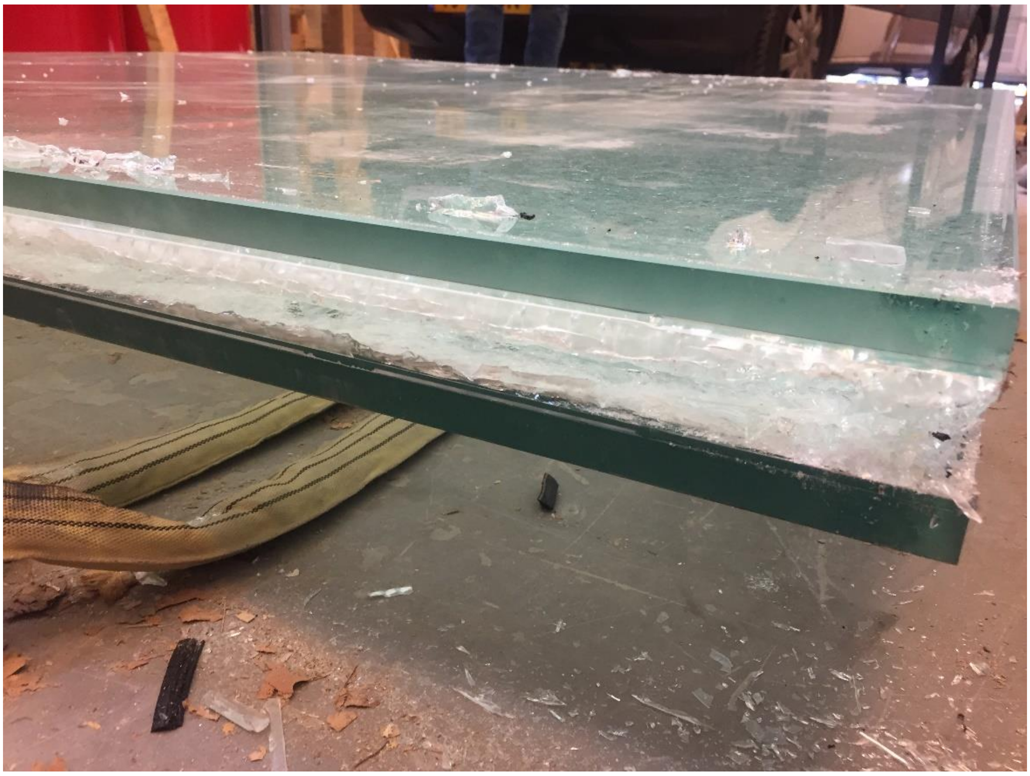

D.4. Test 2

D.4.1. Summary test panel 2

We did a total of 8 tests. The panel eventually broke the two back layers by object 2 at a speed of 3.2 m/s. No delamination occurred and the three broken glass layers and two Sentryglass layers exhibited minimal deformation during transportation on the forklift.

Table D-4: Summary test 2

Test	Impact object	Speed	E_{kin}	Remarks
1	Object 1	$< 2.83\ m/s$	$< 560\ Nm$	No damage.
2	Object 1	$< 2.83\ m/s$	$< 560\ Nm$	No damage.
3	Object 1	$2.83\ m/s$	$560\ Nm$	No damage.
4	Object 2	$< 3.0\ m/s$	$< 1710\ Nm$	No damage.
5	Object 2	$3.0\ m/s$	$1710\ Nm$	No damage.
6	Object 2	$3.2\ m/s$	$1946\ Nm$	Two layers fractured at the back of the glass.
7	Object 2	$3.1\ m/s$	$1826\ Nm$	Last layer fractured
8	Object 2	$3.29\ m/s$	$2056\ Nm$	No further damage except more glass falling from the three already broken layers.

D.4.2. Test 2.3

Panel 2; Impact object 1; test 3/8; no failure
The high speed camera is said to take 60 frames per second. The 4 frames 2.3.1, 2.3.2, 2.3.3 and 2.3.4 are taken apart right before impact without failure.
Approximately 10 cm displacement between frames. Frame 1 and 2 turned out to be the same, so there are 2/60 second between the frames instead of 1/60.

$$u/t = m/s = 0.0944/\frac{2}{60} = 2.83\ m/s$$

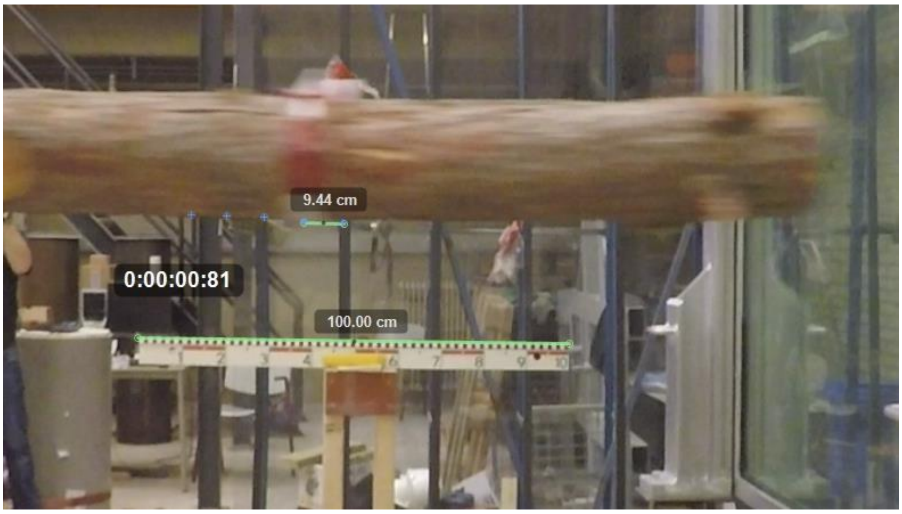

Figure D-18: Frame 2.3.1

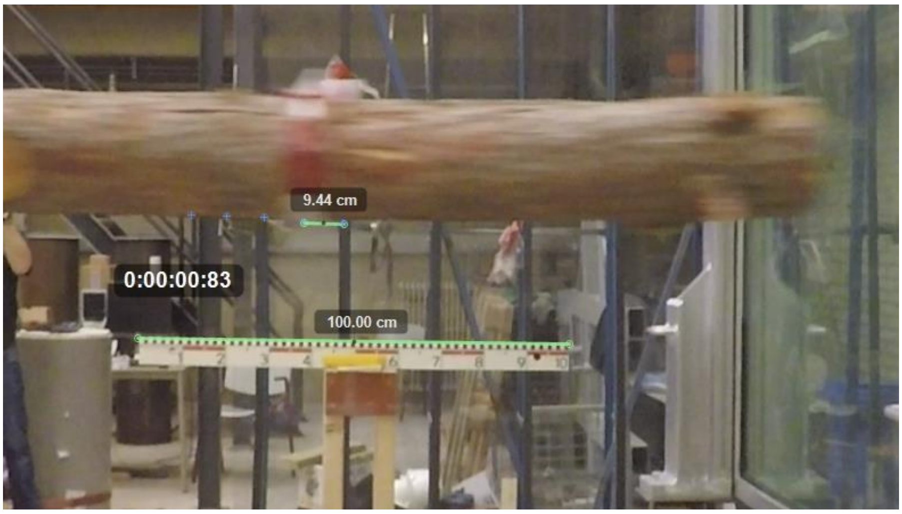

Figure D-19: Frame 2.3.2

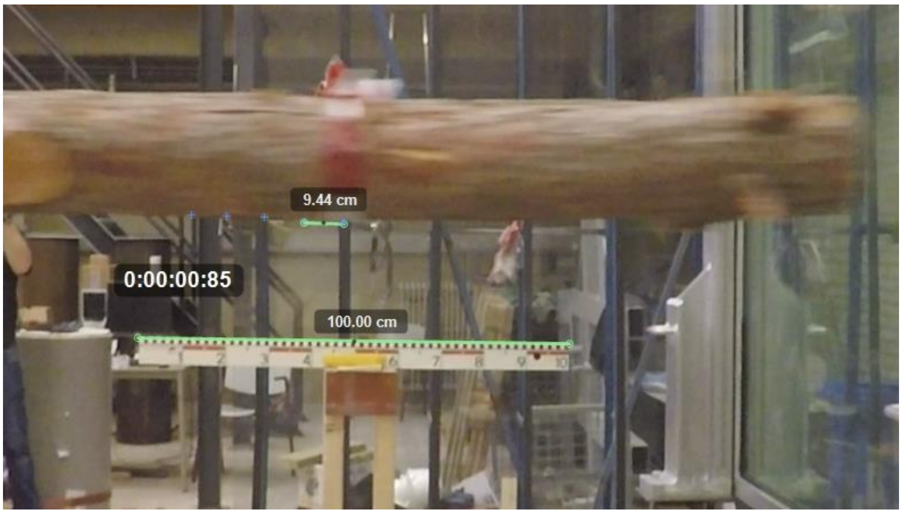

Figure D-20: Frame 2.3.3

Figure D-21: Frame 2.3.4

Check over a longer period of time using the timer on screen gives:

$$u/t = m/s = 0.3585/0.13 = 2.76\, m/s$$

Figure D-22: Speed measure using time difference test 2.3, at 0.73 second.

Figure D-23: Speed measure using time difference test 2.3, at 0.86 second.

Reflection on test 2.3

As expected from test 1; impact object 1 did not cause any damage when released from the highest point possible(the backside of the tree was restricted by a wall). The kinetic energy of impact object 1 was:

$$0.5 \cdot 140 \cdot 2.83^2 = 560\ Nm$$

D.4.3. Test 2.5: test before failure

Panel 2; impact object 2; test 5/8 ; no failure
The high speed camera is said to take 60 frames per second. The 3 frames 5.1, 5.2 and 5.3 are taken apart right before impact without failure.
Approximately 10 cm displacement between frames. Frame 1 and 2 turned out to be the same, so there are 2/60 second between the frames instead of 1/60.

$$u/t = m/s = 0.10/\frac{2}{60} = 3\ m/s$$

Figure D-24: Frame 2.5.1

Figure D-25: Frame 2.5.2

Figure D-26: Frame 2.5.3

Check over a longer period of time with the timer:
The timer gives a time difference between frame 5.4 and 5.5 of $1.96 - 1.85 = 0.11$ seconds, the horizontal distance is 0.33 m. This results in:

$$u/t = m/s = 0.33/0.11 = 3\ m/s$$

This comes down to the exact same speed, so the actual impact speed might even be slightly larger as the speed reaches a maximum at the lowest point of the pendulum.

Figure D-27: Frame 2.5.4

Figure D-28: Frame 2.5.5

Reflection on test 2.5

This was the test just before failure, and we were starting to wonder if the second tree trunk would be heavy enough to damage the glass. The maximum speed at which the glass stayed unharmed was approximately $3\ m/s$. With a mass of $380\ kg$ this comes down to:

$$0.5 \cdot 380 \cdot 3^2 = 1710\ Nm$$

D.4.4. Test 2.6: test with failure

Panel 2; impact object 2; test 6/8 ; failure 2/3
The high speed camera is said to take 60 frames per second. These 4 frames 6.1, 6.2, 6.3 and 6.4 are taken apart right before impact with failure.
Approximately 10.66 cm displacement between frames. Frame 1-2 and 3-4 turned out to be the same, so there are 2/60 second between the frames instead of 1/60.

$$\frac{u}{t} = \frac{m}{s} = 0.1066/\frac{2}{60} = 3.2\ m/s$$

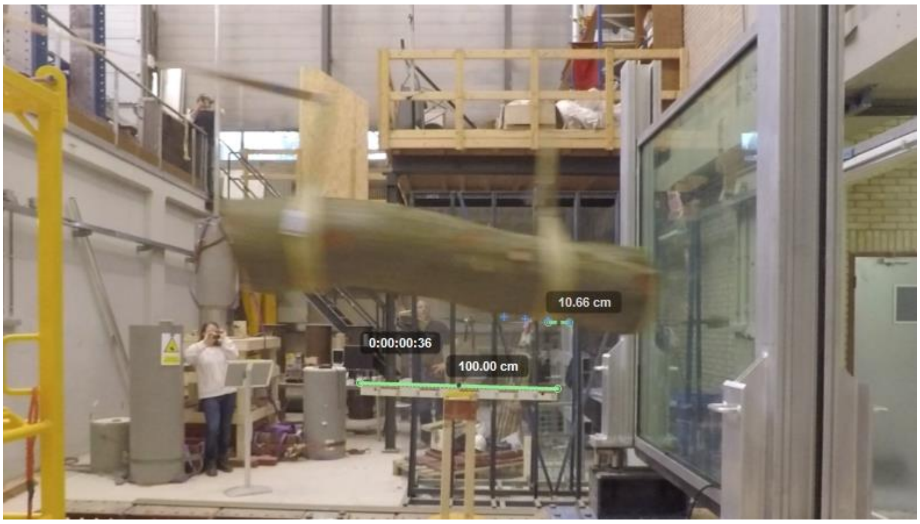

Figure D-29: Frame 2.6.1

Figure D-30: Frame 2.6.2

Figure D-31: Frame 2.6.3

Figure D-32: Frame 2.6.4

Elaboration on test 2.6

After impact, two layers at the back side of the glass were shattered, indicating that the failure was due to moment. Because there were two damaged layers, it was not possible to derive the origin of the failure from the crack pattern. But at the backside, the corner started to crumble as can be seen in Figure D-34. This can be an indication that this location is vulnerable.

Figure D-33:Panel after test 2.6

Figure D-34: Corner failure

The speed at which the two glass layers failed was approximately $3.2\ m/s$. With a mass of $380\ kg$ this comes down to:

$$0.5 \cdot 380 \cdot 3.2^2 = 1946\ Nm$$

D.4.5. Test 2.7

Panel 2; impact object 2; test 7/8 ; failure 3/3
The high speed camera is said to take 60 frames per second. These 4 frames 7.1, 7.2, 7.3 and 7.4 are taken apart right before impact with failure of the last and front layer.
Approximately 10.34 cm displacement between frames. Frame 1-2 and 3-4 turned out to be the same, so there are 2/60 second between the frames instead of 1/60.

$$\frac{u}{t} = \frac{m}{s} = 0.1034/\frac{2}{60} = 3.10\ m/s$$

Figure D-35: Frame 2.7.1

Figure D-36: Frame 2.7.2

Figure D-37: Frame 2.7.3

Figure D-38: Frame 2.7.4

Elaboration on test 2.7

The speed at which the last glass layer failed was approximately $3.1\ m/s$. With a mass of $380\ kg$ this comes down to:

$$0.5 \cdot 380 \cdot 3.1^2 = 1826\ Nm$$

This was the only try, and it is very likely the last glass layer would have failed at lower speeds of the tree.

Figure D-39: Return height test 2.7

In Figure D-39, the return height of the tree is presented. As there was little to no return height in test 2.6, it is interesting to see a trampoline effect that increases as more layers are broken and the displacement under impact also increases.

D.4.6. Test 2.8

Panel 2; impact object 2; test 8/8

The high speed camera is said to take 60 frames per second. These 4 frames 8.1, 8.2, 8.3 and 8.4 are taken apart right before impact where the three glass layers have already failed. Frame 1-2 and 3-4 turned out to be the same, so there are 2/60 second between the frames instead of 1/60. It can be seen that the broken panel still has residual strength and stiffness during and after impact. Approximately 10.97 cm displacement between frames.

$$\frac{u}{t} = \frac{m}{s} = 0.1097/\frac{2}{60} \;\; = 3.29\; m/s$$

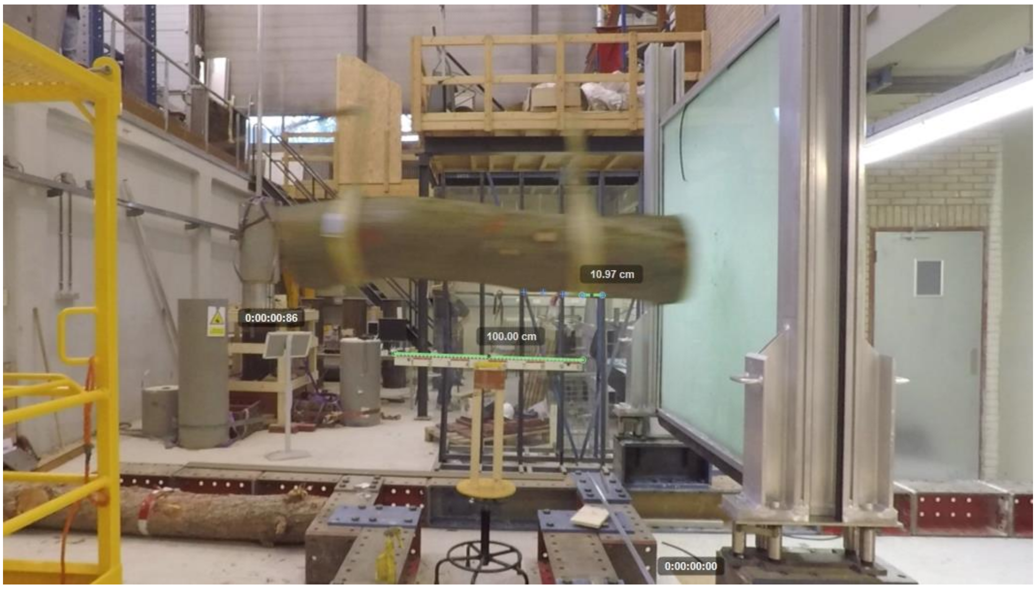

Figure D-40: frame 2.8.1

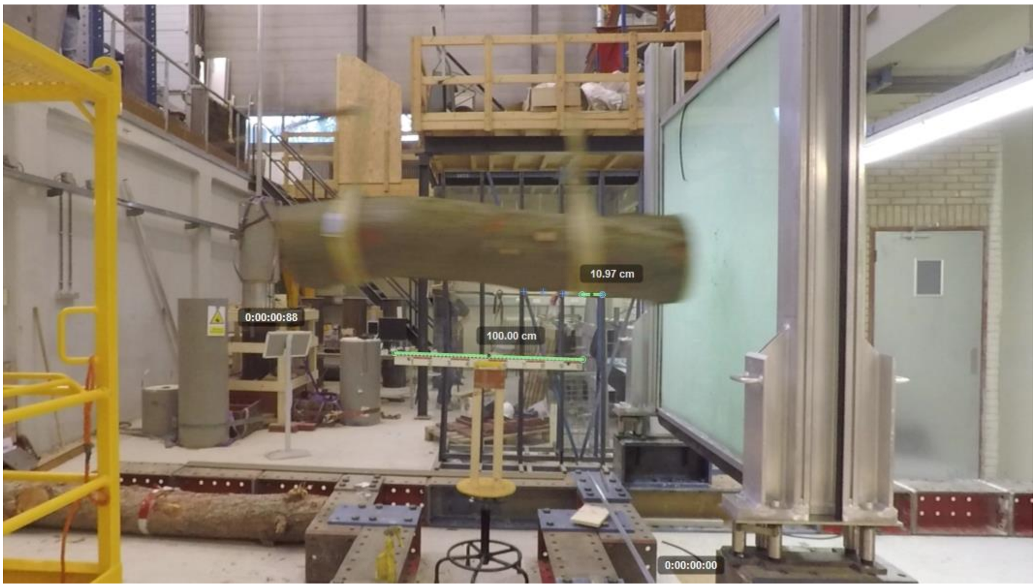

Figure D-41: Frame 2.8.2

Figure D-42: Frame 2.8.3

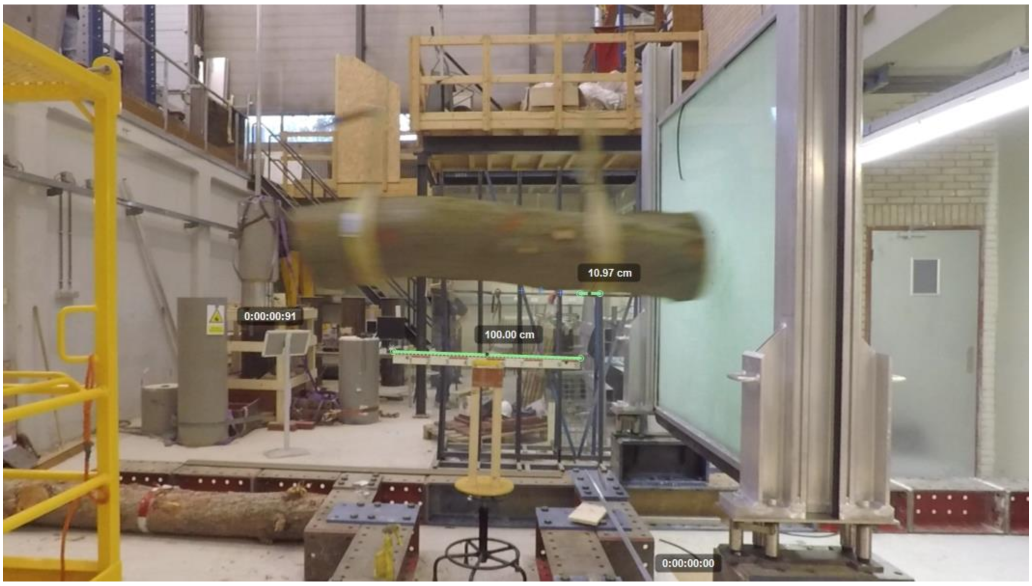

Figure D-43: Frame 2.8.4

Reflection on test 2.8

With the three glass layers broken, the displacement of the glass at the location of impact got larger, therefore increasing the deceleration distance. The latter decreases the equivalent static load. Seemingly acting more as an elastic spring, the impact object bounced back to a significantly larger height than test 2.7. This indicates that the kinetic energy was not fully absorbed by the structure. The kinetic energy of the impact object is approximately:

$$0.5 \cdot 380 \cdot 3.29^2 = 2056\ Nm$$

Figure D-44: Return height test 2.8

Figure D-45: Broken layers test panel 2

Figure D-46: Panel 2 on the forklift 1

Figure D-47: Panel 2 on the forklift 2

D.5. Test 3

D.5.1. Summary of test 3

Test 3 was an interesting experience as we were not able to break the glass with the two impact objects. Impact object 1 was used for the first three tests; impact 2 was used to test 8 times in the middle of the panel without damaging the glass and with the face of the tree trunk flat on the glass. Then we tested two times with the tree at an angle on the glass, so the edge of the tree would hit the glass. After this, we tested at the top of the glass two times. Still no damage. After the 16th test, we decided to attach steel ball to the face of the impact object to create a hard-on-hard material impact. This fractured the two front layers of the glass. We then tried to break the third layer at the back of the glass but the structure reacted more elastic and caused the tree to bounce back without fracturing the last layer. We therefore decided to test the glass with a static load to mimic the water pressure in case of high water levels and put a concrete block on the structure. See Test 4: Remaining bearing capacity test.

Table D-5: Summary test 3

Test	Impact object	Speed	E_{kin}	Remarks
1	Object 1	$< 2.364\ m/s$	$< 391\ Nm$	No damage.
2	Object 1	$< 2.364\ m/s$	$< 391\ Nm$	No damage.
3	Object 1	$2.364\ m/s$	$391\ Nm$	No damage.
4	Object 2	$< 3.150\ m/s$	$< 1885\ Nm$	No damage.
5	Object 2	$< 3.150\ m/s$	$< 1885\ Nm$	No damage.
6	Object 2	$< 3.150\ m/s$	$< 1885\ Nm$	No damage.
7	Object 2	$< 3.150\ m/s$	$< 1885\ Nm$	No damage.
8	Object 2	$< 3.150\ m/s$	$< 1885\ Nm$	No damage.
9	Object 2	$< 3.150\ m/s$	$< 1885\ Nm$	No damage.
10	Object 2	$< 3.150\ m/s$	$< 1885\ Nm$	No damage.
11	Object 2	$3.150\ m/s$	$1885\ Nm$	No damage.
12	Object 2 with edge of tree	$< 3.924\ m/s$	$< 2925\ Nm$	We put the lowest point of the pendulum behind the glass so the edge of the tree would hit the glass. Still no damage.
13	Object 2 with edge of tree	$3.924\ m/s$	$2925\ Nm$	No damage.
14	Object 2 – impact at top	$< 3.366 m/s$	$2153\ Nm$	We changed the location of impact to the top of the structure. No damage.
15	Object 2 – impact at top	$3.366 m/s$	$2153\ Nm$	No damage.
16	Object 2	$3.75\ m/s$	$2672\ Nm$	No damage.
17	Object 2 with steel sphere	$2.226\ m/s$	$941.46\ Nm$	Damaged by the steel sphere: the two front layers were shattered.
18	Object 2	$< 3.588\ m/s$	$< 2446\ Nm$	No further damage except more glass falling from the already broken layers.
19	Object 2	$< 3.588\ m/s$	$< 2446\ Nm$	No further damage except more glass falling from the already broken layers.
20	Object 2	$< 3.588\ m/s$	$< 2446\ Nm$	No further damage except more glass falling from the already broken layers.
21	Object 2	$< 3.588\ m/s$	$< 2446\ Nm$	No further damage except more glass falling from the already broken layers.
22	Object 2	$3.588\ m/s$	$2446\ Nm$	No further damage except more glass falling from the already broken layers.

After test 22, we decided to stop the impact tests and proceed with test 4 with one layer intact.

Video analysis is done for test 3, test 11, 13, 15, 16, 17, and 22. We build up the speed every time we changed something in the test, therefore the speed of the other tests is not relevant as it is less than the calculated maximum. Since a different (newer version) Gopro was used, two frames apart was $\frac{1}{60}$ of a second instead of $\frac{1}{30}$, as was the case in Test 1 and Test 2.

D.5.2. Test 3.3

Panel 3; impact object 1; test 3/22
Approximately 3.94 cm displacement between frames.

$$\frac{u}{t} = \frac{m}{s} = 0.0394/\frac{1}{60} \;= 2.364\ m/s$$

Figure D-48: Frame 3.3.1

Figure D-49: Frame 3.3.2

D.5.3. Test 3.11

Panel 3; impact object 2; impact location in the middle of panel test; 11/22
Approximately 5.25 cm displacement between frames.

$$\frac{u}{t} = \frac{m}{s} = 0.0525/\frac{1}{60} \ = 3.150\ m/s$$

Figure D-50: Frame 3.11.1

Figure D-51: Frame 3.11.2

D.5.4. Test 3.13

Panel 3; impact object 2; impact location in the middle of panel test; 13/22

Figure D-52: Impact with the surface-edge

Approximately 6.54 cm displacement between frames.

$$\frac{u}{t} = \frac{m}{s} = 0.0654/\frac{1}{60} \ = 3.924\ m/s$$

Figure D-53: Frame 3.13.1

Figure D-54: Frame 3.13.2

D.5.5. Test 3.15

Panel 3; impact object 2; impact location at top of panel test; 15/22
Approximately 5.61 cm displacement between frames.

$$\frac{u}{t} = \frac{m}{s} = 0.0561/\frac{1}{60} \ = 3.366m/s$$

Figure D-55: Frame 3.15.1

Figure D-56: Frame 3.15.2

D.5.6. Test 3.16

Panel 3; impact object 2; impact location in the middle of panel; test 16/22; no damage
Approximately 6.25 cm displacement between frames.

$$\frac{u}{t} = \frac{m}{s} = 0.0625/\frac{1}{60} = 3.75\ m/s$$

Figure D-57: Frame 3.16.1

Figure D-58: Frame 3.16.2

D.5.7. Test 3.17

Panel 3; impact object 2; impact location in the middle of panel; test 17/22; two layers fractured;
In this test we made use of a steel hemisphere as the panel withstood the impact objects at maximum speed. This unnatural addition turned out to be a game changer and the two front layers fractured immediately at impact.

Figure D-59: Impact with steel hemisphere

Approximately 3.71 cm displacement between frames.

$$\frac{u}{t} = \frac{m}{s} = 0.0371/\frac{1}{60} \;\; = 2.226\, m/s$$

Figure D-60: Frame 3.17.1

Figure D-61: Frame 3.17.2

Reflection on test 3.17

In the next two frames the high speed camera captured the moment between the fracturing of first and the second layer. In Frame 3.17.3 the steel sphere broke the first layer, and in Frame 3.17.4 the second layer is broken. It can be seen from the reflection and color of the panel that after the fracturing of two layers, the panel is significantly less transparent.

Figure D-62: Frame 3.17.3

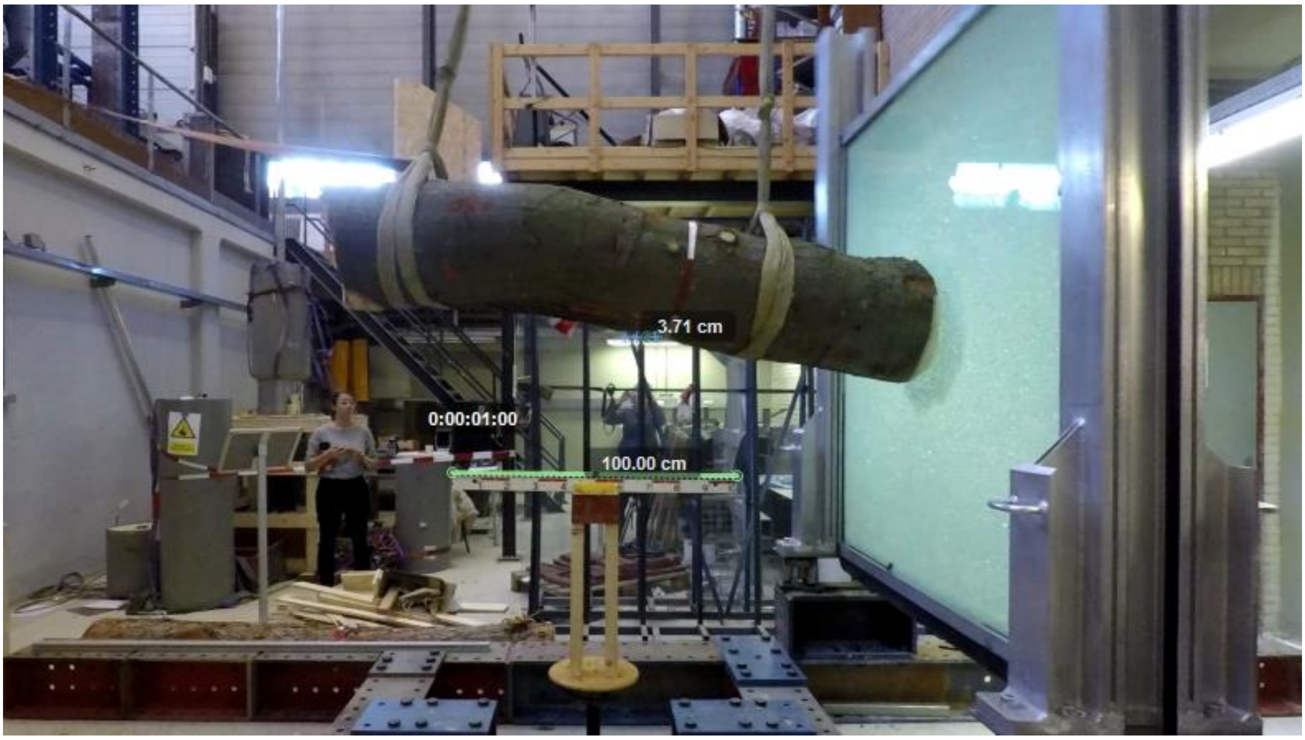

Figure D-63: Frame 3.17.4

Figure D-64: Broken panel 3

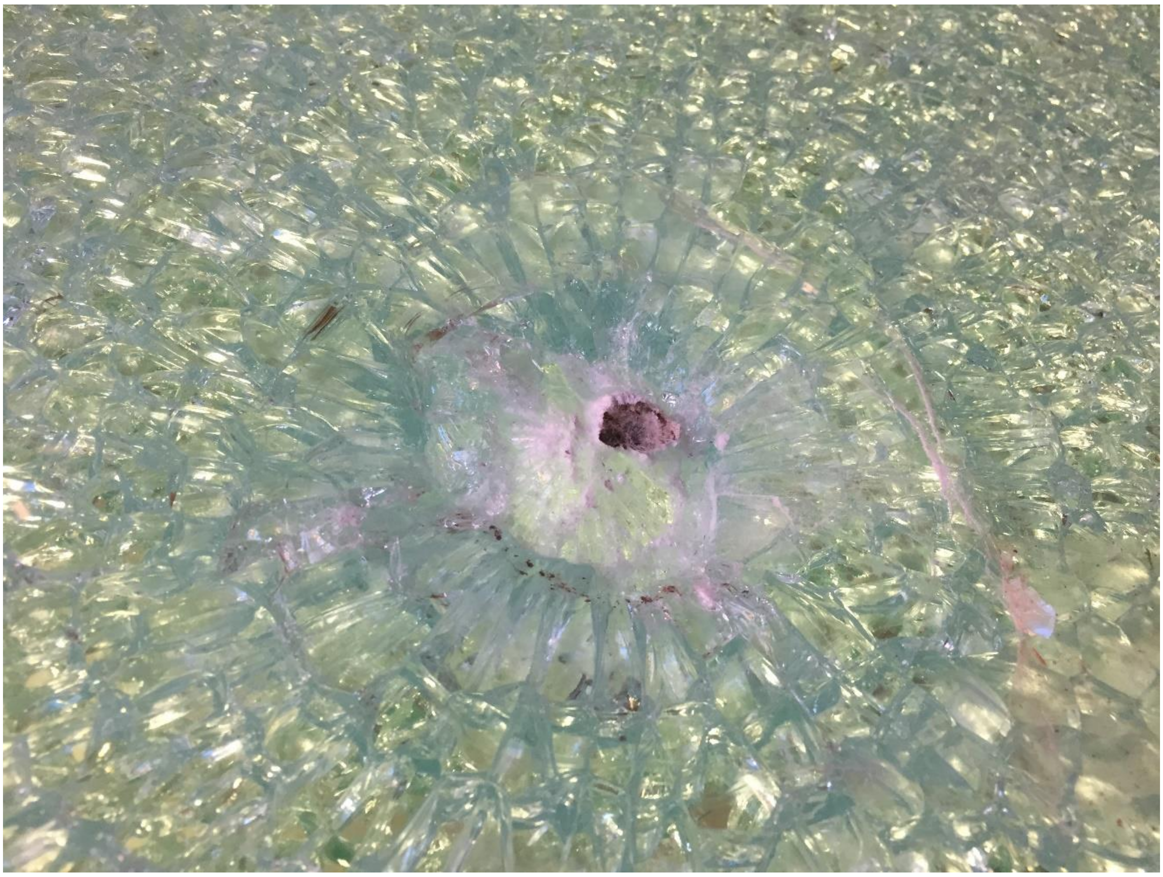

Figure D-65: Location of impact

Figure D-66: Discoloration around impact location

Figure D-67: Visible round color pattern

The steel hemisphere did not survive the hard-on-hard impact either, and exhibited brittle fracture, see Figure D-68.

Figure D-68: The broken steel hemisphere

D.5.8. Test 3.17-Test 3.21

Between test 16 and 22, the panel started to delaminate around the location of impact. Quite similar to what happened in Test 1, except the delamination started in a circle around the location of impact rather than around a still laminated square.

Figure D-69: Delamination circle front view

Figure D-70: Delamination circle side view

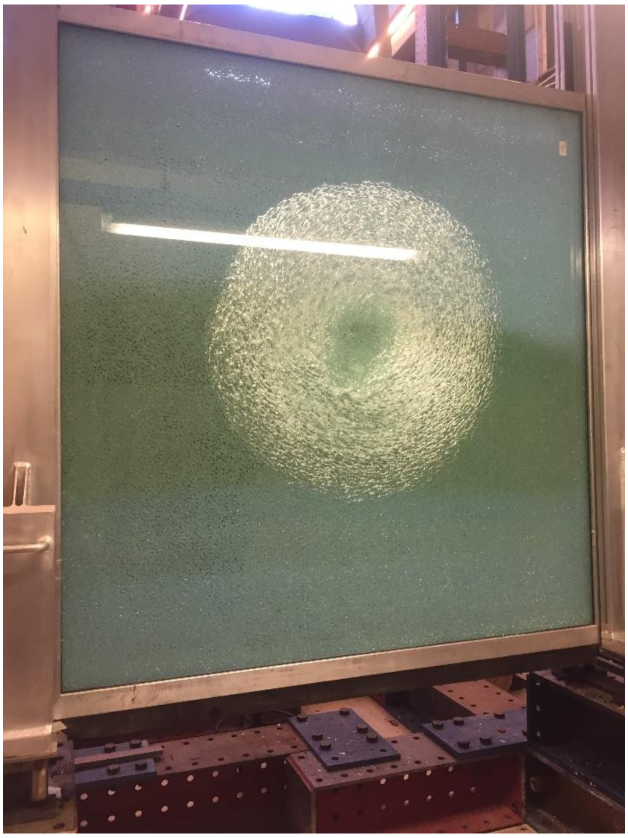

Figure D-71: Back of the glass

Figure D-72: Back of the glass different lighting

D.5.9. Test 3.22

Panel 3; impact object 2; impact location in the middle of panel test; 22/22
Approximately 5.98 cm displacement between frames.

$$\frac{u}{t} = \frac{m}{s} = 0.0598/\frac{1}{60} \;\; = 3.588\, m/s$$

Figure D-73: Frame 3.22.1

Figure D-74: Frame 3.22.2

D.6. Test 4: Remaining bearing capacity test

D.6.1. Static water pressure in FEM

The internal moments m_1 and m_2 for a water load up to the top of the structure are calculated using the FEM model.

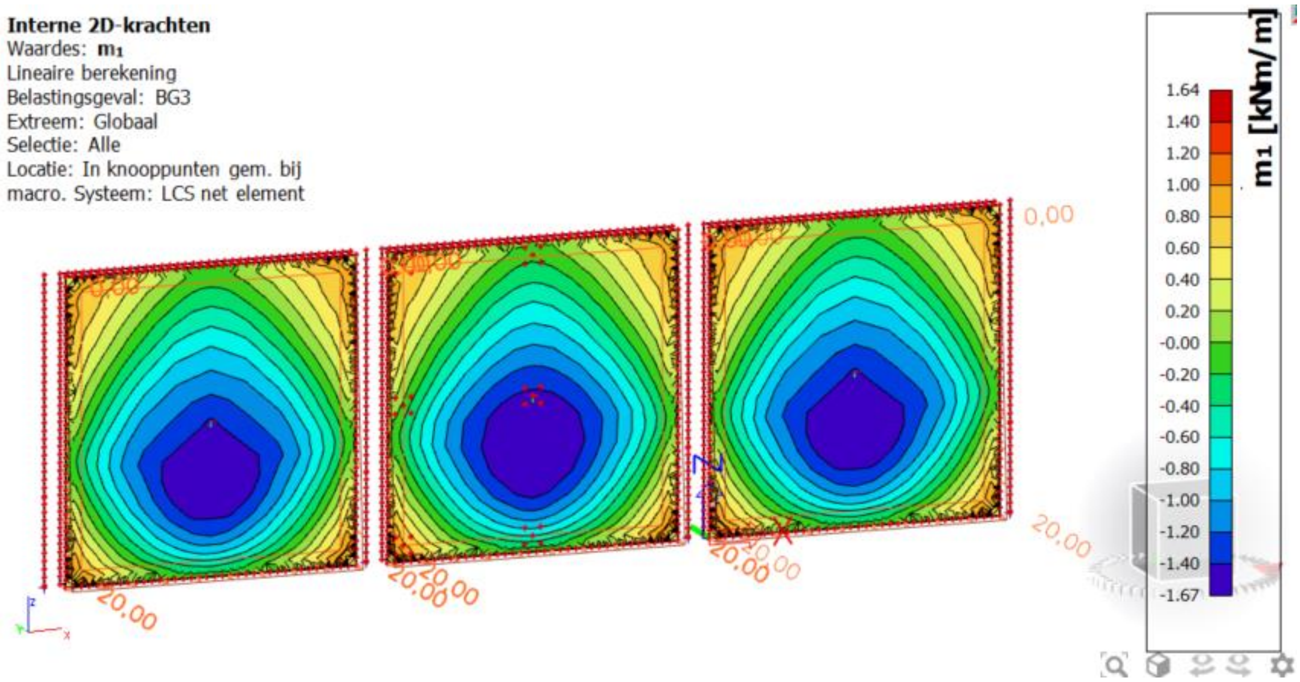

Figure D-75: Internal moments due to water pressure m1

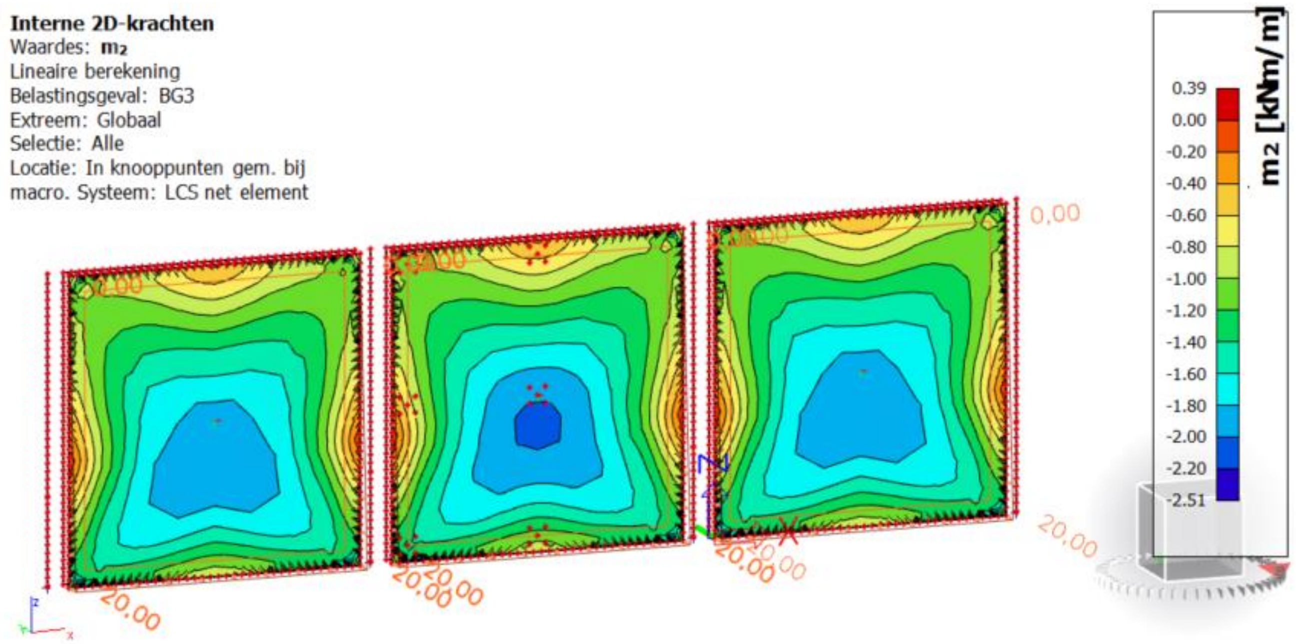

Figure D-76: Internal moments due to water pressure m2

We will put weight on an area of 0.5 by 0.5 meter to simulate the moment from water pressure. FEM analysis showed that similar internal moments occur with a q-load of $50\ kN/m^2$:

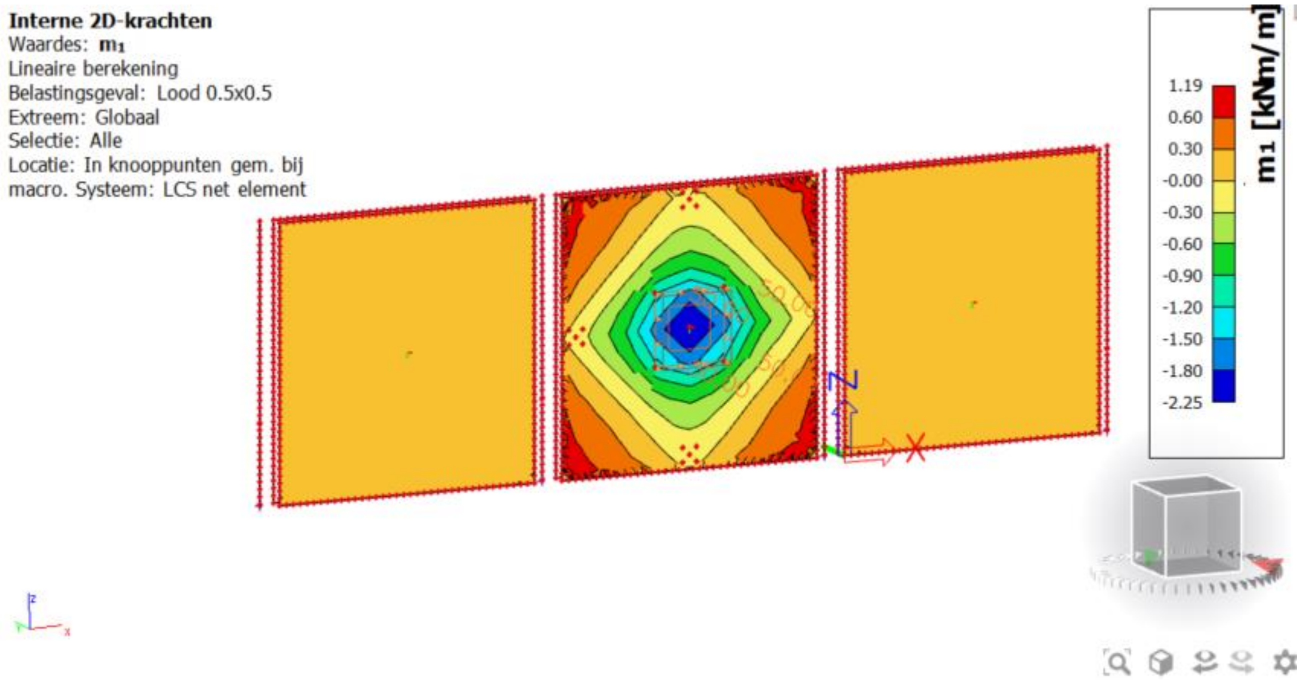

Figure D-77: Internal moments m1 due to distributed load 0.5x0.5 m

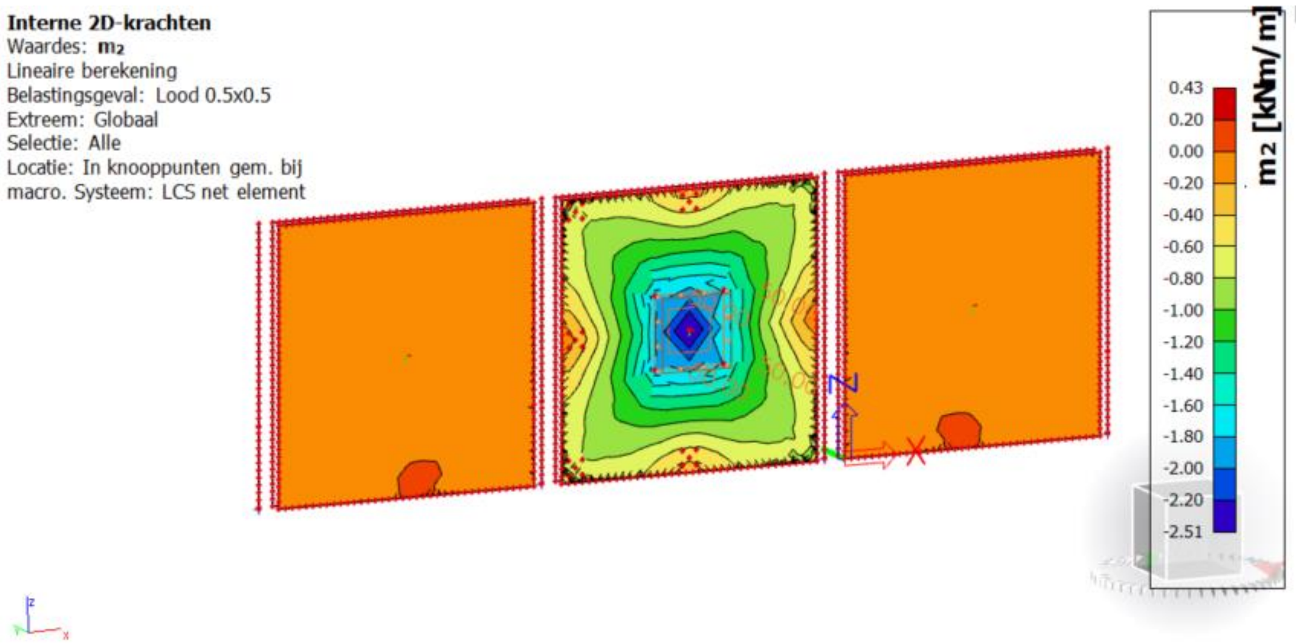

Figure D-78: Internal moments m2 due to distributed load 0.5x0.5 m

50 kN is equal to:
$50/9.81 \cdot 1000$ =5097 kg. we therefore need to put $0.25 \cdot 5097 = 1274\ kg$ on the surface of $0.5 \times 0.5\ m$ to mimic the moment due to water pressure.

D.6.2. Test 4.1

After D.5Test 3, with 2 broken layers, we have put a concrete block of $1174\ kg$ on a surface of $0.5 \times 0.5\ m$, see .

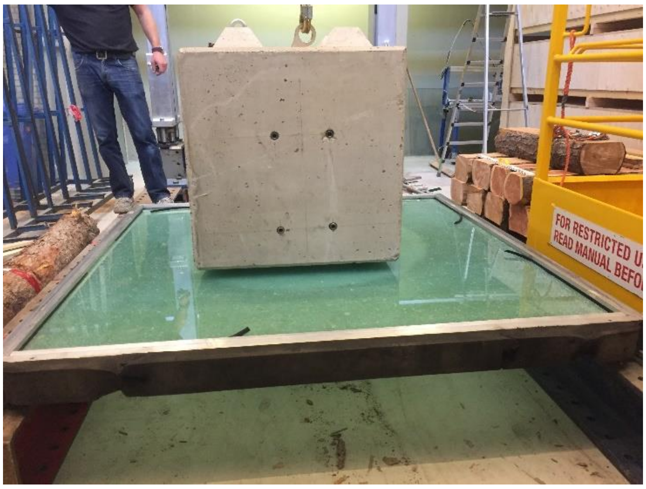

Figure D-79: The placing of the concrete block on a surface of 0.5x0.5 m

Figure D-80: Static load test

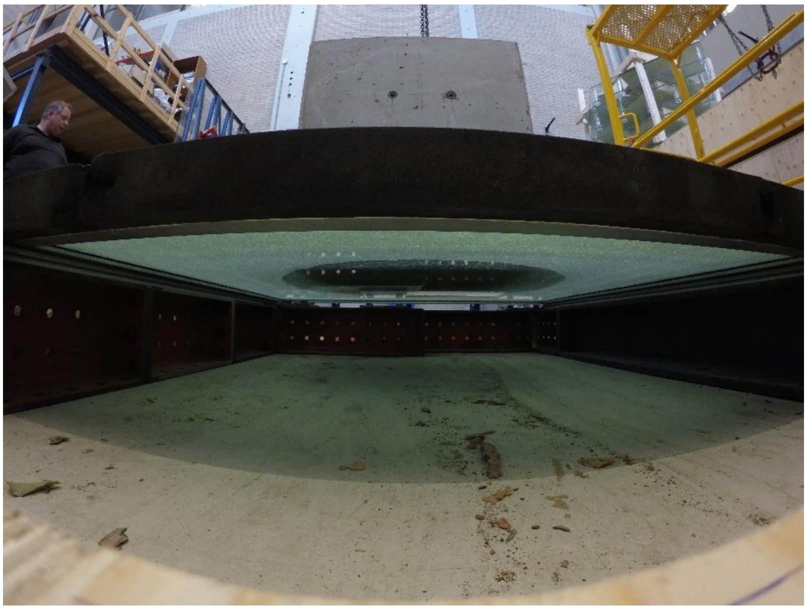

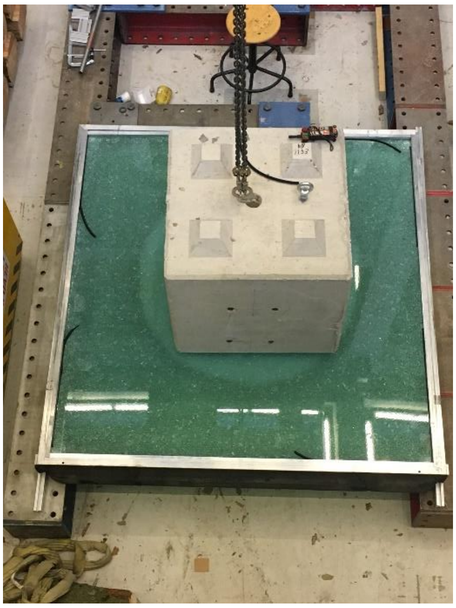

Figure D-81: Static load test view from below

Figure D-82: Static load test view from top

We left the load on the glass for three days, and nothing happened.

D.6.3. Test 4.2

After three days, we lifted the concrete of the glass, broke the third and last layer and put the weight back on. The glass cracked and squeaked for a few minutes, and deflected 1-2 cm. Then it stopped and an equilibrium was reached. In Figure D-86, the impact point of the hammer is visible as a discoloration.

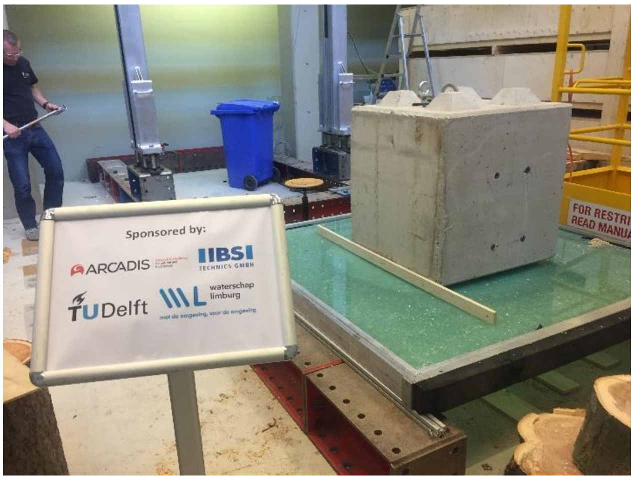

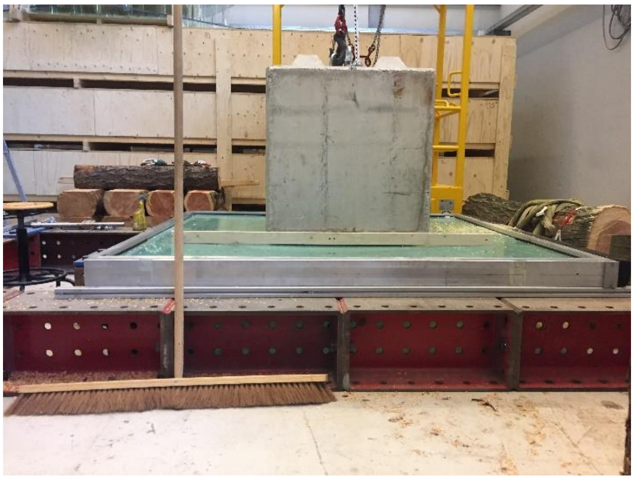

Figure D-83: Free standing concrete block on three broken layers

Figure D-84: Side view test 4.2

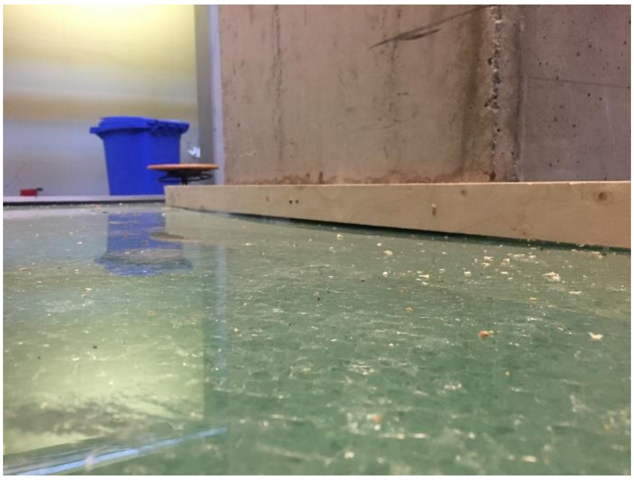

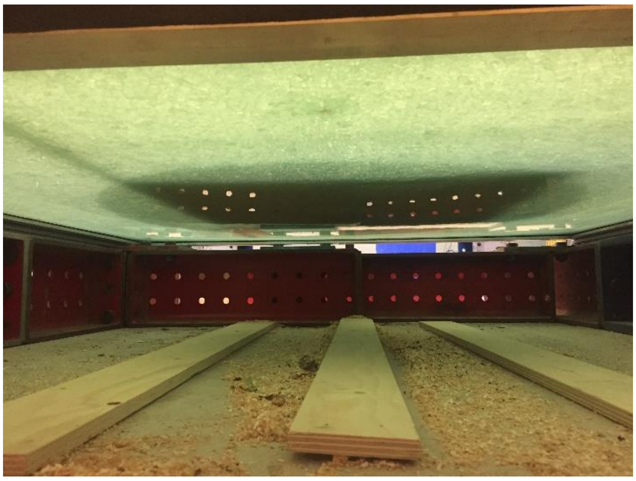

Figure D-85: Visible sag of the panel

Figure D-86: View under the panel, with location of hammer impact visible

E. Glass Calculations

E.1. Intro

There is no Eurocode yet available for structural calculations on glass, in this appendix 3 methods from 3 different building codes are elaborated on and used for glass calculations. We start with the Dutch code(NEN 2608;2014), as this is most relevant for the glass structures that will be constructed along the Meuse river. After this, a more recent method is used, taken from the Italian code (CNR-DT 210/2013). Lastly, the method from the German code(TRLV Standard) is presented and used.

E.2. NEN 2608:2014

E.2.1. Design value of plate thickness of glass panel i

The design thickness of the glass panel needs to be determined by the following formula:

$$t_{pl;i} = t_{pl} = t_{nom} - \varDelta_t$$

Where:

$t_{pl;i}$ = the glass plate thickness of glass panel i, in mm
t_{pl} = the glass thickness of a single glass sheet, in mm
t_{nom} = the nominal thickness of single glass sheet, in mm
$\varDelta_t$ = the maximum allowable deviation, in mm

For a glass plate with thickness of 19 mm, $\varDelta_t$ is 1.0 mm.

E.2.2. Equivalent glass thickness

For calculations with layered glass, the glass panel can be assigned an equivalent thickness. This equivalent thickness $t_{gg;u}$ can be used for displacement and stress checks, and can be determined by the following formulas:

$$t_{gg;u} = MIN(t_{gg;i;u})$$

$$t_{gg;i;u} = \sqrt{\frac{(1-\omega_\sigma) \cdot \sum_{j=1}^{n} t_{pl;j}^3 + \omega_\sigma \cdot \left(\sum_{j=1}^{n} t_{pl;j}\right)^3}{t_{pl;i} + 2 \cdot \omega_\sigma \cdot t_{m;i}}}$$

In ULS, and:

$$t_{gg;ser} = \sqrt[3]{(1-\omega_W) \cdot \sum_{i=1}^{n} t_{pl;i}^3 + \omega_W \cdot (\sum_{i=1}^{n} t_{pl;i})^3}$$

In SLS, where:

$t_{gg;u}$ = the equivalent thickness of layered glass in ultimate limit state (ULS) , in mm
$t_{gg;i;u}$ = the design thickness of a glass plate in a layered glass panel in ULS, in mm
$t_{gg;ser}$ = the equivalent thickness of layered glass in serviceability limit state (SLS) , in mm
ω_σ = coupling factor of the interlayer in stress $0 \leq \omega_\sigma \leq 1$
ω_W = coupling factor of the interlayer in bending $0 \leq \omega_w \leq 1$
$t_{pl;j,i}$ = the glass plate thickness of glass panel i or j in mm
n = the number of glass plates in the panel
$t_{m;i}$ = the distance from the middle of the glass plate i, and the middle of the glass panel, without taking the thickness of the interlayer into account.

The coupling factors are determined by the following formulas:

$$\omega_\sigma = \frac{1}{1 + \frac{\beta}{L_\sigma}}$$

$$\omega_W = \frac{1}{1 + \frac{\beta}{L_W}}$$

$$\beta = \frac{1}{2} \cdot \frac{\pi^2}{L_A^2} \cdot \frac{E_g}{1 - v_g^2} \cdot \frac{X}{G_{tl}}$$

Where:
L_W = form factor of bending dependent on the shape and supporting conditions of the plate
L_σ = form factor of stress dependent on the shape and supporting conditions of the plate
L_A = form factor dependent on the length and width of the plate
E_g = elasticity modulus of glass (=70 000 N/mm²)
v_g = Poisson number of glass (= 0.23)
X = maximum value of equations below
G_{tl} = shear modulus of the interlayer (also determined at the EET method)

X is the maximum value of: $X_1 = \sum_{i=1}^{n-1}(t_{pl;i} + t_{V;i})$ or $X_2 = \sum_{i=2}^{n}(t_{pl;i} + t_{V;i-1})$
In which
$t_{V;i-i}$ = The thickness of the interlayer, in mm

Since we use glass plies and interlayers of identical thickness, X_1 and X_2 are the same value.
We consider two types of support situations:

1. A 3-sided support for a concrete structure, even if an upper beam is implemented in the design, this beam is not supported directly.
2. A 2-sided support for an aluminum frame, the sides are directly supported, bottom and upper beam provide some support to the glass panel but are neglected as full support.

For a <u>2-sided</u> supported panel the following equations can be used:

$$L_A^2 = l_0^2$$

$$L_w = 1.002 \cdot \left(\frac{2 \cdot l_0}{z}\right)^{-0.04354}$$
$$L_\sigma = 1.832 \cdot \left(\frac{2 \cdot l_0}{z}\right)^{-0.60906}$$

$$z = \frac{B_1 + H_1}{2}$$

Where
L_A = the form factor dependent on the length and width of the panel
l_0 = the length of the unsupported side of the panel in mm
L_w = the form factor for bending dependent on the form and support situation of the panel
L_σ = the form factor for tension dependent on the form and support situation of the panel
B_1 = the length of the loading area parallel to side B in mm
H_1 = the length of the loading area parallel to side H in mm

For a <u>3-sided</u> supported panel the following equations can be used:

$$L_A^2 = \frac{1}{(\frac{1}{\ ^2} + \frac{1}{H^2})} \cdot (1-\theta) + l_0^2 \cdot \theta$$

$$L_w = k_w \cdot \left(\frac{2 \cdot a}{z}\right)^{-0.04354} \cdot (1-\theta) + 1.002 \cdot \left(\frac{2 \cdot l_0}{z}\right)^{-0.04354} \cdot \theta$$

$$L_\sigma = k_\sigma \cdot \left(\frac{2 \cdot a}{z}\right)^{-0.60906} \cdot (1-\theta) + 1.832 \cdot \left(\frac{2 \cdot l_0}{z}\right)^{-0.60906} \cdot \theta$$

$$\theta = \frac{l-y}{l-x} \leq 1$$

$$z = \frac{B_1 + H_1}{2}$$

Where:
L_A = the form factor dependent on the length and width of the panel
B = the width of the panel in mm
H = the length of the panel in mm
l_0 = the length of the unsupported side of the panel in mm
L_w = the form factor for bending dependent on the form and support situation of the panel
k_w = the factor for bending according to table C.3
a = the length of the shortest side of the panel in mm
L_σ = the form factor for tension dependent on the form and support situation of the panel
k_σ = the factor for tension according to table C.3
l = the length of the panel perpendicular to l_0 in mm
y = the distance from side l_0 to the middle of the loading area according to C.1 in mm
x = the smallest distance from side l to the middle of the loading area according to C.1 in mm, where $\frac{x}{l} \leq 0.5$
B_1 = the length of the loading area parallel to side B in mm
H_1 = the length of the loading area parallel to side H in mm

For both load situations:
$\frac{B}{H} = \frac{2}{2} = 1$; $k_w = 1.002$; $k_\sigma = 1.832$;

For load situation 1:
B_1=2m; H_1=2m

For load situation 2:
B_1=0.1m; H_1=0.1m

The configuration of the glass used in the IBS structure is $3x19\ mm$ FTG with Sentryglass foils, and the FEM model of the IBS structure showed that the glass is mainly supported by the side supports and is therefore 2-sided supported. The governing values are showed in green.

In the Maple calculations the following effective thicknesses are calculated for $3x19\ mm$, $4x15\ mm$ and $4x19\ mm$ plates with $2.19\ mm$ Sentryglass foils. The calculation for a $3 \times 19\ mm$ panel is done at the end of this Appendix. Shear modulus of the interlayer is assumed to be 114 MPa.

Table E-1: Summary effective thicknesses 2-sided support

2-sided support	$t_{gg;i;u}$			$t_{gg;ser}$		
	3x19mm	4x15 mm	4x19 mm	3x19mm	4x15 mm	4x19 mm

Load situation 1	53.69	57.66	71.48	53.00	56.65	69.95
Load situation 2	52.45	56.30	69.41	53.03	59.69	70.00

Table E-2: Summary effective thicknesses 3-sided support

3-sided support	$_{gg;i;u}$			$t_{gg;ser}$		
	3x19mm	4x15 mm	4x19 mm	3x19mm	4x15 mm	4x19 mm
Load situation 1	53.69	57.66	71.48	53.00	56.65	69.95
Load situation 2	52.45	56.30	69.41	53.03	59.69	70.00

E.2.3. Determination of the design value of the bending strength of prestressed glass $f_{mt;u;d}$:

$$f_{mt;u;d} = \frac{k_a \cdot k_e \cdot k_{mod} \cdot k_{sp} \cdot f_{g;k}}{\gamma_{m;A}} + \frac{k_e \cdot k_z \cdot (f_{b;k} - k_{sp} \cdot f_{g;k})}{\gamma_{m;V}}$$

Table E-3: Explanation of symbols design value of strength NEN

Symbol	Meaning	Formula or explanation	Value
$f_{mt;u;d}$	Design value of the bending strength	See above	TBD
k_e	The factor for the edge quality	Heat strengthened Loaded out of plane	1.0
k_a	The factor for the surface effect	$1.664 \cdot A^{-(\frac{1}{25})}$ for concentrated load or non-linear calculation of bending stress 1.0 for distributed loading	TBD
A	The loading surface	$H1 \times B1$ of the load in mm^2	TBD
k_{mod}	The modification factor	$(\frac{5}{t})^{\frac{1}{c}}$	TBD
c	Corrosion constant	For middle zone For edge zone	18 16
t	Time duration of loading	Dependent on situation	TBD
k_{sp}	The factor for surface structure	Float glass	1.0
$f_{g;k}$	The characteristic bending strength of glass	Float glass	45 [N/mm²]
$f_{b;k}$	The characteristic bending strength of prestressed glass	Fully Tempered Glass	120 [N/mm²]
$\gamma_{m;A}$	The material factor of glass	Other load than isochoric pressure or wind pressure	1.8
$\gamma_{m;V}$	The material factor of prestressed glass	Fixed	1.2
k_z	Factor for the loading zone	It is assumed the load will not occur in the corners of the glass, and these will partly be protected	1.0

The following value for the design bending strength for a short duration load is calculated:

$$t = 3$$

$$A = 100 \cdot 100 = 100000$$

$$k_a = 1.664 \cdot 100000^{-\left(\frac{1}{25}\right)} = 1.151$$

$$k_{mod} = (\frac{5}{t})^{\frac{1}{c}} = 1.0288$$

$$f_{mt;u;d} = \frac{1.151 \cdot 1.0 \cdot 1.0288 \cdot 1.0 \cdot 45}{1.8} + \frac{1.0 \cdot 1.0 \cdot (120 - 1.0 \cdot 45)}{1.2} = 92.1\ MPa$$

The following value for the design bending strength for a long duration load is calculated:

$$t = 60 \cdot 60 \cdot 24 \cdot 30 = 2592000$$
$$A = 0.1 \cdot 0.1 = 0.01$$
$$k_a = 1.0$$
$$k_{mod} = (\frac{5}{t})^{\frac{1}{c}} = 0.481$$

$$f_{mt;u;d} = \frac{1.0 \cdot 1.0 \cdot 0.481 \cdot 1.0 \cdot 45}{1.8} + \frac{1.0 \cdot 1.0 \cdot (120 - 1.0 \cdot 45)}{1.2} = 74.5\ MPa$$

Table E-4: Stress limits different load situations NEN

Load situation	Duration and load area	
1	Duration: 3-5 sec Load surface area: 0.1x0.1m	92.10 [MPa]
2	Duration: 1 week Load surface area: 2x2m	74.53 [MPa]

E.2.4. Ultimate limit state unity check

The unity check for the maximum allowable stress is as follows:

$$\frac{\sigma_{pl;mt;i;d}}{f_{mt;u;d}} \leq 1.0$$

Where:

$\sigma_{pl;mt;i;d}$ = the design value of the bending stress in glass pane i
$f_{mt;u;d}$ = the design value of the bending strength according to the formula

The occurring stresses are calculated and checked in Appendix I: FEM Model

E.3. CNR-DT 210/2013

The Italian code for structural glass is considered(by some) to be most accurate as it uses the most recent research to calculate various aspects of design. To calculate the maximum stress and deflection, this code provides the method of Enhanced Effective Thickness(EET), proposed by Laura Galuppi and Gianni Royer-Carfagni. This method gives accurate results in comparison to FEM calculations. Especially for multi-layered laminates the method is found to be accurate where some other methods are not(for example the Bennison-Wölfel approach from the American code ASTM E1300-09). It will therefore be used in the calculation of a multi layered plate and compared to the calculations from the NEN and layered calculations from the TRLV.

E.3.1. Design value of strength

The design value of the bending strength of glass according to the CNR-DT 210/2013 can be calculated with the following formula and is of the same base as the NEN:

$$f_{g;d} = \frac{k_{mod} \cdot k_{ed} \cdot k_{sf} \cdot \lambda_{gA} \cdot \lambda_{gL} \cdot f_{g;k}}{R_M \gamma_M} + \frac{k'_{ed} \cdot k_v \cdot (f_{b;k} - f_{g;k})}{R_{M;v} \gamma_{M;v}}$$

It is assumed all structural elements are in CC2, consequence class 2 of the Eurocode.

Table E-5:Explanation of symbols design value of strength CNR

Symbol	Meaning	Formula or explanation	Value	
$f_{g;d}$	Design value of the bending strength	See above	TBD	
k_{mod}	Reduction factor for environmental conditions and load duration	 LEFM prEN16612	<u>3-5 sec</u> 0.88 – 0.91 1.0	<u>1 month</u> 0.39 0.41
k_{ed}	Factor for edge or hole quality	Loaded in bending	1.0	
k'_{ed}	Factor for edge or hole quality	Loaded in bending	1.0	
k_{sf}	Reduction factor of surface treatment	No treatment floatglass	1.0	
k_v	Reduction factor for the heat treatment process	Horizontal heat treatment	1.0	
λ_{gA}	Scale factor for the surface area	Distance from edge $> 5 \cdot t \rightarrow \lambda_{gA} = 1.0$	1.0	
λ_{gL}	Scale factor for the stress near element edge	Plates in bending	1.0	
$f_{g;k}$	The characteristic bending strength of glass	Float glass	45 [N/mm²]	
$f_{b;k}$	The characteristic bending strength of prestressed glass	Fully Tempered Glass	120 [N/mm²]	
γ_M	The material factor of annealed glass	Fixed for ULS	2.5	
R_M	Reduction factors of partial factor	Class 2	1.0	
$\gamma_{M;v}$	The material factor of prestressed glass	Fixed for ULS	1.35	
$R_{M;v}$	Reduction factors of the partial material factor	Class 2	1.0	

Where LEFM is short for Linear-Elastic Fracture model, and all descriptions and values can be derived from tables in chapter 7.4 in de CNR-DT 210/2013.

The following value for the design bending strength for a short duration load is calculated:

$$t = 3$$
$$k_{mod} = 0.88$$

$$f_{g;d} = \frac{0.88 \cdot 1.0 \cdot 1.0 \cdot 1.0 \cdot 1.0 \cdot 45}{1.0 \cdot 2.5} + \frac{1.0 \cdot 1.0 \cdot (120 - 45)}{1.0 \cdot 1.35} = 71.40$$

The following value for the design bending strength for a long duration load is calculated:

$$t = 60 \cdot 60 \cdot 24 \cdot 30 = 2592000$$
$$k_{mod} = 0.481$$

$$f_{g;d} = \frac{0.39 \cdot 1.0 \cdot 1.0 \cdot 1.0 \cdot 1.0 \cdot 45}{1.0 \cdot 2.5} + \frac{1.0 \cdot 1.0 \cdot (120 - 45)}{1.0 \cdot 1.35} = 62.58$$

Table E-6: Stress limits different load situations CNR

Load situation	Duration and load area	
1	Duration: 3-5 sec Surface area: 0.1x0.1m	71.40 [MPa]
2	Duration: 1 week Surface area: 2x2m	62.58 [MPa]

These values are lower than the values obtained with the NEN calculation.

E.3.2. The Enhanced Effective Thickness (EET) method:

In the CNR-DT a few calculations examples are made with the EET method and compared to FEM-calculations, with promising similarities. Therefore, a calculation with this method is also made in this report.
The maximum stress in the plate is expressed as:

$$\sigma_{i,max} = \max_x \frac{6|M(x)|}{b\hat{h}_{1;\sigma}^2} = \max_x \left| \frac{N_i(x)}{A_i} \pm \frac{M_i(x)}{I_i}\frac{h_i}{2} \right|$$

Where the deflection-effective thickness of both plates and beams is calculated with:

$$\hat{h}_w = \sqrt[3]{\frac{1}{\dfrac{\eta}{\sum_{i=1}^{N} h_i^3 + 12\sum_{i=1}^{N}(h_i d_i^2)} + \dfrac{(1-\eta)}{\sum_{i=1}^{N} h_i^3}}}$$

And the stress-effective thickness is calculated with:

$$\hat{h}_{i;\sigma} = \sqrt{\frac{1}{\dfrac{2\eta|d_i|}{\sum_{i=1}^{N} h_i^3 + 12\sum_{i=1}^{N}(h_i d_i^2)} + \dfrac{h_i}{\hat{h}_w^3}}}.$$

In the above-mentioned formula, the generic coefficient $\eta$is used for both plates and beams and all load cases. The definition of this coefficient, however, is given for the calculation of multi-layered <u>beams</u>, and <u>two-layered</u> plates, while we want to calculate the effective thickness of three or four (multi-)layered plates. Both governing formulas are presented below and will be converted into an expression for a three-layered laminated glass plate. It must be noted that the shear modulus of Sentryglass is time and temperature dependent,

E.3.3. Monolithic and layered behavior

D_{abs} for a plate or J_{abs} for a beam is the behavior of separate plates of glass, sliding over each other without friction, and D_{full} is the behavior of full cooperation between plates: the plate behaves as monolithic. In reality, the value of the stiffness is in between these values and this can be approached by using the interlayer properties to calculate a coupling factor. In the EET method this coupling factor is called η(eta).
D_{abs} or J_{abs} is calculated as the sum of all separate plate stiffnesses. D_{full} and J_{full} are calculated as the sum of all thicknesses as one plate/beam thickness to calculate the stiffness. See the 2 examples for plate stiffness D_{abs} and D_{full} below:

$$J_{full} = \sum_{i=1}^{n} (J_i + A_i d_i^2) = J_{abs} + \sum_{i=i}^{n} A_i d_i^2 \,,$$

for beams with 2 plies

$$J_{full} = \frac{Nb}{12}[h^3 + h(h+h_{int})^2(N-1)(N+1)]$$

for beams with multiple plies

$$D_{full} = D_{abs} + \frac{E}{(1-\nu^2)} \frac{h_1 h_2}{h_1 + h_2} d^2 .$$

for plates with 2 plies

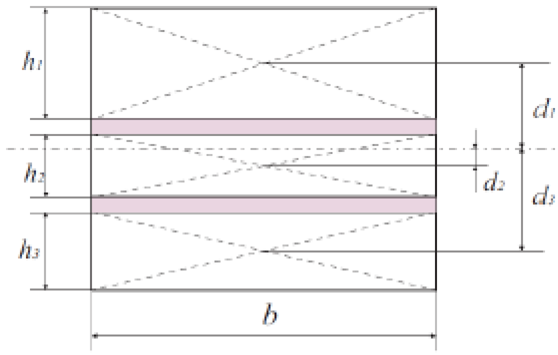

Figure E-1: Glass layers and interlayers

To calculate η(eta), the following expression is used for 3 plies:

$$\eta_{1D,3} = \frac{1}{1 + \dfrac{E\Psi}{G_{int}\left(\sum_{i=1}^{3} h_i^3 + 12\sum_{i=1}^{3} h_i d_i^2\right)\left(\dfrac{(d_1+d_2)^2}{h_{int,1}} + \dfrac{(d_2+d_3)^2}{h_{int,2}}\right)} \sum_{i=1}^{3} h_i^3 \sum_{i=1}^{3} h_i d_i^2}$$

This formula gives the solution for η when there are 3 plies of various thicknesses. The next formula for η(eta) holds for multiple plies of the same thickness:

$$J_{full} = \frac{Nb}{12}[h^3 + h(h+h_{int})^2(N-1)(N+1)]$$

e

$$\eta_{1D,N} = \frac{1}{1 + \dfrac{Eh_{int}}{12G_{int}} \dfrac{Nh^3(N+1)}{h^2 + (h+h_{int})^2(N^2-1)}\Psi}$$

When η is determined, $\hat{h}_{i;\sigma}$ and $\hat{h}_w$ can be calculated. After all these parameters are known, it is time to calculate the maximum stress and deflection. To be able to vary with some of the parameters, maple is used for the calculation. The maximum moment in the "beam" and the maximum stresses due to water load are calculated in maple file "glass calculation water pressure" We will consider the first two load combinations separately as their duration and shape functions are different. The stresses that occur from the load combinations, however, need to be combined as these loads occur simultaneously. The hand calculation is done for a square plate of 2000x2000mm. For both combinations the shear modulus of the interlayer is chosen at 20 degrees Celsius, because it is unlikely that the water temperature in the Maas will be higher than that during a flood(floods occur in wintertime and the water cools the glass). The higher the temperature, the lower the shear modulus so this is considered to be on the safe side. For the collision (load duration: 3 sec) the G modulus of Sentryglass is 211 MPa. For the water level (load duration: 1 day-1 month) G=~120 MPa. Because the shear modulus varies a lot a safety factor of 1.5 is applied.

Table E-7: Design value of shesr modulus

Design value of shear modulus	**T=20°, t=3 sec**	**T=20°, t= 1 month**
$\frac{G_{int}}{1.5}$	140 MPa	114 MPa

See table from the Kuraray Sentryglass Datasheet:

Table E-8: Shear modulus Sentryglass

SHEAR MODULUS: SENTRYGLAS®

		Load Duration						
	Shear Modulus G MPa (psi)	1 s	3 s	1 min	1 h	1 day	1 mo	10 yrs
Temperature	10 °C (50 °F)	240. (34 800)	236. (34 220)	225. (32 625)	206. (29 870)	190. (27 550)	171. (24 795)	153. (22 185)
	20 °C (68 °F)	217. (31 465)	211. (30 595)	195. (28 275)	169. (24 505)	146. (21 170)	112. (16 240)	86.6 (12 557)
	24 °C (75 °F)	200. (29 000)	193. (27 985)	173. (25 085)	142. (20 590)	111. (16 095)	73.2 (10 614)	43.3 (6 279)
	30 °C (86 °F)	151. (21 895)	141. (20 445)	110. (15 950)	59.9 (8 686)	49.7 (7 207)	11.6 (1 682)	5.31 (770)
	40 °C (104 °F)	77.0 (11 165)	63.0 (9 135)	30.7 (4 452)	9.28 (1 346)	4.54 (658.3)	3.29 (477.1)	2.95 (427.8)
	50 °C (122 °F)	36.2 (5 249)	26.4 (3 828)	11.3 (1 639)	4.20 (609)	2.82 (408.9)	2.18 (316.1)	2.00 (290)
	60 °C (140 °F)	11.8 (1 711)	8.18 (1 186)	3.64 (527.6)	1.70 (246.5)	1.29 (187.1)	1.08 (156.6)	0.97 (140.7)
	70 °C (158 °F)	3.77 (546.7)	2.93 (424.9)	1.88 (272.6)	0.84 (121.8)	0.59 (85.6)	0.48 (69.6)	0.45 (69.6)
	80 °C (176 °F)	1.55 (224.8)	1.32 (191.4)	0.83 (120.4)	0.32 (46.4)	0.25 (36.3)	0.21 (30.5)	0.18 (26.1)

E.4. Effective thickness

As can be seen from the table below, ψ is $10/l^2$, in the case that the length of the plate(height) is 2 meters, ψ is 2,5. This is also the case for the point load, so:

$$\psi = \frac{10}{2^2} = 2.5\ [-]$$

Table E-9: Determination of value ψ

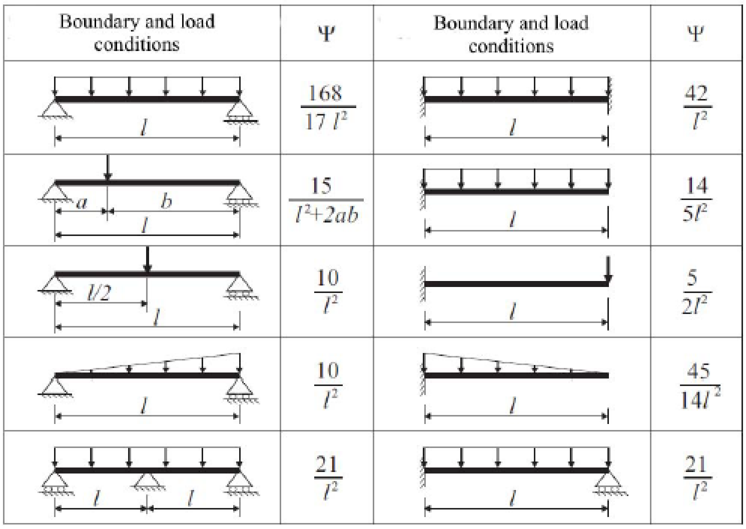

Boundary and load conditions	Ψ	Boundary and load conditions	Ψ
	$\frac{168}{17\,l^2}$		$\frac{42}{l^2}$
	$\frac{15}{l^2+2ab}$		$\frac{14}{5l^2}$
	$\frac{10}{l^2}$		$\frac{5}{2l^2}$
	$\frac{10}{l^2}$		$\frac{45}{14l^2}$
	$\frac{21}{l^2}$		$\frac{21}{l^2}$

A shear modulus of the interlayer of 114 MPa is assumed. Number of plies is 3.

$$E = 70000000\ kN/m^2$$
$$h = 0.018\ m$$
$$v = 0.23$$
$$G_{int} = 114000\ kN/m^2$$
$$h_{int} = 0.00229\ m$$
$$\psi = 2.5$$
$$N = 3$$
$$d = h + h\_int$$

$$eta_{2DN} = \frac{1}{1 + \frac{E * h_{int}}{12 * G_{int} * (1 - v^2)} * \frac{N * h^3 * (N+1)}{h^2 + (h + h_{int})^2 * (N^2 - 1)} * \psi} = 0.995$$

$$h_w = \sqrt[3]{\frac{1}{\frac{eta_{2DN}}{N * h^3 + 12 * (N-1) * (h * d^2)} + \frac{1 - eta_{2DN}}{N * h^3}}} = 0.0571\ m$$

$$h_{i;sigma} = \sqrt{\frac{1}{\frac{2 * eta_{2DN} * \sqrt{(d^2)}}{12 * (N-1) * d^2 * h + N * h^3} + \frac{h}{h_w^3}}} = 0.0574\ m$$

Table E-10: Summary effective thickness CNR

Effective thickness	3x19 mm	4x15 mm	4x19 mm
Deflection related	57.1	53.5	65.1
Stress related	57.4	57.3	69.9

E.5. TRLV Standard 2006

The German standard on glass codes only consider coupled behavior (to some extend) of plates when the glass is annealed. If the glass is laminated and prestressed (heat-strengthened or tempered), layered behavior is assumed, but the allowable stress maxima are increased:

E.5.1. Limit stress:

For long duration loads on laminated annealed glass the maximum allowable stress is increased from $12\ MPa$ to $15\ MPa$.
For short duration loads the maximum allowable stress is increased from $18\ MPa$ to $22.5\ MPa$. For overhead glazing the conditions of long duration loading apply for any situation.

The limit stress for ESG(FTG) is $50\ N/mm^2$, which is considerably lower that the stress limits calculated with the NEN and the CNR codes.

E.5.2. Effective thickness

The German code neglect the cooperation between glass panes “Ohne verbund”, and the effective thickness becomes the lower limit of the layered theory by multiply the stiffnesses of the 3 separate panes:

$$D = N \cdot \frac{Et^3}{12(1-v^2)} = 3 \cdot \frac{70000 \cdot 18^3}{12(1-0.23^2)} = 108 \cdot 10^6\ Nmm$$

This corresponds to an effective thickness of:

$$\frac{70000 \cdot t_{eff}^3}{12(1-0.23^2)} = 108 \cdot 10^6\ Nmm \rightarrow t_{eff} = 25.96\ mm$$

Not taking the interlayer into account decreases the effective thickness drastically. It can be concluded that the German standard is the most conservative of the three considered building codes.

E.6. Conclusion

In the three different codes, the behavior of laminated glass is assumed to be between monolithic and layered. These are the upper and lower boundaries of the strength and bending behavior of the laminated glass. Monolithic behavior means full cooperation between the plates, as if it was one glass plate, this makes the stiffest and strongest plate or beam and is considered the upper boundary of the laminated glass strength.
Layered means the behavior of separate plates of glass, sliding over each other without friction. In reality, the value of the stiffness is in between these values and this can be approached by using the interlayer properties to calculate a coupling factor. The coupling factor represents the extent to which the plates are coupled and its value lies between 0 and 1. In the Italian CNR-DT 210/2013 this coupling factor is called η(eta). In the NEN 2608:2014, this coupling factor is called ω_σ or ω_W, depending on the limit state.
The German code does not take any coupling of the plates into account and assumes the lower limit of layered behavior of the glass panels.
The latter results in very conservative and uneconomic design compared to the other two methods, especially if the glass is laminated with Sentryglass, which is a quite expensive interlayer that results for short loads in a coupling factor close to 1, resulting in almost monolithic behavior.

F. Location analysis

F.1. Intro

The project locations are a few dike trajects in Waterschap Limburg, in former Waterschap Peel en Maasvallei, directly situated along the river the Maas. Currently, a total length of 3.2 km is protected by demountable flood defences, these are Aluminum structures where only the frame and foundation are permanent. In case of high water these defences can be build up relatively quick but erecting 3.2 km of these defences takes quite some time and manhours. Maintaining these defences is expensive, and and there are many failure mechanisms and difficulties that may occur when erecting these flood defences. For example, strong winds or snowfall could slow down the build-up process and if the road is obstructed the workers and/or materials might be unable to reach the flood defences in time. It is also very expensive to maintain through the years as the workmen responsible for the build-up need yearly training, and the materials have to be stored and tested frequently. [Arcadis. (2016)]

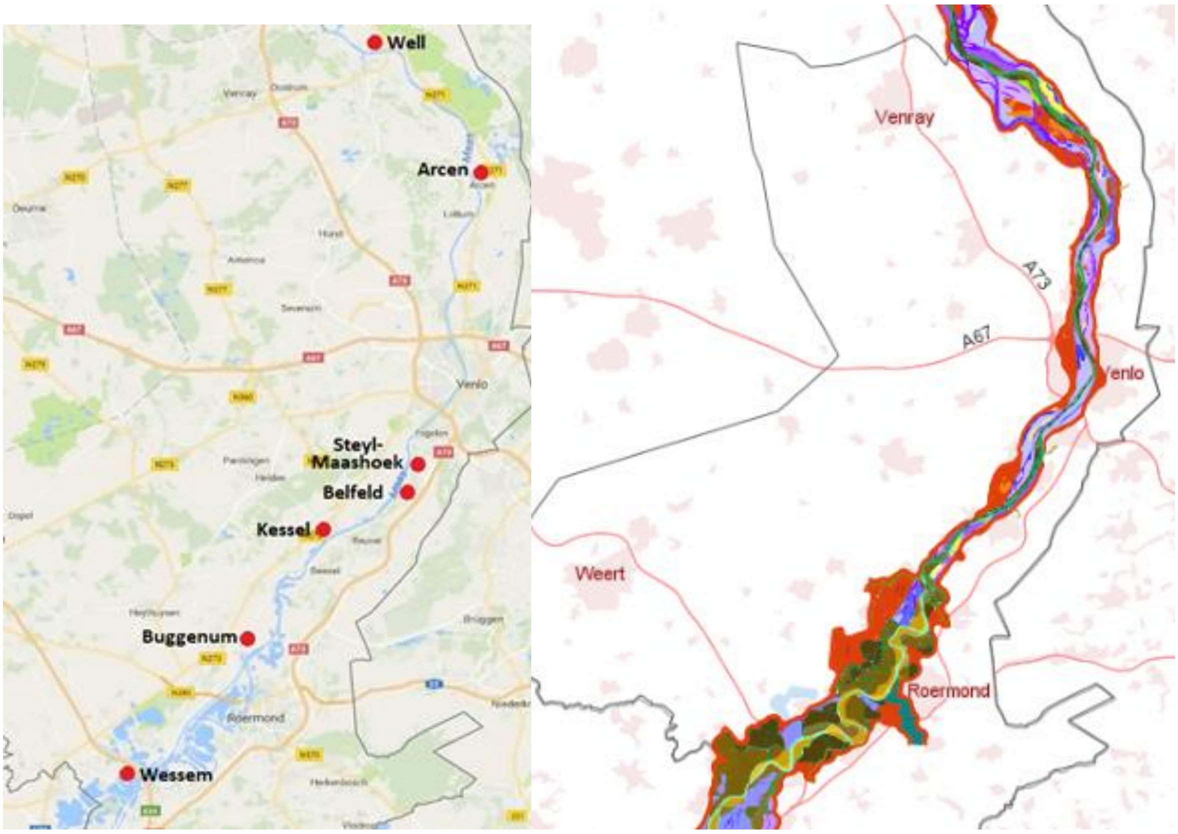

Figure F-1: Left: geographical locations along the maas (google maps); right geomorphogenetical map locations [GIS(2017)]

Figure F-2: Example of a demountable flood defence in Steyl, Limburg [Arcadis (2016)]

Besides the demountable flood defences, also some concrete flood walls could be replaced by glass walls. A few locations that are candidates for a glass flood wall are stated in the "Memo ontwerpuitgangspunten glazen keringen". These are summarized below.

Table F-1: Summary locations

Loacation	Description
Well	The flood defence divides the Maas and a cemetery, a parking lot and a dining area
Arcen	The current flood defence consists of demountable flood defences, flood walls and dike disconnections. A large part of the system is situated in the back yards of residents.
Steyl-Maashoek	The flood defence is situated directly between the Maas and a road with parking spaces, along residential homes and a village centre. It consists of a demountable flood defence and a permanent flood wall.
Belfeld	There is a concrete floodwall present, interrupted at some places by demountable flood defences. Also mainly situated in the gardens of residents.
Kessel	Kessel is currently protected by a dike, with a very large foreshore. A road, the Haagweg, separates the crest of the dike and residential homes. The flood defence could be placed on the crest of the dike, the foreshore and mild slope of the dike can protect the glass wall against larger impact
Buggenum	The flood defence is situated between a small road, the Dorpsstraat, and an elongated port, which is protected from the Maas by a longitudinal dam.
Wessem	On top of the current dike, a small masonry structure (30 cm) protects the road and houses on top of the dike along the Maasboulevard, which later transitions into the Polstraat, seemingly without this masonry structure.

F.2. System scope

In this project the system will consist of the river the Maas, the flood defence, and the hinterland including roads and houses. Most of the possible locations have little to no foreshore.

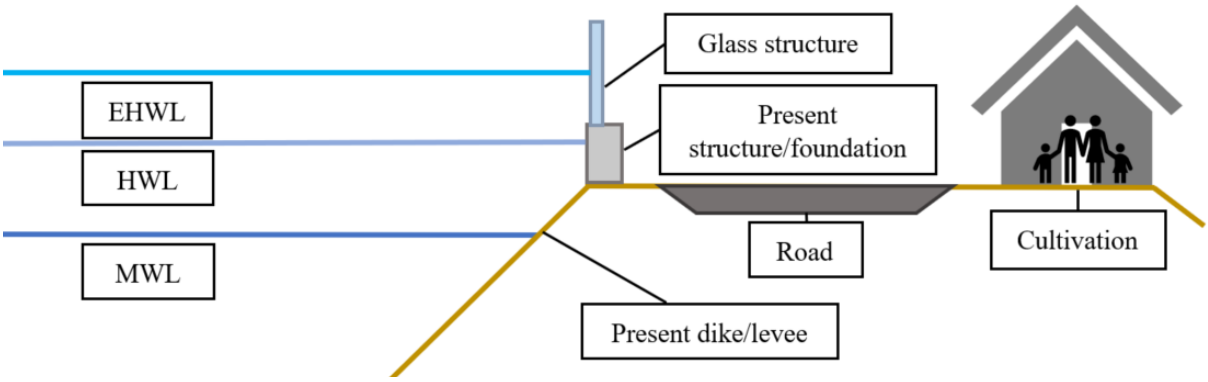

Figure F-3: Typical future situation with Mean Water Level(MWL), High Water Level(HWL) and Extreme High Water Level(EHWL)

F.3. Well

F.3.1. Visualization and geographical location flood defence line

Figure F-4: F.3.1. Visualization and geographical location flood defence line[Arcadis(2016)]

Figure F-5: probe locations Well [Dino loket (2017)]

F.3.2. Geotechnical parameters

The relevant ground probes are summarized below:

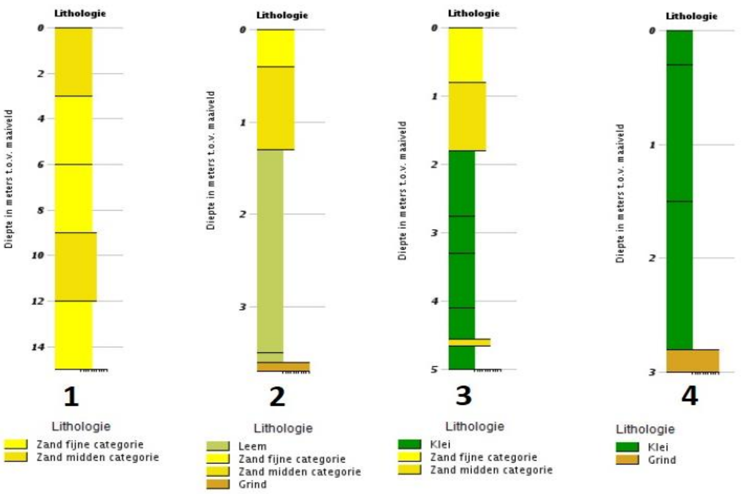

Figure F-6: Inventory ground probes Well [Dino Loket (2017)]

Inventory ground probes Source: Dino Loket

Due to the Maas different deposits and river progressions, the ground layers along this traject seem to vary enormously. From left to right the compositions changes from mainly sand to mainly leem to mainly clay. When building a structure at these locations, foundation enhancements and more geotechnical research is in order.

Table F-2: Water height information measure point Well

Water level	Height [m]
Low water level	<11.05
Normal water level	11.05-12.60
Above normal water level	>12.60
High water level	>14.30
Extremely high water level	>15.00

Table F-3: Height of ground level at probe locations

Probe	Probe depth [m]	Height from NAP [m]	Distance from MWL Maas to probe location
1	0-15	14	
2	0-3.7	13	
3	0-5	14.50	
4	0-3	13	

Additional information from [Memo ontwerpuitgangspunten glazen keringen]:

- The governing water height that needs to be retained is NAP +16 m
- There is a foreshore of 10 m present with a mild slope up to NAP +13.5
- Ships can reach the flood defence if their draught is less than 2.5 meter
- On the other side of the river there are a few mooring places for recreational boats
- Upstream there are almost no mooring places for boats, this means with a shipping restriction, there is little chance of collision

F.4. Arcen

Visualization

Figure F-7:Visualization Arcen [Arcadis(2017)]

Geographical location flood defence line

Figure F-8: Left: indication flood defence line Right: inventory ground probes

From the map it is visible that the height around the location of the flood defence varies around 13-18 m

Geotechnical parameters

The six relevant ground probes are summarized below:

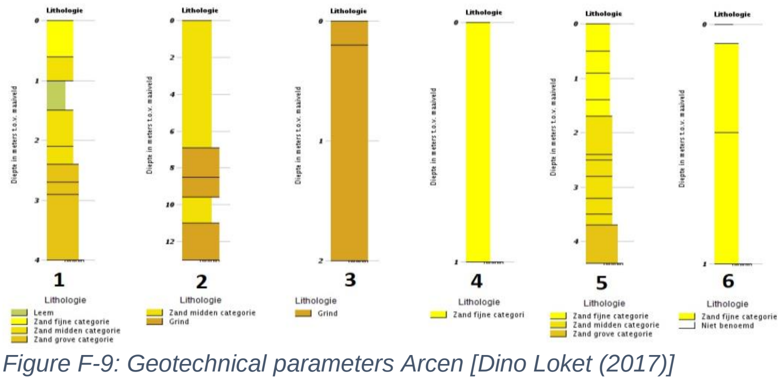

Figure F-9: Geotechnical parameters Arcen [Dino Loket (2017)]

The 6 probes, ranging from 0-1 [m] to 0-12,5 [m], give insight in the main ground layers that are present below the flood defence. Typical for a situation in Limburg, the largest part of the underlayer consists of coarse to fine sand. Sand layers are usually stable and have minimal consolidation, which is a good quality for an underlayer. From the six probes, the majority has a top layer (1 [m]) of fine sand. It can be assumed the middle layers consist of varying layers of coarse and fine sand and below this a layer of gravel.

The mean water level at Arcen is calculated over a period of time from the year 1849 to date 31-12-1995. MWL= +10.538 m above NAP.

Water height information Arcen:

The measure location of Arcen has been dissolved since 1995. The information is retrieved by interpolation between the measurements of Well and Venlo and may not be accurate.

Table F-4: Water levels Arcen

Water level	Height [m] Well	Height [m] Venlo
Low water level	<11.05	<11.05
Normal water level	11.05-12.60	11.05-14.60
Above normal water level	>12.60	>14.60
High water level	>14.30	>16.60
Extremely high water level	>15.00	>17.90

Height of ground level at probe locations:

Table F-5: Height of ground level at probe locations Arcen

Probe	Probe depth [m]	Height from NAP	Distance from MWL Maas to probe location
1	0-4	16.5	+5.962
2	0-13	16	+5.462
3	0-2	4,90 (unknown)	-
4	0-1	15.57	+5.032
5	0-4.40	15.99	+5.452
6	0-1	16.06	+5.522

Additional information from [Memo ontwerpuitgangspunten glazen keringen]:

- The governing water height that needs to be retained is NAP 18.40+ m
- The possibility of drifting ships is small, there are no mooring places in the direct neighborhood
- Upstream a camping is present, from which canoe’s/kayaks might float to the flood defence
- According to the Maas-model of Rijkswaterstaat(RWS) the water speed present at the location will be 1.90 m/s
- Kinetic energy is therefore assumed to have an angle of incidence of 22.5°

F.5. Steyl-Maashoek

Visualization

Figure F-10: Visualization Steyl-Maashoek[Arcadis(2017)]

Geographical location flood defence line

Figure F-11: Left: indication flood defence line (Arcadis report) Right: inventory ground probes [Dino Loket (2017)]

Geotechnical parameters

The relevant ground probes are summarized below:

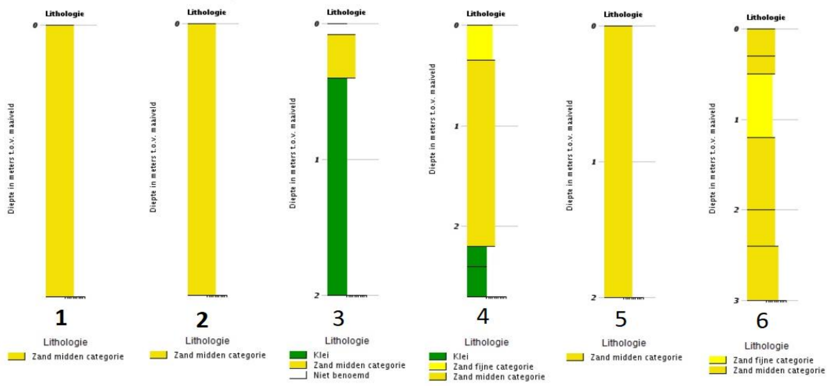

Figure F-12: Inventory ground probes Steyl-Maashoek [Dino Loket(2017)]

For this location the first two probes are less than one meter, and the others are also quite shallow measurements. The top layers consist of sand, with clay layers below. Information about the deeper layers is missing.

Height of ground level at probe locations:

Table F-6: Height of ground level at probe locations Steyl-Maashoek

Probe	Probe depth [m]	Height from NAP	Distance from MWL Maas to probe location
1	0-0.70	16.82	
2	0-0.60	16.88	
3	0-2	17.11	
4	0-2.70	16.97	
5	0-2	16.88	
6	0-3	16.75	

Water height information measurement point "Belfelt beneden":

Table F-7: Water height information measurement point "Belfelt beneden":

Water level	Height [m]
Low water level	<11.05
Normal water level	11.05-14.80
Above normal water level	>14.80
High water level	>17.00
Extremely high water level	>18.40

Additional information from [Memo ontwerpuitgangspunten glazen keringen]:

- The governing water height that needs to be retained is NAP 20.5+ m
- There is a foreshore of 20 m present with a mild slope up to NAP +17
- Ships can reach the flood defence if their draught is less than 3.5(in report 2.5?) m
- There is a relevant possibility ships can drift from the mooring place in between the flood defence and the upstream weir and sluice
- The flood defence is situated in a river bend, the angle of incidence of the kinetic energy will therefore be assumed to be around 40.0°
- According to the Maas-model of RWS, the water speed will be around 1.33 m/s

F.6. Belfelt

Visualization and geographical location flood defence line

Figure F-13: Left: Visualization [Arcadis (2017)] Right: indication flood defence line [Arcadis(2017)]

Geotechnical parameters

No relevant ground parameters were found at the location.

Water height information measure point “Belfelt boven”:

Table F-8: Water height information measurement point “Belfelt boven”:

Water level	Height [m]
Low water level	<13.90
Normal water level	13.90-15.10
Above normal water level	>15.10
High water level	>17.30
Extremely high water level	>18.70

Additional information from [Memo ontwerpuitgangspunten glazen keringen]:

- The governing water height that needs to be retained is NAP 20.1+ m
- There is a small strip of foreshore m present with a mild slope up to NAP +18.5
- Ships can reach the flood defence if their draught is less than 2.6 m
- 2.5 km upstream a yacht marina is located, with moored recreational ships
- Due to the course of the river and the large distance from the marina it is unlikely that ships will collide with the flood defence
- According to the Maas-model of RWS, the water speed will be around 2.0 m/s
- Kinetic energy is assumed to have a minimum angle of incidence of 22.5°

F.7. Kessel

Visualization

Figure F-14: Visualization Kessel [Funda(2017), Haagweg 28]

Geographical location flood defence line

Figure F-15: Left: Indication flood defence line [Arcadis(2017)] Middle: Inventory ground probes Right: Ground probes [Dino Loket(2017)]

Unfortunately, there is but one relevant probing available, which is measured until 3 m below ground level. The ground layers are built up from gravel, sand and clay. It can be concluded that the amount of information about this location is insufficient.

Probe	Probe depth [m]	Height from NAP	Distance from MWL Maas to probe location
1	0-3	15.86	

Water height information Kessel:
There is no measurement station present at Kessel. The information can be retrieved by interpolation between the measurements of "Belfelt Boven" and "Neer".

Table F-9: Water levels Kessel

Water level	Height "Belfelt Boven"	Height [m] "Neer"
Low water level	<13.90	<14.05
Normal water level	13.90-15.10	14.05-16.10
Above normal water level	>15.10	>16.10
High water level	>17.30	>18.20
Extremely high water level	>18.70	>19.90

Additional information from [Memo ontwerpuitgangspunten glazen keringen]:

- The governing water height that needs to be retained is NAP +21 m
- There is a large foreshore of 150 m present with a mild slope up to NAP +17 m
- Ships are able to reach the flood defence if their draught is less than 4 m
- According to the Maas-model of RWS, the water speed will be around 1.72 m/s
- Kinetic energy is assumed to have a minimum angle of incidence of 22.5°

F.8. Buggenum

Visualization

Figure F-16: Visualization Buggenum [Arcadis (2017)]

Geographical location flood defence line

Figure F-17: Left: indication flood defence line (Arcadis report) Right: Inventory ground probes Buggenum

Geotechnical parameters

The relevant ground probes are summarized below:

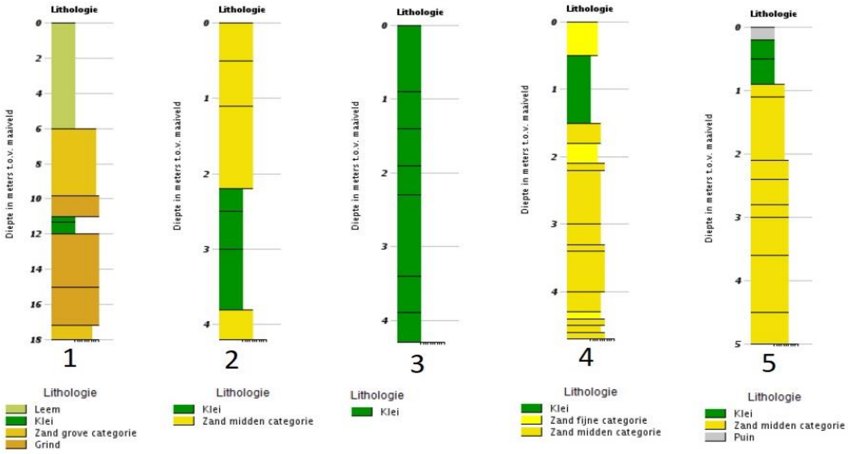

Figure F-18: Inventory ground probes [Dino Loket(2017)]

Height of ground level at probe locations:

Table F-10: Height of ground level at probe locations Buggenum

Probe	Probe depth [m]	Height from NAP	Distance from MWL Maas to probe location
1	0-18	17	
2	0-4.20	19.77	
3	0-4.30	18.78	
4	0-4.70	20	
5	0-5	19.07	

Water height information “Buggenum”:

Table F-11: Water height information “Buggenum”

Water level	Height [m]
Low water level	<13.75
Normal water level	13.75-16.50
Above normal water level	>16.50
High water level	>18.40
Extremely high water level	>20.00

Additional information from [Memo ontwerpuitgangspunten glazen keringen]:

- The governing water height that needs to be retained is 21.5 NAP+m
- The Asseltse plassen, where a lot of recreational shipping takes place, are near the flood defence but the chances that a ship will reach the flood defence are small
- Ships can reach the flood defence if their draught is less than 3 m

- There is a mooring area in front of the flood defence, but separated by a bank with height of NAP +18.5
- The flood defence is situated in a river bend, upstream ships are able to reach the flood defence
- According to the Maas-model of RWS, the water speed will be around 1.40 m/s
- Kinetic energy is assumed to have a minimum angle of incidence of 22.5°

F.9. Wessem

Visualization

Figure F-19: Visualization Wessem; left: Maasboulevard [Arcadis(2017)], right: Polstraat [Arcadis(2017)]

Geographical location flood defence line

Figure F-20: Indication flood defence line Wessem [Arcadis(2016)]

Figure F-21: Left: inventory ground probes Maasboulevard Right: inventory ground probes Polstraat

Geotechnical parameters

The relevant ground probes of the Maasboulevard are summarized below:

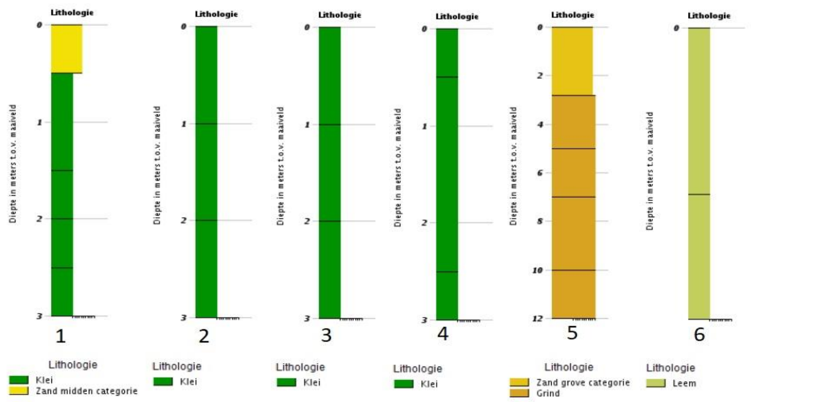

Figure F-22: ground probes of the Maasboulevard Wessem [Dino Loket(2017)]

Height of ground level at probe locations:

Table F-12: Height of ground level at probe locations Wessem Maasboulevard

Probe	Probe depth [m]	Height from NAP
1	0-3	-
2	0-3	-
3	0-3	-
4	0-3	-
5	0-12	22.50
6	0-0.70	23.00

The relevant ground probes of the Polstraat are summarized below:

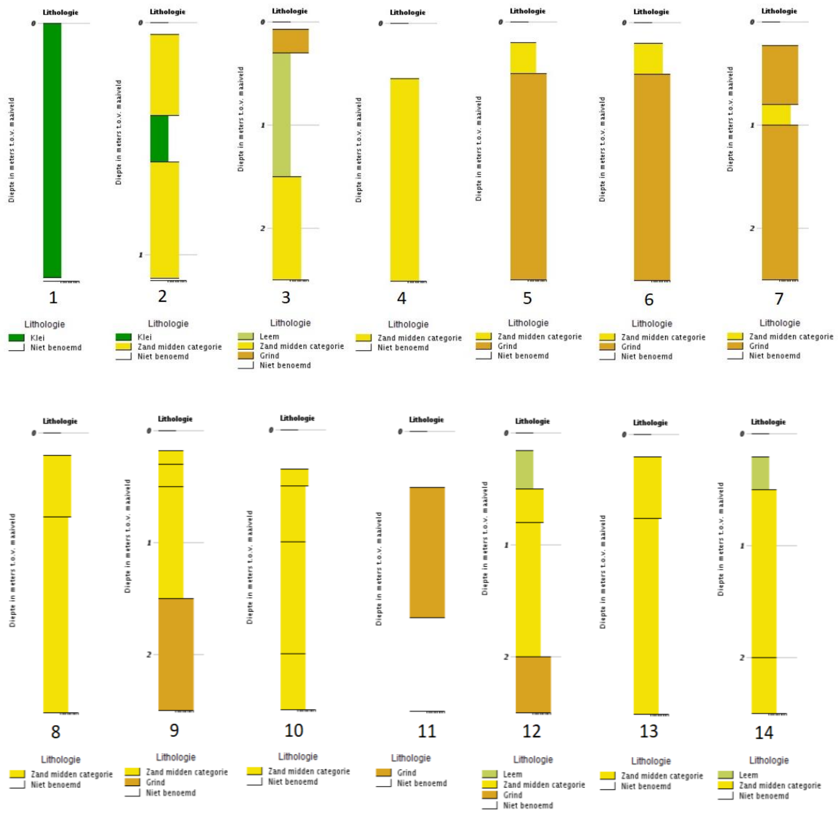

Figure F-23: Ground probes at Polstraat Wessem [Dino Loket(2017)]

It can be seen that the ground layers at the Maasboulevard are clay for the larger part, whereas the layers at the polstraat are mostly sand. All probes except Maasboulevard-5 are quite shallow.

Table F-13: Height of ground level at probe locations Wessem Polstraat

Probe	Probe depth [m]	Height from NAP
1	0-0.71	-
2	0-1.11	-
3	0-2.50	-
4	0-0.7	-
5	0-0.50	-
6	0-0.50	-
7	0-0.50	-
8	0-0.50	-
9	0-0.2.5	-
10	0-0.50	-
11	0-0.75	-
12	0-2.50	-
13	0-0.50	-
14	0-2.50	-

Water height information Wessem:

There is no measurement station present at Wessem, but Wessem is located between two sluice complexes, the relevant measurement station is “Heel Boven”.

Table F-14: Water height information Wessem

Water level	Height “Heel boven” [m]
Low water level	<20.70
Normal water level	20.70-21.15
Above normal water level	>21.15
High water level	>21.80
Extremely high water level	22.50

Additional information from [Memo ontwerpuitgangspunten glazen keringen]:

- The governing water height that needs to be retained is NAP 24.3+ m
- The location is situated next to a port. Ships that can reach this port are up to CEMT class II
- Ships can reach the flood defence if their draught is less than 2 m
- There is a fairway in front of the flood defence, separated by a bank with height of NAP +22.3
- The flood defence is situated in a river bend, there is a large angle of incidence
- According to the Maas-model of RWS, the water speed will be around 2.4 m/s

F.10. Conclusion

From all the different locations where a glass wall can be implemented the underground consists of river clay, sand and gravel. It is important to realize that building a structure on sand provides high stability and very little consolidation but the risk of underflow and piping increases. When the flood duration and water levels are extreme, piping can cause outflow of sand particles which can lead to complete failure of the structure. For these locations grouting, sheet piling or other options to reduce the risk of piping is recommended. This needs to be investigated further at every specific location when the flood defences are implemented.
For the locations where there is a lot of clay present, the clay needs to be examined for consolidation parameters and hydraulic conductivity coefficients. Increasing the stability and bearing capacity by piling or sheet piling to decrease underflow might be necessary.

G. Reference projects

G.1. Reference projects

Introduction

There are only a few reference projects in the Netherlands, which are significantly smaller than the additional defence height needed in Waterschap Limburg. In the United Kingdom, and Germany glass flood defences are used on a slightly larger scale. A few examples from the Netherlands and the United Kingdom:

Ketelhaven (2004)

Port manager Dick van Dijk wanted to keep his view on the port, so when the flood defence at ketelhaven was rejected on height, it was decided that a part of the new structure would be built as a transparent glass wall.

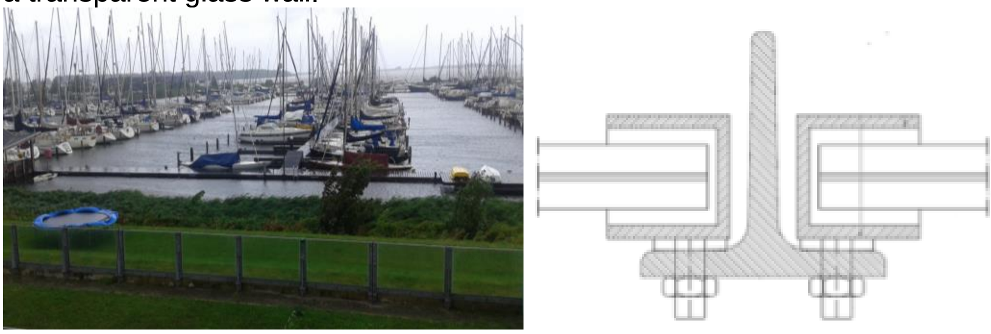

Figure G-1: Left: Glass flood wall Ketelhaven port, source: www.jachthavenketelmeer.nl Right: Cross section design with T-shaped pillars, source: Bestaande Keringen Arcadis(2016)

Wells-next-to-the-sea (2012)

Wells-next-to-the-sea in Norfolk lies, as the name already gives away, next to the sea. In the same North Sea flood, that had cost the lives of 1863 people in the Netherlands on 31st of January in 1953, around 400 lost their lives in the UK. Wells-next-to-the-sea was one of the regions that was heavily affected by the flood. The historic town used to have a wooden flood wall, which blocked the view completely and was not very appealing.

Figure G-2: Left: Old situation, source:Flood Control International. (2017). Right: New situation, source:Flood Control International. (2017).

Above you can see the wooden structure which Flood Control International (FCI) replaced by a 1 m high glass flood defence on top of the existing brick flood wall in June 2012, it also includes a sliding gate in the system to allow cars to go into the parking lot. The glass plates are 2x1 m and are enclosed by the frame on four sides, while the frame is mounted on the brick wall. It also makes use of self-cleaning coatings and stainless steel for optimal protection in marine environments. If the structure needs to be raised in the future, additional demountable flood defences can be installed on top of the system. The 80 m long system cost 116 000 British Pounds(around €1630 per meter).

Keswick (2011)

In 2011, IBS Engineered Products Ltd installed a prestigious glass flood wall in the small town of Keswick. With an aluminum frame and EPDM seals it is a robust and watertight system. It is part of the Environment Agency's flood risk management scheme to protect the area from the river Greta. It is supposedly the largest of its kind in terms of squared meters: 94 m². It's length is about 120 meters. Source: [VolkerStevin (2012)]

Figure G-3: The flood defence before and after overtopping. Photo credit: Stuart Holmes

During storm Desmond heavy rainfall flooded the river and the large amount of water overtopped the flood defence [itv News, 2015], leaving many people disappointed in the recently build, expensive glass wall. But the 'failure' was only due to overtopping, which is only a matter of height. While the water level was at its maximum, floating debris and trees crashed into the flood defence at high speed, but leaving only superficial damage. The glass panels withstood the loads they were designed for and gave the town time to evacuate. The large impact the water had on the road behind the wall could be seen the day after the storm: a large part of the footpath washed away and left a deep scour hole. [BBC, 2016]

Figure G-4: Left: a tree washed over the flood wall. Photo credit: Dan Potts Right: a scour hole was left behind the structure after the flood. Photo credit: Rick Cooper

The same flood defence structure is used in Keulen(Germany), Decin (Czech republic), Norwich and Leeds [Arcadis Bestaande Keringen(2016)] and Littlehampton. Other reference projects in the Netherlands are found in Breskens, and in Roermond the implementation of a glass flood defence is still in progress. Hereafter a summary of the reference structures with their dimensions is given.

G.2. Summary reference projects

Table G-1 Summary reference projects [Source: All values are found in the Bestaande Keringen Arcadis or websites of IBS and FCI]

	Length	Glass width	Glass height	Sheets [mm]	Inter-layer	Glass types	€/m	Support materials
Ketelhaven	50 m	1,5 m	1 m	2 x12	PVB	FTG	555	RVS Neopreen
IBS system (Keswick)	120m	Up to 3 m	1 m	Total 42	PVB	FTG or HSG	-	Aluminum EPDM
FCI system (W-N-T-T-S)	80 m	4.2	1 m	Total up to 70	-	HSG	1630	RVS EPDM
Breskens	295 m	1,5	1-1.2 m	Total 39,6	-	-	800	RVS
Roermond design	380	0.97-1.58m	0.56 m	2x11.7	-	HSG	-	Steel Neopreen

H. FEM Model

H.1. Intro

3 panels are modelled to approach the behavior of the structure as a whole as realistically as possible. Numbering of figures is not done in this Appendix. All images are from SCIA Engineer or the supplier drawings for the IBS structure.

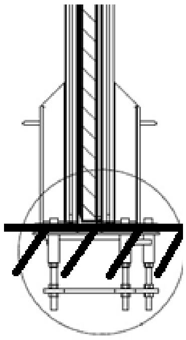

H.2. Foundation

For the FEM analysis the posts are assumed to be clamped into the foundation, where in reality the anchor plates will deform a little and allow a rotation. Since we are only looking at ULS this rotation is no problem and will only contribute to a decrease of the dynamic load and can therefore be neglected.

H.3. Glass panels

The glass panels are modelled as monolithic plates of 1909x1850 ($height \times width$) with an stress-equivalent thickness (ULS) of $53.31\ mm$ and a displacement-equivalent thickness(SLS) of $51.86\ mm$, and are connected to the supports with hinges in all directions.
(for thickness see Appendix Glass Calculations) To simplify the procedure, the same thickness of 53 mm is used for the model as this is a conservative value for both the deflection and stress calculations:
Displacement equivalent thickness:
Higher thickness→less deflection→higher dynamic load
Stress equivalent thickness:
Lower thickness→higher stress

H.4. Numerical input support structure

The profiles that are used in the structure are extruded Aluminum profiles, and have various openings in the profile. SCIA engineer does not have these types of profiles and therefore they have to be defined numerically in the model. The following section values need to be defined in SCIA Engineer:

Table H-1: SCIA input parameters with explanation

Symbol	Dimension	Explanation	Calculation/method
$\boldsymbol{A}$	m^2	The surface area of the profile	See calculation 1
$\boldsymbol{A_y}$	m^2	Shear surface area in principal y-direction	FEM/calculation 2
$\boldsymbol{A_z}$	m^2	Shear surface area in principal z-direction	FEM/calculation 2
$\boldsymbol{A_L}$	m^2/m	Circumference per length unit	See calculation 3
$\boldsymbol{A_D}$	m^2/m	Cure surface	See calculation 3
$\boldsymbol{cYUCS}$	m	Center of gravity coordinates from input axis-system in y-direction	$\frac{b}{2}$
$\boldsymbol{cZUCS}$	m	Center of gravity coordinates from input axis-system in z-direction	$\frac{h}{2}$
$\boldsymbol{\alpha}$	°	Rotation from principal axis system	0

$\boldsymbol{I_y}$	m^4	Moment of inertia in y-direction (in these calculations: I_{zz})	See calculation 1
$\boldsymbol{I_z}$	m^4	Moment of inertia in z-direction (in these calculations: I_{yy})	See calculation 1
$\boldsymbol{i_y}$	mm	Inertial radius in y-direction	$\sqrt{I_{zz}/A}$
$\boldsymbol{i_z}$	mm	Inertial radius in z-direction	$\sqrt{I_{yy}/A}$
$\boldsymbol{W_{el,y}}$	m^3	Elastic moment of resistance around y-axis (in our calculations: $W_{el,zz}$)	I_{zz}/z_{max}
$\boldsymbol{W_{el,z}}$	m^3	Elastic moment of resistance around z-axis (in our calculations: $W_{el,yy}$)	I_{yy}/y_{max}
$\boldsymbol{W_{pl,y}}$	m^3	Plastic moment of resistance around y-axis	See calculation 4
$\boldsymbol{W_{pl,z}}$	m^3	Plastic moment of resistance around z-axis	See calculation 4
$\boldsymbol{M^+_{pl,y}}$	Nm	Plastic moment around y-axis for a positive M_y moment	$W_{pl,y} \cdot f_y$
$\boldsymbol{M^-_{pl,y}}$	Nm	Plastic moment around y-axis for negative M_y moment	$W_{pl,y} \cdot f_y$
$\boldsymbol{M^+_{pl,z}}$	Nm	Plastic moment around y-axis for a positive M_z moment	$W_{pl,z} \cdot f_y$
$\boldsymbol{M^-_{pl,z}}$	Nm	Plastic moment around y-axis for negative M_z moment	$W_{pl,z} \cdot f_y$
$\boldsymbol{d_y}$	mm	Shear center coordinate in principal y direction	0 or FEM
$\boldsymbol{d_z}$	mm	Shear center coordinate in principal z direction	0 or FEM
$\boldsymbol{I_t}$	m^4	Torsion moment	See calculation 5
$\boldsymbol{I_w}$	m^6	Constant of incidence	See calculation 5
$\boldsymbol{\beta_y}$	mm	Mono-symmetric constant around principal y-direction	0 or FEM
$\boldsymbol{\beta_z}$	mm	Mono-symmetric constant around principal z-direction	0 or FEM

H.5. Material input

The Aluminum posts are made of Extruded Profiles AW6005, with thickness $10 < t \leq 25\ mm$.

The top and bottom supports are made of Extruded Profiles AW6082, with thickness $t \leq 25\ mm$

Table H-2: Aluminum properties [NEN-EN 1999-1-1+A1:2011]

Legering EN-AW	Product vorm	Toestand	Dikte t mm 1) 3)	f_o 1) N/mm²	f_u 1) N/mm²	A 5) 2) %	$f_{o,haz}$ 4) N/mm²	$f_{u,haz}$ 4) N/mm²	HAZ-factor 4) $\rho_{o,haz}$	HAZ-factor 4) $\rho_{u,haz}$	BC 6)	n_p 7)
6005A	EP/O, ER/B	T6	$t \leq 5$	225	270	8			0,51	0,61	A	25
			$5 < t \leq 10$	215	260	8			0,53	0,63	A	24
			$10 < t \leq 25$	200	250	8	115	165	0,58	0,66	A	20
	EP/H, ET	T6	$t \leq 5$	**215**	**255**	8			0,53	0,65	A	26
			$5 < t \leq 10$	**200**	**250**	8			0,58	0,66	A	20
6082	EP,ET,ER/B	T4	$t \leq 25$	110	205	14	100	160	0,91	0,78	B	8
	EP	T5	$t \leq 5$	230	270	8	125	185	0,54	0,69	B	28
	EP, ET	T6	$t \leq 5$	250	290	8			0,50	0,64	A	32
			$5 < t \leq 15$	260	310	10	125	185	0,48	0,60	A	25
	ER/B	T6	$t \leq 20$	250	295	8			0,50	0,63	A	27
			$20 < t \leq 150$	260	310	8			0,48	0,60	A	25
	DT	T6	$t \leq 5$	255	310	8			0,49	0,60	A	22
			$5 < t \leq 20$	240	310	10			0,52	0,60	A	17

H.5.1. Side-supports

The extruded Aluminum profiles that form the side supports are build up from 2 parts: one Aluminum I-profile and two Aluminum T-profiles for extra support at the bottom part. Because of symmetry, the neutral axis is in the middle of the I-profile for both x- and y-directions. As the side he length of the lower profile is $26.97 \times 20 = 539.4\ mm$.

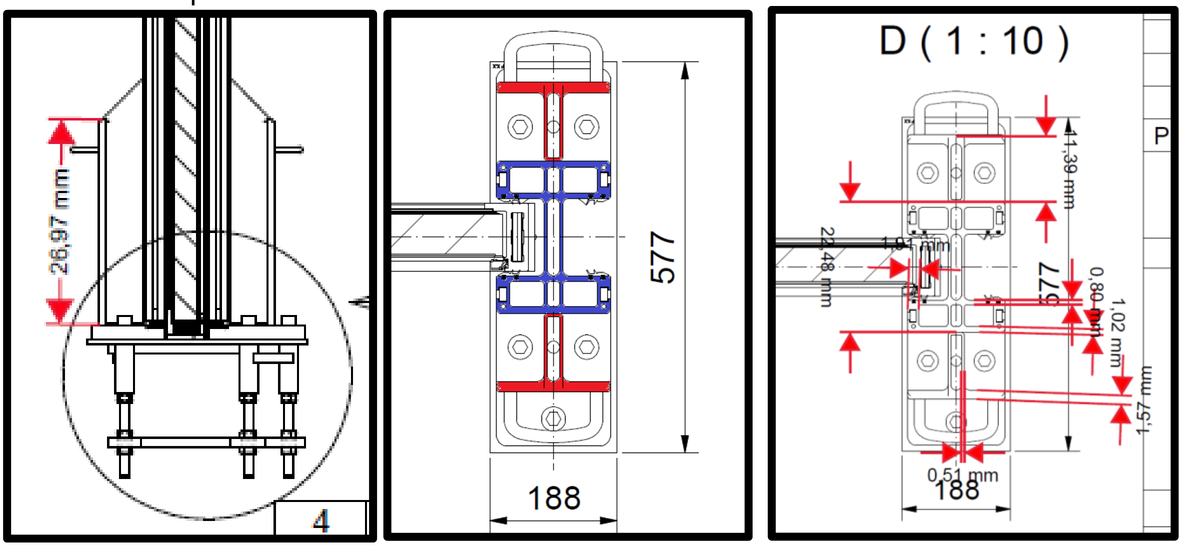

H.5.2. I-profile calculation 1: A, I_{zz} and I_{yy}

The surface area A and the moments of inertia I_{zz} and I_{yy} of the I-profile are determined first:

$$I_{zz} = I_{z,tot} - 4 \cdot (I_1 + A_1 \cdot z_1) - 2 \cdot (I_2 + A_2 \cdot z_2) - 2 \cdot (I_3 + A_3 \cdot z_3) - 4 \cdot (I_4 + A_4 \cdot z_4) - I_{y,5}$$
$$\rightarrow I_{zz} = I_{z,tot} - 4 \cdot (I_{z,1,tot}) - 2 \cdot (I_{z,2,tot}) - 2 \cdot (I_{z,3,tot}) - 4 \cdot (I_{z,4,tot}) - I_{z,5}$$

$$I_{yy} = I_{y,tot} - 4 \cdot (I_{y,1} + A_1 \cdot y_1) - 2 \cdot (I_{y,2} + A_2 \cdot y_2) - 2 \cdot (I_{y,3} + A_3 \cdot y_3) - 4 \cdot (I_{y,4} + A_4 \cdot y_4) - I_{y,5}$$
$$\rightarrow I_{yy} = I_{y,tot} - 4 \cdot (I_{y,1,tot}) - 2 \cdot (I_{y,2,tot}) - 2 \cdot (I_{y,3,tot}) - 4 \cdot (I_{y,4,tot}) - I_{y,5}$$

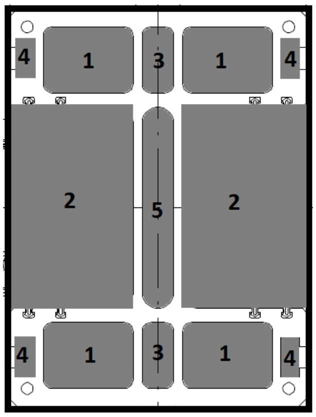

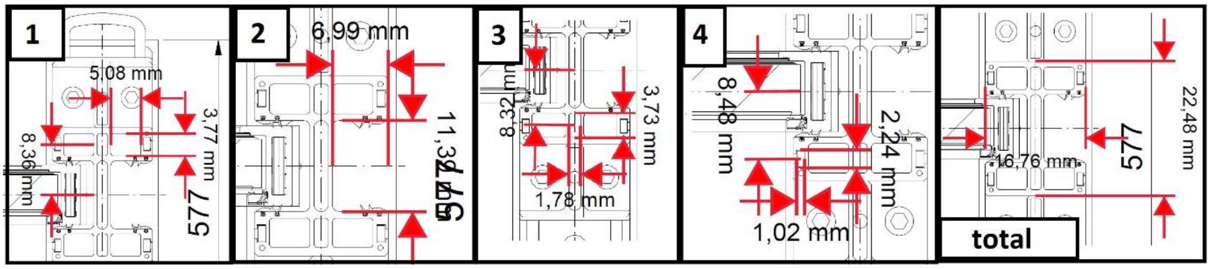

$$I_{z,tot} = \frac{1}{12} \cdot 167{,}6 \cdot 224.8^3 = 158.67 \cdot 10^6$$

$$I_{z,1,tot} = \frac{1}{12} \cdot 50.8 \cdot 37.7^3 + 83.6^2 \cdot 50.8 \cdot 37.7 = 13.61 \cdot 10^6$$
$$I_{2,tot} = \frac{1}{12} \cdot 69.9 \cdot 113.9^3 = 8.61 \cdot 10^6$$
$$I_{z,3,tot} = \frac{1}{12} \cdot 17.8 \cdot 37.3^3 + 83.2^2 \cdot 17.8 \cdot 37.3 = 4.67 \cdot 10^6$$
$$I_{z,4,tot} = \frac{1}{12} \cdot 10.2 \cdot 22.4^3 + 84.8^2 \cdot 10.2 \cdot 22.4 = 1.65 \cdot 10^6$$
$$I_{z,5} = \frac{1}{12} \cdot 17.8 \cdot 113.9^3 = 2.19 \cdot 10^6$$

The total adds up to:

$$I_{zz} = 10^6 \cdot (158.67 - 4 \cdot (13.61) - 2 \cdot (8.61) - 2 \cdot (4.67) - 4 \cdot (1.65) - 2.19) = 68.88 \cdot 10^6$$
$$I_{zz} = 68.88 \cdot 10^6 [mm^4]$$

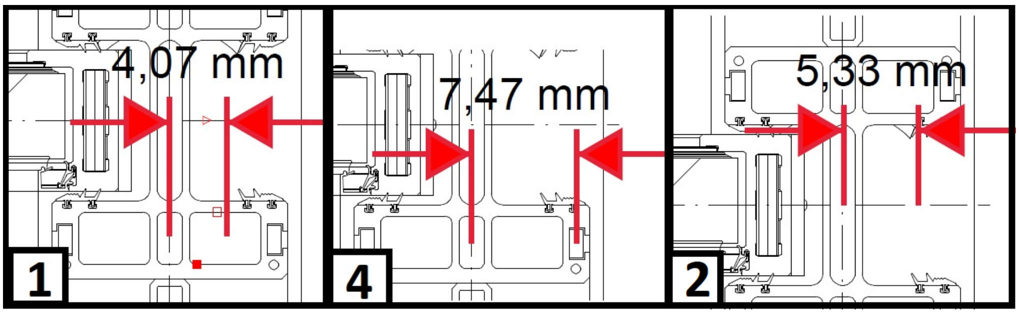

$$I_{y,tot} = \frac{1}{12} \cdot 224.8 \cdot 167{,}6^3 = 88.19 \cdot 10^6$$
$$I_{y,1,tot} = \frac{1}{12} \cdot 37.7 \cdot 50.8^3 + 40.7^2 \cdot 50.8 \cdot 37.7 = 3.58 \cdot 10^6$$

$$I_{y,2,tot} = \frac{1}{12} \cdot 113.9 \cdot 69.9^3 + 53.3^2 \cdot 113.9 \cdot 69.9 = 25.86 \cdot 10^6$$
$$I_{y,3,tot} = \frac{1}{12} \cdot 37.3 \cdot 17.8^3 = 0.018 \cdot 10^6$$
$$I_{y,4,tot} = \frac{1}{12} \cdot 22.4 \cdot 10.2^3 + 74.7^2 \cdot 10.2 \cdot 22.4 = 1.28 \cdot 10^6$$
$$I_{y,5} = \frac{1}{12} \cdot 113.9 \cdot 17.8^3 = 0.054 \cdot 10^6$$

The total adds up to:

$$I_{yy} = 10^6 \cdot (88.19 - 4 \cdot (3.58) - 2 \cdot (25.86) - 2 \cdot (0.018) - 4 \cdot (1.28) - 0.054) = 16.94 \cdot 10^6$$
$$I_{yy} = 16.94 \cdot 10^6 [mm^4]$$

And the total surface area of the I-profile is:

$$A_{tot} = 167.6 \cdot 224.8 - 4 \cdot 50.8 \cdot 37.7 - 2 \cdot 69.9 \cdot 113.9 - 2 \cdot 17.8 \cdot 37.3 - 4 \cdot 10.2 \cdot 22.4 - 113.9 \cdot 17.8 = 9823.4\ mm^2$$

H.5.3. I-profile calculation 2: The shear surface area's

SCIA Engineer makes use of the theory of Grasshof-Zuravski to calculate the shear surface area in the principal directions (Source: SCIA Help)

The shear surface area is calculated by the following formula:

$$A_z = \frac{A}{\beta_z}$$

Where the value of β_z is calculated by shear stresses. This will not be elaborated on further and a value of β_z and β_y is obtained by using a simplified section with comparable properties and take the largest value of beta.

We compare the obtained value for A_z of a simplified section in SCIA by the following NEN formula to check whether the values match with each other in order of magnitude.

The shear surface area for a I-profile $A_{v,z}$ can be determined by the following NEN formula:

$$A_{v,z} = A - 2 \cdot b \cdot t_f + 2(t_w + 2 \cdot r)t_f$$

This is an estimation of the area that is affected by shear, and basically only counts the surface of the web and takes a small part of the flange into account:

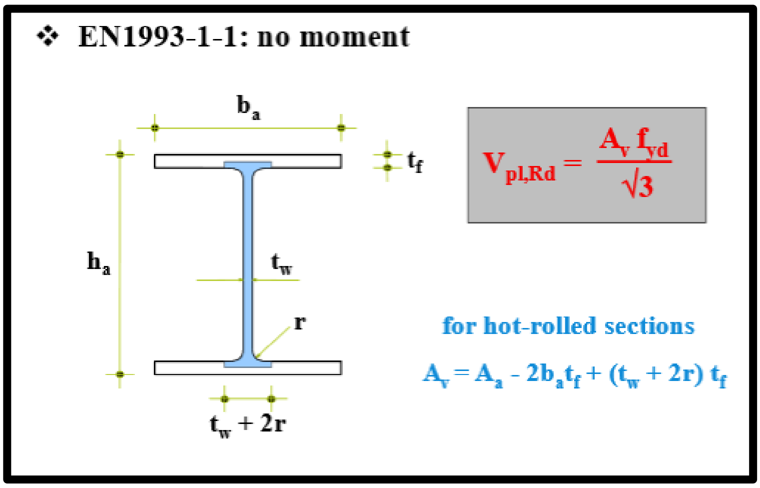

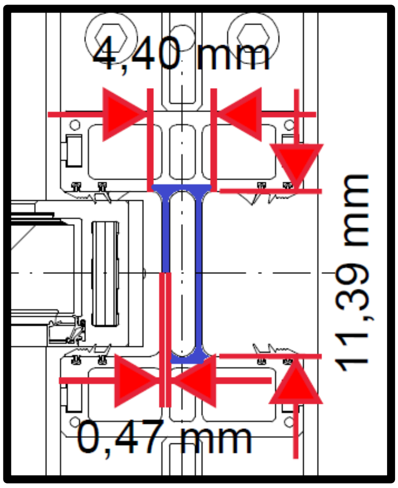

Source left: steel structures 3 lecture slides composite structures

Estimation of the shear surface area A_y:

$$2 \cdot 113.9 \cdot 4.7 + 44 \cdot 4.7 = 1277.47\ mm^2$$

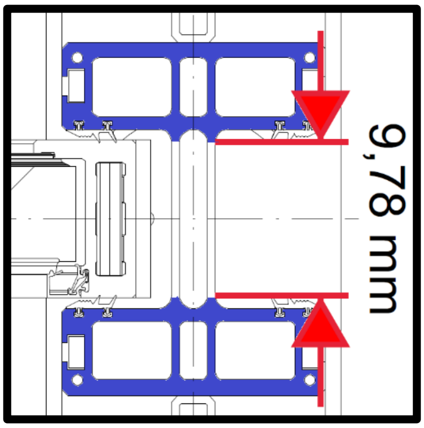

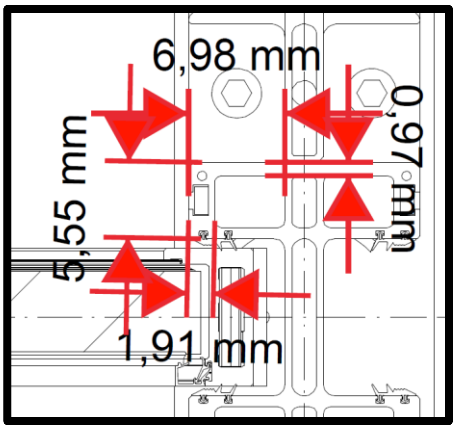

We can do the same for shear around the z-axis:

$$A_z = 9823.4 - 2 \cdot 97.8 \cdot 4.7 = 8904.1\ mm^2$$

Now we have made an estimation of the shear surface area, we need to compare these values to values obtained from a simplified section in SCIA Engineer. The simplified section is presented below and the following values are compared:

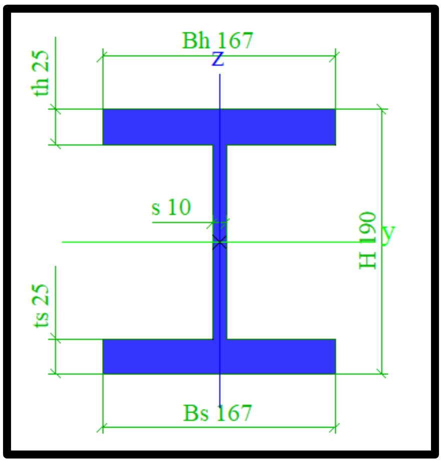

Property	I-section	Simplified section
A	0,982e-02	0,975e-02
I_y	68.88e-06	59,55e-06
I_z	16.94e-06	19,41e-06
A_y	0,890e-02	0,767e-02
A_z	0,128e-02	0,196e-02

It can be seen that the values are of similar magnitudes, but in y-direction the simplified section gives a lower value, and the smallest β's are taken as governing:

$$\beta_y = \frac{0.975}{0.767} = 1.27 \qquad \beta_z = \frac{0.975}{0.128} = 7.62$$

These beta values will also be used for the whole section(including the additional T-profiles).

H.5.4. I-profile calculation 3: A_L and L_D

The circumference per length unit and cure surface are the same value and are the circumference of the section. For the I-profile; this value is measured to be $1033{,}2\ mm$.

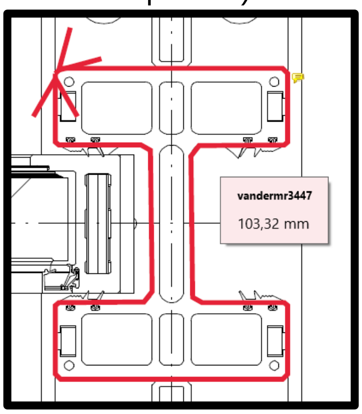

H.5.5. I-profile calculation 4: Plastic moment of resistance

Plastic behavior can occur in the Aluminum structure and the sections of profiles that are used in the structure are of section class 1, checked with chapter 5.6 of NEN-EN 1993-1-1:

Internal parts:

$$\frac{c}{t} \leq 72\varepsilon \rightarrow \frac{97.8}{2 \cdot 4.7} = 10.4 \leq 72$$

External parts

$$\frac{c}{t} \leq 9\varepsilon \rightarrow \frac{74.7}{8 + 10.2} = 4.1 \leq 9$$

Since the Aluminum profiles have a lower yield strength than steel S235, ε is 1. The profiles are of section class 1 and plastic behavior can occur.

To speed up the calculation the flanges are simplified to solid strips.

$$A_{web} = 2 \cdot (113.9 \cdot 4.7 + 2 \cdot 4.7^2) = 1159\, mm^2$$

$$A_{flange} = \frac{9823.4 - 1159}{2} = 4332.2$$

$$W_{zz,pl} = \sum A_i \cdot z_i = 4332.2 \cdot 170.3 + 0.5 \cdot 1159 \cdot 53.1 = 0.769 \cdot 10^6\, mm^3 = 0.769 \cdot 10^{-3}\, m^3$$

$$W_{yy,pl} = \sum A_i \cdot y_i = 4332.2 \cdot 0.5 \cdot 167.6 + 0.5 \cdot 1159 \cdot 22.5 = 0.376 \cdot 10^6\, mm^3 = 0.376 \cdot 10^{-3}\, m^3$$

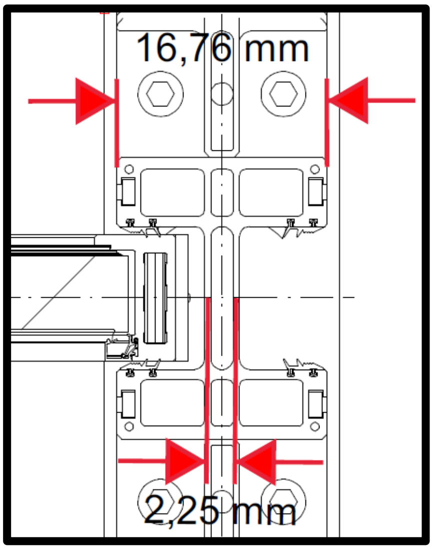

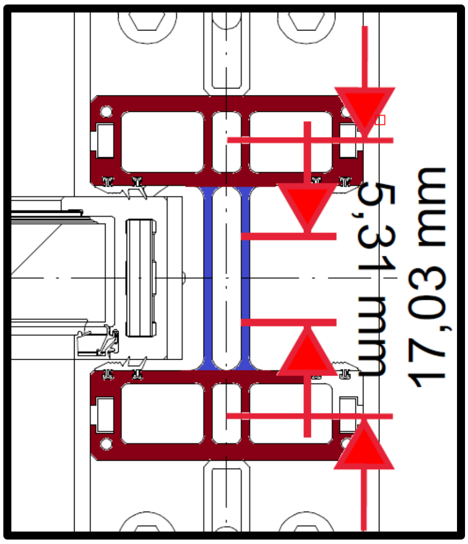

H.5.6. I-profile calculation 5: The incidence and torsional constant I_w and I_t

In Dutch: Welvingsconstante I_w, this value is estimated for the I-profile by making use of a simple formula for I-profiles: $I_w = h_f^2 \cdot I_z / 4$ (with I_z the moment of inertia around the weak axis)

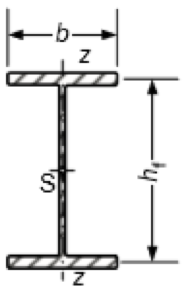

$$I_w = \frac{h_f^2 I_z}{4}$$

$$h_f^2 \cdot \frac{I_z}{4} = (0.0836 \cdot 2)^2 \cdot 16.94 \cdot \frac{10^{-6}}{4} = 1.18 \cdot 10^{-7}$$

H.5.7. Torsional constant

The torsional constant I_t for slender open profiles according to the NEN-EN 1999-1-1+A1:2011 is:

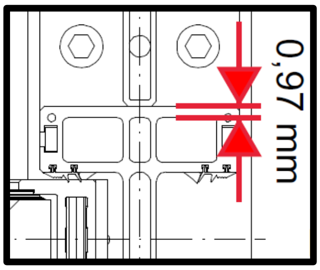

$$\sum_{i=1}^{n} dA_i \cdot \frac{(t_i)^2}{3} = 2 \cdot (t_f \cdot b_f) \cdot \frac{t_f^2}{3} + (t_w \cdot b_w) \cdot \frac{t_w^2}{3}$$

$$I_t = 2 \cdot \frac{(2 \cdot 9.7 \cdot 167.6) \cdot (2 \cdot 9.7)^2}{3} + \frac{((2 \cdot 4.7) \cdot 97.8) \cdot (2 \cdot 4.7)^2}{3}$$
$$= 0.84 \cdot 10^6 \, mm^4 = 0.84 \cdot 10^{-6} \, m^4$$

Where t_f and t_w are simplified as solid strips.

:

Table H-3: Summary of calculated values of the top profile

Symbol	Dimension	Calculation/explanation	Numeric input Scia
$\boldsymbol{A}$	m^2	$9823.4 \cdot 10^{-6}\, m$	0,982e-02
$\boldsymbol{A_y}$	m^2	$\frac{A}{\beta_y} = \frac{0.982}{1.27} = 0.762\, m^2$	0,767e-02
$\boldsymbol{A_z}$	m^2	$\frac{A}{\beta_z} = \frac{0.982}{7.62} = 0.128\, m^2$	0,128e-02
$\boldsymbol{A_L}$	m^2/m	$1033.2\, mm$	1,0332
$\boldsymbol{A_D}$	m^2/m	$1033.2\, mm$	1,0332
$\boldsymbol{cYUCS}$	mm	$0.5 \cdot 167.6$	83,8
$\boldsymbol{cZUCS}$	mm	$0.5 \cdot 224.8$	112,4
$\boldsymbol{\alpha}$	$^\circ$	No rotation of axis	0
$\boldsymbol{I_y}$	m^4	$I_{zz} = [mm^4] \to [m^4] = 68.88 \cdot \frac{10^6}{(10^3)^4}$	68.88e-06
$\boldsymbol{I_z}$	m^4	$I_{yy} = [mm^4] \to [m^4] = 16.94 \cdot \frac{10^6}{(10^3)^4}$	16.94e-06
$\boldsymbol{i_y}$	mm	$\sqrt{I_{zz}/A} = \sqrt{68.88 \cdot 10^6/9823.4}$	83,74
$\boldsymbol{i_z}$	mm	$\sqrt{I_{yy}/A} = \sqrt{16.94 \cdot 10^6/9823.4}$	41,52
$\boldsymbol{W_{el,y}}$	m^3	$I_{zz}/z_{max} = 68.88 \cdot 10^{-6}/0.1124$	6,13e-04
$\boldsymbol{W_{el,z}}$	m^3	$I_{yy}/y_{max} = 16.94 \cdot 10^{-6}/0.0838$	2,02e-04
$\boldsymbol{W_{pl,y}}$	m^3	$0.769 \cdot 10^{-3}\, m^3$	7,69e-04
$\boldsymbol{W_{pl,z}}$	m^3	$0.376 \cdot 10^{-3}\, m^3$	3,76e-04
$\boldsymbol{M_{pl,y}^+}$	Nm	$W_{pl,y} \cdot f_y = 0.769 \cdot 10^{-3} \cdot 200 \cdot 10^6$	1,54e05
$\boldsymbol{M_{pl,y}^-}$	Nm	$W_{pl,y} \cdot f_y = 0.769 \cdot 10^{-3} \cdot 200 \cdot 10^6$	1,54e05
$\boldsymbol{M_{pl,z}^+}$	Nm	$W_{pl,y} \cdot f_y = 0.376 \cdot 10^{-3} \cdot 200 \cdot 10^6$	0,75e05
$\boldsymbol{M_{pl,z}^-}$	Nm	$W_{pl,y} \cdot f_y = 0.376 \cdot 10^{-3} \cdot 200 \cdot 10^6$	0,75e05
$\boldsymbol{d_y}$	mm	Symmetry	0
$\boldsymbol{d_z}$	mm	Symmetry	0
$\boldsymbol{I_t}$	m^4	$\sum_{i=1}^{n} dA_i \cdot (t_i)^2/3$	0,84e-06
$\boldsymbol{I_w}$	m^6	$h_f^2 \cdot \frac{I_z}{4} = (0.0836 \cdot 2)^2 \cdot 16.94 \cdot 10^{-6}/4$	1,18e-07

$\boldsymbol{\beta_y}$	mm	Symmetry	0
$\boldsymbol{\beta_z}$	mm	Symmetry	0

H.6. T-profile

There are two T-profiles connected to the bottom and top flange of the I-profile. This additional material can be divided into three parts, one top flange and the web in 2 parts. The small contribution of the rest(closure of profile at bottom of the web) is neglected.

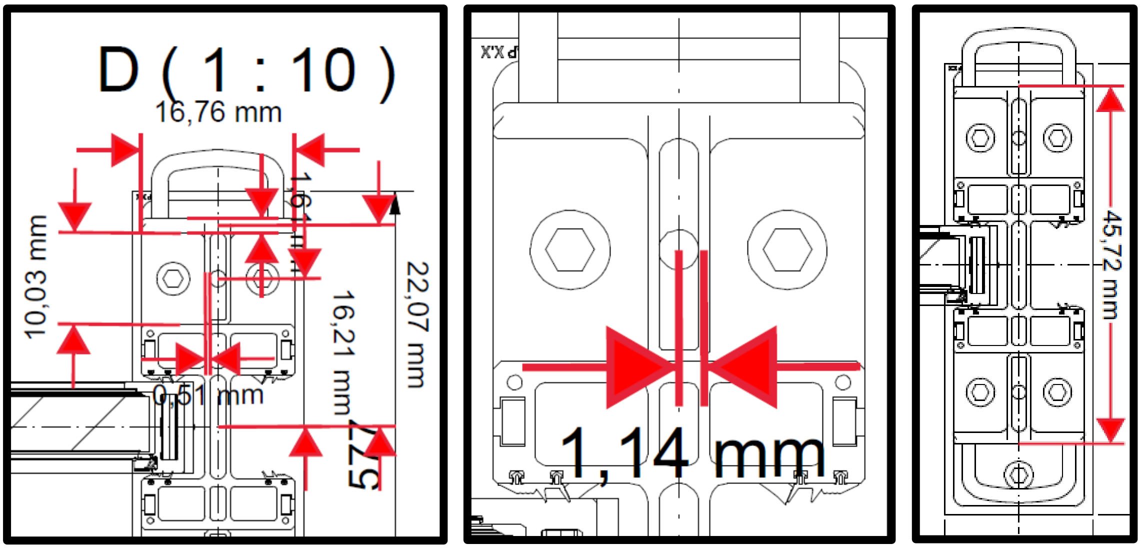

H.6.1. T-profile calculation 1: A, I_{zz} and I_{yy}

The surface area A and the moments of inertia I_{zz} and I_{yy} of the T-profile are determined by adding up the three different parts that contribute to the stiffness:

$$I_{zz} = \left(I_{z,flange} + A_{flange} \cdot z_{flange}\right) + 2 \cdot \left(I_{z,web} + A_{web} \cdot z_{web}\right)$$
$$\rightarrow I_{zz} = I_{flange,total} + 2 \cdot I_{web,total}$$

Where z is the distance from the center of gravity of each part to the neutral z-axis.

$$I_{z,flange,total} = \frac{1}{12} \cdot 167.6 \cdot 16.1^3 + 220.7^2 \cdot 167.6 \cdot 16.1 = 131.49 \cdot 10^6$$
$$I_{z,web,total} = \frac{1}{12} \cdot 5.1 \cdot 100.3^3 + 162.1^2 \cdot 5.1 \cdot 100.3 = 13.87 \cdot 10^6$$

This adds up to:

$$I_{zz,T} = 10^6 \cdot (131.49 + 2 \cdot 13.87) = 159.23 \cdot 10^6$$

And the moment of inertia in y direction:

$$I_{yy} = I_{y,flange} + 2 \cdot \left(I_{y,web} + A_{web} \cdot y_{web}\right)$$

$$I_{y,flange} = \frac{1}{12} \cdot 16.1 \cdot 167.6^3 = 6.31 \cdot 10^6$$
$$I_{y,web} = \frac{1}{12} \cdot 100.3 \cdot 5.1^3 + 11.4^2 \cdot 5.1 \cdot 100.3 = 0.068 \cdot 10^6$$

$$I_{yy,T} = 6.31 \cdot 10^6 + 2 \cdot (0.068 \cdot 10^6) = 6.45 \cdot 10^6$$

The surface area of the T-profile is:

$$A_T = 16.1 \cdot 167.6 + 2 \cdot 100.3 \cdot 5.1 = 3721.4$$

H.6.2. Total lower profile calculation 1: $\boldsymbol{A}$, $\boldsymbol{I_{zz}}$ and $\boldsymbol{I_{yy}}$

In summary:
The upper part is only the I-profile:

$$I_{zz,upper} = 68.88 \cdot 10^6 [mm^4]$$
$$I_{yy,upper} = 16.94 \cdot 10^6 [mm^4]$$
$$A_{upper} = 24880\ [mm^2]$$

The lower part of the side support is stiffened by the 2 additional T-profiles, the two total moments of inertia are:

$$I_{zz,lower} = I_{zz,I} + 2 \cdot I_{zz,T} = 68.88 \cdot 10^6 + 2 \cdot 159.23 \cdot 10^6 = 387.34 \cdot 10^6\ mm^4$$
$$I_{yy,lower} = I_{yy,I} + 2 \cdot I_{yy,T} = 16.94 \cdot 10^6 + 2 \cdot 6.45 \cdot 10^6 = 29.84 \cdot 10^6\ mm^4$$
$$A_{lower} = 9823.4 + 2 \cdot 3721.4 = 17266.2\ mm^2$$

It can be seen that the lower part of the side supports has a much larger stiffness in Z-direction due to the two additional T-profiles, this is mainly caused by the large distance between the center of gravity of the T-profiles and the neutral axis of the total section.

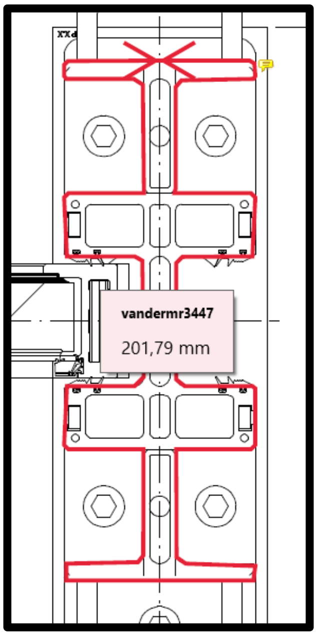

H.6.3. Total lower profile calculation 2: The shear surface area's

As determined for the I-profile, the beta's for the whole section are assumed to be of the same value:

$$\beta_y = 1.27 \rightarrow \frac{A}{\beta_y} = \frac{1.727}{1.27} \cdot 10^{-2} = 1.36 \cdot 10^{-2}$$

$$\beta_z = 7.62 \rightarrow \frac{A}{\beta_z} = \frac{1.727}{7.62} \cdot 10^{-2} = 0.227 \cdot 10^{-2}$$

H.6.4. Total lower profile calculation 3: $\boldsymbol{A_L}$ and $\boldsymbol{L_D}$

The circumference per length unit and cure surface are the same value and are the circumference of the section. For the I-profile; this value is measured to be $2017.9\ mm$.

H.6.5. Total lower profile calculation 4: Plastic moment of resistance

The addition of each T-profile to the plastic moments resistance is:

$$W_{pl,y,add} = 167.6 \cdot 16.1 \cdot 220.7 + 2 \cdot 5.1 \cdot 100.3 \cdot 162.1 = 768472.6\ mm^3 = 0.761 \cdot 10^{-3}\ m^3$$

$$W_{pl,y,lower} = 0.769 + 2 \cdot 0.761) \cdot 10^{-3} = 0.002292\ m^3$$

$$W_{pl,z,add} = 0.5 \cdot 167.6 \cdot 16.1 \cdot 0.5 \cdot 167.7 + 5.1 \cdot 100.3 \cdot 2 \cdot 11.4 = 124791.6\ mm^3 = 0.125 \cdot 10^{-3}\ m^3$$

$$W_{pl,z,lower} = (0.376 + 2 \cdot 0.125) \cdot 10^{-3}\ m^3$$

H.6.6. Total lower profile calculation 5: The incidence and torsional constant I_w and I_t

The incidence constant I_w is calculated with the same formula as for

$$h_f^2 \cdot \frac{I_z}{4} = (0.4572)^2 \cdot 29.84 \cdot 10^{-6}/4$$

The torsional constant I_t for slender open profiles according to the NEN-EN 1999-1-1+A1:2011 is:

$$I_t = \sum_{i=1}^{n} dA_i \cdot \frac{(t_i)^2}{3} = I_{t,I} + 2 \cdot I_{t,T}$$

$$I_{t,T} = 2 \cdot \frac{(t_w \cdot b_w) \cdot t_w^2}{3} + \frac{\left(t_f \cdot b_f\right) \cdot t_f^2}{3} = 2 \cdot \frac{(5.1 \cdot 100.3) \cdot 5.1^2}{3} + \frac{(16.1 \cdot 167.6) \cdot 16.1^2}{3} = 242017\ mm^4$$
$$= 0.241 \cdot 10^{-6}\ m^4$$

$$(0.84 + 2 \cdot 0.241) \cdot 10^{-6} = 1.32 \cdot 10^{-6}\ m^4$$

Table H-4: Summary of calculated values of the lower profile

Symbol	Dimension	Calculation/explanation	Numeric input SCIA
$\boldsymbol{A}$	m^2	$32322.8\ \cdot 10^{-6}\ m$	1,727e-02
$\boldsymbol{A_y}$	m^2	$\frac{A}{\beta_y} = \frac{1.727}{1.27} = 1.36$	1,36e-02
$\boldsymbol{A_z}$	m^2	$\frac{A}{\beta_z} = \frac{1.727}{7.62} = 0.227$	0,227e-02
$\boldsymbol{A_L}$	m^2/m	$2017.9\ mm$	2,018
$\boldsymbol{A_D}$	m^2/m	$2017.9\ mm$	2,018
$\boldsymbol{cYUCS}$	mm	$0.5 \cdot 167.6$	83,8
$\boldsymbol{cZUCS}$	mm	$0.5 \cdot 224.8 + 100.3 + 16.1$	228,8
$\boldsymbol{\alpha}$	°	No rotation of axis	0
$\boldsymbol{I_y}$	m^4	$I_{zz} = [mm^4] \rightarrow [m^4] = 387.34 \cdot \frac{10^6}{(10^3)^4}$	387,34e-06
$\boldsymbol{I_z}$	m^4	$I_{yy} = [mm^4] \rightarrow [m^4] = 29.84 \cdot \frac{10^6}{(10^3)^4}$	29,84e-06
$\boldsymbol{i_y}$	mm	$\sqrt{I_{zz}/A} = \sqrt{387.34 \cdot 10^6/32322.8}$	109,5
$\boldsymbol{i_z}$	mm	$\sqrt{I_{yy}/A} = \sqrt{29.84 \cdot 10^6/32322.8}$	30,4
$\boldsymbol{W_{el,y}}$	m^3	$I_{zz}/z_{max} = \frac{387.34}{0.4572/2} \cdot 10^{-6}$	16,55e-04
$\boldsymbol{W_{el,z}}$	m^3	$I_{yy}/y_{max} = 29.84 \cdot 10^{-6}/0.0838$	3,56e-04
$\boldsymbol{W_{pl,y}}$	m^3	$(0.769 + 2 \cdot 0.761) \cdot 10^{-3} = 0.002292\ m^3$	22,92e-04
$\boldsymbol{W_{pl,z}}$	m^3	$(0.376 + 2 \cdot 0.125) \cdot 10^{-3}\ m^3$	6,26e-04
$\boldsymbol{M_{pl,y}^+}$	Nm	$W_{pl,y} \cdot f_y = 22.92 \cdot 10^{-4} \cdot 200 \cdot 10^6$	4,58e05
$\boldsymbol{M_{pl,y}^-}$	Nm	$W_{pl,y} \cdot f_y = 22.92 \cdot 10^{-4} \cdot 200 \cdot 10^6$	4,58e05
$\boldsymbol{M_{pl,z}^+}$	Nm	$W_{pl,y} \cdot f_y = 6.26 \cdot 10^{-4} \cdot 200 \cdot 10^6$	1,25e05
$\boldsymbol{M_{pl,z}^-}$	Nm	$W_{pl,y} \cdot f_y = 6.26 \cdot 10^{-3} \cdot 200 \cdot 10^6$	1,25e05
$\boldsymbol{d_y}$	mm	Symmetry	0
$\boldsymbol{d_z}$	mm	Symmetry	0
$\boldsymbol{I_t}$	m^4	$(0.84 + 2 \cdot 0.241) \cdot 10^{-6} = 1.32 \cdot 10^{-6}\ m^4$	1,32e-06

$\boldsymbol{I_w}$	m^6	$h_f^2 \cdot \frac{I_z}{4} = (0.4572)^2 \cdot 29.84 \cdot 10^{-6}/4$	1,56e-07
$\boldsymbol{\beta_y}$	mm	Symmetry	0
$\boldsymbol{\beta_z}$	mm	Symmetry	0

H.6.7. Top and bottom support profile (closed L-profile)

The framework consists of the top and bottom beam, and 2 sides. For the fem model, the frames on the side are neglected assumed they are only used to transfer the loads to the side supports. The top and bottom beam are taken into account as support.

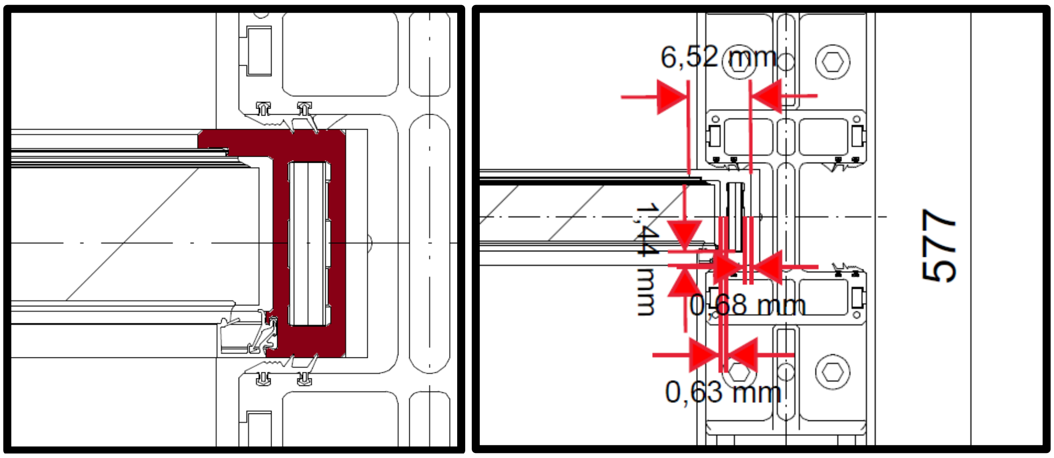

This profile is not symmetric and first, the center of gravity needs to be determined, this is done from the bottom and from the right side.

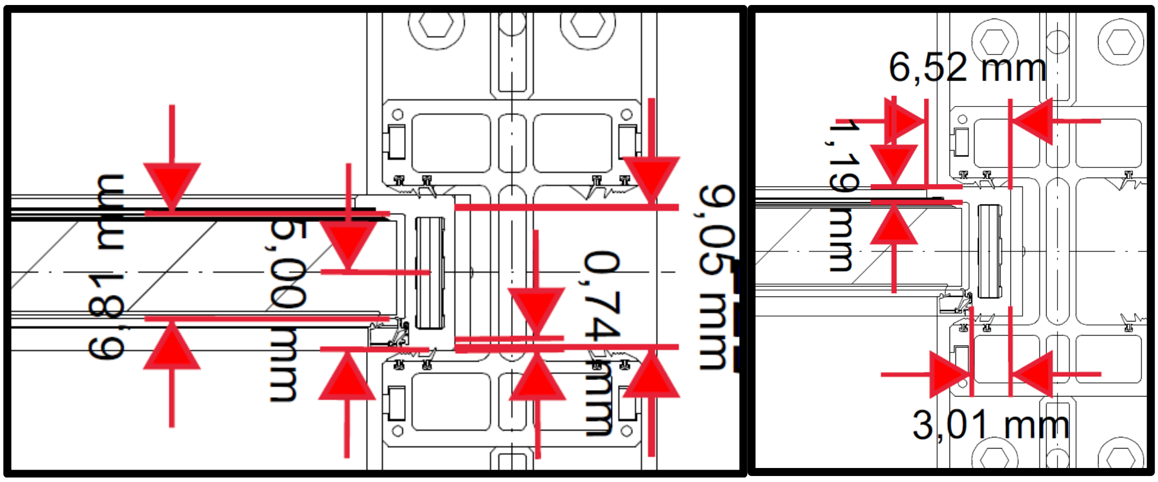

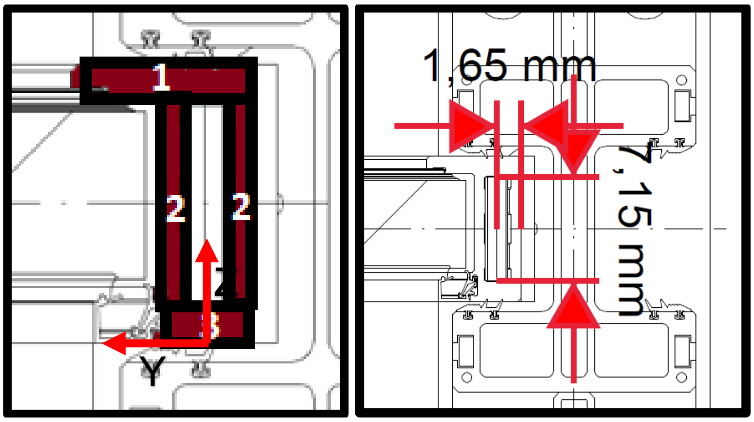

$$z = \frac{z_1 \cdot A_1 + 2 \cdot z_2 \cdot A_2 + z_3 \cdot A_3}{A_1 + 2 \cdot A_2 + A_3}$$

$$z = \frac{90.5 \cdot 65.2 \cdot 11.9 + 2 \cdot 50 \cdot 6.5 \cdot 61.8 + 7.4 \cdot 30.1 \cdot 14.4}{65.2 \cdot 11.9 + 2 \cdot 6.5 \cdot 61.8 + 30.1 \cdot 14.4} = 56.4\, mm$$

$$y = \frac{y_1 \cdot A_1 + 2 \cdot y_2 \cdot A_2 + y_3 \cdot A_3}{A_1 + 2 \cdot A_2 + A_3}$$

$$y = \frac{(0.5 \cdot 65.2) \cdot 65.2 \cdot 11.9 + 2 \cdot 16.5 \cdot 6.5 \cdot 61.8 + (0.5 \cdot 30.1) \cdot 30.1 \cdot 14.4}{65.2 \cdot 11.9 + 2 \cdot 6.5 \cdot 61.8 + 30.1 \cdot 14.4} = 22.4\, mm$$

Both coordinates are located as expected.

Now we can determine the moments of inertia from the determined center of gravity:

$$I_{zz} = \left(I_{z,1} + A_1 \cdot |(z_1 - z)|\right) + 2 \cdot \left(I_{z,2} + A_2 \cdot |(z_2 - z)|\right) + \left(I_{z,3} + A_3 \cdot |(z_3 - z)|\right)$$

$$\begin{aligned} I_{zz} = &\left(\frac{1}{12} \cdot 65.2 \cdot 11.9^3 + 65.2 \cdot 11.9 \cdot |(90.5 - 56.4)|^2\right) + 2 \\ &\cdot \left(\frac{1}{12} \cdot 6.5 \cdot 61.8^3 + 6.5 \cdot 61.8 \cdot |(50 - 56.4)|^2\right) \\ &+ \left(\frac{1}{12} \cdot 30.1 \cdot 14.4^3 + 30.1 \cdot 14.4 \cdot |(7.4 - 56.4)|^2\right) \end{aligned}$$

$$I_{zz} = 911357.1 + 288605.4 + 1048179.3 = 2248141 = 2.25 \cdot 10^6\, mm^4$$

$$I_{yy} = \left(I_{y,1} + A_1 \cdot |(y_1 - y)|^2\right) + 2 \cdot \left(I_{y,2} + A_2 \cdot |(y_2 - y)|^2\right) + \left(I_{y,3} + A_3 \cdot |(y_3 - y)|^2\right)$$

$$\begin{aligned} I_{yy} = &\left(\frac{1}{12} \cdot 11.9 \cdot 65.2^3 + 65.2 \cdot 11.9 \cdot |(65.2 \cdot 0.5 - 22.4)|^2\right) + 2 \\ &\cdot \left(\frac{1}{12} \cdot 61.8 \cdot 6.5^3 + 6.5 \cdot 61.8 \cdot |(16.5 - 22.4)|^2\right) \\ &+ \left(\frac{1}{12} \cdot 14.4 \cdot 30.1^3 + 30.1 \cdot 14.4 \cdot |(0.5 \cdot 30.1 - 22.4)|^2\right) \end{aligned}$$

$$I_{yy} = 355580.6 + 30795.0 + 56140 = 442516.2 = 0.44 \cdot 10^6\, mm^4$$

The surface area is:

$$A = A_1 + 2 \cdot A_2 + A_3 = 11.9 \cdot 65.2 + 2 \cdot 61.8 \cdot 6.5 + 30.1 \cdot 14.4 = 2012.7\ mm^2$$

The circumference area is:

$$A_L = 2 \cdot 65.2 + 2 \cdot (11.9 + 66.8 + 14.4) =$$

FEM input summary for the top and bottom support L:

$$I_{zz,L} = 2.25 \cdot 10^6\ mm^4$$
$$I_{yy,L} = 0.44 \cdot 10^6\ mm^4$$
$$A_L = 2012.7\ mm^2$$

Since this profile is mainly a closed square with a small extra contribution to the stiffness for the I_{yy}, this profile is modelled in SCIA as an rectangular hollow Aluminum profile:

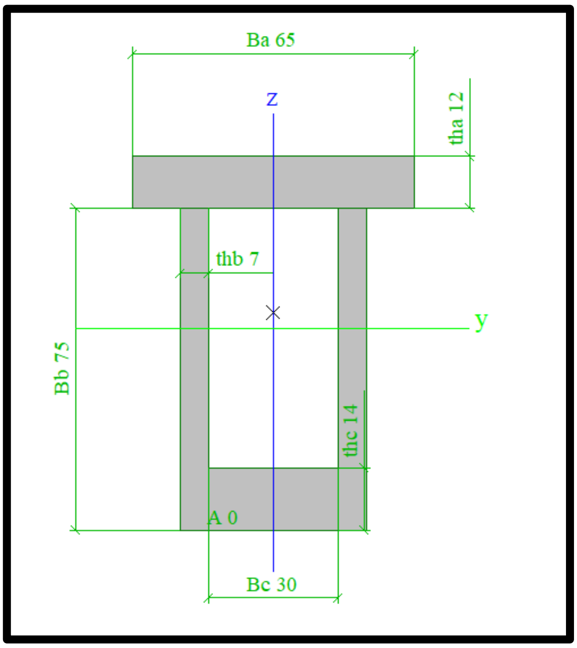

Figure H-1: Frame profile

Table H-5: Input SCIA

Parameters	
Materiaal	EN-AW 6082 (EP,ET,ER/B) T4 (0-25)
Ba [mm]	65
tha [mm]	12
Bb [mm]	75
thb [mm]	7
Bc [mm]	30
thc [mm]	14
A [mm]	0
Algemeen	
Tekenkleur	Normale kleur
Kleur	
AutoDesign restricties	
Bouwwijze	extrusie
Initiële vorm	
Inschakelen	☐
Vezels en Onderdel...	
Vezels tekst zoom	1.0
Bewerk benoemde on...	
2D EEM analyse	
Pas 2D EEM analyse toe	☑
Netgrootte [mm]	0
Min. puntafstand [mm]	0
Afschuifvlak Ay	Zonder τ xz
Afschuifvlak Az	Zonder τ xy
Toon net	☐
Eigenschap Modifi...	
Wijzig afschuif- en tor...	☐
Gebruik eigenschap ve...	☐

Eigenschap	
A [m^2]	2,1843e-03
Ay [m^2]	1,1911e-03
Az [m^2]	1,0908e-03
AL [m^2/m]	3,0420e-01
AD [m^2/m]	4,8560e-01
cYUCS [mm]	33
cZUCS [mm]	47
α [deg]	0,00
Iy [m^4]	2,1425e-06
Iz [m^4]	6,3753e-07
iy [mm]	31
iz [mm]	17
Wely [m^3]	4,5662e-05
Welz [m^3]	1,9556e-05
Wply [m^3]	6,2871e-05
Wplz [m^3]	3,3751e-05
Mply+ [Nm]	6,92e+03
Mply- [Nm]	6,92e+03
Mplz+ [Nm]	3,71e+03
Mplz- [Nm]	3,71e+03
dy [mm]	0
dz [mm]	4
It [m^4]	1,1383e-06
Iw [m^6]	2,2621e-10
β y [mm]	-10
β z [mm]	0

H.7. Dummy section

To connect the glass panels to the Aluminum frame, dummy bars are used to have realistic behavior and cooperation between model members. The following tables are the input for these sections in SCIA.

Naam	DUMMY
Normonafhankelijk	
Materiaaltype	Algemeen materiaal
Thermische uitzetting ...	0,00
Massa eenheid [kg/m...	0,0
E-modulus [MPa]	1,0000e+10
Poisson coeff.	0,3
Onafhankelijke G-mod...	☐
G-modulus [MPa]	3,8462e+09
Log. decrement (niet-...	0,15
Kleur	
Specifieke hitte [J/gK]	6,0000e-01
Thermische geleiding ...	4,5000e+01

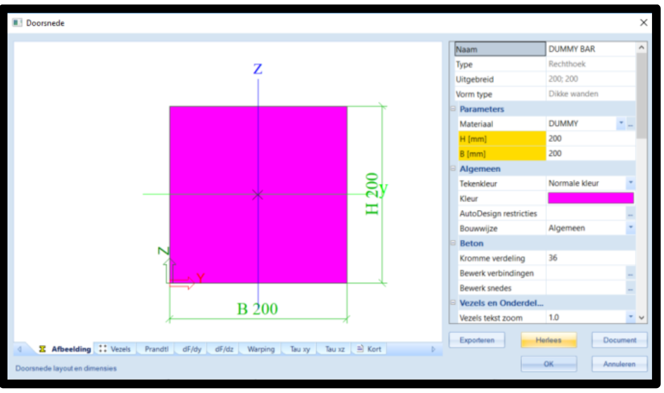

Figure H-2: Properties dummy section

H.8. Test prediction with FEM

To predict possible outcomes of the test, three different scenario's will be worked out:

1. The conservative approach based on Eurocode and NEN standards, the Ultimate Limit State. This is the minimum energy that should be absorbed by the structure without failure of the panel. ($f_g \approx 92$)
2. The expected outcome, based on mean strength values. ($f_g \approx 120$)

3. An optimistic outcome, previous impact tests showed that glass strength is even higher with short duration loads like impact. ($f_g \approx 140$)

H.8.1. Ultimate Limit State

In Appendix F the maximum allowed stress in the ULS of the glass is determined for a short duration concentration load according to the Dutch NEN [Appendix F]:

$$92.10\ MPa$$

With a concentrated force of $10200\ kN/m^2$ on a surface of $0.1x0.1m$, the total load is $102\ kN$. The principal stresses are $91.7\ N/mm^2$

H.8.2. 3D principal stress σ_1

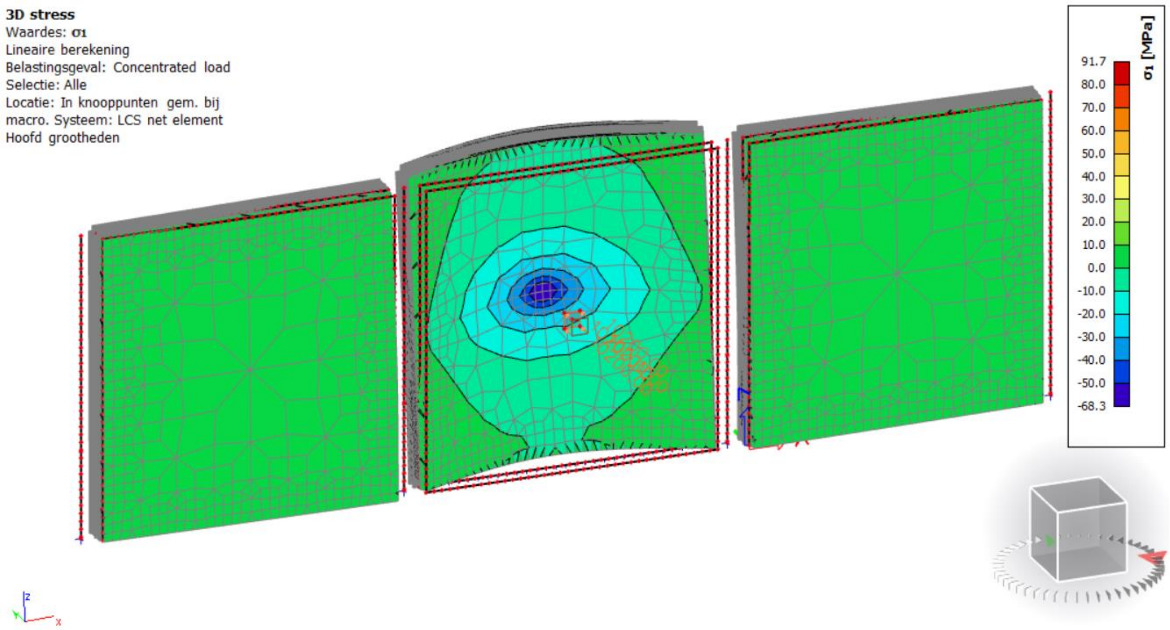

Figure H-3: 3D stresses σ_1 Impact load ULS

H.8.3. 3D principal stress σ_2

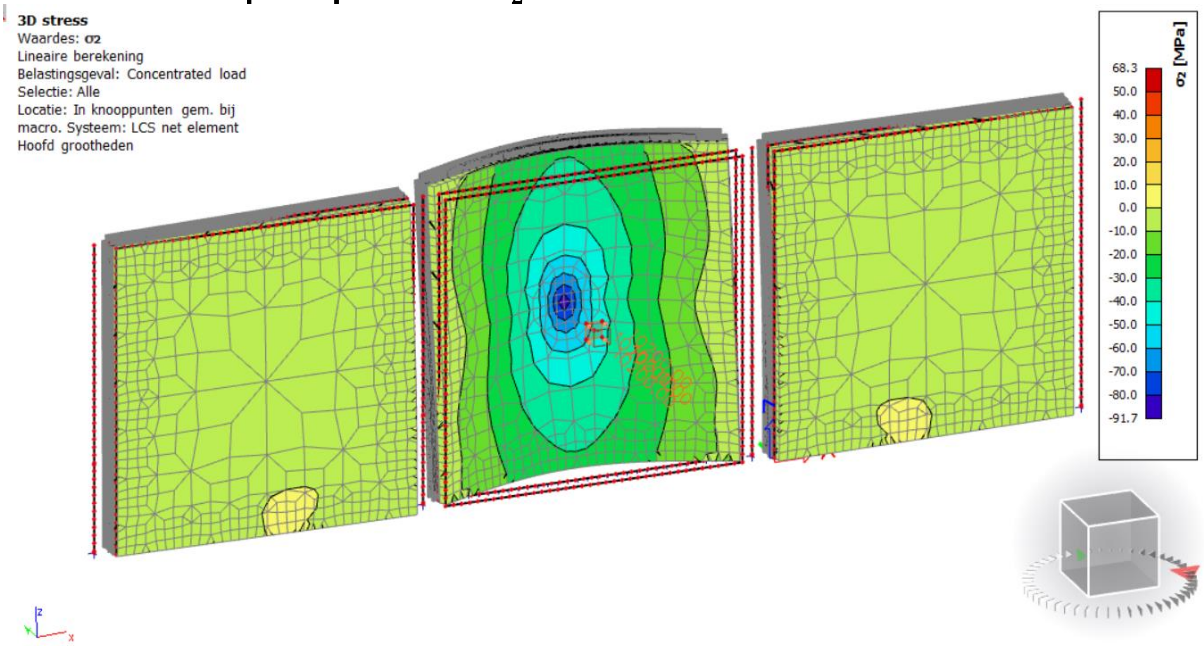

Figure H-4: 3D stresses σ_2 Impact load ULS

And the displacement that occurs is 9.6 mm.

H.8.4. 3D displacement u_{max}

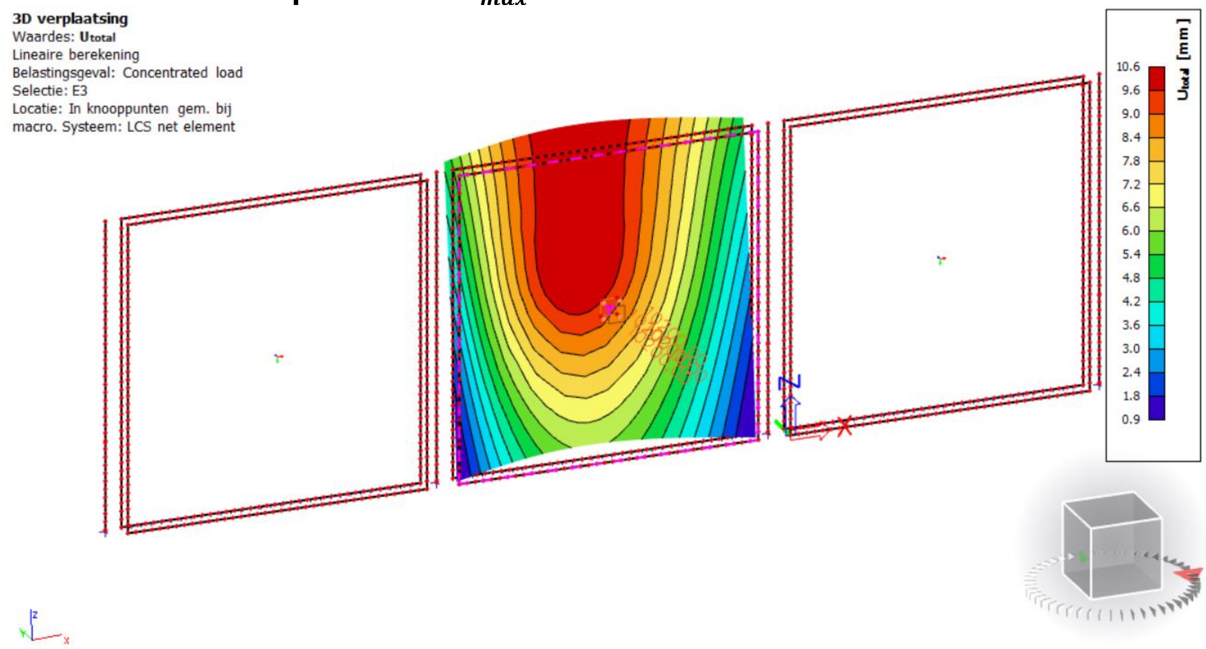

Figure H-5: 3D Displacement impact load ULS

H.8.5. Conclusion Ultimate Limit State

At this point the critical stress according to the NEN is reached. The concentrated load is $102\ kN$ and the displacement $u_{max} = \Delta x = 0.096\ m$. According to the formula derived in Appendix B; the (linear) relation $F \cdot \Delta x = 2 \cdot E_{kin,max}$, the energy absorbed by the structure becomes:

$$E_{absorbed} = \frac{F \cdot \Delta x}{2} = \frac{102 \cdot 0.096}{2} = 0.490\ kNm = 490\ Nm$$

This value corresponds with the energy of a tree trunk of $200\ kg$, with a speed of $2.213\ m/s$

$$E_{kin} = 0.5 \cdot 200 \cdot 2.213^2 = 490\ kg \cdot m^2/s^2 = 490\ Nm$$

This energy is absorbed by the structure without inclination of the impact object, which is a conservative assumption.

H.9. Expected outcome

For this calculation the nominal value of FTG will be used:

$$120\ MPa$$

With a concentrated force of $13350\ kN/m^2$ on a surface of $0.1x0.1m$, the total load is $133.5\ kN$. The principal stresses are $120\ N/mm^2$

H.9.1. 3D principal stress σ_1

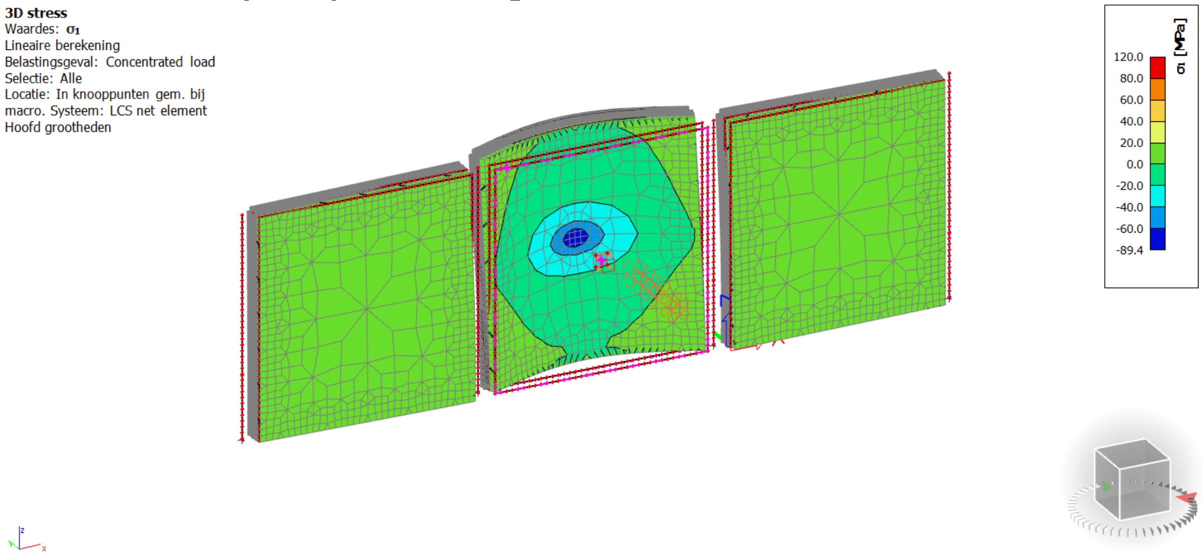

Figure H-6: 3D Principal stress σ_1 expected outcome

H.9.2. 3D principal stress σ_2

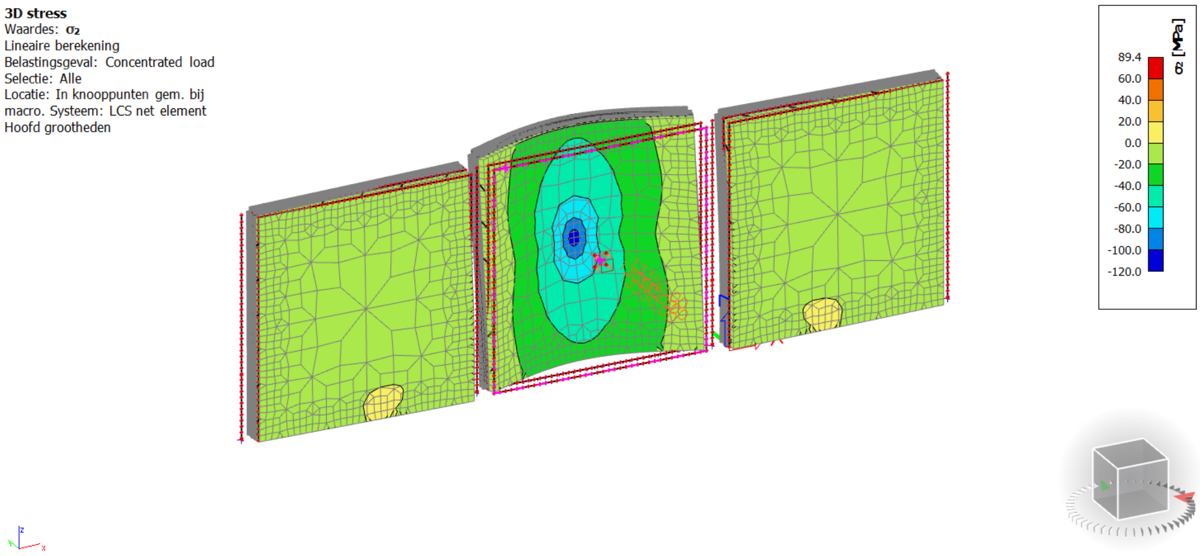

Figure H-7: 3D Principal stress σ_2 expected outcome

And the displacement that occurs is 12 mm.

H.9.3. 3D displacement u_{max}

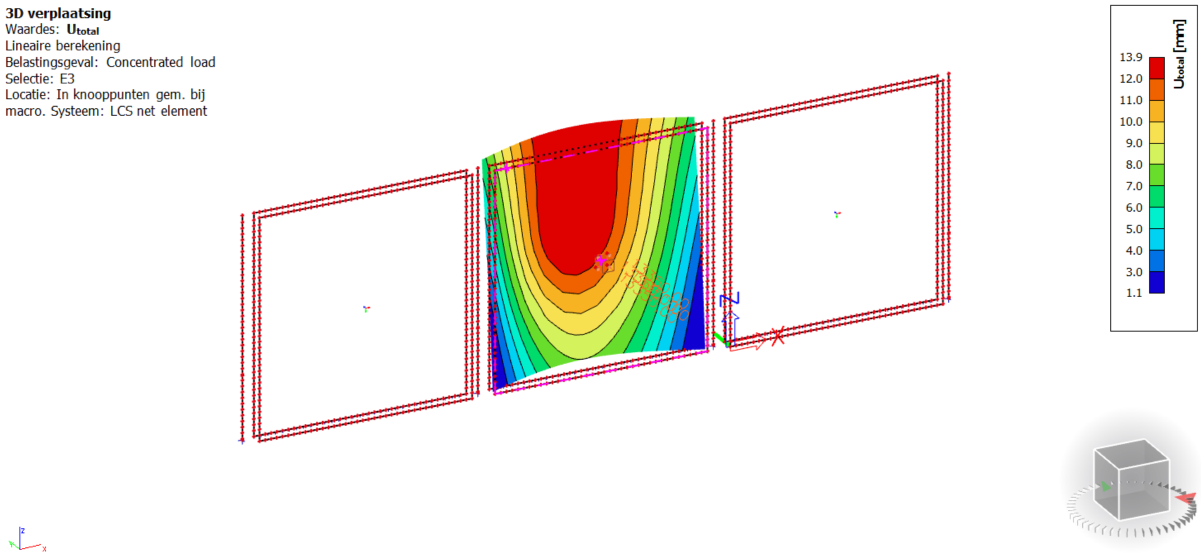

Figure H-8: 3D displacement expected outcome

H.9.4. Conclusion Expected Outcome

At this point the nominal strength is reached. The concentrated load is $133.5\ kN$ and the displacement $u_{max} = \Delta x = \ 0.012\ m$. According to the formula derived in Appendix B; the (linear) relation $F \cdot \Delta x = 2 \cdot E_{kin,max}$, the energy absorbed by the structure becomes:

$$E_{absorbed} = \frac{F_c \cdot \Delta x}{2} = \frac{133.5 \cdot 0.012}{2} = 0.801\ kNm = 801\ Nm$$

This value corresponds with the energy of a tree trunk of $200\ kg$, with a speed of $2.32\ m/s$

$$E_{kin} = 0.5 \cdot 200 \cdot 2.830^2 = 801\ kg \cdot m^2/s^2 = 801\ Nm$$

This energy is <u>without</u> inclination of the impact object, which is a conservative assumption. If we do take the inclination of the tree trunk into account, the total displacement between the two masses increases. The springs are in series and a linear relation is assumed. The stiffness of the structure at this point is:

$$k_s = \frac{133.5}{0.012} = 11125$$

An upper boundary for the spring stiffness of the tree trunk is determined in Appendix B; $k_b = 1508\ kN/m$. An equivalent spring stiffness is derived by:

$$k_{eq} = \frac{1}{\frac{1}{k_s} + \frac{1}{k_b}} = \frac{1}{\frac{1}{11125} + \frac{1}{1508}} = 1328\ kN/m$$

With the governing force of $133.5\ kN$ based on the critical stress in the glass plate the total inclination of both plate and tree becomes:

$$u_{eq} = \frac{F_c}{k_{eq}} = \frac{133.5}{1328} = 0.101\ m$$

The absorbed energy then becomes:

$$E_{absorbed} = \frac{F_c \cdot u_{eq}}{2} = \frac{133.5 \cdot 0.1}{2} = 6.710\ kNm = 6710\ Nm$$

This value corresponds with the energy of a tree trunk of $200\ kg$, with a speed of $8.17\ m/s$

$$E_{kin} = 0.5 \cdot 200 \cdot 8.19^2 = 6710\ kg \cdot m^2/s^2 = 6710\ Nm$$

Side note: In reality the spring stiffness of the tree is not linear and becomes larger during the inclination, as the fibers are pushed together and become denser. The total energy that can be absorbed will then be between the values of $801\ Nm$ and $6710\ Nm$ and is hard to predict.

H.10. Optimistic Outcome

For this calculation an optimistic value of glass strength will be used, it is

$$140\ MPa$$

This value will never be used to design safe structures, but as is often the case, the real strength and redundancy of materials and structures usually exceeds the design values.
With a concentrated force of $13350\ kN/m^2$ on a surface of $0.1x0.1m$, the total load is $133.5\ kN$. The principal stresses are $120\ N/mm^2$

H.10.1. 3D principal stress σ_1

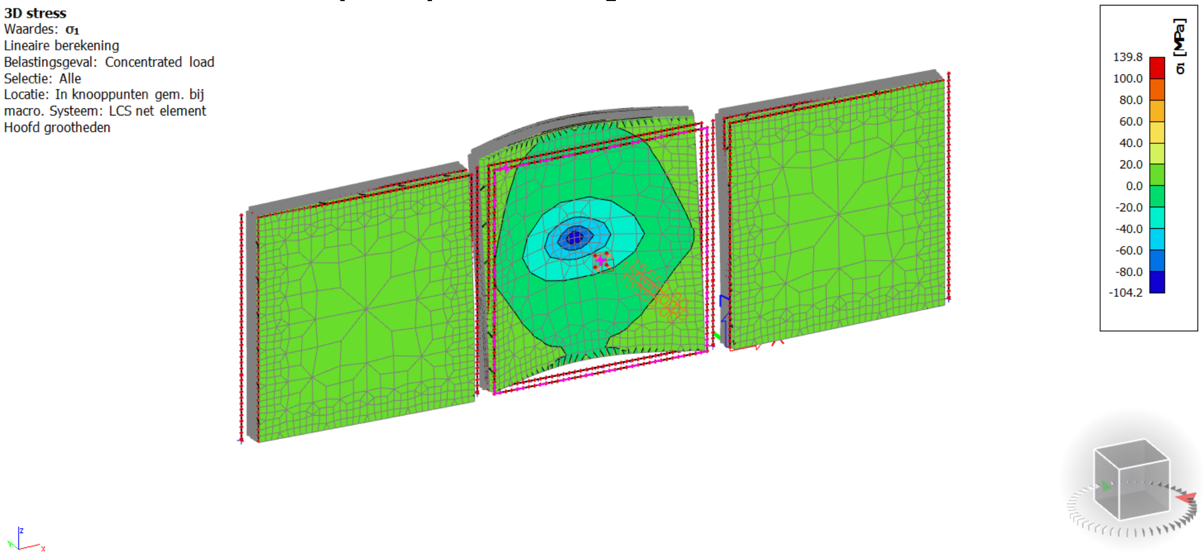

Figure H-9: 3D Principal stress σ_1 optimistic outcome

H.10.2. 3D principal stress σ_2

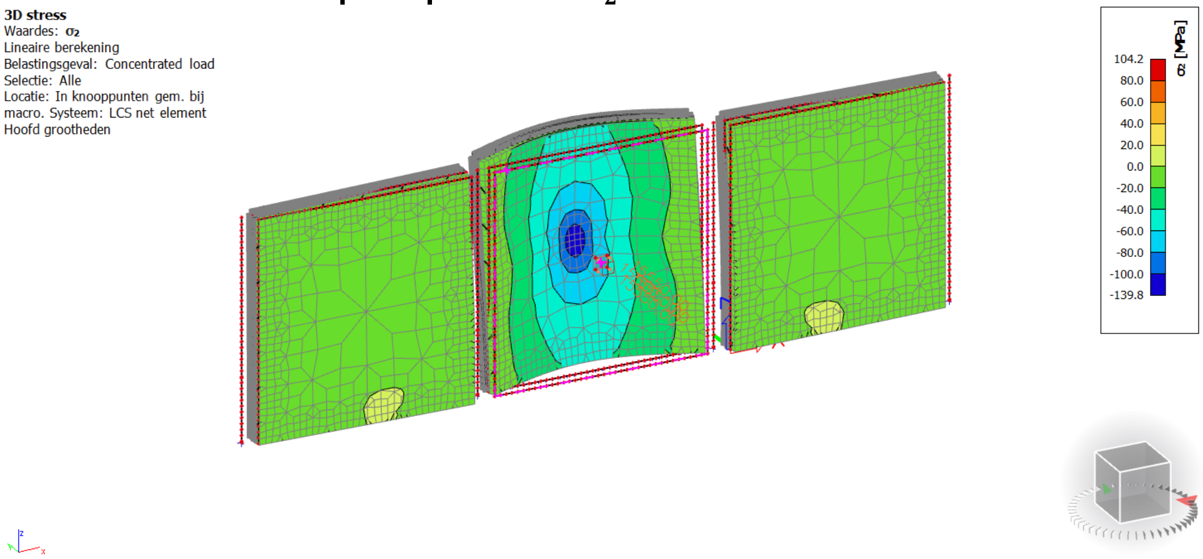

Figure H-10: 3D Principal stress σ_2 optimistic outcome

And the displacement that occurs is 15 mm.

H.10.3. 3D displacement u_{max}

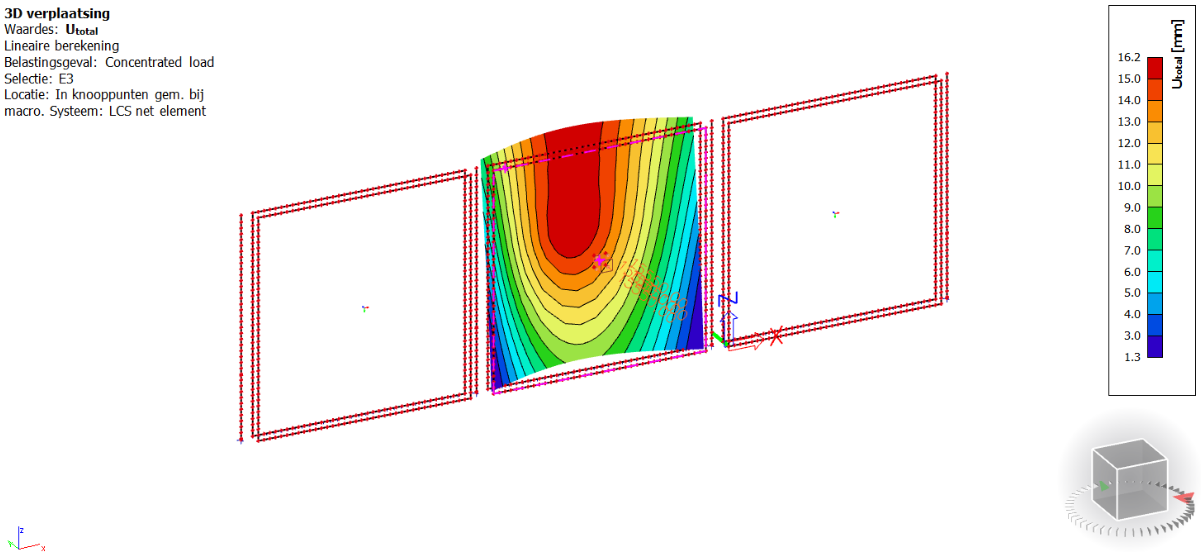

Figure H-11: 3D displacement optimistic outcome

H.10.4. Conclusion Optimistic Outcome

At this point the optimistic glass strength is reached. The concentrated load is $155.5\ kN$ and the displacement $u_{max} = \Delta x = \ 0.015\ m$. According to the formula derived in Appendix B; the (linear) relation $F \cdot \Delta x = 2 \cdot E_{kin,max}$, the energy absorbed by the structure becomes:

$$E_{absorbed} = \frac{F_c \cdot \Delta x}{2} = \frac{155.5 \cdot 0.015}{2} = 1.166\ kNm = 1166\ Nm$$

This value corresponds with the energy of a tree trunk of $200\ kg$, with a speed of $2.32\ m/s$

$$E_{kin} = 0.5 \cdot 200 \cdot 3.415^2 = 1166\ kg \cdot m^2/s^2 = 1166\ Nm$$

This energy is <u>without</u> any inclination of the impact object, which is a conservative assumption. If we do take the inclination of the tree trunk into account, the total displacement between the two masses increases. The springs are in series and a linear relation is assumed. The stiffness of the structure at this point is:

$$k_s = \frac{155.5}{0.015} = 10367\ kN/m$$

An upper boundary for the spring stiffness of the tree trunk is determined in Appendix B; $k_b = 1508\ kN/m$. An equivalent spring stiffness is derived by:

$$k_{eq} = \frac{1}{\frac{1}{k_s} + \frac{1}{k_b}} = \frac{1}{\frac{1}{10367} + \frac{1}{1508}} = 1316\ kN/m$$

With the governing force of $133.5\ kN$ based on the critical stress in the glass plate the total inclination of both plate and tree becomes:

$$u_{eq} = \frac{F_c}{k_{eq}} = \frac{155.5}{1316} = 0.118\ m$$

The absorbed energy then becomes:

$$E_{absorbed} = \frac{F_c \cdot u_{eq}}{2} = 155.5 \cdot 0.118 = 9.175\ kNm = 9175\ Nm$$

This value corresponds with the energy of a tree trunk of $200\ kg$, with a speed of $9.578\ m/s$

$$E_{kin} = 0.5 \cdot 200 \cdot 9.578^2 = 9175\ kg \cdot m^2/s^2 = 9175\ Nm$$

Side note: In reality the spring stiffness of the tree is not linear and becomes larger during the inclination, as the fibers are pushed together and become denser. The total energy that can be absorbed will then be between the values of $1166\ Nm$ and $9175\ Nm$ and is hard to predict.

H.11. Summary

Three scenarios with a few different assumptions are elaborated on and the results of these iterative calculations are summarized below:

Table H-6: Summary critical impact energy

Scenario	E_c Without inclination impact object $[kNm]$	E_c With inclination impact object $[kNm]$
ULS	0.54	-
Expected	0.801	6.710
Optimistic	1.166	9.175

H.12. Water level resistance

A FEM analysis of the water level resistance of the glass panel at maximum water pressure is done below.

The maximum allowed stress for a long duration distributed load is:

$$74.53\ MPa$$

The displacements in this case are not important as it is an Ultimate Limit State situation. The displacement is therefore not presented. The analysis is done in both SLS and ULS.

3D principal stress σ_1 with $t_{eff} = 50.01$

SLS

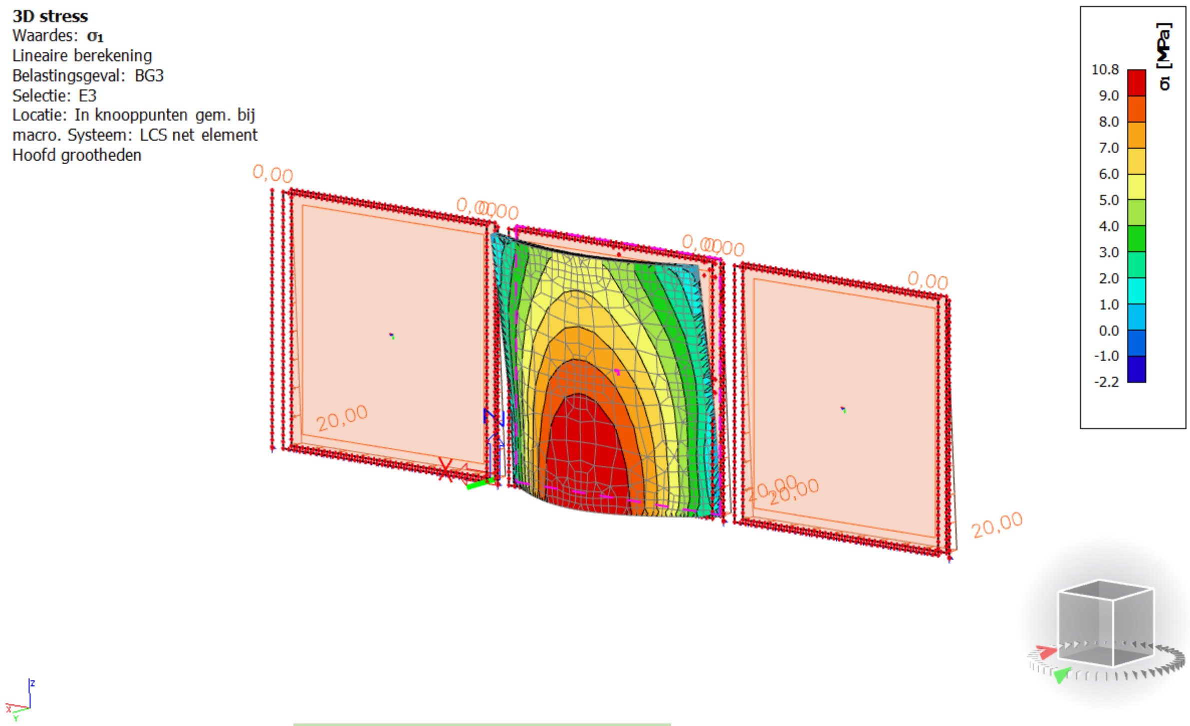

Maximum tensile stress is $10.8\ N/mm^2 < 74.53\ N/mm^2$

ULS

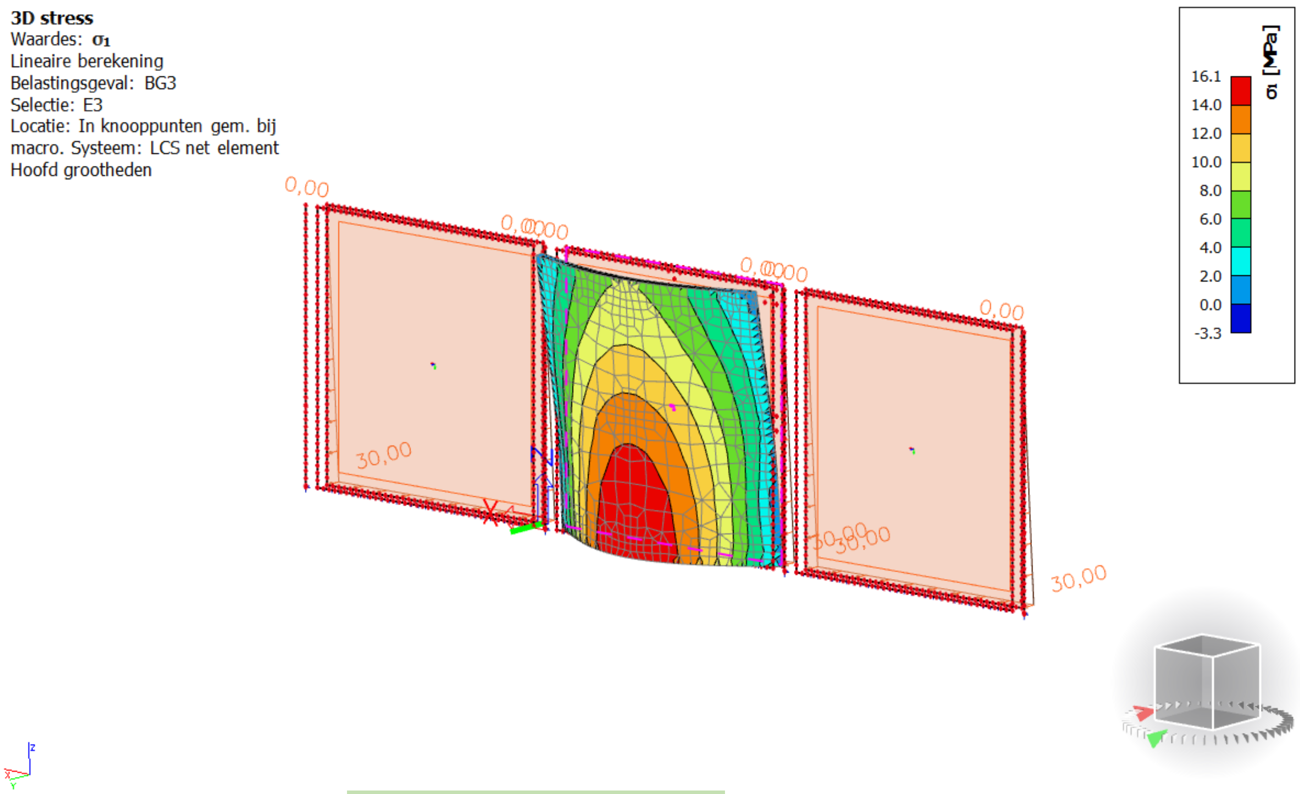

Maximum tensile stress is $16.1\ N/mm^2 < 74.53\ N/mm^2$

3D principal stress σ_2 with $t_{eff} = 50.01$

SLS

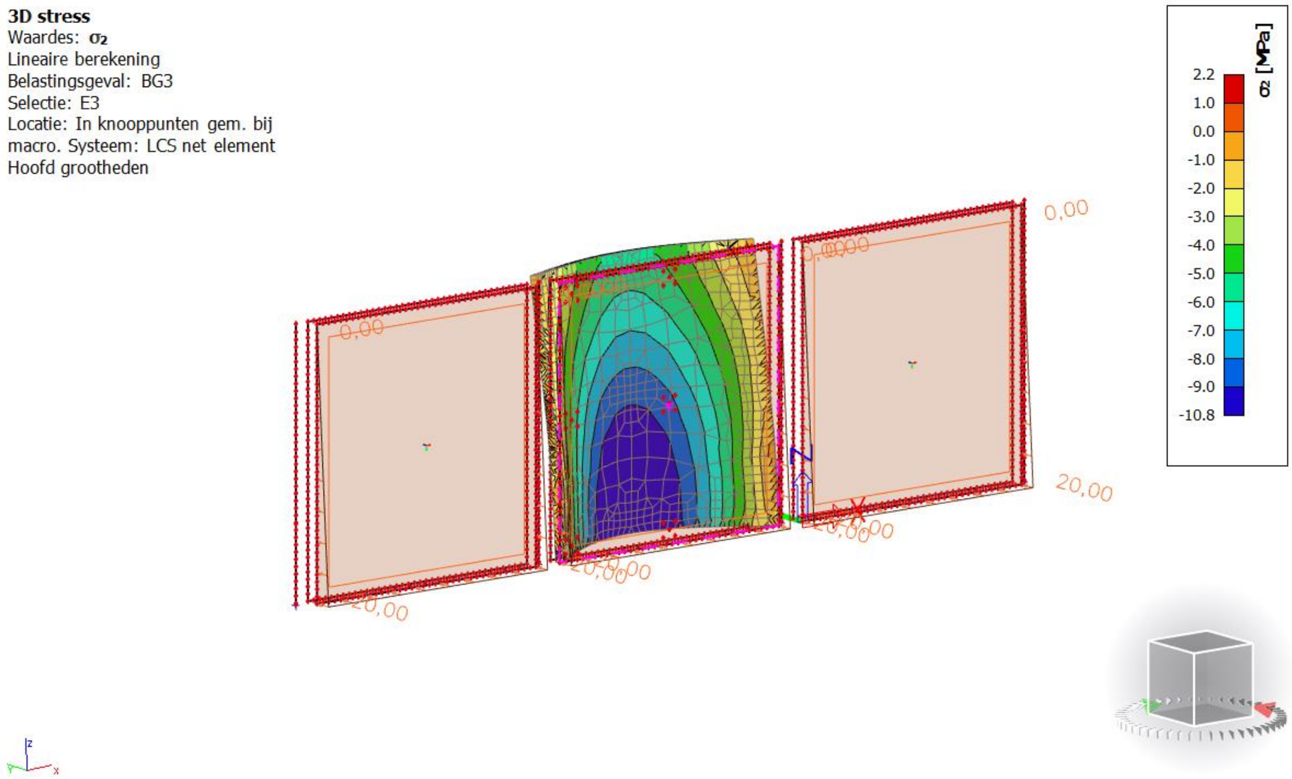

Maximum tensile stress is $2.2\ N/mm^2 < 74.53\ N/mm^2$

ULS

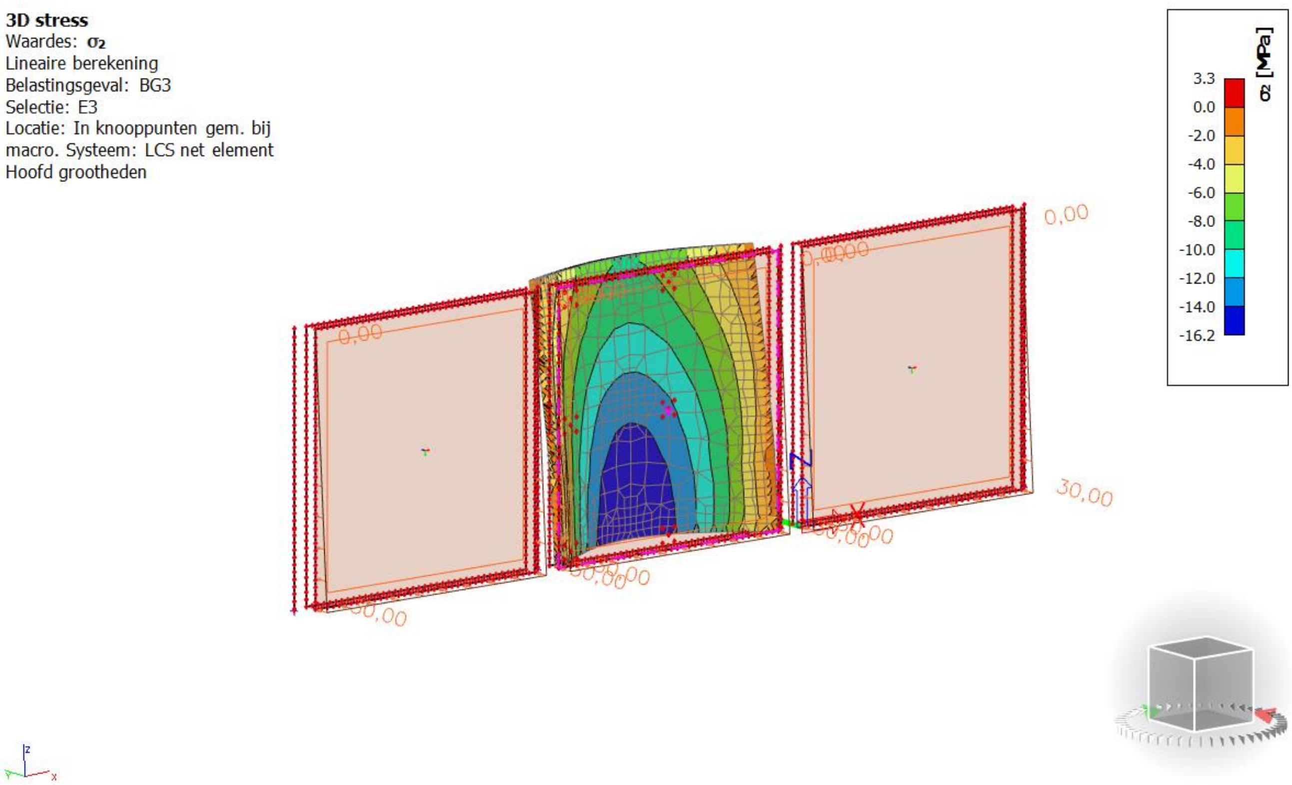

Maximum tensile stress is $3.3\ N/mm^2 < 74.53\ N/mm^2$

H.13. Water level resistance after impact

In case of an impact, one, two or all plies can be broken. If the water level is still high at the time of impact, this can cause the panel to fail completely resulting in a flood. In the FEM model, the residual strength with the effective thicknesses of one and two plies is checked in the following paragraphs.

H.13.1. Water level capacity of two remaining plies

The maximum allowed stress for a long duration distributed load is:

$$74.53\ MPa$$

The displacements in this case are not important as it is an Ultimate Limit State situation. The displacement is therefore not presented.

Coupled

If the two remaining plies are still coupled, and only one of the outer plies are broken, the effective thickness is based on 7.3:

$$t_{gg;ser} = \sqrt[3]{(1-\omega_W)\cdot\sum_{i=1}^{n} t_{pl;i}^3 + \omega_W\cdot\left(\sum_{i=1}^{n} t_{pl;i}\right)^3} = 35.72$$

3D principal stress σ_1 with $t_{eff} = 35.72$

SLS

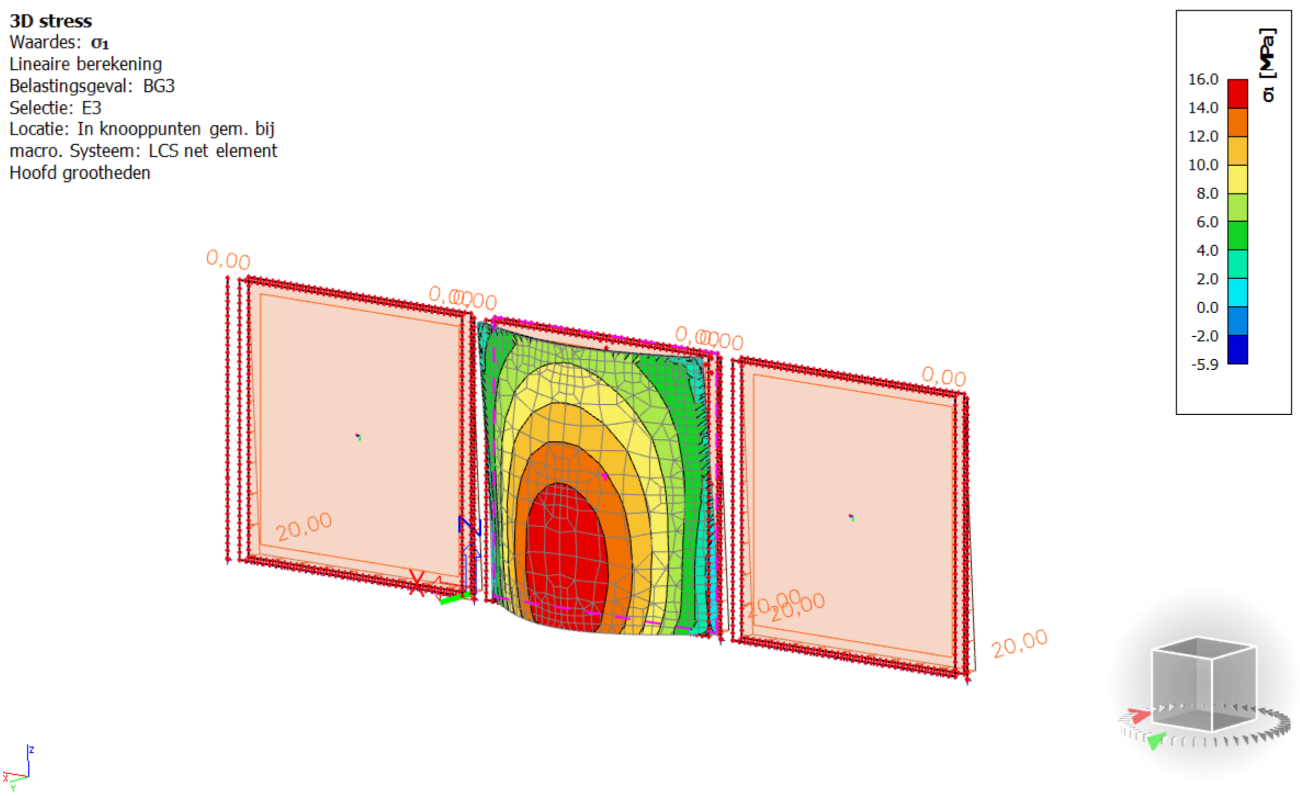

Figure H-12: 3D principal stress σ_1 with t_eff=35.72 in SLS

Maximum tensile stress is $16.0\ N/mm^2 < 74.53 N/mm^2$

ULS

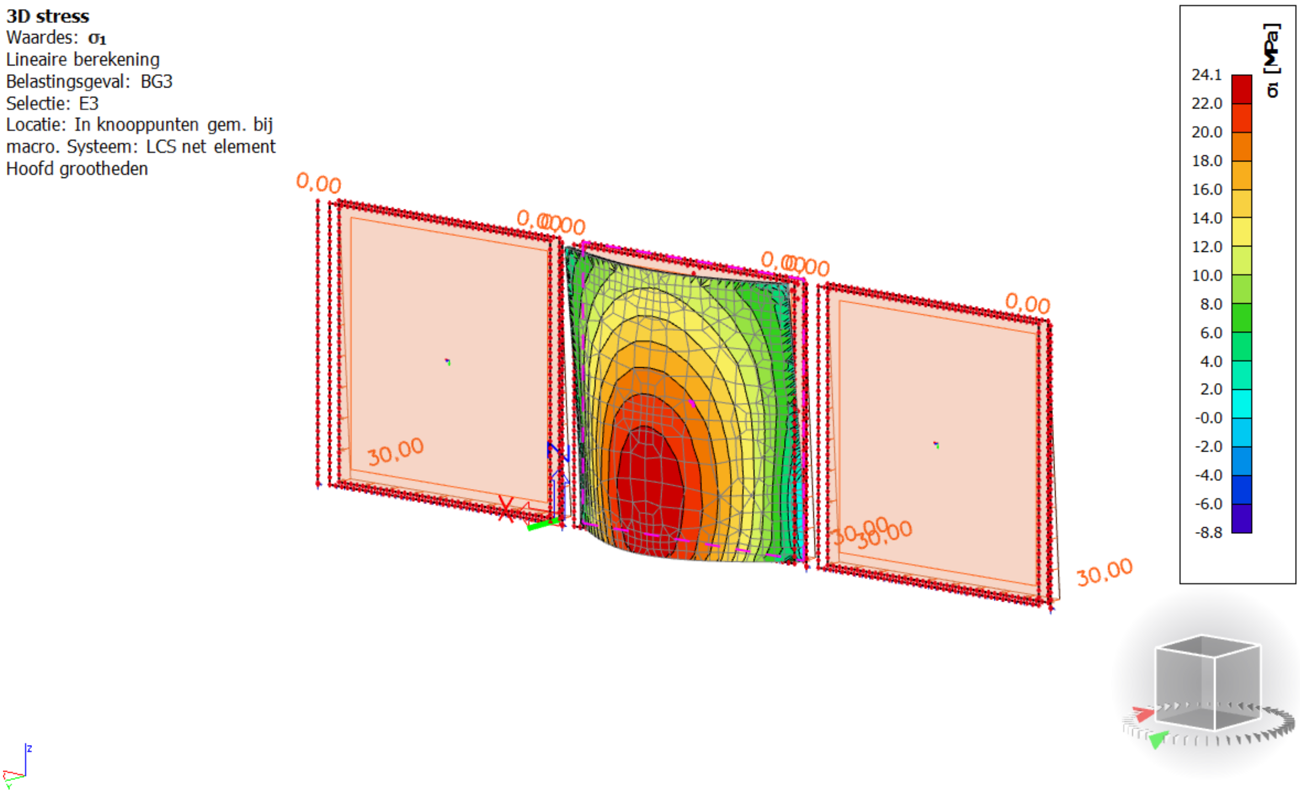

Figure H-13: 3D principal stress σ_1 with t_eff=35.72 in ULS

Maximum tensile stress is $24.1\ N/mm^2 < 74.53N/mm^2$

3D principal stress σ_2 with $t_{eff} = 35.72$

SLS

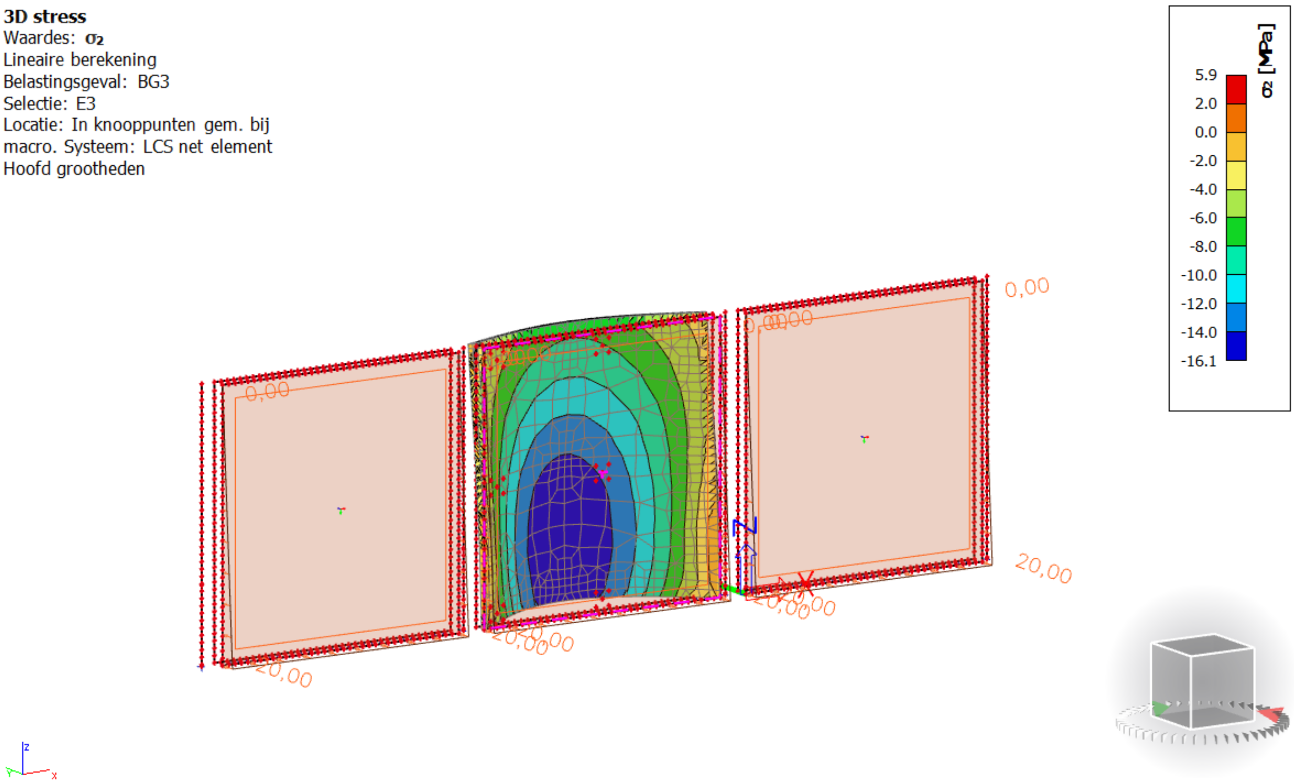

Figure H-14: 3D principal stress σ_2 with t_eff=35.72 in SLS

Maximum tensile stress is $5.9\ N/mm^2 < 74.53\ N/mm^2$

ULS

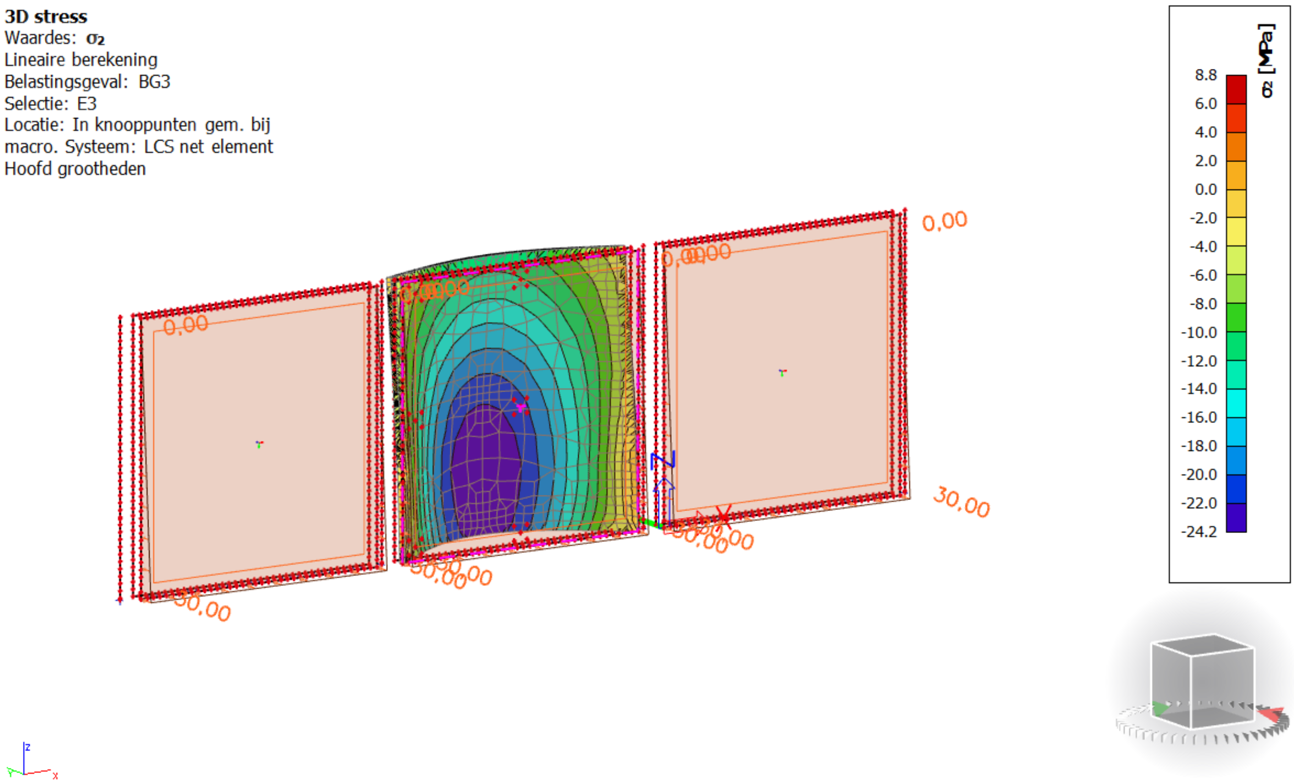

Figure H-15: 3D principal stress σ_2 with t_eff=35.72 in ULS

Maximum tensile stress is $8.8\ N/mm^2 < 74.53N/mm^2$

Uncoupled

If the middle ply fractures, and delamination occurs, there is no coupling of the plates. This means the two plates slide over each other. The effective plate stiffness can be calculated by using the standard formula for plate thickness:

$$D = \frac{Et^3}{12(1-v^2)}$$

As the plate stiffness is the sum of two plies, the stiffness D becomes:

$$D = 2 \cdot \frac{\cancel{70000} \cdot 18^3}{\cancel{12(1-0.23^2)}} = \frac{\cancel{70000} \cdot t_{eff}^3}{\cancel{12(1-0.23^2)}} \rightarrow t_{eff} = \sqrt[3]{2 \cdot 18^3} = 22.68$$

3D principal stress σ_1 with $t_{eff} = 22.68$

SLS

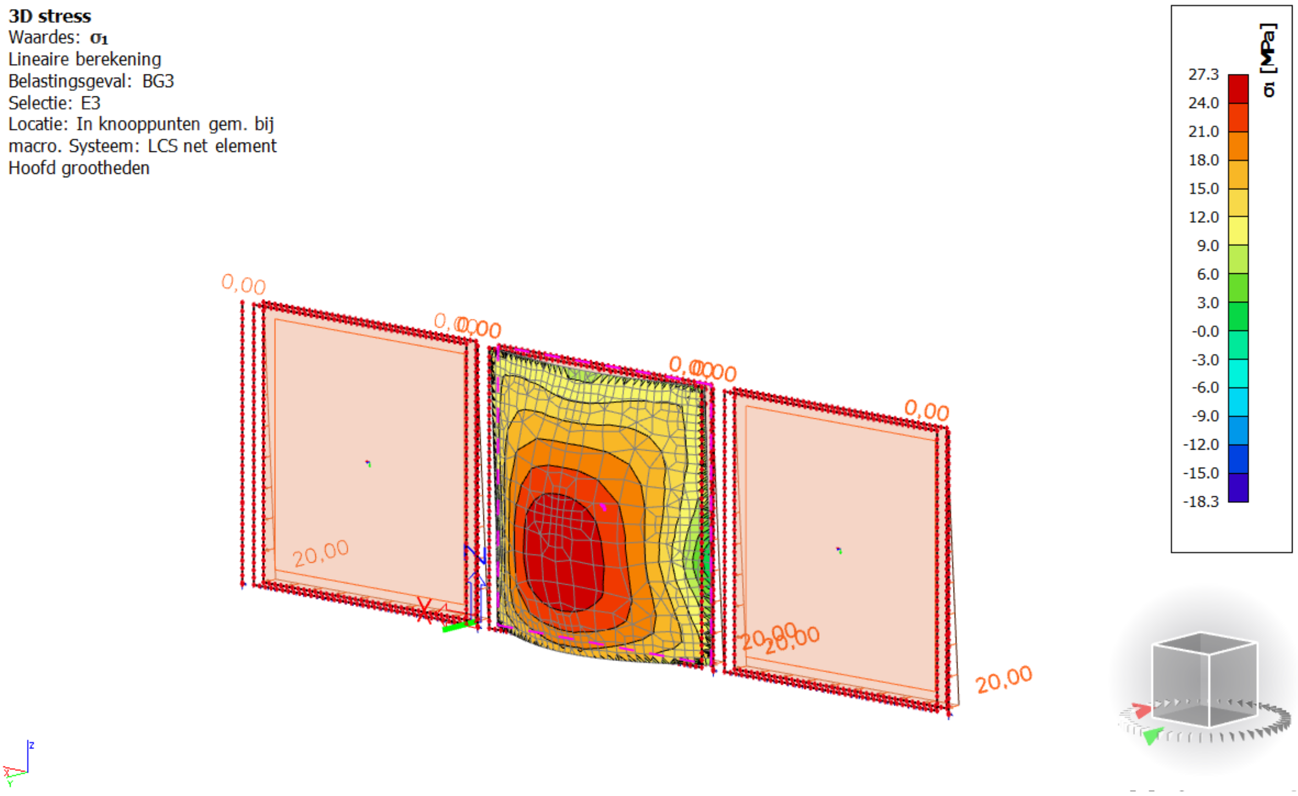

Figure H-16: 3D principal stress σ_1 with t_eff=22.68 in SLS

Maximum tensile stress is $27.3\ N/mm^2 < 74.53N/mm^2$

ULS

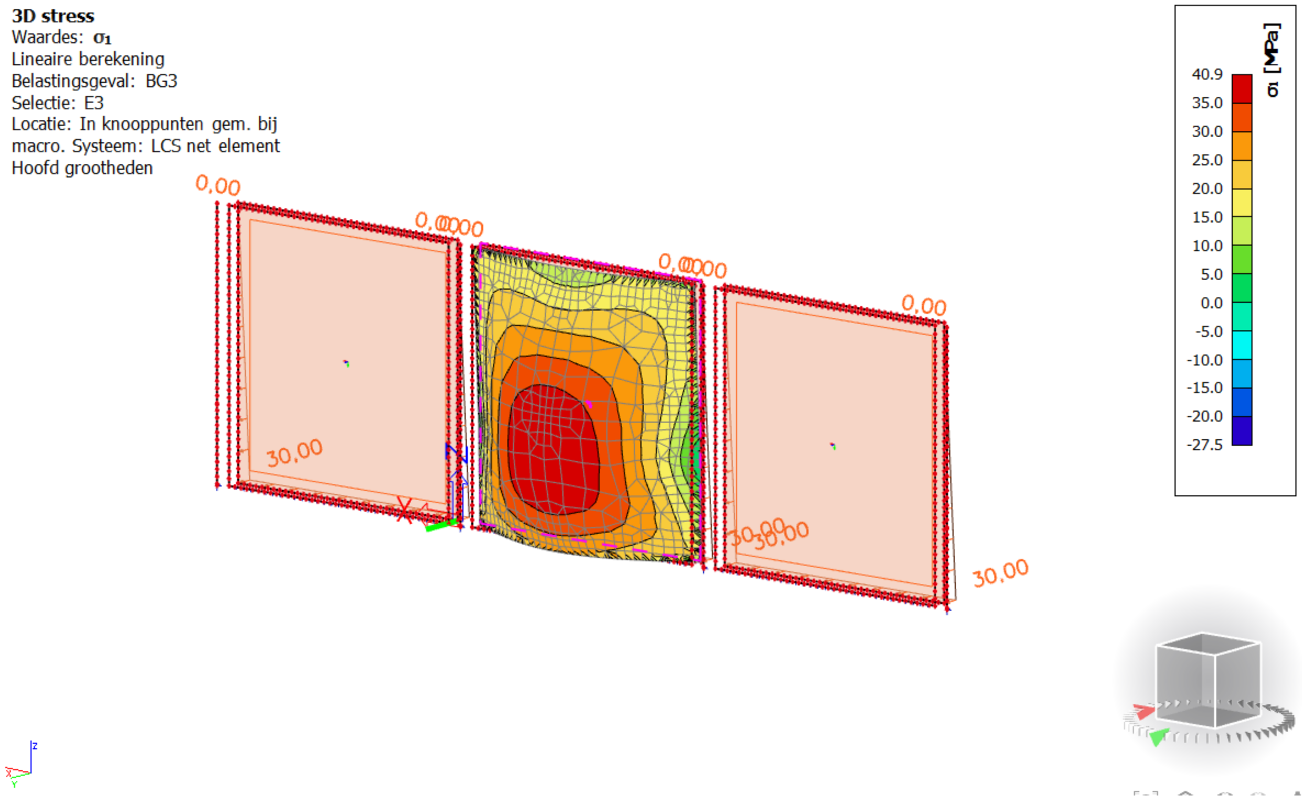

Figure H-17: 3D principal stress σ_1 with t_eff=22.68 in ULS

Maximum tensile stress is $40.9/mm^2 > 74.53N/mm^2$

3D principal stress σ_2 with $t_{eff} = 22.68$

SLS

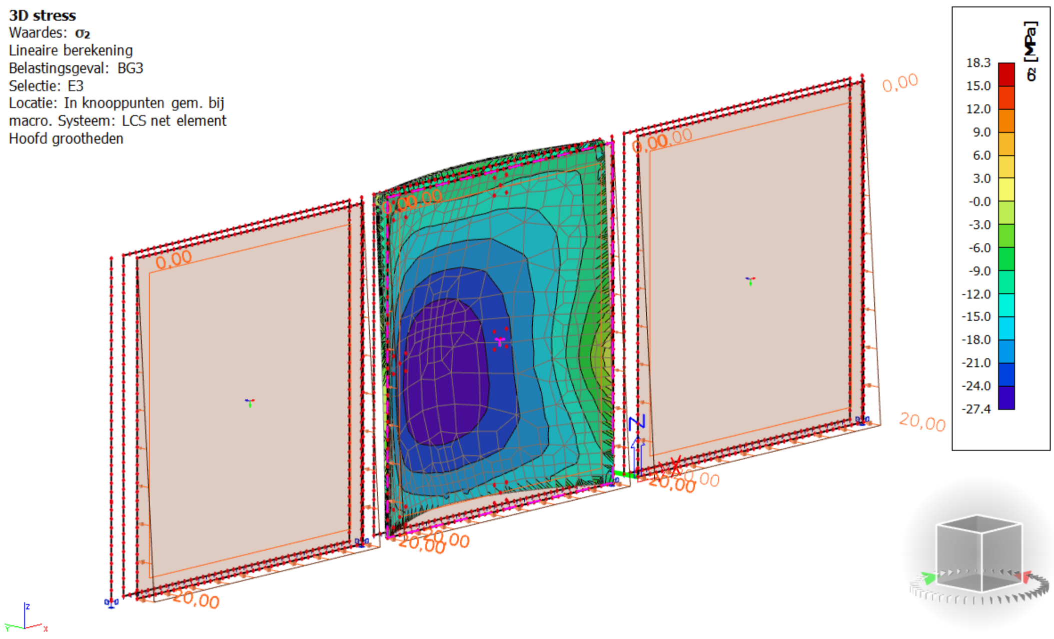

Figure H-18: 3D principal stress σ_2 with t_eff=22.68 in SLS

Maximum tensile stress is $18.3\ N/mm^2 < 74.53N/mm^2$

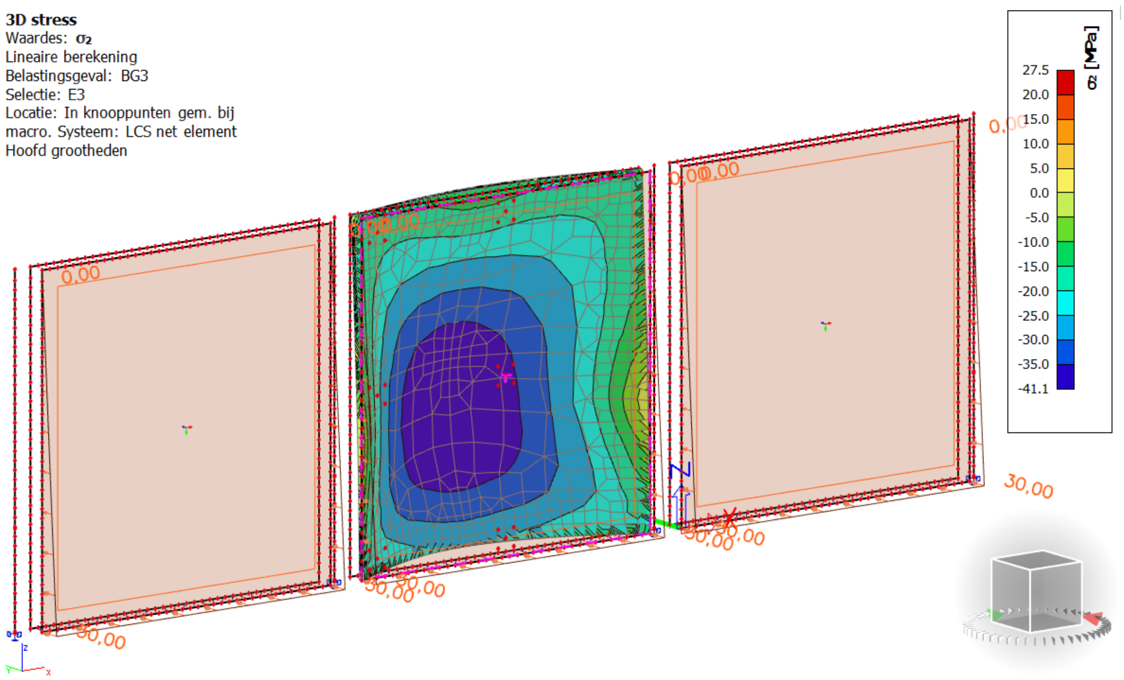

Figure H-19: 3D principal stress σ_2 with t_eff=22.68 in ULS

Maximum tensile stress is $27.5\ N/mm^2 > 74.53\ N/mm^2$

H.13.2. Water level capacity of one remaining ply

With one ply remaining, no coupling of plates occurs and the effective thickness is equal to $18\ mm$, see 7.2.4.

3D principal stress σ_1 with $t_{eff} = 18\ mm$

SLS

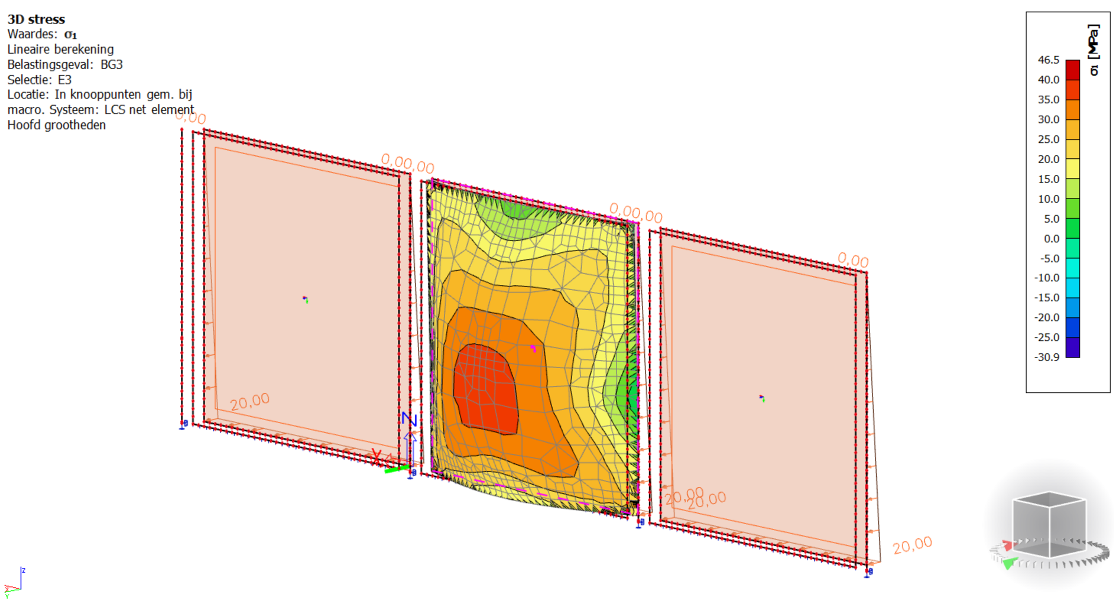

Figure H-20:3D principal stress σ_1 with t_eff=18 mm in SLS

Maximum stress is $46.5 N/mm^2 < 74.53\ N/mm^2$

ULS

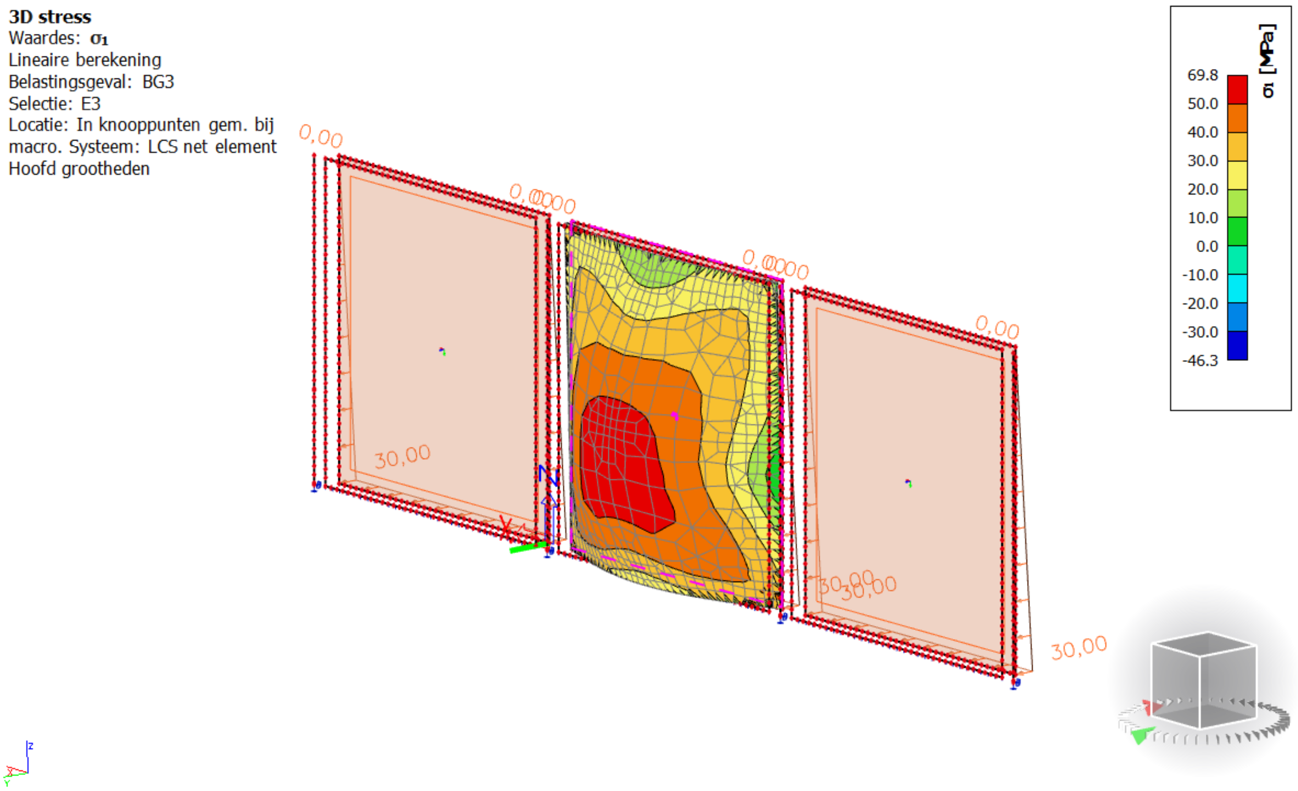

Figure H-21: 3D principal stress σ_1 with t_eff=18 mm in ULS

Maximum stress is $69.8 N/mm^2 > 74.53 N/mm^2$

3D principal stress σ_2 with $t_{eff} = 18\ mm$

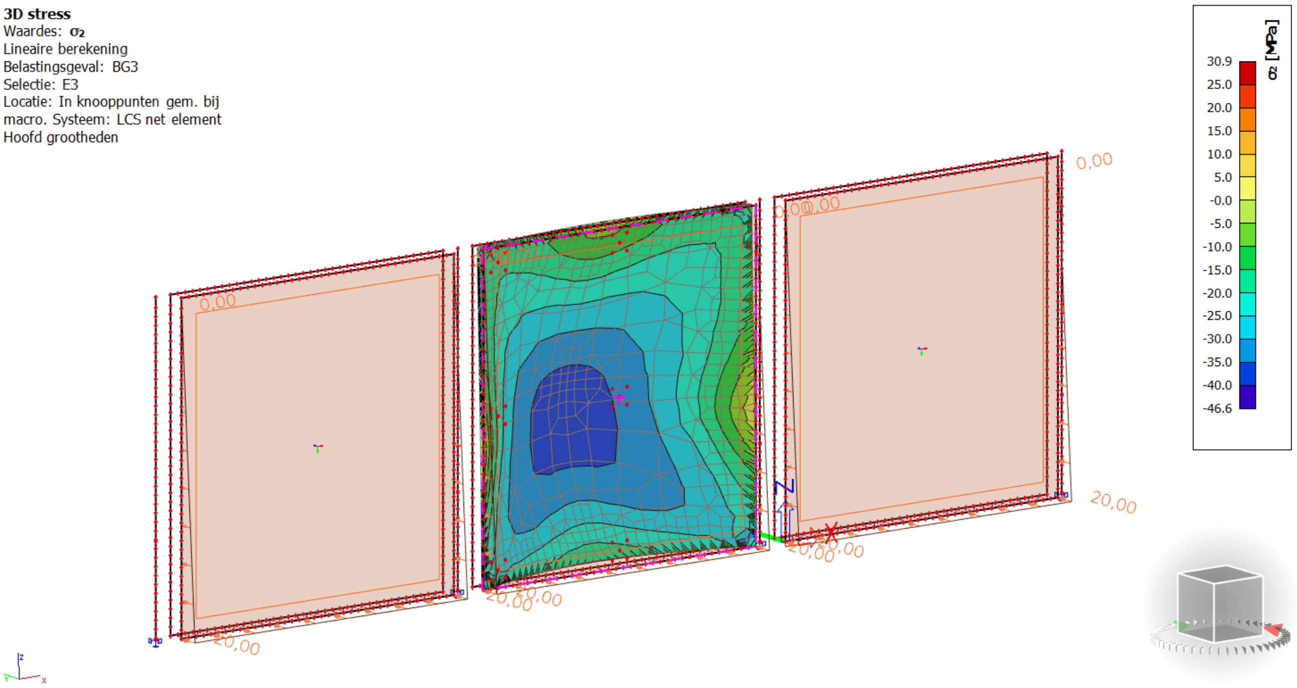

Figure H-22: 3D principal stress σ_2 with t_eff=18 mm in SLS

Maximum tensile stress is $30.9\ N/mm^2 > 74.53 N/mm^2$

ULS

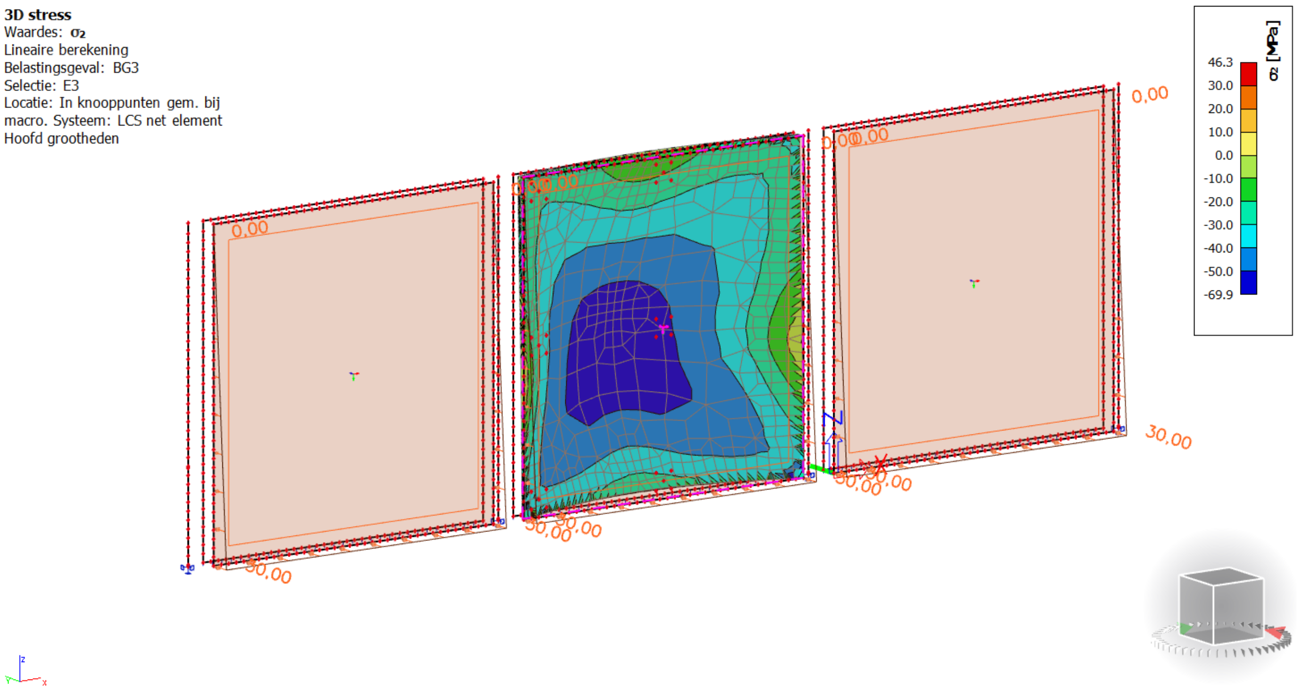

Figure H-23: 3D principal stress σ_2 with t_eff=18 mm in ULS

Maximum tensile stress is $46.3\ N/mm^2 > 74.53 N/mm^2$

H.13.3. Summary of water pressure resistance

By using the maximum allowed stress using the Dutch NEN, and the FEM model made in SCIA, the found maximum stresses of 3 coupled plies, 2 coupled plies, two uncoupled plies and a single ply are summarized in the table below. According to the model with input from the NEN2608, one remaining ply can resist the water pressure. Using only one ply is severely discouraged in terms of safety (no redundancy), but the total thickness of the plate may be optimized concerning the water pressure. Wave pressures are not included in the model.

Table H-7: Summary tensile stresses with different effective thickness relating to the maximum water pressure

t_{eff}	σ_{max} in SLS	σ_{max} in ULS
$\mathbf{50.01\ mm}$	$\mathbf{10.8\ N/mm^2}$	$\mathbf{16.1\ N/mm^2}$
$\mathbf{35.72\ mm}$	$\mathbf{16.0\ N/mm^2}$	$\mathbf{24.1\ N/mm^2}$
$\mathbf{22.68\ mm}$	$\mathbf{27.3\ N/mm^2}$	$\mathbf{40.9\ N/mm^2}$
$\mathbf{18\ mm}$	$\mathbf{46.5\ N/mm^2}$	$\mathbf{69.8\ N/mm^2}$

H.14. Literature

Hartsuijker, C. (2001). *Toegepaste Mechanica, deel 2: Spanningen vervormingen , verplaatsingen*. Amsterdam, Nederland: Academic Service.

Wagemaker. (2017). *Berekening* (Twee bruggen Prinses Irenestraat). Retrieved from https://www.odnzkg.nl/mozard/document/docnr/8401336,,7864674,/W17078%20RAP01_v10_pdf%20.pdf

SCIA Engineer. (2016). *Handboek Doorsneden*. Retrieved from https://help.scia.net/download/17.0/nl/Cross-sections_nld.pdf

Sectional characteristics calculated by FEM [Help]. (n.d.). Retrieved June 15, 2018, from https://help.scia.net/15.1/en/rb/crosssections/sectional_characteristics_calculated_by_fem.htm

CEN. (2011). *NEN-EN 1999-1-1+A1*. Geraadpleegd van https://www.nen.nl/NEN-Shop/Norm/NENEN-199911A12011NB2011-nl.htm

I. Failure mechanisms: Structural Failure

I.1. Intro

The WBI 2017 Standard pursues a full probabilistic approach regarding flood safety in the Netherlands. The failure probability space of structural failure for hydraulic structures in a dike trajectory is 0.02, or 2% [Jonkman]. This 2% of the total failure probability should be divided by the number of hydraulic structures in the dike trajectory to obtain the failure probability space for the glass flood defence. A large portion of mean values μ, coefficients of variation V_r and standard deviations σ are given in the “Schematiseringshandleiding sterkte en stabiliteit” or “Toetsspoorrapport sterkte en stabiliteit”. Some of the remaining values that need to be defined by the user are defined in this Appendix and some general values are explained in Appendix K. All remaining “Input” values are found in the latter.

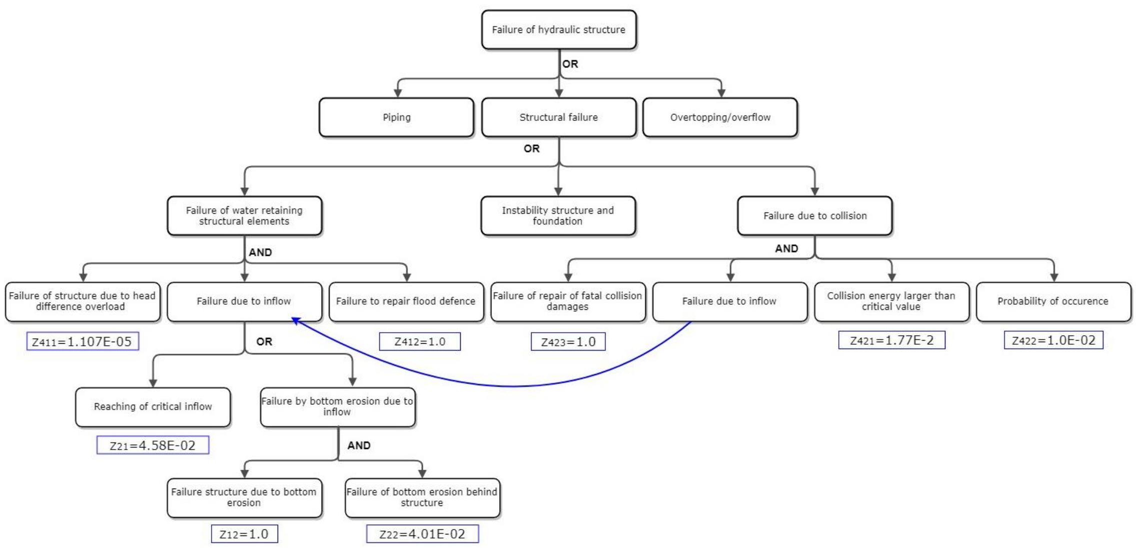

Figure I-1: Failure tree

I.2. Failure mechanisms

The sub- failure mechanisms are:

12. Failure of structure due to bottom erosion → Z_{12}
13. Failure due to the reaching of critical inflow → Z_{21}
14. Failure of bottom erosion behind structure → Z_{22}
15. Failure of structural parts due to head difference overload → Z_{411}
16. Failure to repair flood defence → Z_{412}
17. Collision energy larger than critical value → Z_{421}
18. Probability of occurrence of a collision → Z_{422}
19. Failure to repair the fatal collision damages → Z_{423}
20. Failure of structure due to instability of structure or its foundation → Z_{43}

Z_{12}: Failure of structure due to bottom erosion

This sub mechanism describes the chance of failure of the structure, given that erosion of the bottom protection takes place.

Z-Function

$$Z_{12} = \beta_{kw|erosion} - u$$

Where:

$\beta_{kw|erosion}$ = Reliability index corresponding with the failure probability of the structure given the fact that piping/under seepage is occurring. Value between 0 and 1.

u = Standard normally distributed variable, a tool for the probabilistic sum

Model

$$\beta_{kw|erosion} = \phi^{-1}(P_{f,kw|erosion})$$

ϕ^{-1} = Inverse of the normal distribution

Table I-1: Z-function explanation Z_12

Symbol	Unit	Description	Distribution	μ	V_r/σ
$P_{f,kw\|erosion}$	[-]	Failure probability	Deterministic	1.0	-
u	[-]	Intrinsic uncertainty model	Normal	0	1.0

For this sub mechanism we use the standard value for $P_{f,kw|piping}$: 1.0. This means that the probability is 1.0.

$$P_{f;12} = 1.0$$

Z_{21}: Failure due to the reaching of critical inflow

This failure mechanism describes the probability that the storage capacity is not sufficient to store the inflow of water during breaching of the structure with high water levels.

Z-Function

$$Z_{21} = V_c - V_{inflow}$$

Where:

V_c = Maximum present volume storage capacity in the hinterland, without significant water hindrance. This is the strength (resistance) of the hinterland.

V_{inflow} = Incoming volume due to breaching of the hydraulic structure during high water. This is the load on the hinterland.

Model

$$V_c = m_{kom} \cdot A_{kom} \cdot \Delta h_{kom}$$

Table I-2: Model explanation Z_21 for V_c

Symbol	Unit	Description	Distribution	μ	V_r/σ
m_{kom}	[-]	Model factor storage capacity	Lognormal	1.0	$\sigma = 0.2$
A_{kom}	[m²]	Storage area	Lognormal	Input	$V_r = 0.1$
Δh_{kom}	[m]	Allowed inundation	Lognormal	Input	$\sigma = 0.1$

$$V_{inflow} = m_{in} \cdot f_{ts|open} \cdot t_s \cdot Q_{in|open}$$

Table I-3: Model explanation Z_21 for V_inflow

Symbol	Unit	Description	Distribution	μ	V_r/σ
$Q_{in\|open}$	[m³/s]	Inflow	See formula	-	-
$f_{ts\|opn}$	[-]	Factor duration of high water	Deterministic	1.0	-
m_{in}	[-]	Model factor incoming discharge	Lognormal	1	$\sigma = 0.2$
t_s	[hours]	Storm duration	Lognormal	Input	$V_r = 0.25$

The standard factor duration of high water is 1.0 found in the schematization manual.

The choice is made to assume a situation with no inner water level, the given formula for this expression is:

$$Q_{in|open} = B \cdot m_{OL} \cdot 0.55 \cdot \sqrt{g \cdot (h - h_{threshold})^3}$$

Table I-4: Model explanation Z_21 for Q_in/open

Symbol	Unit	Description	Distribution	μ	V_r/σ
B	[m]	Width of opening	Normal	Input	0.05
m_{OL}	[-]	Model factor free flow	Normal	1.1	$\sigma = 0.03$
h	[m+NAP]	Outer water level	Gumbel	Input	Input
$h_{threshold}$	[m+NAP]	Height of threshold	Normal	Input	$\sigma = 0.1$
g	[m/s²]	Gravitational constant	Deterministic	9.81	-

It is assumed that the inner water level as well as the height of the threshold are equal to $16\ m$. See appendix J.

The calculation results are summarized in the "Prob2B Output" and the total failure probability of this mechanism is:

$$P_{f;21} = 4.58 \cdot 10^{-2}$$

Z_{22}: Failure of bottom erosion behind structure

This failure mechanism describes the probability that the bottom protection behind the structure erodes due to the opening of the structure and instability of the structure can occur.

Z-Function

$$Z_{22} = Q_c - Q_{in|open}$$

Where:

Q_C = The critical discharge at which the bottom protection fails
$Q_{in|open}$ = Occurring discharge in open structure

Model

$$Q_C = q_c \cdot B_{sv}$$

Table I-5: Model explanation Z_22 for Q_c

Symbol	Unit	Description	Distribution	μ	V_r/σ
q_c	[m³/s/m]	Critical discharge	Formula		

$\boldsymbol{B_{sv}}$	[m]	Width of governing bottom protection	Normal	Input	$\sigma = 0.05$

Because the critical flow rate is dependent on a few different probabilistic parameters, this will become an expression:

$$q_c = (h - h_{threshold}) \cdot u_c$$

Table I-6: Model explanation Z_22 for q_c

Symbol	Unit	Description	Distribution	$\boldsymbol{\mu}$	$\boldsymbol{V_r/\sigma}$
$\boldsymbol{u_c}$	$[m/s]$	Critical flow rate	Normal	Input	$\sigma = 0.1$
$\boldsymbol{h}$	$[m + NAP]$	Outer water level	Gumbel	Input	Input
$\boldsymbol{h_{in}}$	$[m + NAP]$	Inner water level	Normal	Input	$\sigma = 0.1$

The incoming volume per second is the same as for failure mechanism z_{21}:

$$Q_{in|open} = B \cdot m_{OL} \cdot 0.55 \cdot \sqrt{g \cdot (h - h_{threshold})^3}$$

Table I-7: Model explanation Z_22 for Q_in/open

Symbol	Unit	Description	Distribution	$\boldsymbol{\mu}$	$\boldsymbol{V_r/\sigma}$
$\boldsymbol{B}$	[m]	Width of opening	Normal	Input	0.05
$\boldsymbol{m_{free}}$	[-]	Model factor free flow	Normal	1	$V_r = 0.10$
$\boldsymbol{h_{in}}$	[m+NAP]	Inner water level	Normal	Input	$\sigma = 0.1$
$\boldsymbol{h}$	[m+NAP]	Outer water level	Gumbel	Input	Input
$\boldsymbol{h_{threshold}}$	[m+NAP]	Height of threshold	Normal	Input	$\sigma = 0.1$
$\boldsymbol{g}$	[m/s²]	Gravitational constant	Deterministic	9.81	-

It is assumed that the inner water level as well as the height of the threshold are equal to $16\ m$. See appendix J.

The calculation results are summarized in the “Prob2B Output” and the total failure probability of this mechanism is:

$$P_{f;22} = 4.1 \cdot 10^{-2}$$

Z_{411}: Failure of structural parts due to head difference overload

This sub mechanism describes the probability of failure of individual structural parts, due to hydraulic load including wave loading. Every structural part needs to be checked individually, where the Z function consists of the strength of a structural member and the load R that works on that member. Since there is no water behind the structure, the load function is linear.

$$Z_{411,L} = R_{lin} - m_s S_{lin}$$

The structural parts that are prone to this load are identified as:

Table I-8: Loads on structural parts

Structural member	Load type	Variation coefficient
The glass panel	• Bending moment in the middle of the plate • Corner stresses	$V_R = 0.3$ (same as for masonry)
Aluminum anchor posts	• Moment • Shear	$V_R = 0.1$
Steel bolts in anchor plate	• Tension	$V_R = 0.1$

	• Shear (3 sub mechanisms)

Other structural parts or details are considered non-governing; the anchor plate has a relatively large thickness and failure mechanisms like local buckling, the developing of plastic hinges by prying forces, rupture or failure of the welding are therefore not taken into account in the probabilistic calculation.

The calculation results of all sub mechanisms of Z_{411} are summarized in the “Prob2B Output” and the total failure probability of this mechanism is:

$$P_{f411} = P_{f411;1} + P_{f411;2} + P_{f411;3} + P_{f411;4} + P_{f411;5} + P_{f411;6;1} + P_{f411;6;2} + P_{f411;6;3}$$

$$P_{f411} = 7.135 \cdot 10^{-7} + 3.634 \cdot 10^{-7} + 0 + 0 + 0 + 0 + 1 \cdot 10^{-5} = 1.107 \cdot 10^{-5}$$

I.2.1. $Z_{411;1}$ Bending moment in the middle of the plate

Bending moments in the plate can cause the outer ply to fracture. It is assumed that failure occurs when one ply is overloaded and fractures. The failure mechanisms related to glass failure are based on the FEM model, this model assumed high water levels up to the top of the structure. It is assumed that “high water” occurs when there is water reaching the top of the structure ($h = 18$), conform the FEM model. The probability of high water is calculated with Prob2B.

$$P_{f;highwater} = 6.057 \cdot 10^{-4}$$

Model

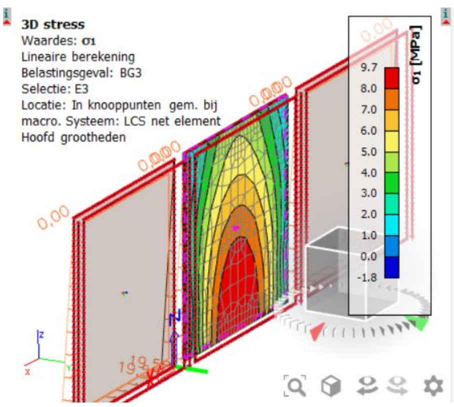

Figure I-2: Stresses in the plate due to waterpressure

The occurring maximal tensile stress due to high water is calculated by the SCIA model:

$$\sigma_{max} = 9.7\ MP$$

The probability of bending moment failure of the glass due to high water pressure is very small due to the large difference between characteristic strength and the occurring load.

$$Z_{411;1} = f_g - 9.7 \cdot m_s$$

The calculation results are summarized in the “Prob2B Output” and the total failure probability of this mechanism is:

$$P_{f;411;1} = 6.057 \cdot 10^{-4} \cdot 1.178 \cdot 10^{-3} = 7.135 \cdot 10^{-7}$$

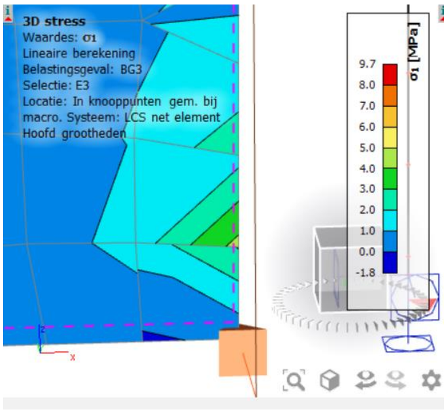

Figure I-3: corner stresses in the plate

I.2.2. $Z_{411;2}$ Corner stresses in the plate

When the plate deforms to a bulge due to a pressure, the corners want to deform to the opposite side due to the rotation caused by the bulging. If restrained, high stresses can occur in the corners of the plate. From the model it can be seen that these stresses are not larger than the stresses that occur in the middle of the plate and are estimated to be $6\ MPa$.

$$Z_{411;2} = f_g - 6 \cdot m_s$$

The calculation results are summarized in the “Prob2B Output” and the total failure probability of this mechanism is:

$$P_{f;411;2} = 6.057 \cdot 10^{-4} \cdot 6 \cdot 10^{-4} = 3.634 \cdot 10^{-7}$$

I.2.3. $Z_{411;3}$ Moment in the anchor posts

The stresses caused by shear and bending moments have to be checked for the two different cross sections, at their critical locations(lowest). This will be done by hand as the input in SCIA for these cross sections was numerical and results are not visible. It is assumed that there is only one moment M_z and M_y is neglected as there is no force present in that direction. Axial force and torsion are also neglected as the anchor posts are mainly loaded in bending and shear.
Basic mechanic formula’s for pure bending moments without safety factors:

$$S_{411;3;lower} = \sigma_z = \frac{M_{z;lower} \cdot z_{lower}}{I_{z:lower}}$$

$$S_{411;3;upper} = \sigma_z = \frac{M_{z;upper} \cdot z_{upper}}{I_{z:upper}}$$

$$R_{411:3} = f_0 = 200\ MPa$$

To add wave pressure in a simple way, the load from water pressure is increased by 25%

$$M_{z,lower} = \frac{1}{6} \cdot (h - h_{threshold})^3 \cdot \gamma_w \cdot g \cdot B \cdot 1.25(wave)[Nm]$$

$$M_{z,upper} = \frac{1}{6} \cdot (h - h_{threshold} - l_1)^3 \cdot \gamma_w \cdot g \cdot B \cdot 1.25(wave)[Nm]$$

With a maximum water level of 2,5 meter, due to the fact that the structure will overflow at this point.

Where the height of the water level is relative to the structure, meaning $h_{w,0} = z$. the water level is at the top of the structure B is the system width of the structure, the width of water pressure one anchor post needs to resist is the post-to-post distance: 2 meter. For a characteristic calculation the water level has deterministic value of 2 meter in height, $h_w = 2$. The weight of the water is $1000\ kg/m^3$ and gravitational acceleration is $9.81\ m/s^2$.

The input parameters are:

Table I-9: Explanation of symbols Z_411;3

Symbol	Unit	Description	Distribution	μ	V_r/σ
f_0	$[N/m^2]$	Strength of Aluminum	Normal	$200 \cdot 10^6$	$V_r = 0.1$
γ_w	$[Kg]$	Specific weight of water	Normal	1000	$\sigma = 5$
h	$[m + NAP]$	Outer water level	Gumbel	Input	Input
$h_{threshold}$	[m+NAP]	Height of threshold	Normal	Input	$\sigma = 0.1$
z_{lower}	$[m]$	Height of section	Deterministic	0.4572	-
z_{upper}	$[m]$	Height of section	Deterministic	0.2248	-
$I_{z;lower}$	$[m^4]$	Moment of inertia	Normal	$387.34 \cdot 10^{-6}$	$V_r = 0.1$
$I_{z;upper}$	$[m^4]$	Moment of inertia	Normal	$68.88 \cdot 10^{-}6$	$V_r = 0.1$
g	$[m/s^2]$	Gravitational constant	Deterministic	9.81	-
B	$[m]$	Width of opening	Normal	Input	$V_r = 0.05$

Characteristic:

$$M_{z,lower} = \frac{1}{6} \cdot 2^3 \cdot 9.81 \cdot 1000 \cdot 2 \cdot 1.25 = 32700\ Nm$$

$$Z_{411;3} = R_{411:3} - S_{411;3} \cdot m_s$$

The calculation results are summarized in the “Prob2B Output” and the total failure probability of this mechanism is:

$$P_{f;411;3} = 0$$

I.2.4. $Z_{411;4}$ Shear in the anchor posts

The stresses caused by shear and bending moments have to be checked for the two different cross sections, at their critical locations(lowest). This will be done by hand as the input in SCIA for these cross sections was numerical and results are not visible. It is assumed that there is only shear in one direction as there is no force present in other directions. Axial force and torsion are also neglected as the anchor posts are mainly loaded in bending and shear. Because the section is of a complicated kind, the Z-function $Z_{411;4}$ is expressed in shear force and shear capacity (averaged over the surface area) and not in stress and yield strength.
Basic mechanic formula’s for shear without safety factors:

$$V_{pl,R,lower} = A_{v;lower}\left(\frac{f_0}{\sqrt{3}}\right) = 1570\ kN$$
$$V_{pl,R,upper} = A_{v;upper}\left(\frac{f_0}{\sqrt{3}}\right) = 880\ kN$$

Where:

f_0	$= 200\ N/mm^2$	[Appendix I]
$A_{v;upper}$	$= 0.762 \cdot 10^{-2}\ m^2 = 7620\ mm^2$	[Appendix I]
$A_{v;lower}$	$= 1.36 \cdot 10^{-2}\ m^2 = 13600\ mm^2$	[Appendix I]

To add wave pressure in a simple way, the load from water pressure is increased by 25%

$$V_{S,lower} = \frac{1}{2} \cdot (h - h_{threshold})^2 \cdot \gamma_w \cdot g \cdot B \cdot 1.25(wave)$$
$$V_{S,upper} = \frac{1}{2} \cdot (h - l_1 - h_{threshold})^2 \cdot \gamma_w \cdot g \cdot B \cdot 1.25(wave)$$

With a maximum water level of 2,5 meter, due to the fact that the structure will overflow at this point.

Where:
l_1 = $0.5394\ m$ Appendix I]
B = $2\ m$ [Appendix I]
γ_w = $1000\ kg/m^3$
g = $9.81\ m/s^2$
h_w = $2\ m$ deterministic or a probabilistic Gumbel distribution

Expected outcomes of the formula with high water are:

$$V_{S,lower} = \frac{1}{2} \cdot 2^2 \cdot \cancel{1000} \cdot 9.81 \cdot 2 \cdot 1.25(wave)\cancel{/1000} = 49.05\ kN$$

$$V_{S,upper} = \frac{1}{2} \cdot (2 - 0.270)^2 \cdot \cancel{1000} \cdot 9.81 \cdot 2 \cdot 1.25(wave)/\cancel{1000} = 26.16\ kN$$

Z-functions are:

$$Z_{411;4;lower} = V_{pl,R,lower} - V_{S,lower} \cdot m_s$$

And:

$$Z_{411;4;upper} = V_{pl,R,lower} - V_{S,lower} \cdot m_s$$

The input parameters are:

Table I-10: Explanation of symbols Z_411;4

Symbol	Unit	Description	Distribution	μ	V_r/σ
f_0	$[N/m^2]$	Strength of Aluminum	Normal	$200 \cdot 10^6$	$V_r = 0.1$
γ_w	$[Kg]$	Specific weight of water	Normal	1000	$\sigma = 5$
h	$[m + NAP]$	Outer water level	Gumbel	Input	Input
$h_{threshold}$	$[m + NAP]$	Height of threshold	Normal	Input	$\sigma = 0.1$
l_1	$[m]$	Height of lower profile	Normal	0.5394	$V_r = 0.05$
$A_{v;upper}$	$[m^2]$	Shear surface upper	Normal	$7.620 \cdot 10^{-3}$	$V_r = 0.05$
$A_{v;lower}$	$[mm^2]$	Shear surface lower	Normal	$13.60 \cdot 10^{-3}$	$V_r = 0.05$
g	$[m/s^2]$	Gravitational constant	Deterministic	9.81	-
B	$[m]$	Width of opening	Normal	Input	$V_r = 0.05$

The calculation results are summarized in the “Prob2B Output” and the total failure probability of this mechanism is:

$$P_{f;411;4} = 0$$

I.2.5. $Z_{411;5}$ Steel bolts in tension

Due to a bending moment at the bottom of the anchor posts, the outer bolts connecting the anchor plate to the foundation are loaded in tension. The bolts that are used in the structure are: DIN 912 M24 x 110, of stainless steel 8.8. These bolts have a tensile strength of $f_u = 800\ N/mm^2$ and a shank surface area of $A_s = 352\ mm^2$.
The tension in the bolts is induced by the bending moment, which is the same bending moment calculated for $M_{z,lower}$:

$$M_{anchor} = \frac{1}{6} \cdot (h - h_{threshold})^3 \cdot \gamma_w \cdot g \cdot B \cdot 1.25(wave)[Nm]$$

The anchor plate is relatively thick and the rotation is assumed to occur at the end of the plate at the land-side. There is one outer bolt with a rotation distance of $0.5165\ m$, and 2 bolts in the second row, with a distance of 0.4129.

When we fill in deterministic values the working moment becomes:

$$M_{S;bolts} = \frac{1}{6} \cdot 2^3 \cdot 9.81 \cdot 1000 \cdot 2 \cdot 1.25 = 32700\ Nm$$

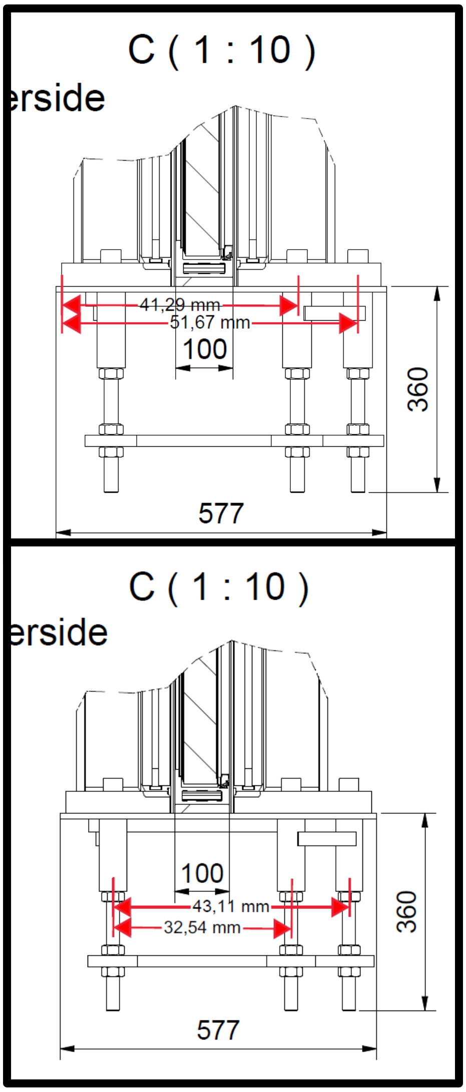

A resultant force from the 3 bolts in tension resists the tensile force from the working moment. The moment capacity in the case that no plastic hinge occurs at the location of the inner(land-side) hinge is calculated by the following:
The lever arm of the resultant force is:

$$d = \frac{1 \cdot 0.5167 + 2 \cdot 0.4129}{3} = 0.4475$$

The tensile strength of one bolt is[EN 1993-1-8, table 3.4]:

$$F_{t,u} = k_2 \cdot f_{ub} \cdot A_s$$

Where:
$k_2 = 0.9$ =reduction based on tests

The resultant resistant force when plastic behavior of the bolt group occurs is:

$$F_T = 3 \cdot k_2 \cdot f_{ub} \cdot A_s = 3 \cdot 0.9 \cdot = 760320\ N$$

The resisting moment then becomes:

$$M_{R;bolts} = 760320 \cdot 0.4475 = 340243\ Nm$$

For the situation where a plastic hinge occurs at the location of the inner bolt row:

$$d = \frac{1 \cdot 0.4311 + 2 \cdot 0.3254}{3} = 0.3606$$

This value for the lever arm is governing.

$$M_{R;bolts;Pl} = 760320 \cdot 0.3606 = 274196\ Nm$$

Table I-11: Explanation of symbols Z_411;5

Symbol	Unit	Description	Distribution	μ	V_r/σ
$\boldsymbol{k_2}$	-	-	Deterministic	0.9	-
$\boldsymbol{\gamma_w}$	$[Kg]$	Specific weight of water	Normal	1000	$\sigma = 5$
$\boldsymbol{h}$	$[m + NAP]$	Outer water level	Gumbel	Input	Input
$\boldsymbol{h_{threshold}}$	$[m + NAP]$	Height of threshold	Normal	Input	$\sigma = 0.1$
$\boldsymbol{d}$	$[m]$	Lever arm	Normal	0.3606	$V_r = 0.05$
$\boldsymbol{f_{ub}}$	$[N/m^2]$	Bolt tensile strength	Normal	$800 \cdot 10^6$	$V_r = 0.05$
$\boldsymbol{A_s}$	$[m^2]$	Shaft area	Normal	$352 \cdot 10^{-6}$	$V_r = 0.05$
$\boldsymbol{g}$	$[m/s^2]$	Gravitational constant	Deterministic	9.81	-
$\boldsymbol{B}$	$[m]$	Width of opening	Normal	Input	$V_r = 0.05$

The calculation results are presented in the “Prob2B Output” and the total failure probability of this mechanism is:

$$P_{f;411;5} = 0$$

I.2.6. $Z_{411;6}$ Steel bolts in shear

The three main failure modes for bolts in shear are:

1. Tensile strength net section plate
2. Shear failure bolt
3. Plate bearing resistance (shearing out of plate/hole ovalisation)

1. The tensile strength of the net section plate

The plate is most vulnerable at the location where two bolt-holes are present. The influence of the aluminum section on the end plate is neglected as this contributes in a positive manner. Plate properties:

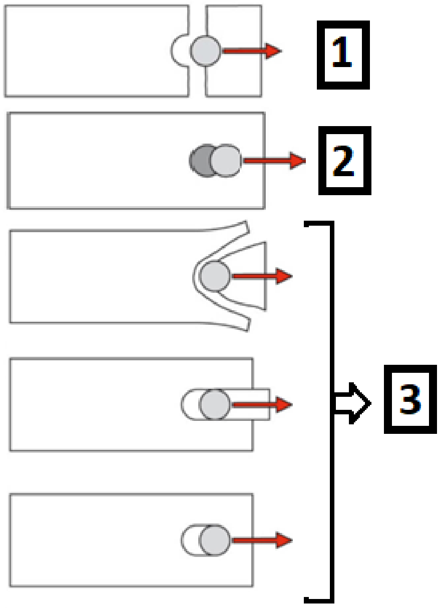

Figure I-4: Failure modes bolts in shear [EN 1993-1-1 art. 6.2.3]

Aluminum grade: AW6005
Tensile strength $f_u \,/\, f_0 = 200N/mm^2$
Thickness $t = 39.3\ mm$
Width of the plate $w = 167.6\ mm$
Hole clearance $hc = 2$ [NEN-EN1090-2]
Width per opening $o = d + hc = 24 + 2 = 26\ mm$
Total section steel plate:

$$A_{net} = 39.3 \cdot (167.6 - 2 \cdot 26) = 4700\ mm^2$$

Occurring tensile stress is the same as for the bottom support:

$$V_{S,lower} = \frac{1}{2} \cdot h_w^2 \cdot \gamma_w \cdot g \cdot B \cdot 1.25(wave)$$

$$S_{411;6;1} = V_{S,lower}$$

$$R_{411;6;1} = 0.9 \cdot A_{net} \cdot f_u = 0.9 \cdot 4700 \cdot 200 = 846000\ N$$

$$Z = R_{411;6;1} - S_{411;6;1} \cdot m_s$$

Deterministic values:

$$V_{S,lower} = \frac{1}{2} \cdot 2^2 \cdot \cancel{1000} \cdot 9.81 \cdot 2 \cdot 1.25(wave)/\cancel{1000} = 49.05\ kN$$

$$\sigma_{plate} = 49050/4700 = 10.43$$

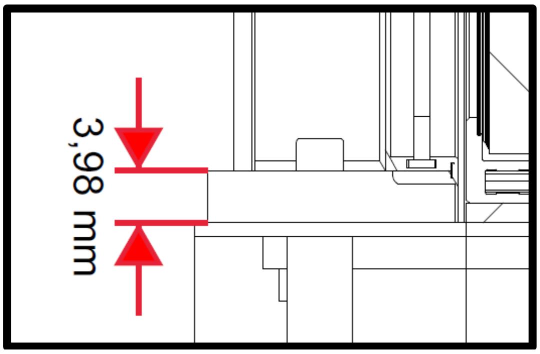

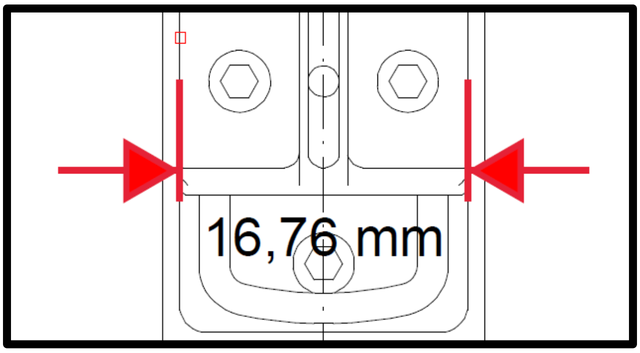

Table I-12: Explanation of symbols Z_411;6;1

Symbol	Unit	Description	Distribution	μ	V_r/σ
t	$[m]$	Thickness of the plate	Normal	0.0393	$V_r = 0.05$
w	$[m]$	Width of the plate	Normal	0.1676	$V_r = 0.05$
γ_w	$[Kg]$	Specific weight of water	Normal	1000	$\sigma = 5$
h	$[m + NAP]$	Outer water level	Gumbel	Input	Input
$h_{threshold}$	$[m + NAP]$	Height of threshold	Normal	Input	$\sigma = 0.1$
o	$[m]$				
f_0	$[N/m^2]$	Strength of Aluminum	Normal	$200 \cdot 10^6$	$V_r = 0.1$
A_s	$[m^2]$	Shaft area	Normal	$352 \cdot 10^{-6}$	$V_r = 0.05$
g	$[m/s^2]$	Gravitational constant	Deterministic	9.81	-
B	$[m]$	Width of opening	Normal	Input	$V_r = 0.05$

The calculation results are summarized in the “Prob2B Output” and the total failure probability of this mechanism is:

$$P_{f;411;6;1} = 0$$

2. *Shear failure bolt*

The shear resistance of a single bolt can be calculated by the following formula:

$$F_{V;Rd} = \frac{\alpha_v \cdot f_{ub} \cdot A_s}{\gamma_{M2}}$$

And without the safety factors:

$$F_V = \alpha_v \cdot f_{ub} \cdot A_s = 0.6 \cdot 800 \cdot 352 = 168960\ N = 169\ kN$$

Where:

α_v = 0.6 ($\approx \frac{1}{\sqrt{3}}$)
f_{ub} = 800 N/mm^2
A_s = 352 mm^2

There are 5 bolts that resist the total shear resistance:

$$R_{411;6;2} = 5 \cdot F_V = 5 \cdot 168960 = 844800\ N$$
$$S_{411;6;2} = V_{S,lower}$$

$$V_{S,lower} = \frac{1}{2} \cdot h_w^2 \cdot \gamma_W \cdot g \cdot B \cdot 1.25(wave)$$

$$Z = R_{411;5;2} - S_{411;6;2} \cdot m_s$$

Table I-13: Explanation of symbols Z_411;6;2

Symbol	Unit	Description	Distribution	μ	V_r/σ
α_v	-	-	Deterministic	0.6	-
γ_w	$[Kg]$	Specific weight of water	Normal	1000	$\sigma = 5$
h	$[m + NAP]$	Outer water level	Gumbel	Input	Input
$h_{threshold}$	$[m + NAP]$	Height of threshold	Normal	Input	$\sigma = 0.1$
f_{ub}	$[N/m^2]$	Bolt tensile strength	Normal	$800 \cdot 10^6$	$V_r = 0.05$
A_s	$[m^2]$	Shaft area	Normal	$352 \cdot 10^{-6}$	$V_r = 0.05$

$\boldsymbol{g}$	$[m/s^2]$	Gravitational constant	Deterministic	9.81	-
$\boldsymbol{B}$	$[m]$	Width of opening	Normal	Input	$V_r = 0.05$

The calculation results are summarized in the "Prob2B Output" and the total failure probability of this mechanism is:

$$P_{f;411;6;2} = 0$$

3. *Plate bearing resistance*

$$S_{411;6;3} = V_{S,lower}$$

General expression for the bearing resistance of a bolted plate (without safety factors):

$$R_{411;6;3} = F_b = k_1 \cdot \alpha_b \cdot f_u \cdot t \cdot d \qquad \text{[EN 1993-1-8, table 3.4]}$$

With:
k_1 = 2.5
α_b = $\frac{f_u}{f_{ub}} = \frac{200}{800} = 0.25$
t = 39.3 mm
f_u = 200 N/mm^2 Normal distribution
d = 24 mm

$$Z = R_{411;6;3} - S_{411;6;3} \cdot m_s$$

Table I-14: : Explanation of symbols Z_411;6;3

Symbol	Unit	Description	Distribution	μ	V_r/σ
$\boldsymbol{k_1}$	-	-	Deterministic	2.5	-
$\boldsymbol{\alpha_b}$	-	-	Deterministic	0.25	-
$\boldsymbol{\gamma_w}$	$[Kg]$	Specific weight of water	Normal	1000	$\sigma = 5$
$\boldsymbol{h}$	$[m + NAP]$	Outer water level	Gumbel	Input	Input
$\boldsymbol{h_{threshold}}$	$[m + NAP]$	Height of threshold	Normal	Input	$\sigma = 0.1$
$\boldsymbol{f_0}$	$[N/m^2]$	Strength of Aluminum	Normal	$200 \cdot 10^6$	$V_r = 0.1$
$\boldsymbol{d}$	$[m]$	Diameter of bolt	Normal	0.024	$V_r = 0.1$
$\boldsymbol{g}$	$[m/s^2]$	Gravitational constant	Deterministic	9.81	-
$\boldsymbol{B}$	$[m]$	Width of opening	Normal	Input	$V_r = 0.05$

The calculation results are summarized in the "Prob2B Output" and the total failure probability of this mechanism is:

$$P_{f;411;6;1} = 1 \cdot 10^{-5}$$

Z_{412}: Failure to repair flood defence

When failure occurs and there is incoming water, attempts to close the flood defense can by made by the use of sandbags, or; in the case of our structure; replace the glass panel by Aluminum parts(demountable flood defence) if water inflow is not too severe and the structure can be reached.

Z-function

$$Z_{412} = \beta_{f,repairdefence} - u$$

Where
$\beta_{f,repairdefence}$ = The reliability index corresponding to the failure probability of the hydraulic structure, given the failure of the bottom protection with the occurring of erosion and scour holes. Value between 0 and 1.

u = Standard normally distributed variable, a tool for the probabilistic sum

$$\beta_{f,repairdefence} = -\phi^{-1}(P_{f,repairdefence})$$

ϕ^{-1} = Inverse of the normal distribution

The standard value for $(P_{f,repairdefence})$ in this failure mechanism is 1.0 [Schematiseringshandleiding kunstwerken sterkte en stabiliteit], which means the failure probability of this mechanism is also 1.0.

Table I-15: Explanation of Z-function Z_412

Symbol	Unit	Description	Distribution	μ	V_r/σ
$P_{f,repairdefence}$	[-]	Failure probability	Deterministic	1.0	-
u	[-]	Intrinsic uncertainty model	Normal	0	$\sigma = 1.0$

Z_{421}: Collision energy larger than critical value

This sub-mechanism describes the probability that the value of the collision energy is larger that the energy that can be absorbed by the structure. For this function, multiple models and disciplinaries are involved and simplified for the purpose of the probabilistic sum. These models and explanation of the Z-models are based on structural mechanics, FEM models of the structure and assumptions of the author and can't be used for other applications than this thesis without further investigation.

Z-Function

$$Z_{421} = E_c - E_0$$

Where:
E_c = Critical value collision energy
E_0 = Occurring collision energy

Model $\mathrm{E_0}$

The load is determined by the kinetic energy of the ship, or impact object that must be transferred to the structure. This is explained in Appendix B. For the probabilistic calculation a model uncertainty m_E is added.

$$E_0 = m_E \cdot \frac{1}{2} \cdot m \cdot v_{\perp}{}^2 \;\; [Nm]$$

For the mass and speed of the impact object values are estimated. The case study is a tree trunk of around 200 kg, with an impact speed perpendicular to the structure that depends on the speed of the object and impact angle.

$$v_{\perp} = v_s \cdot \sin(\alpha)$$

Table I-16: Explanation of symbols Z_412

Symbol	Unit	Description	Distribution	μ	V_r/σ
m_E	[-]	Model factor for collision	Normal	1.0	$V_r = 0.2$
m	[kg]	Mass of incoming object	Normal	Input	$V_r = 0.2$
v_s	[m/s]	Speed of incoming object	Normal	Input	$V_r = 0.55$
α	[°]	Angle of incidence	Normal	Input	Input

It is assumed that the impact speed a floating object is equal to the speed of the water flow in the river. The angle of incidence and flow velocity have been analyzed for a few possible locations for a glass flood defence along the Meuse river and the following values were found [Arcadis] by using the Meuse river model of Rijkswaterstaat and google maps:

Table I-17: Impact specifics different locations

Loacation	Flow velocity v_s	Angle of incidence α
Well	-	-
Arcen	1.9 [m/s]	22.5°
Steyl-Maashoek	1.33 [m/s]	40°
Belfeld	2.0 [m/s]	22.5°
Kessel	1.72 [m/s]	22.5°
Buggenum	1.40 [m/s]	22.5°
Wessem	2.4 [m/s]	Large (45° is assumed)

I.2.7. Distribution flow velocity v

The formula for standard deviation:

$$S_x^2 = \frac{\sum(x_i - \bar{x})^2}{n_x - 1}$$

Where:

x_i = Individual value

$\bar{x} = \frac{1.9+1.33+2+1.72+1.4+2.4}{6} = 1.79$ = Mean value (μ)

$n_x = 6$ = Number of values

$S_x = \sqrt{(1.90-1.79)^2 + (1.33-1.79)^2 + (2.0-1.79)^2 + (1.72-1.79)^2 + (1.40-1.79)^2 + (2.4-1.79)^2)/5} = 0.40$

= The standard deviation

The standard error is $\frac{s_x}{\sqrt{n}} = \frac{0.40}{\sqrt{6}} = 0.163$ and coefficient of variation $V_r = \frac{s_x}{\mu} = \frac{0.40}{1.79} = 0.22$

But since a larger coefficient of variation (0.55) is already given in the schematization manual, this value will be used. This means that the standard deviation becomes $0.55 \cdot 1.79 = 0.9845$.

I.2.8. Distribution angle of incidence α

$$S_x^2 = \frac{\sum(x_i - \bar{x})^2}{n_x - 1}$$

Where:

x_i = Individual value

$\bar{x} = \frac{4 \cdot 22.5+40+45}{6} = 29.2$ = Mean value (μ)

$n_x = 6$ = Number of values

$S_x = \sqrt{(4 \cdot (22.5-29.2)^2 + (40-29.2)^2 + (45-29.2)^2)/5} = 10.45$ = The standard deviation

The standard error is $\frac{s_x}{\sqrt{n}} = \frac{10.45}{\sqrt{6}} = 4.27$ and coefficient of variation $V_r = \frac{s_x}{\mu} = \frac{10.45}{29.2} = 0.36$

Table I-18: Probabilistic distributions velocity and angle of incidence

Parameter	Object velocity v_s	Angle of incidence α
$\boldsymbol{\mu}$	1.79	29.2
$\boldsymbol{s_x/\sigma}$	0.9845	10.45
$\boldsymbol{V_r}$	$V_r = 0.55$	0.36

Model E_c

The critical energy E_c that can be absorbed by the structure depends on the maximum concentrated force that is applied on the structure and its location. It is assumed that this force will always be

applied on the glass panel and nine possible locations on this panel have been analyzed to determine the critical stiffness k_c and the critical force F_c per location. The collision force is dependent on the stiffness of the structure, the stiffness of the collision object k_s, the mass m_s, and speed of the collision object perpendicular to the panel.
The location of the impact on the glass is also of importance, therefore the glass panel is divided into nine different regions where the structure's stiffness and critical concentrated force are determined:

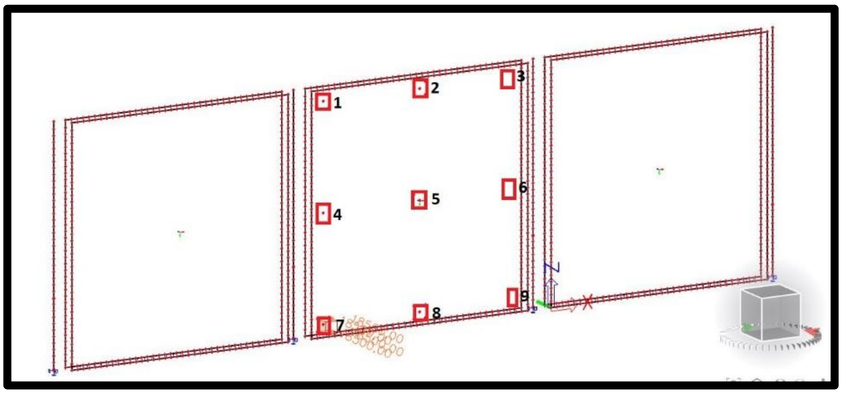

Figure I-5: Possible impact locations on the glass panel

To simplify the procedure, the additional water pressure is taken into account by reducing the allowable stress at any point by $9.7\ N/mm^2$(see maximum stress caused by high water in failure mechanism $Z_{411;1}$). The allowable stress in the plate now is $120 - 9.7 = 110.3\ N/mm^2 \approx 110\ N/mm^2$

Below, one example of the procedure is done, the rest of the calculations is done in the same matter. The procedure is of an iterative nature, as the maximum allowed stress at each point of the plate needs to be found by adjusting the value of the force and also the displacement differs per location.

Example

We start by modelling a concentrated pressure near one of the lower corners and check if the limit stress $110\ N/mm^2$ is reached. There are no safety factors used on the applied force.

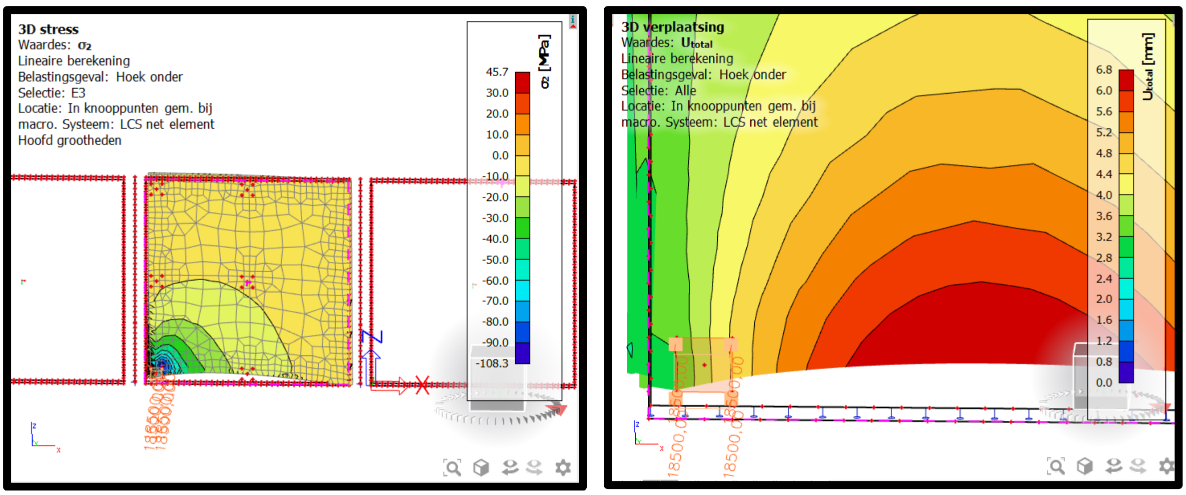

Figure I-6: Example energy calculation

The limit stress will (almost) be reached with $108.3\ MPa$ at a pressure of $18500\ kN/m^2$. With a force surface of $0.1 \cdot 0.1 = 0.01\ m^2$, the distributed force over this area is a concentrated critical load F_c of $185\ kN$. The displacement at the impact location is $\sim 3.6\ mm$. The corresponding critical stiffness then becomes: $k_s = \frac{F}{u} = \frac{185}{0.0036} = 51388\ kN/m$ with a critical concentrated force of 185 kN.

The conservative value of the critical energy assumes only deformation of the structure:

$$E_c = \frac{F_c \cdot u}{2}$$

For location 7, this critical energy E_c is $E_c = \frac{185 \cdot 0.0036}{2} = 0.333\ kNm$

The stiffness of the impact object is smaller than the structure stiffness, and can therefore be taken into account. A deterministic value of 1508 kN/m is chosen to be used for the stiffness k_b. This value is explained is Appendix B. The two springs in series have an equivalent stiffness of:

$$k_{eq} = \frac{1}{\frac{1}{k_s} + \frac{1}{k_b}}$$

In the case of location 7 this equivalent stiffness becomes: $k_{eq;7} = \frac{1}{\frac{1}{51388} + \frac{1}{1508}} = 1465\ kN/m$

The total inclination of both structure and object at the limit load becomes:

$$u_{eq} = \frac{F}{k_{eq}}$$

For case 7 this is: $u_{eq;7} = \frac{185}{1465} = 0.126\ m$

The (linear) relation $F(= F_c) \cdot \Delta x\big(= u_{eq}\big) = 2 \cdot E_{kin,max}(= E_c)$ is derived in Appendix B. The critical energy that can be absorbed by the structure AND impact object then is:

$$E_c = \frac{F_c \cdot u_{eq}}{2}$$

In the case of location 7 the critical energy with a wooden pole then becomes:

$$E_{c;7;wood} = \frac{F_{c;7} \cdot u_{eq;7}}{2} = \frac{185 \cdot 0.126}{2} = 11.66\ kNm$$

I.2.9. Summary of critical energy with inclination of a wooden pole with $k_b = 1508\ kN/m$

Table I-19 Summary of critical energy with inclination of a wooden pole with $k_b = 1508\ kN/m$

Location	Critical load F_c [kN]	Deformation u at location [m]	Structure stiffness k_s [kN/m]	Equivalent Stiffness k_{eq} [kN/m]	Equivalent inclination u_{eq} [m]	E_c [kNm]
1	230	0.036	6389	1220	0.188	21.66
2	85	0.020	4250	1113	0.076	3.23
3	230	0.036	6389	1220	0.188	21.66
4	220	0.010	22000	1411	0.156	17.16
5	120	0.011	10909	1324	0.091	5.46
6	220	0.010	22000	1411	0.156	17.16
7	185	0.0036	51388	1465	0.126	11.66
8	90	0.012	7500	1255	0.072	3.24

9	185	0.0036	51388	1465	0.126	11.66

I.2.10. Summary of critical energy with inclination of a boat's bow with $k_b = 15000\ kN/$

Table I-20: Summary of critical energy with inclination of a boat's bow with k_b=15000 kN/

Location	Critical load F_c [kN]	Deformation u at location [m]	Structure stiffness k_s [kN/m]	Equivalent Stiffness k_{eq} [kN/m]	Equivalent inclination u_{eq} [m]	E_c [kNm]
1	230	0.036	6389	4480	0.051	5.87
2	85	0.020	4250	3312	0.026	1.11
3	230	0.036	6389	4480	0.051	5.87
4	220	0.010	22000	8919	0.025	2.75
5	120	0.011	10909	6316	0.019	1.14
6	220	0.010	22000	8919	0.025	2.75
7	185	0.0036	51388	11611	0.016	1.48
8	90	0.012	7500	5000	0.018	0.81
9	185	0.0036	51388	11611	0.016	1.48

I.2.11. Summary of critical energy <u>without</u> inclination of an impact object (Conservative)

Table I-21: Summary of critical energy without inclination of an impact object (Conservative)

Location	Critical load F_c [kN]	Deformation u at location [m]	Structure stiffness k_s [kN/m]	E_c [kNm]
1	230	0.036	6389	4.14
2	85	0.020	4250	0.85
3	230	0.036	6389	4.14
4	220	0.010	22000	1.10
5	120	0.011	10909	0.66
6	220	0.010	22000	1.10
7	185	0.0036	51388	0.33
8	90	0.012	7500	0.54
9	185	0.0036	51388	0.33

It can be seen from the table that, although there is a high critical force at the two bottom supports, its critical energy is lowest due to the large stiffness-small deceleration distance.

I.2.12. Distribution critical energy E_c

It can be seen that due to the large stiffness of the glass flood defence the influence of the inclination of the impact object is very larger, even when conservative values of a wooden pole are used. The distribution of the critical energy E_c is based on the conservative values without inclination of the impact object. Due to this choice of using the conservative approach, a dynamic enhancement factor is not included. The panel is split up in the 9 areas, which all contribute with 11.11% to the failure probability.

Probability of failure

The calculation results are summarized in the "Prob2B Output" and the total failure probability of this mechanism is:

$$P_{f;421} = 1.777 \cdot 10^{-2}$$

Note: It is assumed failure occurs when the critical bending stress of the outer glass ply is reached, this is a conservative assumption as it does not directly mean that water flows in, the structure can still have residual strength in the other glass plies and/or interlayer. This is however not taken into account in this calculation.

I.2.13. Z_{422}: Probability of a collision

For this sub-mechanism, only the risk of a collision during high water needs to be accounted for due to the fact that there is no flood risk due to failure of the glass flood defence when there is no water above the foot of the flood defence. Therefore it is combined with the probability of the reaching of critical inflow. In this sub-mechanism the probability of a significant impact object reaching the flood defence and colliding with the glass panel is elaborated on.

A collision is one of the most uncertain events that can occur, along with the probability of explosions, vandalism, earthquakes, traffic and ice-damage it is an incidental load. High water occurs in the wintertime, while it is still cold. Ship-traffic is prohibited and recreational activities have reached a low. Most objects will float in the middle of the river, parallel to the structure. The author estimated the probability that an object with *significant* mass, speed, stiffness and angle of incident reaches the structure to be 1% per year. A further study about the objects floating in the river during high water is highly advised.

$$P_{f;collision} = 0.01$$

I.2.14. Z_{423}: Failure to repair the fatal collision damages

After a fatal collision, water flows in and the breach in the structure needs to be closed. In the case of glass panel failure, there is a probability that the structure can be repaired by temporarily substituting the glass panel by Aluminum beams as the frame structure is also used for the demountable flood defences [IBS]. Other measures may also be possible. This sub mechanism describes the probability that the structure can't be repaired in time. It must be noted that a collision may happens when there is no person to witness the breaching of the flood defence, therefore a large probability that the failure will go unnoticed also needs to be taken into account.

Z-Function

$$Z_{423} = v_{c;sluit} - v_0$$

Where:

$v_{c;closure}$	= Critical flow velocity in which the flood defence can be closed after a collision
v_0	= Occurring flow velocity

Model

The occurring flow velocity at the structure during a breach of the flood defence can be described with the following formula:

$$v_0 = m_{OL} \cdot \sqrt{2 \cdot g \cdot \frac{h - h_{threshold}}{3}}$$

The critical flow velocity $v_{c;closure}$ must be estimated. As it is hard to close a breach in general, and the probability that water reaches the structure is already taken into account, the failure probability of this sub-mechanism is chosen to be 1.0. Further investigation in the probability that the structure can be repaired is necessary.

Table I-22: Explanation symbols Z_423

Symbol	Unit	Description	Distribution	μ	V_r/σ
g	$[m/s^2]$	Gravitational constant	Deterministic	9.81	-

$\boldsymbol{m_{OL}}$	[-]	Model factor free flow	Normal	1.1	$\sigma = 0.03$
$\boldsymbol{h}$	$[m + NAP]$	Outer water level	Gumbel	Input	Input
$\boldsymbol{h_{threshold}}$	$[m + NAP]$	Height of threshold	Normal	Input	$\sigma = 0.1$
$\boldsymbol{v_{c;closure}}$	$[m/s]$	Critical flow velocity	Normal	Input	$V_r = 0.2$

$$P_f = 1.0$$

Z_{43}: Failure of structure due to instability of structure or its foundation

This sub mechanism describes the probability that the structure or its foundation becomes unstable due to hydraulic loads. It is assumed that the stability of the structure and its foundation is sufficient to withstand these loads and therefore this sub mechanism is not worked out.

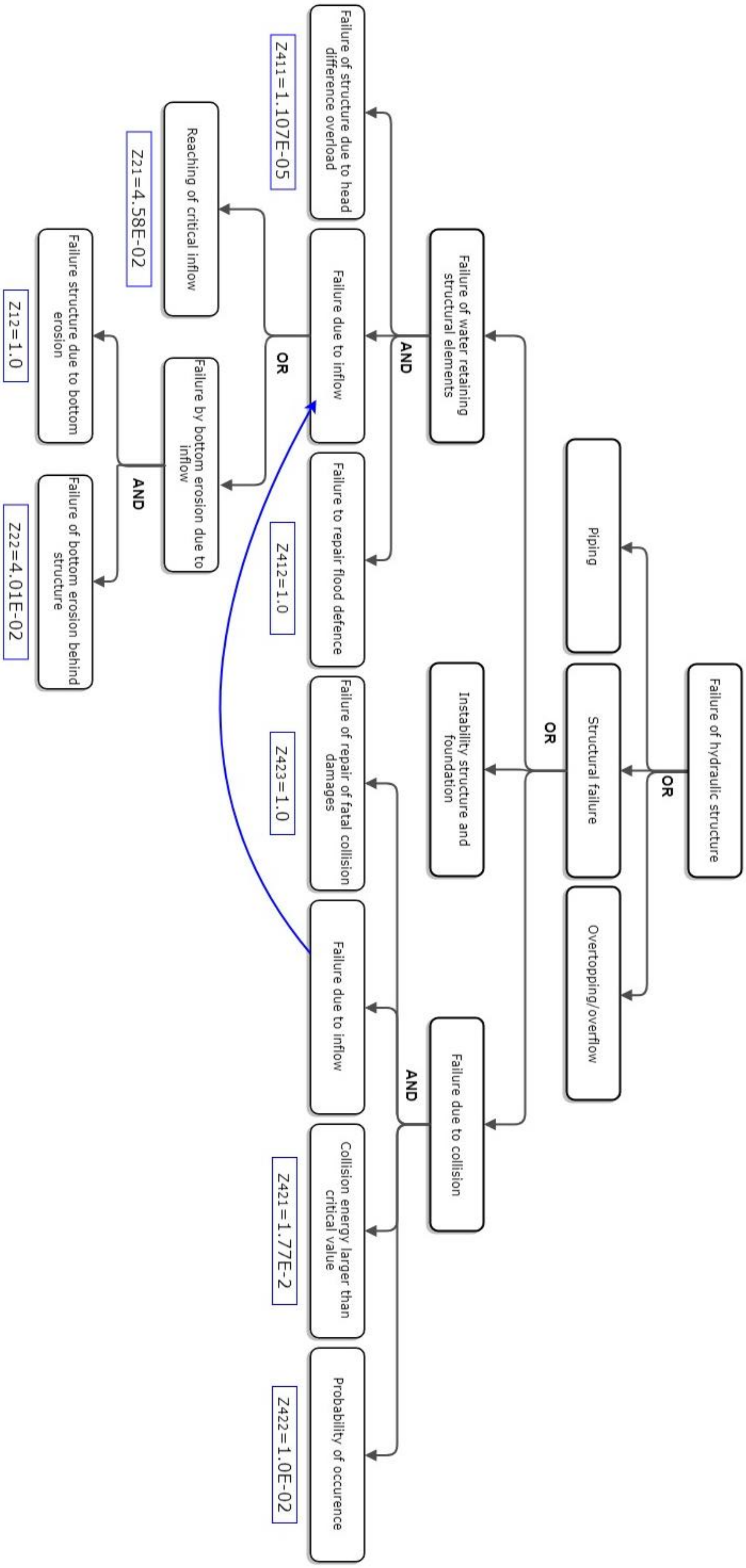

Figure I-7: Failure probability tree

I.3. Total failure probability

The probability of flooding in dike trajectory 65 (Arcen) is $1/100$ [VNK/i-viewer].The failure probability of a section of an hydraulic structure is extracted from the i-viewer and is $1/470$ per year. The failure probability space of an hydraulic structure is 0.08, with 0.02 reserved for structural failure [S.N. Jonkman et al.]. The total failure probability space for this mechanism then becomes:

$$P_{f;space} = 1/470 \cdot 0.02 = 4.255 \cdot 10^{-5}$$

I.3.1. OR

Due to sometimes unknown correlations between failure mechanisms and sub-mechanisms the failure probabilities per failure mechanism are not simply added when the OR function is used. Correlations are taken into account by giving an upper and a lower limit of the total failure probability. This means that the lower limit assumes full correlation between failure mechanisms, while the upper limit corresponds to the situation that the failure mechanisms are independent and there is no correlation between the failure probabilities. [S.N. Jonkman et al.]

Lower limit OR: $P_{combi} = Max(P_i)$
Upper limit OR: $P_{combi} = \sum(P_i)$

To be on the safe side, the upper limit must be assumed and the probabilities are added up to each other. The reality will be in between.

I.3.2. AND

When the function AND is used, it means that all sub-mechanisms need to happen independently to cause system failure. Sometimes these sub-mechanisms are highly correlated, and can therefore not be multiplied with each other. For example when water retaining elements fail due to head difference overload, it is highly possible that the hydraulic load is high, and the probability of reaching the critical inflow is close to one. The lower limit in this case is that the failure mechanisms are completely independent and can be multiplied with one another. The upper limit assumes full correlation and the largest probability is governing.

Lower limit AND: $P_{combi} = P_1 \cdot P_2 \ldots \cdot P_i$
Upper limit AND: $P_{combi} = Max(P_i)$

I.3.3. Analysis failure tree

Some correlations can be easily identified, as the probability of “Failure of the structure due to head difference overload” and “Failure due to inflow” are highly correlated. When “Failure of the structure due to head difference overload” occurs, “Failure due to inflow” almost certainly also occurs, this is the domino effect. The other way around is almost impossible: there is no inflow if the water retaining elements do not fail. This is not always the case, but for this particular structure, inflow becomes critical very fast as there is no inner water level.
Other failure mechanisms such as the “Probability of occurrence” of a collision and the “Collision energy larger than critical value” are independent.

In the sub mechanism “Failure of water retaining structural elements” it can be concluded that the upper limit is equal to the probability of failure of “Failure due to head difference overload” $Z_{411} = 1.107 \cdot 10^{-5}$.

In the sub-mechanism failure due to collision all events needs to happen to cause a flood. The events are independent of each other so the failure probability becomes:
Failure due to inflow =$4.01 \cdot 10^{-2} \cdot 1.0 + 4.58 \cdot 10^{-2} = 8.59 \cdot 10^{-2}$
Failure due do collision $= 1.0 \cdot 10^{-2} \cdot 1.77 \cdot 10^{-2} \cdot 8.59 \cdot 10^{-2} = 1.52 \cdot 10^{-5}$

Total failure probability:

$$P_{f;total} = 1.52 \cdot 10^{-5} + 1.107 \cdot 10^{-5}\left(+P_{f;instability} \approx 0\right) = 2.627 \cdot 10^{-05}$$

This probability is smaller than the failure probability space. More information about the probability of a collision and the distributions of floating debris in the Meuse is however needed as a large portion of this calculations are based on estimations of the author.

I.4. Prob2B output

The sub- failure mechanisms are:

I.4.1. Z_{12} Failure of structure due to bottom erosion

$$P_{f;12} = 1.0$$

I.4.2. Z_{21} Failure due to the reaching of critical inflow

A Monte Carlo Simulation was performed with Prob2B, a probabilistic calculation tool provided by TNO. The results are stated below:

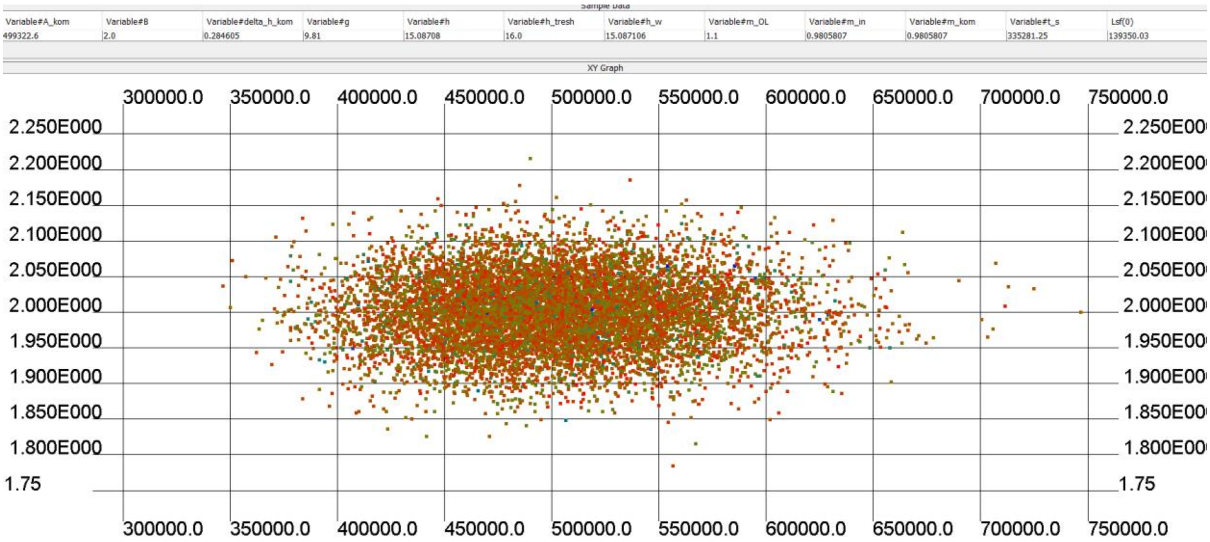

Figure I-8: Example of the Crude Monte Carlo simulation

Number of calculations (Crude Monte Carlo) : 10002

Beta : 1.687E000
P_f : 4.580E-02

Table I-23: Crude Monte Carlo output Z_21

	Model	Parameter	alfa	X
1	Variable	A_kom	-1.744E-01	5.142E005
2	Variable	B	2.084E-01	1.982E000
3	Variable	delta_h_kom	1.457E-01	2.628E-01
4	Variable	g	4.165E-02	9.810E000
5	Variable	h	-7.115E-01	1.581E001
6	Variable	h_tresh	4.693E-01	1.592E001
7	Variable	h_w	3.863E-01	1.481E001
8	Variable	m_OL	9.390E-02	1.095E000
9	Variable	m_in	-3.270E-02	9.914E-01
10	Variable	m_kom	-1.247E-01	1.022E000

11	Variable	t_s	-4.599E-02	3.417E005

	z-value
1	1.394E005
10002	1.381E005

$$P_{f;21} = 4.58 \cdot 10^{-2}$$

I.4.3. Z_{22} Failure of bottom erosion behind structure

A Monte Carlo Simulation was performed with Prob2B, a probabilistic calculation tool provided by TNO. The results are stated below:

Number of calculations (Crude Monte Carlo) : 10002

Beta : 1.739E000
P_f : 4.100E-02

Table I-24: Crude Monte Carlo output Z_22

	Model	Parameter	alfa	X
1	Variable	A_kom	-6.161E-02	5.047E005
2	Variable	B	-7.044E-02	2.006E000
3	Variable	B_sv	-4.865E-01	4.042E000
4	Variable	delta_h_kom	-4.960E-02	2.927E-01
5	Variable	g	-2.100E-01	9.810E000
6	Variable	h	6.381E-01	1.464E001
7	Variable	h_tresh	-2.686E-01	1.605E001
8	Variable	h_w	-7.447E-02	1.515E001
9	Variable	m_OL	1.079E-01	1.094E000
10	Variable	m_in	-8.013E-02	1.008E000
11	Variable	m_kom	1.294E-01	9.378E-01
12	Variable	t_s	-4.236E-01	4.020E005
13	Variable	u_c	-9.408E-02	5.164E-01

	z-value
1	0.000E00
10002	0.000E00

$$P_{f;22} = 4.1 \cdot 10^{-2}$$

I.4.4. Z_{411} Failure of structural parts due to head difference overload

$\mathbf{Z_{411;1}}$ *Bending moment in the middle of the plate*

First the yearly probability that high water occurs is calculated as will be multiplied by the probability of failure of the glass.

$$Z_{highwater} = (h_{threshold} + 2) - h$$

A Form and a Monte Carlo Simulation was performed with Prob2B, a probabilistic calculation tool provided by TNO. The results are stated below:

Number of calculations (FORM) : 281

Beta : 3.222E000
P_f : 6.369E-04

Table I-25: FORM output Z_411

	Model	Parameter	alfa	X
1	Variable	A_kom	0.000E00	4.993E005
2	Variable	B	0.000E00	2.000E000
3	Variable	B_sv	0.000E00	4.000E000
4	Variable	delta_h_kom	0.000E00	2.846E-01
5	Variable	g	0.000E00	9.810E000
6	Variable	h	-9.978E-01	1.798E001
7	Variable	h_tresh	6.650E-02	1.598E001
8	Variable	h_w	0.000E00	1.509E001
9	Variable	m_OL	0.000E00	1.100E000
10	Variable	m_in	0.000E00	9.806E-01
11	Variable	m_kom	0.000E00	9.806E-01
12	Variable	t_s	0.000E00	3.353E005
13	Variable	u_c	0.000E00	5.000E-01

Number of calculations (Crude Monte Carlo) : 165113

Beta : 3.236E000
P_f : 6.057E-04

Table I-26: Crude Monte Carlo output Z_411

	Model	Parameter	alfa	X
1	Variable	A_kom	-4.071E-02	5.059E005
2	Variable	B	4.945E-02	1.992E000
3	Variable	B_sv	-4.332E-02	4.007E000
4	Variable	delta_h_kom	-1.395E-01	3.295E-01
5	Variable	g	1.558E-01	9.810E000
6	Variable	h	-8.669E-01	1.742E001
7	Variable	h_tresh	-1.770E-01	1.606E001
8	Variable	h_w	-1.380E-01	1.532E001
9	Variable	m_OL	3.531E-01	1.066E000
10	Variable	m_in	1.001E-01	9.197E-01
11	Variable	m_kom	4.425E-02	9.532E-01
12	Variable	t_s	-1.066E-01	3.650E005
13	Variable	u_c	-2.106E-02	5.068E-01

	z-value
1	2.913E000
165113	6.389E-01

$$P_{f;high\,water} = 6.057 \cdot 10^{-4}$$

Now the failure probability of the bending stresses in the plate due to high water are calculated with a Monte Carlo Simulation and the Weibull distribution of glass strength.

Number of calculations (Crude Monte Carlo) : 100002

Beta : 4.013E000
P_f : 3.000E-05

Table I-27: Crude Monte Carlo output $\boldsymbol{Z_{411}}$ Weibull glass strength

	Model	Parameter	alfa	X
1	Variable	f_g_1	9.958E-01	8.258E000
2	Variable	f_g_2	-9.060E-02	1.331E002
3	Variable	m_s	1.490E-02	9.970E-01

z-value
1 9.484E001
100002 -1.413E000

And with the Normal distribution of glass strength:

Number of calculations (Crude Monte Carlo) : 84891

Beta : 3.041E000
P_f : 1.178E-03

Table I-28: Crude Monte Carlo output $\boldsymbol{Z_{411}}$ Normal distribution glass strength

	Model	Parameter	alfa	X
1	Variable	f_g_1	-1.724E-01	1.203E002
2	Variable	f_g_2	9.848E-01	1.218E001
3	Variable	m_s	-2.078E-02	1.003E000

z-value
1 1.103E002
84891 2.447E000

As the latter probability is larger, this will be used to compute the total failure probability of this failure mechanism

$$P_{f;411;1} = 6.057 \cdot 10^{-4} \cdot 1.178 \cdot 10^{-3} = 7.135 \cdot 10^{-7}$$

$\boldsymbol{Z_{411;1}}$ *Corner stresses in the plate*

A Monte Carlo Simulation was performed with Prob2B, a probabilistic calculation tool provided by TNO. The results are stated below:

Weibull glass strength:

Number of calculations (Crude Monte Carlo) : 100002

Beta : 4.265E000
P_f : 1.000E-05

Table I-29: Crude Monte Carlo output $\boldsymbol{Z_{411;1}}$ Weibull glass strength

	Model	Parameter	alfa	X
1	Variable	f_g_1	8.808E-01	1.060E001
2	Variable	f_g_2	7.004E-02	1.092E002
3	Variable	m_s	-4.682E-01	1.100E000

z-value
1 9.854E001
100002 4.004E000

Normal distribution glass strength:

Number of calculations (Crude Monte Carlo) : 100002

Beta : 3.239E000
P_f : 6.000E-04

Table I-30: Crude Monte Carlo output Z_(411;1) Normal distribution glass strength

	Model	Parameter	alfa	X
1	Variable	f_g_1	-5.517E-02	1.100E002
2	Variable	f_g_2	9.984E-01	3.586E000
3	Variable	m_s	-1.253E-02	1.002E000

z-value
1 1.140E002
100002 -2.426E000

The latter is governing

$$P_{f;411;2} = 4.1 \cdot 10^{-2} \cdot 6 \cdot 10^{-4} = 2.46 \cdot 10^{-5}$$

$Z_{411;2}$ *Moment in the anchor posts*

A Monte Carlo Simulation was performed with Prob2B, a probabilistic calculation tool provided by TNO. The results are stated below:

$Z_{411;2;lower}$

number of Warnings: 1
1 warning number: 701
Geen designpunt doordat de faalkans gelijk is aan 0.

Number of calculations (Crude Monte Carlo) : 100002

Beta : 3.705E001
P_f : 1.003E-300

Table I-31: Crude Monte Carlo output Z_(411;2;lower)

	Model	Parameter	alfa	X
1	Variable	B	-2.887E-01	3.070E000
2	Variable	I_z_lower	-2.887E-01	8.016E-04
3	Variable	I_z_upper	-2.887E-01	1.426E-04
4	Variable	f_o	-2.887E-01	4.139E008
5	Variable	g	-2.887E-01	9.810E000
6	Variable	$gamma\_w$	-2.887E-01	1.053E003
7	Variable	h	-2.887E-01	4.003E001
8	Variable	h_tresh	-2.887E-01	1.707E001

9	Variable	l_1	-2.887E-01	8.279E-01
10	Variable	m_s	-2.887E-01	1.535E000
11	Variable	z_lower	-2.887E-01	4.572E-01
12	Variable	z_upper	-2.887E-01	2.248E-01

z-value
1 2.000E008
100002 3.235E008

$Z_{411;2;upper}$

Number of calculations (Crude Monte Carlo) : 100002

Beta : 3.705E001
P_f : 1.003E-300

Table I-32: Crude Monte Carlo output Z_(411;2;upper)

	Model	Parameter	alfa	X
1	Variable	B	-2.887E-01	3.070E000
2	Variable	l_z_lower	-2.887E-01	8.016E-04
3	Variable	l_z_upper	-2.887E-01	1.426E-04
4	Variable	f_o	-2.887E-01	4.139E008
5	Variable	g	-2.887E-01	9.810E000
6	Variable	gamma_w	-2.887E-01	1.053E003
7	Variable	h	-2.887E-01	4.003E001
8	Variable	h_tresh	-2.887E-01	1.707E001
9	Variable	l_1	-2.887E-01	8.279E-01
10	Variable	m_s	-2.887E-01	1.535E000
11	Variable	z_lower	-2.887E-01	4.572E-01
12	Variable	z_upper	-2.887E-01	2.248E-01

z-value
1 2.000E008
100002 3.391E008

$$P_{f;411;3} = 0$$

$\mathbf{Z_{411;3}}$ *Shear in the anchor posts*

A Monte Carlo Simulation was performed with Prob2B, a probabilistic calculation tool provided by TNO. The results are stated below:

Calculation upper profile

Number of calculations (FORM) : 276

Beta : 1.000E001
P_f : 7.769E-24

Table I-33: FORM output Z_(411;3;upper)

	Model	Parameter	alfa	X
1	Variable	Av_lower	0.000E00	1.360E-02
2	Variable	Av_upper	5.001E-04	7.598E-03
3	Variable	B	0.000E00	2.000E000
4	Variable	f_o	1.000E00	-3.900E002
5	Variable	g	0.000E00	9.810E000
6	Variable	gamma_w	0.000E00	1.000E003
7	Variable	h	0.000E00	1.454E001
8	Variable	h_tresh	0.000E00	1.600E001
9	Variable	l_1	0.000E00	5.394E-01
10	Variable	m_s	0.000E00	1.000E000

	z-value
1	8.776E005
276	-1.711E000

number of Warnings: 1
1 warning number: 701
Geen designpunt doordat de faalkans gelijk is aan 0.

Number of calculations (Crude Monte Carlo) : 100002

Beta : 3.705E001
P_f : 1.003E-300

Table I-34: Crude Monte Carlo output Z_(411;3;upper)

	Model	Parameter	alfa	X
1	Variable	Av_lower	-3.162E-01	2.157E-02
2	Variable	Av_upper	-3.162E-01	1.205E-02
3	Variable	B	-3.162E-01	3.172E000
4	Variable	f_o	-3.162E-01	4.343E008
5	Variable	g	-3.162E-01	9.810E000
6	Variable	gamma_w	-3.162E-01	1.059E003
7	Variable	h	-3.162E-01	1.491E002
8	Variable	h_tresh	-3.162E-01	1.717E001
9	Variable	l_1	-3.162E-01	8.554E-01
10	Variable	m_s	-3.162E-01	1.586E000

	z-value
1	8.776E005
100002	2.934E006

Calculation lower profile

number of Warnings: 1
1 warning number: 701
Geen designpunt doordat de faalkans gelijk is aan 0.

Number of calculations (Crude Monte Carlo) : 100002

Beta : 3.705E001
P_f : 1.003E-300

Table I-35:Crude Monte Carlo output Z_(411;3;lower)

	Model	Parameter	alfa	X
1	Variable	Av_lower	-3.162E-01	2.157E-02
2	Variable	Av_upper	-3.162E-01	1.205E-02
3	Variable	B	-3.162E-01	3.172E000
4	Variable	f_o	-3.162E-01	4.343E008
5	Variable	g	-3.162E-01	9.810E000
6	Variable	gamma_w	-3.162E-01	1.059E003
7	Variable	h	-3.162E-01	1.491E002
8	Variable	h_tresh	-3.162E-01	1.717E001
9	Variable	l_1	-3.162E-01	8.554E-01
10	Variable	m_s	-3.162E-01	1.586E000

z-value
1 1.570E006
100002 5.204E006

Number of calculations (FORM) : 276

Beta : 1.000E001
P_f : 7.769E-24

Table I-36: FORM output Z_(411;3;lower)

	Model	Parameter	alfa	X
1	Variable	Av_lower	5.001E-04	1.360E-02
2	Variable	Av_upper	0.000E00	7.600E-03
3	Variable	B	-2.252E-10	2.000E000
4	Variable	f_o	1.000E00	-3.900E002
5	Variable	g	0.000E00	9.810E000
6	Variable	gamma_w	-2.252E-11	1.000E003
7	Variable	h	0.000E00	1.454E001
8	Variable	h_tresh	-2.385E-04	1.600E001
9	Variable	l_1	0.000E00	5.394E-01
10	Variable	m_s	-2.252E-10	1.000E000

z-value
1 1.594E006
276 -3.062E000

$$P_{f411;4} = 0$$

$\mathrm{Z}_{411;5}$ *Steel bolts in tension*

A Monte Carlo Simulation was performed with Prob2B, a probabilistic calculation tool provided by TNO. The results are stated below:

number of Warnings: 1
1 warning number: 701
Geen designpunt doordat de faalkans gelijk is aan 0.

Number of calculations (Crude Monte Carlo) : 100002

Beta : 3.705E001
P_f : 1.003E-300

Table I-37: Crude Monte Carlo output Z_(411;5)

	Model	Parameter	alfa	X
1	Variable	As	-2.774E-01	5.329E-04
2	Variable	B	-2.774E-01	3.028E000
3	Variable	I_z	-2.774E-01	7.854E-04
4	Variable	d	-2.774E-01	3.606E-01
5	Variable	f_o	-2.774E-01	4.055E008
6	Variable	f_ub	-2.774E-01	1.211E009
7	Variable	g	-2.774E-01	9.810E000
8	Variable	gamma_w	-2.774E-01	1.051E003
9	Variable	h	-2.774E-01	3.819E001
10	Variable	h_tresh	-2.774E-01	1.703E001
11	Variable	k_2	-2.774E-01	9.000E-01
12	Variable	m_s	-2.774E-01	1.514E000
13	Variable	z	-2.774E-01	4.572E-0

1

z-value
1 2.742E005
100002 -9.266E007

$$P_{f;411;5} = 0$$

$\mathbf{Z_{411;6;1}}$ *Steel bolts in shear: Tensile strength net section plate*

A Monte Carlo Simulation was performed with Prob2B, a probabilistic calculation tool provided by TNO. The results are stated below:

number of Warnings: 1
1 warning number: 701
Geen designpunt doordat de faalkans gelijk is aan 0.

Number of calculations (Crude Monte Carlo) : 100002

Beta : 3.705E001
P_f : 1.003E-300

Table I-38: Crude Monte Carlo output Z_(411;6;1)

	Model	Parameter	alfa	X
1	Variable	As	-2.673E-01	5.263E-04
2	Variable	B	-2.673E-01	2.990E000
3	Variable	I_z	-2.673E-01	7.709E-04
4	Variable	f_o	-2.673E-01	3.980E008
5	Variable	f_ub	-2.673E-01	1.196E009
6	Variable	g	-2.673E-01	9.810E000
7	Variable	gamma_w	-2.673E-01	1.050E003
8	Variable	h	-2.673E-01	3.661E001
9	Variable	h_tresh	-2.673E-01	1.699E001

10	Variable	k_2	-2.673E-01	9.000E-01
11	Variable	m_s	-2.673E-01	1.495E000
12	Variable	o	-2.673E-01	3.887E-02
13	Variable	t	-2.673E-01	5.876E-02
14	Variable	w	-2.673E-01	2.506E-01
15	Variable	z	0.000E00	4.572E-01

z-value
1 2.000E008
100002 -6.921E008

$411;6;1$

$$P_{f;411;6;1} = 0$$

$\mathbf{Z_{411;6;2}}$ *Steel bolts in shear: Shear failure bolt*

A Monte Carlo Simulation was performed with Prob2B, a probabilistic calculation tool provided by TNO. The results are stated below:

number of Warnings: 1
1 warning number: 701
Geen designpunt doordat de faalkans gelijk is aan 0.

Number of calculations (Crude Monte Carlo) : 100002

Beta : 3.705E001
P_f : 1.003E-300

Table I-39: Crude Monte Carlo output Z_(411;6;2)

	Model	Parameter	alfa	X
1	Variable	As	-2.673E-01	5.263E-04
2	Variable	B	-2.673E-01	2.990E000
3	Variable	I_z	-2.673E-01	7.709E-04
4	Variable	f_o	-2.673E-01	3.980E008
5	Variable	f_ub	-2.673E-01	1.196E009
6	Variable	g	-2.673E-01	9.810E000
7	Variable	gamma_w	-2.673E-01	1.050E003
8	Variable	h	-2.673E-01	3.661E001
9	Variable	h_tresh	-2.673E-01	1.699E001
10	Variable	k_2	-2.673E-01	9.000E-01
11	Variable	m_s	-2.673E-01	1.495E000
12	Variable	o	-2.673E-01	3.887E-02
13	Variable	t	-2.673E-01	5.876E-02
14	Variable	w	-2.673E-01	2.506E-01
15	Variable	z	0.000E00	4.572E-01

z-value
1 8.129E005
100002 -9.254E006

$$P_{f;411;6;2} = 0$$

$Z_{411;6;3}$ *Steel bolts in shear: Plate bearing resistance (shearing out of plate/hole ovalisation)*

A Monte Carlo Simulation was performed with Prob2B, a probabilistic calculation tool provided by TNO. The results are stated below:

Number of calculations (Crude Monte Carlo) : 100002

Beta : 4.265E000
P_f : 1.000E-05

Table I-40: Crude Monte Carlo output Z_(411;6;3)

	Model	Parameter	alfa	X
1	Variable	B	-3.060E-01	2.131E000
2	Variable	ab	2.820E-01	2.500E-01
3	Variable	d	-1.123E-01	2.457E-02
4	Variable	f_o	9.622E-02	1.918E008
5	Variable	f_ub	1.509E-01	7.743E008
6	Variable	g	-3.599E-01	9.810E000
7	Variable	gamma_w	4.977E-02	9.989E002
8	Variable	h	-7.236E-01	1.780E001
9	Variable	h_tresh	2.054E-01	1.591E001
10	Variable	k_1	1.425E-01	2.500E000
11	Variable	m_s	2.499E-01	9.467E-01
12	Variable	o	-2.423E-02	2.613E-02
13	Variable	t	3.303E-02	3.902E-02

	z-value
1	1.179E005
100002	7.115E004

$$P_{f;411;6;1} = 1 \cdot 10^{-5}$$

Z_{412} *Failure to repair flood defence*

$$P_{f;412} = 1.0$$

Z_{421} *Collision energy larger than critical value*

Nine Monte Carlo Simulations were performed with Prob2B, a probabilistic calculation tool provided by TNO. The results are stated below:

Location 1 and 3

Monte Carlo found no design point, therefore a FORM analysis is performed.
Number of calculations (FORM) : 210

Beta : 5.241E000
P_f : 8.022E-08

Table I-41: Crude Monte Carlo output Z_(421) Location 1 and 3

	Model	Parameter	alfa	X
1	Variable	E_c13	2.303E-01	3.640E003

2	Variable	E_c2	0.000E00	8.500E002
3	Variable	E_c46	0.000E00	1.100E003
4	Variable	E_c5	0.000E00	6.600E002
5	Variable	E_c79	0.000E00	3.300E002
6	Variable	E_c8	0.000E00	5.400E002
7	Variable	alpha	-4.844E-01	5.573E001
8	Variable	m	-3.026E-01	2.634E002
9	Variable	m_E	-3.026E-01	1.317E000
10	Variable	v_s	-7.275E-01	5.543E000

	z-value
1	4.188E003
210	8.864E-02

Location 2

Number of calculations (Crude Monte Carlo) : 29002

Beta : 2.702E000
P_f : 3.448E-03

Table I-42: : Crude Monte Carlo output Z_(421) Location 2

	Model	Parameter	alfa	X
1	Variable	E_c13	-4.716E-02	4.193E003
2	Variable	E_c2	1.030E-01	8.263E002
3	Variable	E_c46	1.263E-01	1.062E003
4	Variable	E_c5	1.101E-01	6.404E002
5	Variable	E_c79	1.380E-01	3.177E002
6	Variable	E_c8	4.857E-02	5.329E002
7	Variable	alpha	-6.835E-01	4.850E001
8	Variable	m	-3.545E-02	2.038E002
9	Variable	m_E	3.618E-02	9.805E-01
10	Variable	v_s	-6.841E-01	3.610E000

	z-value
1	7.737E002
29002	9.611E001

Location 4 and 6

Number of calculations (Crude Monte Carlo) : 84530

Beta : 3.040E000
P_f : 1.183E-03

Table I-43: : Crude Monte Carlo output Z_(421) Location 4 and 6

	Model	Parameter	alfa	X
1	Variable	E_c13	-1.907E-01	4.380E003
2	Variable	E_c2	1.096E-01	8.217E002
3	Variable	E_c46	2.462E-01	1.018E003
4	Variable	E_c5	-9.276E-02	6.786E002
5	Variable	E_c79	-4.946E-02	3.350E002

6	Variable	E_c8	1.472E-01	5.158E002
7	Variable	alpha	-5.697E-01	4.730E001
8	Variable	m	-1.658E-01	2.202E002
9	Variable	m_E	8.589E-02	9.478E-01
10	Variable	v_s	-7.063E-01	3.904E000

	z-value
1	1.024E003
84530	1.590E002

Number of calculations (FORM) : 199

Beta : 2.929E000
P_f : 1.698E-03

Table I-44: : FORM output Z_(421) Location 4 and 6

	Model	Parameter	alfa	X
1	Variable	E_c13	0.000E00	4.140E003
2	Variable	E_c2	0.000E00	8.500E002
3	Variable	E_c46	1.544E-01	1.050E003
4	Variable	E_c5	0.000E00	6.600E002
5	Variable	E_c79	0.000E00	3.300E002
6	Variable	E_c8	0.000E00	5.400E002
7	Variable	alpha	-5.268E-01	4.533E001
8	Variable	m	-2.547E-01	2.298E002
9	Variable	m_E	-2.547E-01	1.149E000
10	Variable	v_s	-7.543E-01	3.965E000

	z-value
1	1.024E003
199	1.175E-01

Location 5

Number of calculations (Crude Monte Carlo) : 11253

Beta : 2.370E000
P_f : 8.888E-03

Table I-45: : Crude Monte Carlo output Z_(421) Location 5

	Model	Parameter	alfa	X
1	Variable	E_c13	-2.536E-01	4.389E003
2	Variable	E_c2	-1.833E-01	8.869E002
3	Variable	E_c46	1.467E-01	1.062E003
4	Variable	E_c5	2.681E-01	6.181E002
5	Variable	E_c79	-1.589E-01	3.424E002
6	Variable	E_c8	1.176E-01	5.250E002
7	Variable	alpha	-3.838E-01	3.871E001
8	Variable	m	1.647E-01	1.844E002
9	Variable	m_E	-4.086E-01	1.194E000
10	Variable	v_s	-6.544E-01	3.317E000

	z-value
1	5.837E002
11253	1.446E002

Number of calculations (FORM) : 199

Beta : 2.211E000
P_f : 1.352E-02

Table I-46: FORM output Z_(421) Location 5:

	Model	Parameter	alfa	X
1	Variable	E_c13	0.000E00	4.140E003
2	Variable	E_c2	0.000E00	8.500E002
3	Variable	E_c46	0.000E00	1.100E003
4	Variable	E_c5	1.338E-01	6.405E002
5	Variable	E_c79	0.000E00	3.300E002
6	Variable	E_c8	0.000E00	5.400E002
7	Variable	alpha	-5.341E-01	4.154E001
8	Variable	m	-2.338E-01	2.207E002
9	Variable	m_E	-2.338E-01	1.103E000
10	Variable	v_s	-7.665E-01	3.458E000

	z-value
1	5.837E002
199	8.388E-02

Location 7 and 9

Number of calculations (Crude Monte Carlo) : 1667

Beta : 1.580E000
P_f : 5.706E-02

Table I-47: : Crude Monte Carlo output Z_(421) Location 7 and 9

	Model	Parameter	alfa	X
1	Variable	E_c13	-2.229E-01	4.286E003
2	Variable	E_c2	-5.475E-03	8.507E002
3	Variable	E_c46	2.726E-01	1.053E003
4	Variable	E_c5	1.772E-01	6.415E002
5	Variable	E_c79	-2.973E-01	3.455E002
6	Variable	E_c8	6.652E-02	5.343E002
7	Variable	alpha	-7.644E-01	4.182E001
8	Variable	m	-8.364E-02	2.053E002
9	Variable	m_E	-2.487E-01	1.079E000
10	Variable	v_s	-3.140E-01	2.278E000

	z-value
1	2.537E002
1667	8.996E001

Location 8

Number of calculations (Crude Monte Carlo) : 5556

Beta : 2.101E000
P_f : 1.782E-02

Table I-48: : Crude Monte Carlo output Z_(421) Location 8

	Model	Parameter	alfa	X
1	Variable	E_c13	8.599E-02	4.065E003
2	Variable	E_c2	3.247E-01	7.920E002
3	Variable	E_c46	7.163E-02	1.083E003
4	Variable	E_c5	1.465E-01	6.397E002
5	Variable	E_c79	-2.217E-02	3.315E002
6	Variable	E_c8	2.089E-01	5.163E002
7	Variable	alpha	-4.126E-01	3.826E001
8	Variable	m	-2.697E-01	2.227E002
9	Variable	m_E	-1.497E-02	1.006E000
10	Variable	v_s	-7.571E-01	3.356E000

	z-value
1	4.637E002
5556	3.251E001

Number of calculations (FORM) : 199

Beta : 1.952E000
P_f : 2.548E-02

Table I-49: : Form output Z_(421) Location 8

	Model	Parameter	alfa	X
1	Variable	E_c13	0.000E00	4.140E003
2	Variable	E_c2	0.000E00	8.500E002
3	Variable	E_c46	0.000E00	1.100E003
4	Variable	E_c5	0.000E00	6.600E002
5	Variable	E_c79	0.000E00	3.300E002
6	Variable	E_c8	1.265E-01	5.267E002
7	Variable	alpha	-5.354E-01	4.012E001
8	Variable	m	-2.255E-01	2.176E002
9	Variable	m_E	-2.255E-01	1.088E000
10	Variable	v_s	-7.718E-01	3.273E000

	z-value
1	4.637E002
199	7.434E-02

Table I-50: Probability percentages per location and total failure probability

Location	E_c [Nm]	σ	$\%\ of\ probability$	P_f	$\% \cdot P_f$
1	4140	414	11.111	8.022E-08	8.913E-09
2	850	85	11.111	3.448E-03	3.831E-04
3	4140	414	11.111	8.022E-08	8.913E-09
4	1100	110	11.111	1.698E-03	1.887E-04

5	660	66	11.111	1.352E-02	1.502E-03
6	1100	110	11.111	1.698E-03	1.887E-04
7	330	33	11.111	5.706E-02	6.340E-03
8	540	54	11.111	2.548E-02	2.831E-03
9	330	33	11.111	5.706E-02	6.340E-03
Total	-	-	100	-	1.777E-02

$$P_f = 1.777 \cdot 10^{-2}$$

I.4.5. Z_{422} Probability of occurrence of a collision

$$P_{f;422} = 1 \cdot 10^{-2}$$

I.4.6. Z_{423} Failure to repair the fatal collision damages

$$P_{f;423} = 1.0$$

I.4.7. Z_{43} Failure of structure due to instability of structure or its foundation

Assumed sufficiently small.

$$P_{f;43} \approx 0$$

I.5. Literature

CEN. (2007). *NEN-EN 1993-1-8:2006/NB:2007*. Geraadpleegd van https://www.nen.nl/NEN-Shop/Norm/NENEN-1993182006NB2007-nl.htm
EN 1993-1-1 art. 6.2.3

CEN. (2011). *NEN-EN 1090-2:2008+A1:2011 nl*. Geraadpleegd van https://www.nen.nl/NEN-Shop/Norm/NENEN-109022008A12011-nl.htm

CEN. (2011). *NEN-EN 1999-1-1+A1*. Geraadpleegd van https://www.nen.nl/NEN-Shop/Norm/NENEN-199911A12011NB2011-nl.htm

CEN. (2016). *NEN-EN 1993-1-1+C2+A1:2016*. Geraadpleegd van https://www.nen.nl/NEN-Shop/Norm/NENEN-199311C2A12016-nl.htm

Jonkman, S. N., Jorissen, R. E., Schweckendieck, T., & Van den Bos, J. P. (2017). *Flood Defences Lecture notes CIE5314* (2nd ed.). Retrieved from TU Delft Blackboard

Veer, F., Louter, P., & Bos, F. (2009). The strength of annealed, heat-strenghtened and fully tempered float glass. Fatigue & Fracture of Engineering Materials & Structures, 32, 18-25

WBI 2017. (2015). *Toetsspoorrapport Sterkte en Stabiliteit puntconstructies*. Retrieved from: https://www.helpdeskwater.nl/onderwerpen/waterveiligheid/primaire/beoordelen-wbi/producten-wbi/

WBI 2017. (2017). *Schematiseringshandleiding sterkte en stabiliteit kunstwerk*. Retrieved from: https://www.helpdeskwater.nl/algemene-onderdelen/structuur-pagina/zoeken-site/@178897/laag-2-1/

J. Parameter List

J.1. Explanations of parameters in the probabilistic assessment

J.1.1. Water height h_w

The water level is one of the most important input variables of the probabilistic analysis. It is assumed this parameter has a Gumbel-distribution. The values obtained from the Pim-platform(a data-tool provided by the waterboard of Limburg), which are extracted from Hydra are:

Figure J-1: Hydraulic boundary conditions Arcen

Waterstand zonder onzekerheidstoeslag 1/10: 15.869
Waterstand zonder onzekerheidstoeslag 1/30: 16.368
Waterstand zonder onzekerheidstoeslag 1/100: 16.845
Waterstand zonder onzekerheidstoeslag 1/300: 17.208
Waterstand zonder onzekerheidstoeslag 1/1000: 17.497
Waterstand zonder onzekerheidstoeslag 1/3000: 17.695
Waterstand zonder onzekerheidstoeslag 1/10000: 17.902
Waterstand zonder onzekerheidstoeslag 1/30000: 18.092

The probability density function of a Gumbel(maximum) distribution are:

$$f(x) = \frac{1}{\beta} \cdot e^{-\frac{x-\mu}{\beta}} \cdot e^{-e^{-\frac{x-\mu}{\beta}}}$$

And the cumulative distribution is:

$$F(x,\mu,\beta) = e^{-e^{\frac{x-\mu}{\beta}}}$$

So the probabilistic distribution must follow the values extracted from the i-viewer or Pim platform. β and μ are the unknowns of the probability density function. We use 2 values to determine μ and β:
For $F = 0.90$; $x = 16.325$ and for $F = 0.99$; $x = 17.426$

$$0.900 = e^{-e^{\frac{16.325-\mu}{\beta}}}; \; 0.99 = e^{-e^{\frac{17.426-\mu}{\beta}}}$$

$$ln(-ln(0.900)) = -2.25 = \frac{15.869-\mu}{\beta} \rightarrow \beta = \frac{15.869-\mu}{-2.25}$$

$$ln\big(-ln(0.99)\big) = -4.60 = \frac{17.426-\mu}{\beta} = -2.25 \cdot \frac{16.845-\mu}{15.869-\mu} \rightarrow \mu = 14.935 \rightarrow \beta = -0.415$$

According to the found parameters the following water levels and their probabilities are:

$$F(x,\mu,\beta) = e^{-e^{\frac{x-14.935}{-0.415}}}$$

Table J-1: Yearly probability of occurrence of water levels

Yearly probability	Water level [NAP+m]	Est. water level [NAP+m]
1/10	15.869	15.869
1/30	16.368	16.339
1/100	16.845	16.844
1/300	17.208	17.301
1/1000	17.497	17.801
1/3000	17.695	18.258
1/10000	17.902	18.757
1/30000	18.092	19.213

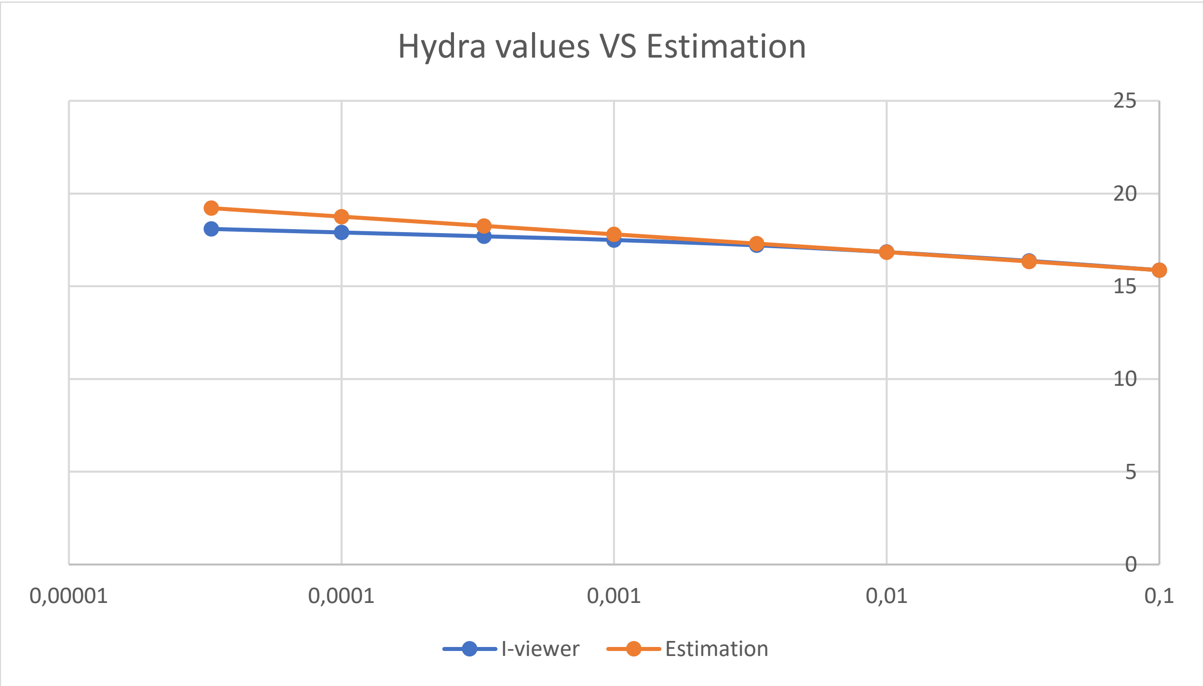

Figure J-2: Hydra values VS Estimation

The found parameters for μ and β lead to an overestimation of the height per probability, but these values will be used as this overestimation starts only from the probabilities smaller than $1/1000$.

The input for prob2B contains 2 values:

$$u = \mu = 14.935$$
$$\alpha = \frac{1}{\beta} = \frac{1}{0.415} = 2.41$$

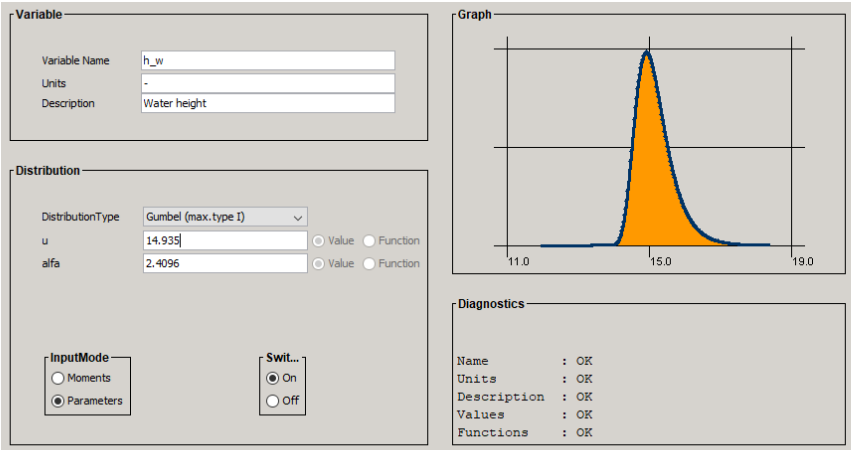

Figure J-3: Probabilistic distribution water level at Arcen

J.1.2. A_{kom} and Δh_{kom}

The storage area of Arcen is assumed to be smaller than reality, only the village is taken into account as economic damages occur when this area is flooded.
With an area measurement tool [www.kilometerafstanden.nl] the area is determined to be $501813\ m$. The critical inundation height is $0.3\ m$

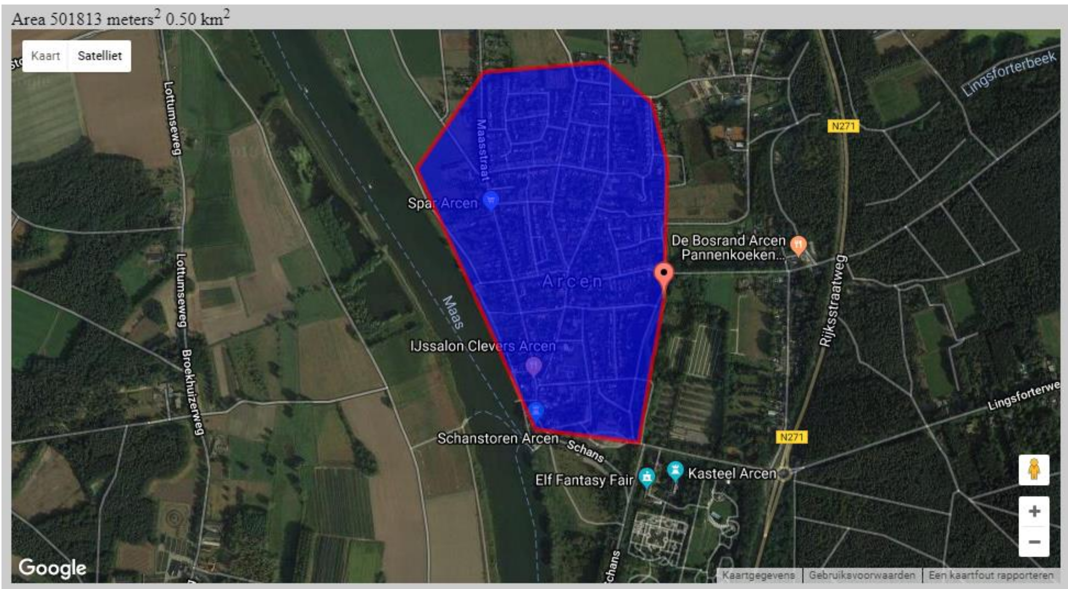

Figure J-4: Inundation area [www.kilometerafstanden.nl(2018)]

J.1.3. h_{in} and $h_{threshold}$

There is no water behind the structure and the mean height in the affected area is around 16 meter above NAP. Therefore both the inner water level and the threshold height are set to be $NAP + 16\ m$. (Height that needs to be retained is $18.40\ m + NAP$, the structure's height is 2 meter so a threshold value of $16\ m + NAP$ is conservative)

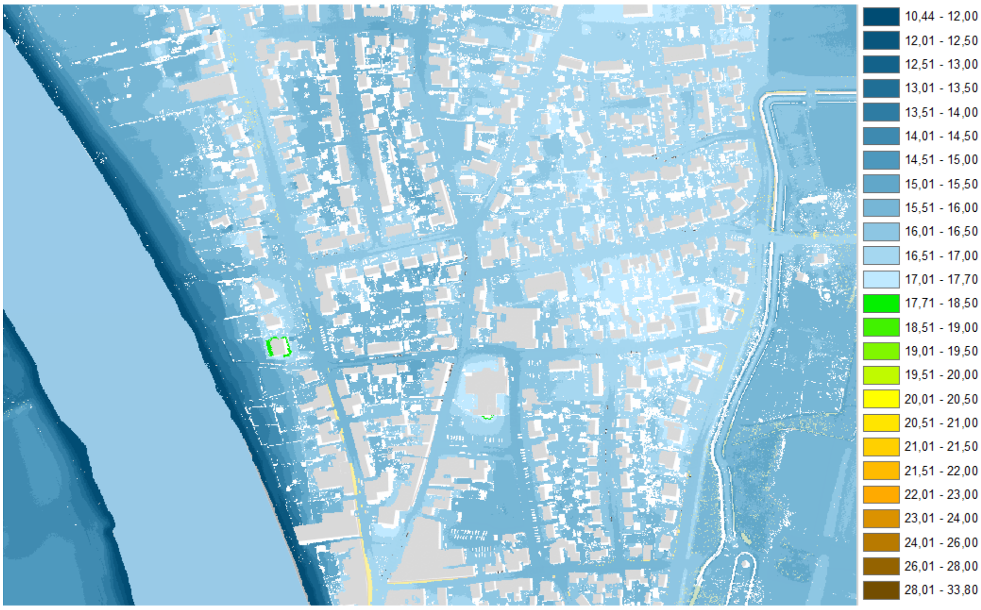

Figure J-5: Height map Arcen [Source: Pimplatform.nl; AHN2 PDOK, Actuality: 2008-2012]

J.1.4. q_c and B_{sv}

The critical flow rate q_c can be determined by using the critical flow velocity and the water level difference. Since there is no water behind the structure, the water level difference is that between the outer water height h and the height of the threshold $h_{threshold}$.

Grondsoort	u_c [m/s]
fijn zand	0,10
matig fijn zand	0,15
matig grof zand	0,20
grof zand	0,30
veen	0,30-0,60
kleiig zand	0,40-0,50
Slappe klei	0,60-0,80
Redelijk vaste klei	0,80-1,00
Vaste klei	1,00-1,20
grind	1,00

The critical flow velocity is assumed to be sandy clay, which has a u_c of 0.5 m/s and will also be given a Normal distribution with $\sigma = 0.1$

The width of the governing bottom protection is assumed to be 4. See image below.

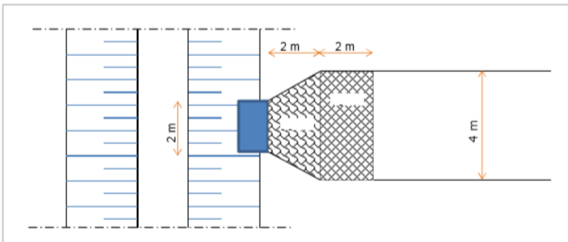

Figure J-6: Left: Table foundations [Handleiding schematisatie] Right: Governing width bottom protection [Handleiding schematisatie]

J.1.5. The strength of glass f_g

The material glass has a large spread when it comes to the (tensile) strength. Not only does the type of loading have an effect on the maximum stress, also load duration, manufacturing an heat treatments have large influence on this value. The nominal value for the tensile strength of FTG is $120\ N/mm^2$, which is discounted with many factors in the NEN to obtain a safe value to use for structural calculations. In the Eurocode calculations [Appendix F] two values were obtained for 2 different load situations. The first load situation was a short duration(3 seconds) concentrated load, and the second was a longer duration(1 week) distributed load on the glass panel.
The obtained values of NEN calculations are:

Long duration load	[MPa]	74.536
Short duration load	[MPa]	98.097

Figure J-7: Summary NEN calculations

In the schematization manual for the failure mechanism Structural Failure, the variational coefficient for masonry is $V_r = 0.3$. Since masonry is quite similar to glass: not very resistant to tensile stresses, brittle and quite unpredictable, it is assumed the same variational coefficient may be used for glass.

Many tests have been done in this area of expertise, and in their research, [Veer Louter Bos] have found the following values for standing fully tempered glass specimens:

Table J-2: Found failure stress standing tempered glass

Average failure stress	[MPa]	98.0
Standard deviation	[% of average]	13.7
Average prestress	[MPa]	-100.6
Standard deviation of prestress	[% of average]	12.9

Jorrit Kentrop (2016) used the following (conservative) values for a Weibull distribution of the glass strength in his thesis:

$$u = 114.76$$
$$k = 3.93$$

It can be concluded that there is not one distribution possible that describes the failure stress of glass as different distributions need to be used for different load and load duration types. The choice is made to use the variational coefficients of and the Weibull distribution of Jorrit Kentrop and compare failure probabilities.

J.1.6. Storm duration t_s

At the locations at the Meuse, high water levels can occur for several days straight. Therefore a storm duration value of 4 days instead of 6-7 hours is chosen to be governing. This value then becomes $4 \cdot 24 \cdot 60 \cdot 60 = 345600$, with a standard deviation of $\sigma = 0.25 \cdot 345600 = 86400$.

J.2. Summary of used parameters

Table J-3: Summary of used parameters

Symbol	Unit	Description	Distribution	μ	V_r/σ
h_w	$[m]$	Water level at location	Gumbel	$u = 14.935$	$\alpha = 2.41$
A_{kom}	$[m^2]$	Storage area	Lognormal	501813	$V_r = 0.1$
Δh_{kom}	$[m]$	Allowed inundation	Lognormal	0.30	$\sigma = 0.1$
h_{in}	$[m]$	Inner water level	Normal	16	$\sigma = 0.1$
$h_{threshold}$	$[m]$	Height of the threshold	Normal	16.40	$\sigma = 0.1$
u_c	$[m/s]$	Critical flow velocity	Normal	0.5	$\sigma = 0.1$
B_{sv}	$[m]$	Width of governing bottom protection	Normal	4	$\sigma = 0.05$
t_s	[hours]	Storm duration	Lognormal	345600	$\sigma = 86400$
f_g	$[\frac{N}{mm^2}]$	Tensile strength of glass	Weibull	$u = 114.76$	$k = 3.93$
			Normal	$\mu = 120$	$\sigma = 36$
B	$[m]$	Width of opening	Normal	2	0.05
g	$[m/s^2]$	Gravitational constant	Deterministic	9.81	-

J.3. Literature

I-viewer tool/Pimplatform.nl

www.kilometerafstanden.nl

WBI 2017. (2017). *Schematiseringshandleiding sterkte en stabiliteit kunstwerk*. Geraadpleegd van https://www.helpdeskwater.nl/algemene-onderdelen/structuur-pagina/zoeken-site/@178897/laag-2-1/

https://nl.wikipedia.org/wiki/Gumbel-verdeling

Kentrop, J. (2016). *Design and reliability evaluation of a glass flood defence* (MSc. Thesis). Geraadpleegd van https://repository.tudelft.nl/islandora/object/uuid:7f4a8b7d-e00e-4818-8340-be1d3284b857/datastream/OBJ/download

K. Maple files

K.1. Load situation 1, 3 plies

```
> restart;
```

Calculation on the effective thickness from the NEN in Newtons and mm's. With nominal thickness of 19 mm and 3 plies:

```
> a:=2000; b:=2000; E:=70000: h:=18; v:=0.23; G_int:=114; h_int:=
  2.19; N:=3;
```

$$a := 2000$$
$$b := 2000$$
$$h := 18$$
$$v := 0.23$$
$$G\_int := 114$$
$$h\_int := 2.19$$
$$N := 3 \quad \textbf{(1)}$$

```
Error, missing operator or `;`
> B1:=2000; H1:=2000; l_0:=2000;
```

$$B1 := 2000$$
$$H1 := 2000$$
$$l\_0 := 2000 \quad \textbf{(2)}$$

```
> z:=(B1+H1)/2; L_A:=l_0; L_W:=1.002*(2*l_0/z)^(-0.04354);
  L_sigma:=1.832*(2*l_0/z)^(-0.60906);
```

$$z := 2000$$
$$L\_A := 2000$$
$$L\_W := 0.9722117723$$
$$L\_sigma := 1.201102691 \quad \textbf{(3)}$$

```
> X:=(N-1)*h_int*h;
```

$$X := 78.84 \quad \textbf{(4)}$$

```
> beta:=0.5*(3.14^2/L_A^2)*E/(1-v^2)*X/G_int
```

$$\beta := 0.06299604388 \quad \textbf{(5)}$$

```
> w_sigma:=1/(1+beta/L_sigma);w_W:=1/(1+beta/L_W);
```

$$w\_sigma := 0.9501652503$$
$$w\_W := 0.9391464761 \quad \textbf{(6)}$$

```
> t_gg_i_u:=sqrt(((1-w_sigma)*N*h^3+w_sigma*(N*h)^3)/(h+2*w_sigma*
  (0.5*N*h-0.5*h)));
```

$$t\_gg\_i\_u := 53.68982529 \quad \textbf{(7)}$$

```
> t_gg_i_ser:=((1-w_W)*N*h^3+w_W*(N*h)^3)^(1/3);
```

$$t\_gg\_i\_ser := 53.00824056 \quad \textbf{(8)}$$

K.2. Load situation 1, 2 plies

```
> restart;
```

Calculation on the effective thickness from the NEN in Newtons and mm's. With nominal thickness of 19 mm and 2 plies:

```
> a:=2000; b:=2000; E:=70000: h:=18; v:=0.23; G_int:=114; h_int:=
  2.19; N:=2;
```

$$a := 2000$$
$$b := 2000$$
$$h := 18$$
$$v := 0.23$$
$$G\_int := 114$$
$$h\_int := 2.19$$
$$N := 2 \quad (1)$$

```
> B1:=2000; H1:=2000; l_0:=2000;
```

$$B1 := 2000$$
$$H1 := 2000$$
$$l\_0 := 2000 \quad (2)$$

```
>  z:=(B1+H1)/2; L_A:=l_0; L_W:=1.002*(2*l_0/z)^(-0.04354);
  L_sigma:=1.832*(2*l_0/z)^(-0.60906);
```

$$z := 2000$$
$$L\_A := 2000$$
$$L\_W := 0.9722117723$$
$$L\_sigma := 1.201102691 \quad (3)$$

```
> X:=(N-1)*h_int*h;
```

$$X := 39.42 \quad (4)$$

```
> beta:=0.5*(3.14^2/L_A^2)*E/(1-v^2)*X/G_int
```

$$\beta := 0.03149802194 \quad (5)$$

```
> w_sigma:=1/(1+beta/L_sigma);w_W:=1/(1+beta/L_W);
```

$$w\_sigma := 0.9744458836$$
$$w\_W := 0.9686183970 \quad (6)$$

```
> t_gg_i_u:=sqrt(((1-w_sigma)*N*h^3+w_sigma*(N*h)^3)/(h+2*w_sigma*
  (0.5*N*h-0.5*h)));
```

$$t\_gg\_i\_u := 35.88332912 \quad (7)$$

```
> t_gg_i_ser:=((1-w_W)*N*h^3+w_W*(N*h)^3)^(1/3);
```

$$t\_gg\_i\_ser := 35.71532033 \quad (8)$$

K.3 Load situation 2, 3 plies

```
> restart;
```

Calculation on the effective thickness from the NEN in Newtons and mm's.

```
> a:=2000; b:=2000; E:=70000: h:=18; v:=0.23; G_int:=100; h_int:=
  1.52; N:=3;
```

$$a := 2000$$
$$b := 2000$$
$$h := 18$$
$$v := 0.23$$
$$G\_int := 100$$
$$h\_int := 1.52$$
$$N := 3 \tag{1}$$

```
> B1:=100; H1:=100; l_0:=2000;
```

$$B1 := 100$$
$$H1 := 100$$
$$l\_0 := 2000 \tag{2}$$

```
>  z:=(B1+H1)/2; L_A:=l_0; L_W:=1.002*(2*l_0/z)^(-0.04354);
  L_sigma:=1.832*(2*l_0/z)^(-0.60906);
```

$$z := 100$$
$$L\_A := 2000$$
$$L\_W := 0.8533241357$$
$$L\_sigma := 0.1937201563 \tag{3}$$

```
> X:=(N-1)*h_int*h;
```

$$X := 54.72 \tag{4}$$

```
> beta:=0.5*(3.14^2/L_A^2)*E/(1-v^2)*X/G_int
```

$$\beta := 0.04984454100 \tag{5}$$

```
> w_sigma:=1/(1+beta/L_sigma);w_W:=1/(1+beta/L_W);
```

$$w\_sigma := 0.7953540001$$
$$w\_W := 0.9448114818 \tag{6}$$

```
> t_gg_i_u:=sqrt(((1-w_sigma)*N*h^3+w_sigma*(N*h)^3)/(h+2*w_sigma*
  (0.5*N*h-0.5*h)));
```

$$t\_gg\_i\_u := 52.55890940 \tag{7}$$

```
> t_gg_i_ser:=((1-w_W)*N*h^3+w_W*(N*h)^3)^(1/3);
```

$$t\_gg\_i\_ser := 53.10213762 \tag{8}$$

K.4 Load situation 2, 3 plies

```
> restart;
```

Calculation on the effective thickness from the NEN in Newtons and mm's.

```
> a:=2000; b:=2000; E:=70000: h:=18; v:=0.23; G_int:=100; h_int:=
  1.52; N:=2;
```

$$a := 2000$$
$$b := 2000$$
$$h := 18$$
$$v := 0.23$$
$$G\_int := 100$$
$$h\_int := 1.52$$
$$N := 2 \quad (1)$$

```
> B1:=100; H1:=100; l_0:=2000;
```

$$B1 := 100$$
$$H1 := 100$$
$$l\_0 := 2000 \quad (2)$$

```
>  z:=(B1+H1)/2; L_A:=l_0; L_W:=1.002*(2*l_0/z)^(-0.04354);
  L_sigma:=1.832*(2*l_0/z)^(-0.60906);
```

$$z := 100$$
$$L\_A := 2000$$
$$L\_W := 0.8533241357$$
$$L\_sigma := 0.1937201563 \quad (3)$$

```
> X:=(N-1)*h_int*h;
```

$$X := 27.36 \quad (4)$$

```
> beta:=0.5*(3.14^2/L_A^2)*E/(1-v^2)*X/G_int
```

$$\beta := 0.02492227051 \quad (5)$$

```
> w_sigma:=1/(1+beta/L_sigma);w_W:=1/(1+beta/L_W);
```

$$w\_sigma := 0.8860135662$$
$$w\_W := 0.9716226896 \quad (6)$$

```
> t_gg_i_u:=sqrt(((1-w_sigma)*N*h^3+w_sigma*(N*h)^3)/(h+2*w_sigma*
  (0.5*N*h-0.5*h)));
```

$$t\_gg\_i\_u := 35.45188757 \quad (7)$$

```
> t_gg_i_ser:=((1-w_W)*N*h^3+w_W*(N*h)^3)^(1/3);
```

$$t\_gg\_i\_ser := 35.74277061 \quad (8)$$